MECHANISMS OF RTK SIGNAL TRANSDUCTION ACROSS THE PLASMA MEMBRANE

by

Sarvenaz Sarabipour

A dissertation submitted to Johns Hopkins University in conformity with the requirements for the degree of Doctor of Philosophy

Baltimore, Maryland

March 2015

Abstract

Receptor Tyrosine kinases (RTKs) are a family of membrane proteins with extracellular ligand-binding domains, single transmembrane domains, and intracellular kinase domains. RTKs conduct biochemical signals upon lateral dimerization in the plasma membrane. While RTK activation is postulated to occur in response to ligand binding, recent work suggests that some RTKs are capable of forming ligand-independent dimers. However, the biological significance of RTK unliganded dimers is not well established, and the mechanistic knowledge of RTK signal transduction is incomplete. Here we use a methodology that has been specifically developed to study unliganded dimers, in order to further our understanding of RTK signal transduction across the plasma membrane.

We show that the Fibroblast growth factor receptors, FGFRs, and Vascular endothelial growth factor receptor 2, VEGFR2, form dimers in the absence of their ligands, and we measure the unliganded dimer stabilities. We show that the transmembrane and intracellular domains favor dimerization, while the extracellular domains inhibit dimerization. We demonstrate that the unliganded dimers are phosphorylated. We further show that the unliganded dimers undergo structural changes in response to ligand binding, and this response depends on the identity of the ligand. Such structural changes appear to be a critical aspect of FGFR and VEGFR2 signal transduction across the plasma membrane.

The FGF receptors and VEGF receptor 2 harbor many pathogenic mutations, but the effects of these mutations on signal transduction are not well understood. Here we study five different pathogenic mutations, linked to cancers and growth disorders, and show that these different mutations alter the mechanism of signal transduction in profoundly different ways. Thus, our results provide new basic knowledge about RTK signal transduction across the plasma membrane in health and disease.

Thesis advisor and reader: Dr.Kalina Hristova

Thesis reader: Dr.Michael Edidin

Aknowledgements

I would like to express my deepest gratitude to my thesis advisor, Prof.Kalina Hristova, for her insight and support throughout the years. I would like to acknowledge her strength and perseverance which encouraged me to think critically and enabled me to achieve my scientific goals.

I would like to thank our fantastic lab members. I would like to thank Dr.Janice Lin, Dr.Lijuan He, Dr.Edwin Li, Dr.Fenghao Chen, Dr.Lirong Chen, Dr.Jesse Placone, Gregory Wiedman, Christopher King, Patrick Byrne, Nuala Del Piccolo, Sarah Kim, Kristen Duthie, Angela Feldhaus, Alex Komin, Fozia Ahmed.

I would like to acknowledge the technical assistance that I received from Dr.Andrew Ziman (Nikon Inc), Jeffery Reidler (Nikon Inc), Gregory Kildoff, Joseph Sinclair (Baltimore Precision Instruments) with our lab's confocal microscope.

I would like to thank the entire faculty members and staff at department of Materials Science and Engineering at Johns Hopkins for their support. I have been very inspired by their words of encouragement, their interest in my work and their positive energy.

I would also like to acknowledge many wonderful colleagues, Dr.Luis Santos, Dr.Yang Li, Dr.Stephen Farias, Dr.Thomas Dawidczyk, Dr. Ming-Ling Yeh, Dr.Manu Kanwa, Dr. Brian Chaikind, Dr.Clay Wright, Dr. Elad Firnberg, Ms.Lindsay Clegg, Dr.Joseph Bender and Ms.Anna Frishman in the departments of Materials Science and Engineering, Chemical and Biomolecular Engineering and Biomedical Engineering at Johns Hopkins University.

I was honoured to have Prof.Michael Edidin, Prof.Daniel Leahy, Prof.Feilim Mac Gabhann, Prof.Denis Wirtz, Prof.Peter Searson, Prof.Margarita Herrera-Alonso and

Prof.Kalina Hristova as my thesis defense committee members.I am very inspired by them and their research.

I would like to thank Prof. Ostermeier, Prof. Betenbaugh, Prof.Herrera-Alonso for kindly sharing their facilities with our lab.

I would like to thank wonderful collaborators; Prof.Daniel Leahy at Johns Hopkins School of Medicine, Prof.Kurt Ballmer-Hofer at Paul Scherrer Institute (Switzerland), Dr.Robin Chan and Prof.Gilbert Di Paolo at Columbia University.

I would like to acknowlege the fantastic encouragement of many colleagues, experts in biopolymers, membrane proteins, receptor tyrosine kinases and lipidomics: Prof.Herrera-Alonso (Johns Hopkins University), Prof.Feilim Mac Gabhann (Johns Hopkins University), Prof.Ilya Levental (University of Texas Medical School), Prof.Mark Lemmon (University of Pennsylvania), Prof.Natalia Jura (University of California, San Francisco), Prof.Dirk Schneider (Universität Mainz), Prof.Stephen White (University of California, Irvine), Prof.William Wimley (Tulane University), Prof.Jonathan Sachs (University of Minnesota), Prof.Paulo Almeida (University of North Carolina Wilmington), Prof.Gerald Feigenson (Cornell University).

I would like to thank my parents, Maryam Dabiri and Gholamhossein Sarabipour for their support throughout the years. I am forever inspired by their strength of character, their energy, work ethics and integrity. I would like to thank my adorable brother, Soheil, and sister,Yasamin, for their encouragements and best wishes.

Table of content

Abbreviations xiii

List of Tables xv

List of Figures xvi

Chapter 1 1

1. Literature review 1

1. 1.The plasma membrane 1

1.2. Membrane proteins..1

1.3. Receptor Tyrosine Kinases (RTKs) 2

1.3.1 Fibroblast Growth Factor Receptors (FGFRs) 3

1.3.2. Vascular Endothelial Growth Factor Receptors (VEGFRs)....................................5

1.4. A physico-chemical model for FGFR and VEGFR dimerization and activation.......................……………………………………………………..…………….6

1.5.Quantitative Imaging FRET (QI-FRET) as a direct dimerization assay………………6

1.6. Significance of RTK measurements in this thesis……………………………………9

1.7.Dissertation Objectives.......... ……………………………………………….......11

Chapter 2.Mechanism of FGF receptor Signal transduction across plasma membrane………………………………………………………………………..12

2.1.Introduction.......... ……………………………………………………………….……13

2.2.Abbreviated Methods.......... …………………………………………………..……14

2.2.1.Materials and Methods.......... ……………………………………………………14

2.2.2.Cell culture and transfection for FRET experiments..16

2.2.3.Production of mammalian plasma membrane vesicles..16

2.2.4.QI-FRET Image Acquisition... 16

2.2.5.Western blots...17

2.2.6.Activation with fgf1 and fgf2. 18

2.3.Results.. 18

2.3.1. Full-length FGF receptors dimerize in the absence of ligand, and unliganded FGFR2 and FGFR3 dimers exist at physiological concentrations. 18

2.3.2.Thermodynamic contributions of FGFR domains to unliganded dimerization... …20

2.3.3.Structural changes in FGFR dimers upon fgf1 and fgf2 binding........................ …21

2.3.4.Structural differences in the fgf1 and fgf2 states correlate with phosphorylation levels.. ...23

2.3.5.Insights from a high-resolution NMR structure of the isolated FGFR3 TM dimer………………………………………………... …24

2.3.6.FGFR3 domain dimer structure in the fgf2 state..…….25

2.3.7.FGFR3 TM domain dimer structure in the fgf1 state.. 26

2.3.8.FGFR3 TM domain dimer structure in the unliganded state.................................. 27

2.3.9.Effect of a pathogenic mutation of FGFR3..28

2.3.10.Correlation between TM dimer structure and receptor phosphorylation... 30

2.4.Discussion... 30

2.4.1.Mechanism of FGFR activation. 30

2.4.2.A unified model of RTK activation...31

2.4.3.Interplay of different FGFR domains in dimerization. 32

2.4.4.Multiple active RTK dimers...33

2.4.5.Phosphorylation is correlated with distance between the TM domains. 34

2.4.6.A new molecular mechanism behind FGFR-linked pathologies..........................34

Chapter 3. Mechanism of VEGFR2 Signal transduction across plasma membrane……..60

3.1.Introduction..61

3.2.Materials and Methods...63

3.2.1.Cell culture and transfection...65

3.2.2.Production of mammalian plasma membrane vesicles.. 66

3.2.3.Treatment with VEGF. 66

3.2.4.QI-FRET Image Acquisition...66

3.2.5.QI-FRET data Analysis: Methodology and Protocol..66

3.2.6.Western blots..67

3.2.7.Cross-linking Experiments. 67

3.3.Results..68

3.3.1.Full-length VEGFR2 dimerizes in the absence of ligand...................................... 68

3.3.2.VEGFR2 is autophosphorylated in the absence of ligand.......................................70

3.3.3.The extracellular domain inhibits VEGFR2 dimerization. The intracellular domain is not required for dimerization but significantly stabilizes VEGFR2 dimers. 71

3.3.4.Bound ligand causes a structural change in the receptor. VEGF-A_{121}, VEGF-A_{165}, VEGF-C and VEGF-D induce similar structural change in the VEGFR2 dimer. 72

3.3.5. The C482R mutation induces ligand-independent constitutive dimerization. The mutant unliganded dimer is similar to liganded wild-type dimers……………………………….. 74

3.3.6.The V769E mutation causes a structural change in the isolated TM domain dimer, but stabilizes the dimer when the EC domain is present. .... ….75

3.3.7.The D7(VEGFR2)→D6(VEGFR1) mutation affects ligand-independent and ligand-dependent dimerization, yet VEGFR2 is capable of binding to $VEGFA_{121}$................... 76

3.4. Discussion……………………………………………………………………......78

Chapter 4. FGFR3 unliganded dimer stabilization by the juxtamembrane domain…....100

4.1. Introduction.. 101

4.2. Experimental Methods……….. 102

4.2.1. Cell culture and transfection..104

4.2.2. Production of mammalian plasma membrane vesicles....................................... 105

4.2.3. Fluorescence Image Acquisition. 105

4.2.4. QI-FRET DATA ANALYSIS IN BRIEF..106

4.3. SECONDARY STRUCTURE PREDICTIONS..108

4.4. RESULTS..109

4.4.1. The substitution of an unstructured linker with the FGFR3 JM domain stabilizes FGFR3 dimers in the absence of ligand. 109

4.4.2. The interplay of FGFR3 domain interactions...111

4.4.3. The $(GGS)_5$ linker does not contribute significantly to dimerization. 112

4.4.4. Tethering the JM domain to the membrane does not lead to stabilizing interactions...113

4.4.5. The interactions between the JM domains occur within the N-terminal part of the JM sequence. 114

4.4.6. FGFR3 JM domain stabilizes the A391E FGFR3 dimer......................................115

4.5. DISCUSSION..116

4.5.1. Goals and findings of this study...116

4.5.2. Experimental approach...116

4.5.3. Comparison with EGFR..117

4.5.4. Implications..118

Chapter 5. Strong inter-molecular disulfide linked dimers caused by mutations of key Cysteines in FGF receptors……………………………………………………….130

5.1.Introduction..131

5.2. Materials and Methods. 132

5.2.1. Cell culture and transfection. 134

5.2.2. Production of mammalian plasma membrane vesicles…………………………..134

5.2.3.QI-FRET Image Acquisition. 134

5.2.4. QI-FRET data Analysis: Methodology and Protocol. 135

5.2.5.Western blots. 135

5.3.Results & Discussion..136

5.3.1.FGFR1 C178S…………………………………………………………………….136

5.3.2.FGFR2 C342R. ……………………..139

5.3.3.FGFR3 C228R. 140

5.4.Conclusion..142

Chapter 6. Analytical characterization of plasma membrane-derived vesicles produced via osmotic and chemical vesiculation…………………………………………………153

6.1.Introduction..153

6.2.Materials and Methods...155

6.2.1.Cell culture and vesiculation. 155

6.2.2.Vesicle lipid pelleting.. 155

6.2.3.Liquid chromatography mass spectrometric (LC-MS) analysis of lipids and cholesterol. 155

6.2.4.Thin layer chromatography. 156

6.2.5.^{31}P NMR phospholipid analysis. 157

6.2.6.Annexin V binding to plasma membrane derived vesicles. 157

6.2.7. Plasmids for vesicle content leakage assays. 157

6.2.8. Western blot analysis of EGFR in A431 vesicles. 158

6.2.9. EGF-Rhodamine binding to EGFR in A431 vesicles. 158

6.3. Results 158

6.3.1. Different methods of vesicle production lead to small, but statistically significant differences in cholesterol and lipid composition. 158

6.3.2. Vesicles bind annexin V, independent of production method. 161

6.3.3. Cytoplasmic proteins are not retained in vesicles produced via osmotic vesiculation. 162

6.3.4. EGFR incorporates very efficiently in chloride salt vesicles, but not in DTT/formaldehyde vesicles..163

6.4. Discussion..164

Chapter 7. Uninduced high yield expression of fluorescent proteins…………….........183

Conclusions..192

References……………………………………..…………………..…………...........196

Curriculum vitae………………………….…………………..………………...169

List of Abbreviations

BSA	Bovine serum albumin
CHO	Chinese Hamster Ovary
C-terminus	Carboxy-terminus, C-terminal tail, or COOH-terminus
DTT	Dithiothreitol
E.coli	Escherichia coli
ECD	Extracellular domain
EGFR	Epidermal Growth Factor receptor
FRET	Förster Resonance Energy Transfer
Flk-1	Fetal liver kinase-1 = VEGFR-2=KDR
FGF	Fibroblast Growth Factor
FGFR	Fibroblast Growth Factor Receptor
HEK 293T	Human Embryonic Kidneys 293T
I-FRET	Intrinsic FRET=$\tilde{E}$
JMD	Intracellular juxtamembrane domain
KDR	Kinase Insert Domain Receptor
mCherry	monomeric Cherry
MUT	Mutant
N-terminus	Amino-terminus or NH_2-terminus
NRP	Neuropilins
PCR	Polymerase chain reaction
PLC-γ	Phospholipase C gamma

PLC-δ	Phospholipase C delta
PKC	Protein kinase C
QI-FRET	Quantitative Imaging FRET
RTK	Receptor Tyrosine Kinase
TK	Tyrosine kinase
TMD	Transmembrane domain
VEGF	Vascular Endothelial Growth factor
VEGFR	Vascular Endothelial Growth factor receptor
WT	Wild type
YFP	Yellow Fluorescent Protein

List of Tables

Table 2-1. Parameters describing FGFR unliganded dimerization……………………..35

Table 2-2. Intrinsic FRET efficiencies $\tilde{E}$, measured in the presence of saturating fgf1 and fgf2 concentrations for the truncated EC+TM FGFR constructs………………………..36

Table S1 (2-3). Intrinsic FRET, measured for the full-length receptors in the absence and presence of ligand…………………………………………………………………..47

Table 3-1. Dimerization free energies (dimer stabilities) ΔG and Intrinsic FRET efficiencies $\tilde{E}$. FRET data for full-length and truncated constructs that lack the IC domain (EC+TM) and both EC and IC (TM only)……………………………………...84

Table 4-1. Dimer stabilities and Intrinsic FRET for the proteins containing the juxtamembrane domain…………………………………………………………………120

Table 5-1. Dimerization free energies (dimer stabilities) ΔG and Intrinsic FRET efficiencies $\tilde{E}$. FRET data for wild type and mutant full-length and truncated FGFR constructs that lack the IC domain (EC+TM). The mutations are Cystein mutations…………………………………………………………………………..145

List of Figures

Figure 1. Schematic diagram of Fibroblast growth factor receptor and Vascular endothelial growth factor receptor 2 (VEGFR2) and ligands……………………….…3

Figure 2-1. (A) Measured FRET as a function of receptor concentration, for the three full-length receptors. Every data point represents a single vesicle (B) The donor concentration………..…………………………………………………………………37

Figure 2-2. Dimerization curves for the full-length receptors and truncated FGFRs. …………………………………………………………………………………………38

Figure 2-3. FRET and Western blot results for wild-type FGFR1, FGFR2, and FGFR3. ……………………………………………………………………………………...39

Figure 2- 4. Insights into the fgf1-bound and fgf2-bound FGFR3 dimer structures in the plasma membrane ……………………………………………………………….....41

Figure 2-5. The unliganded FGFR3 dimer structure, based on mutagenesis, guided by the high resolution structure of the isolated FGFR3 TM domain in micelles………………43

Figure 2-6. Effect of the pathogenic A391E FGFR3 mutation on dimer structures in the fgf1 and fgf2 states. …………………………………………………………………45

Figure 2-7. Correlation between Intrinsic FRET and phosphorylation, for FGFR3 and the three studied FGFR3 mutants. Only results for constitutive dimer are included. ……………………………………………………………………………………….46

Figure S1(2-8). The plasmid constructs used in the FRET experiments.………………48

Figure S2(2-9). The plasmid constructs used in Western blot experiments. …………..49

Figure S3(2-10). One vesicle, imaged in the FRET, acceptor, and donor channels. ……………………………………………………………………………………….50

Figure S4(2-11). Relative phosphorylation of mature FGFR1 in the absence of ligand, as a function of FGFR1 expression. ……………………………………………………….51

Figure S5(2-12). FRET efficiencies, donor concentrations and acceptor concentrations, measured for the wild-type EC+TM FGF receptors. ……………………………………52

Figure S6(2-13). Phosphorylation of FGFR1, FGFR2, and FGFR3, characterized via Western blotting. ……………………………………………………………………...53

Figure S7(2-14). FGFR3 TM domain structure in micelles, solved by NMR …………..54

Figure S8(2-15). FRET data for the EC+TM FGFR3 (L377I-G380I-A391I) mutant…...55

Figure S9(2-16). FRET data for the EC+TM FGFR3 (A374I-G375I-S378I) mutant. ….55

Figure S10(2-17).Phosphorylation of the L377I-G380I-A391I and A374I-G375I-S378I mutants, characterized via Western blotting. ……………………………………………56

Figure S11(2-18). FRET data for the A391E EC+TM FGFR3 mutant. ………………...57

Figure S12(2-19). Phosphorylation of the pathogenic A391E mutant, characterized via Western blotting. ……………………………………………………………………...57

Figure S13(2-20). Relative phosphorylation of wild-type FGFR3 and the FGFR3 mutants studied here, in the presence of saturating fgf2 concentrations. ………………………...59

Figure 3-1. FRET data describing VEGFR2 dimerization. ……………………………..82

Figure 3-2. VEGFR2 cross-linking and phosphorylation in CHO cells. ………………..85

Figure 3-3. CHO, HEK293T and MEC (microvascular endothelial) cells stained for VEGF-A. ……………………………………………………………………………...87

Figure 3-4. FRET efficiency measured as a function of acceptor concentration for EC+TM VEGFR2, in the absence of ligand and in the presence of VEGF-A121, VEGFA-165, VEGF C or VEGF D. …………………………..……………………………………..88

Figure 3-5. The model of VEGFR2 dimerization and activation based on our experiments. ……………………………………………………………………………..90

Figure 3-6. FRET data comparing the dimerization of wild-type in the absence of ligand the C482R mutant in the absence of ligand and the C482R mutant in the presence of ligand ………………………………………………………………………………….91

Figure 3-7. Results for the V769E mutant. ……………………………………………...92

Figure 3-8. FRET efficiency plotted as a function of acceptor concentration for WT EC+TM and D7→D6 ECTM VEGFR2. ……………………………………………….94

Figure 3-9. FRET efficiency plotted as a function of acceptor concentration for WT EC+TM and D4→D5 ECTM VEGFR2………………………………………………….96

Figure 3-10. Our proposed dimerization model for VEGFR……………………………97

Figure S1(3-11). The constructs used in the FRET experiments. ………………………98

Figure S2(3-12). The plasmid construct used for western blotting measurements. …….99

Figure 3-13reduced SDS PAGE and Non-reduced SDS PAGE for WT and C482R VEGFR2 followed by western blot staining. ……………………………………………99

Figure 4-1. The plasmid constructs used in the FRET experiments. …………………..121

Figure 4-2. A vesicle, imaged and analyzed in the FRET, acceptor, and donor channels. Images were acquired with a Nikon laser scanning confocal microscope. ……………123

Figure 4-3. Dimerization curves for EC-TM-$(GGS)_5$-YFP/mCherry and EC-TM-JM-YFP/mCherry. The dimer that contains the JM domain is more stable………………...124

Figure 4-4. Dimerization curves for TM-$(GGS)_5$-YFP/mCherry and TM-JM-YFP/mCherry…...………………………………………………...………………124

Figure 4-5. Dimerization curves for three Glycophorin A TM helix constructs in which the fluorescent proteins are attached to the TM helix via different length linkers……………………………………………………… ……………………..125

Figure 4-6. Dimerization curves for GpA-$(GGS)_5$-YFP/mCherry and GpA-(GGS)2-JM-YFP/mCherry. …………………………………………………………………….125

Figure 4-7. Dimerization curves for EC-TM-$(GGS)_5$-YFP/mCherry and EC-TM-JM_{60}-YFP/mCherry. …………………………………………………………………….126

Figure 4-8. Dimerization curves for and EC-TMA391E-$(GGS)_5$-YFP/mCherry and EC-TMA391E-JM_{60}-YFP/mCherry. ……………………………………………………….126

Figure S1(4-9)…………………………………………………………………..127

Figure S2(4-10)…………………………………………………………………127

Figure S3(4-11)…………………………………………………………………128

Figure S4(4-12)…………………………………………………………………128

Figure S5(4-13)…………………………………………………………………129

Figure S6(4-14)…………………………………………………………………129

Figure 5-1. Schematic of FGF receptor structure and location of the three mutations investigated ……………………………………………………………………….142

Figure 5-2. FRET results for wild type FGFR1and C178S FGFR1 …………………..143

Figure 5-3. Anti-FGFR1 staining of non-reducing and reducing western blots for wild type and C178S FGFR1. ……………………………………………………………….144

Figure 5-4. FRET results for wild type FGFR2 and C342R FGFR2…………………...146

Figure 5-5. Anti-FGFR2 staining of non-reducing western blots for wild type and C342R FGFR2. ………………………………………………………………………………...147

Figure 5-6. FRET results for wild type FGFR3 and C228R FGFR3 ………………..…148

Figure 5-7. Anti-FGFR3 staining of non-reducing and reducing western blots for wild type and C228R FGFR3 in HEK293T cells. ………………………………………..149

Figure S1(5-8). Plasmid constructs used for the FRET experiments. ………………….150

Figure S2(5-9). Plasmid constructs used for the Western blot experiments. ………..…151

Figure 6-1. Cholesterol and lipid composition of A431 chloride salt vesicles, A431 DTT/formaldehyde vesicles, and CHO DTT/formaldehyde vesicles, determined by LC-MS. ……………………………………………………………………………………..165

Figure 6-2. Lipid composition of A431 chloride salt vesicles, A431 DTT/formaldehyde vesicles, and CHO DTT/formaldehyde vesicles, calculated by re-scaling the LC-MS data shown in Figure 6-1. ……………………………………………………………...167

Figure 6-3. Phospholipid content of the vesicles, from ^{31}P NMR experiments ………..168

Figure 6-4. Annexin V binding to A431 chloride salt vesicles, A431 DTT/formaldehyde vesicles, and CHO DTT/formaldehyde vesicles. ………………………………………169

Figure 6-5. Chinese Hamster Ovary (CHO) expressing Grb2-Venus (MW ~ 60 kDa) and FGFR2-mCherry. ……………………………………………………………………170

Figure 6-6. Top panel: CHO cells expressing Plcɣ-GFP and FGFR2-mCherry. Bottom panel: Plcɣ-GFP (MW ~ 210 kDa) is not retained in CHO chloride salt vesicles.……………………………………………………………………………171

Figure 6-7. Western blots staining for endogenous Epidermal Growth Factor Receptor (EGFR) in A431 vesicles. ……………………………………………………………..172

Figure 6-8. EGF-Rhodamine binding to A431 vesicles. Left: A341 chloride salt vesicles; Right: A431 DTT/formaldehyde vesicles……………………………………………172

Figure S1(6-9). High Performance Liquid Chromatography Mass Spectrometry (LC-MS) results for A431 chloride salt vesicles, A431 DTT/formaldehyde vesicles, and CHO DTT/formaldehyde vesicles. ………………………………………………………...…173

Figure S2(6-10). Thin-layer chromatogram of lipid extracts from different vesicle preparations. ………………………………………………………………………...174

Figure S3(6-11). ^{31}P NMR spectra (acquired by Avanti Polar Lipids Analytical Services) for (A) A431 chloride salt vesicles sample and (B) A431 DTT/formaldehyde vesicle sample. ………………………………………………………………………………176

Figure S4(6-12). CHO cells expressing the soluble cytoplasmic proteins used in the leakage assays: …………………………………………………………………………177

Figure S5(6-13). Top panel: Chinese Hamster Ovary (CHO) cells co-expressing FGFR2-mCherry and Plcδ1-PH-GFP. ……………………………………………………….178

Figure S6(6-14). CHO cells co-expressing PKCϴ-GFP and FGFR2-mCherry.…….…179

Figure S7(6-15). Top panel: Chinese Hamster Ovary (CHO) co-expressing VVVVVV (Venus x 6) and FGFR2-mCherry. ……………………………………………………180

Figure S8(6-16). CHO cells co-expressing Intersectin II-GFP and FGFR2-mCherry……………………………………………………………………………...181

Figure 7-1. Protocols for fluorescent protein expression *in E. coli*. …………………..188

Figure 7-2. The mCherry pellet……………………………………………………..189

Figure 7-3. Purified stocks of fluorescent proteins in phosphate saline buffer. From left to right: mCherry, mTurquoise, YFP and GFP2 solutions. ………………………………189

Figure 7-4. Excitation and emission spectra of the produced fluorescent proteins: YFP, mCherry, GFP2 and mTurquoise.. ……………………………………………......190

1. Literature review

1. 1.The plasma membrane. The cell plasma membrane is a bilayer consisting of lipids (phospholipids and glycolipids), cholesterol, and proteins in the form of integral and peripheral membrane proteins, channels and transporters. The plasma membrane of mammals contains five major phospholipids; phosphatidylcholine, phosphatidylethanolamine, phosphatidylserine, phosphatidylinositol and sphingomyelin. The lipid bilayer is critical for membrane protein function. It also imposes a barrier which prevents the passage of ions and water-soluble molecules through the plasma membrane (136, 137).

1.2. Membrane proteins. An estimated 30-40% of mammalian cellular proteins are membrane proteins. Proteins are responsible for carrying out specific functions. According to the fluid mosaic model of the plasma membrane (137), membrane proteins are categorized into two classes: peripheral and integral. Peripheral membrane proteins may dissociate from the membrane without disruption of the lipid bilayer. However, integral membrane proteins are stably inserted into the bilayer. Most of the integral membrane proteins are transmembrane proteins. Examples are the 58 Receptors Tyrosine Kinases, and Glycophorin, the integral membrane protein of the red blood cells. In mammalian cells, transmembrane proteins span the lipid bilayer as α-helices of 20-27 hydrophobic amino acids. The structures of many transmembrane proteins are unknown, as they cannot be overexpressed and crystallized. Thus, a variety of other biochemical and biophysical methods have been developed over the past few decades to decipher the structural and functional properties of these proteins. Yet, many questions about the function of membrane proteins remain unanswered.

1.3. Receptor Tyrosine Kinases (RTKs). RTKs, first discovered in 1980s, comprise a superfamily of 58 single pass transmembrane proteins which are subclassified into 20 families. RTKs are essential for many aspects of cell life including proliferation, metabolism, migration, differentiation and survival (7, 39, 76, 126). All the receptors possess a single pass transmembrane domain (TMD), ligand binding extracellular domain (ECD), intracellular juxtamembrane domain (JMD), tyrosine kinase domain (TKD) and a C-terminus tail (Figure 1). The complex RTK signaling output results from receptor dimerization in the two dimensional plane of the plasma membrane. However the mechanistic principles and the propensity of receptor dimerization and activation are only minimally/partially understood. It is now known that dysregulated RTK signaling results in pathologies. RTKs are implicated in initiation and progression of many forms of cancers and skeletal disorders either through point mutations or receptor and or ligand overexpression (7). Numerous approved therapeutics target various domains of these proteins with the goal of inhibition of malignant signaling pathways.

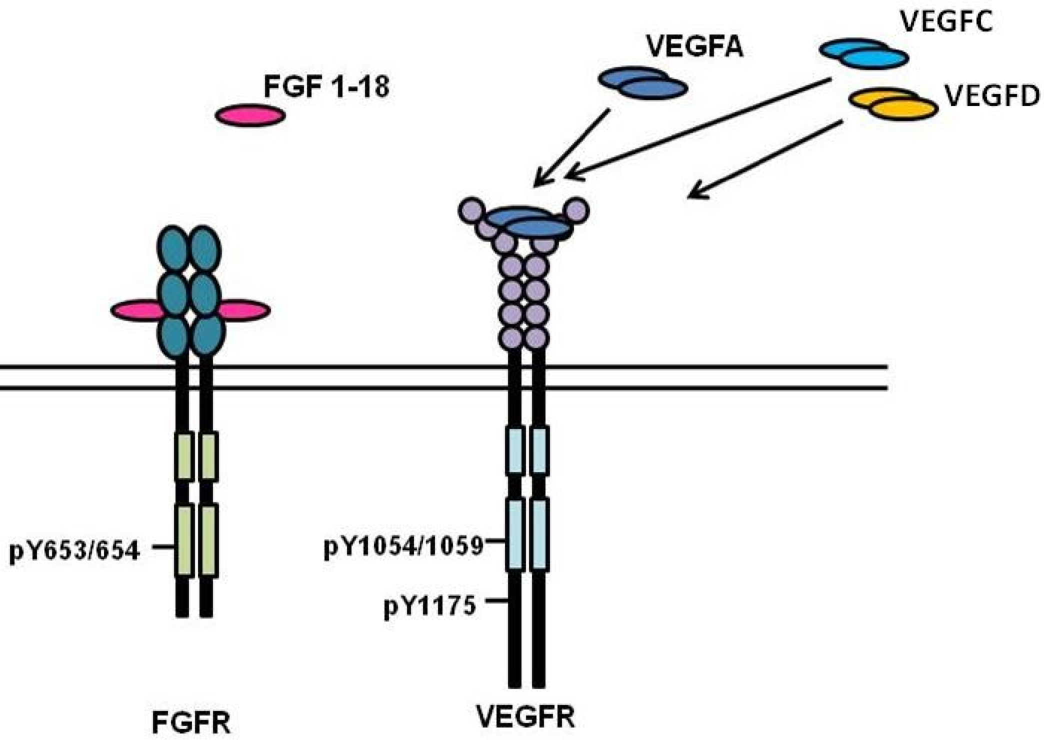

Figure 1. Schematic diagram of Fibroblast growth factor receptor and Vascular endothelial growth factor receptor 2 (VEGFR2) and ligands.

1.3.1 Fibroblast Growth Factor Receptors (FGFRs). FGFR1, FGFR2, FGFR3 and FGFR4 are involved in embryonic and adult skeletal development. The FGFR extracellular domain consists of three Immunoglobulin like (Ig-like) domains, D1, D2 and D3 with ~ 9-20 amino acid linker regions in between the domains. 18 ligands (FGFs) bind to and activate FGFR family members. Human fgfs are 150-300 amino acids long and share 30-60% sequence identity. Human fgfs play diverse functions throughout embryonic and adult development (29, 30, 40, 145). In adults fgfs play critical roles in tissue homeostasis, wound healing and angiogenesis (32, 62). Binding of fgfs to FGFRs stabilizes FGFR dimers and is hypothesized (but not proven) to induce a structural change of the receptor leading to phosphorylation of key tyrosine residues (including tyrosines located in the activation loop). As many as 20 isoforms in some cases have been identified for the FGF receptors. The isoforms are mainly either different at their D3-Ig like domain or the length of their C-terminus tail due to alternative splicing. Crystal structures of FGF receptor ectodomains have revealed that Domain 2 and 3 (D2-D3) and the linker in between are indispensible for ligand (fgf) binding to the receptor (115). The mode of ligand binding to FGFRs is bivalent, with two fgfs and two heparin sulphate proteoglycans (HSPG) forming a complex with two fgf receptors (128). Moreover structural studies have revealed that the two receptors contact each other and HSPG molecules at D2. Domain 1 (D1) and the acid box region of FGFRs has been shown to play an autoinhibitory role in FGFR ligand induced dimerization (47, 68, 97). FGF receptors have been the subject of intense crystallographic studies; however questions remain unanswered regarding the unliganded dimerization of these receptors, the role of the intracellular domain in FGFR dimerization and the role of various fgfs in receptors dimerization and activation.

FGF/FGFR signaling is involved in an array of biological events inside the cell, however the origins of biological specificity largely remain unknown. FGF/FGFR signaling is a major therapeutic target, but only a few strategies have shown promise. Thus, elucidating the exact biophysical/biochemical mechanism of FGFR dimerization and activation will greatly enhance the drug design for these receptors. In Chapter 1, we study the ligand independent and ligand dependent homodimerization of FGFR1, FGFR2 and FGFR3. We investigat the role of various domains in FGFR dimerization. Finally we study the effect of pathogenic mutations in TMD and ECD of FGFRs on receptor dimerization and activation.

1.3.2 Vascular Endothelial Growth Factor Receptors (VEGFRs). VEGFRs play a crucial role in the development of the blood and lymphatic vessels. VEGF ligands (VEGFA/B/C/D and PlGF) selectively bind to and activate VEGFRs on endothelial cells. Upon ligand binding, VEGFR 1, 2 and 3 are activated by trans-phosphorylation of the tyrosines located in the kinase domain and C-terminus tail of these receptors. This regulates the formation, growth and stabilization of blood vessels in cancer, diabetes and cardiovascular disorders.

The VEGF receptor extracellular domain is large and consists of seven Ig-like domains (D1-D7). Crystal structures of VEGFR2 extracellular domain in the presence of VEGF have revealed that ligand binds between D2 and D3 (78). Further biophysical and biochemical studies have shown that receptor contacts exist between D4 domains (D4-D4) and D7 domains (D7-D7) in the liganded receptor structure (65, 120). However, the contribution of these contacts to receptor stability remains unknown. VEGFR dimerization in the presence and absence of ligands is poorly quantified. It is only known that the three VEGF receptors (VEGFR1/FLT1, VEGFR2/FLK1/KDR & VEGFR3/FLT4) homo- and heterodimerize in the presence of ligands such as VEGFA/B/C/D and PlGF. The receptors are also known to form complexes with the VEGF co-receptors (Neuropilins). However, all the possible homo- and heterodimer complexes and their interaction propensities are uncharacterized. In particular, there are no studies of VEGFR homo-dimerization and activation in the presence and absence of ligands. There are no structures for full length VEGFR dimers and the existance of VEGFR unliganded dimers has not been addressed by research in the field so far. In this dissertation, we have investigated these questions for VEGFR2, the major receptor involved in angiogenesis. In Chapter 2, we study the ligand independent and ligand dependent homodimerization of VEGFR2, the role of various domains in receptor dimerization, and the effect of various VEGFs on receptor dimerization and structure. We also study the effect of four mutations on VEGFR2 dimerization and activation.

1.4. A Physical-chemical model for FGFR and VEGFR dimerization and activation.

RTKs transduce signals via lateral dimerization in the plane of the plasma membrane. We used a thermodynamic description of receptor dimerization where receptors exist in a monomer-dimer equilibrium in the absence of ligands. When ligand binds, the unliganded dimers are converted to liganded dimers with different structure. The total receptor concentration is [T]=2[d]+[M]. The dimerization constant (k) is defined for the following model as:

$$M + M \xrightarrow{k} d \tag{1}$$

$$k = \frac{[d]}{[M]^2} \tag{2}$$

1.5. Quantitative Imaging FRET (QI-FRET) as a direct dimerization assay.

Förster resonance energy transfer (FRET) occurs as a result of non-radiative energy transfer between a donor fluorophore and an acceptor fluorophore (44). The requirement for successful FRET is for the emission spectrum of the donor fluorophore to overlap with the excitation spectrum of the acceptor. When the donor and acceptor are at a close distance, excitation of the donor results in emission of the acceptor.

The QI-FRET method has been described previously (22, 23), but it applied here for the first time to full-length RTKs. Soluble YFP and mCherry were produced in *E.coli* and were purified as described previously and in chapter 6 (125). Purified solutions of YFP and mCherry of known concentration were imaged in the donor, FRET and acceptor scans, to obtain the calibration constants for the donor and the acceptor, i_D and i_A, as well the bleed-through coefficients for the donor and the acceptor, β_D and β_A (81). A soluble linked YFP-mCherry protein was also imaged in the three channels to obtain the gauge factor G_F as described by Li et al (81).

Each vesicle co-expressing FGFR-YFP and FGFR-mCherry was imaged in the donor, acceptor and FRET channels (Figure S3). The fluorescence intensities across the plasma membrane, I_D, I_{FRET}, and $I_{A,}$ in the three channels, were determined as described in detail elsewhere (22). The acceptor concentration in each vesicle, C_A, was calculated according to (22):

$$C_A = \frac{I_A}{i_A} \tag{3}$$

The sensitized emission of the acceptor in each vesicle was determined as (81):

$$I_{SEN} = I_{FRET} - \beta_A I_A - \beta_D I_D \tag{4}$$

The donor intensity in the absence of the acceptor $I_{D,corr}$, and the donor concentrations (C_D) were calculated as:

$$I_{D,corr} = I_D + G_F I_{SEN} \tag{5}$$

$$C_D = \frac{I_{D,corr}}{i_D} \tag{6}$$

From equations (1) and (4), the total concentration, T, and the acceptor fraction, x_A, are calculated according to:

$$T = C_A + C_D \tag{7}$$

$$x_A = \frac{C_A}{C_A + C_D} \tag{8}$$

The FRET efficiency, E, was calculated using eq.6:

$$E = 1 - \frac{I_D}{I_{D,corr}} \tag{9}$$

The FRET efficiency was corrected for the so-called "proximity FRET" contribution which describes the close approach of donors and acceptors (within distances of 100 Å or so) in the membrane without specific interactions (70, 140, 163). The dimeric fraction is determined from the corrected FRET efficiency according to:

$$f_D = \frac{E}{x_A \widetilde{E}} \tag{10}$$

The constant $\widetilde{E}$ in equation (8) is the "Intrinsic FRET", the FRET efficiency in a dimer containing a donor and an acceptor. This is a structural parameter, a constant for each receptor dimer, which depends only on the separation and the orientation of the two fluorescent proteins in the dimer, not on the dimerization propensity.

$$E = \frac{1}{1 + (\frac{r}{R_0})^6} \tag{11}$$

x_A is the acceptor fraction. Where R_0 represents the Förster radius.

Based on the law of mass action, the dimeric fraction can be written as a function of the total receptor concentration, *T*, and the dimerization constant *K* according to equation 9:

$$f_D = \frac{1}{T}\left(T - \frac{1}{4K}\left(\sqrt{1+8TK} - 1\right)\right) \qquad (12)$$

Equations (10) and (11) are used to fit the dimerization model to the data while optimizing for two adjustable parameters: the dimerization constant *K*, and the intrinsic FRET, $\tilde{E}$.

The free energy of dimerization is calculated according to:

$$\Delta G = -RT\ln(K) \qquad (13)$$

with the standard state defined as 1 receptor/nm^2. The dissociation constant is 1/K, and is reported in units of μm^{-2} in Table 1.

In the case of 100% dimers ($f_D = 1$), equation (10) can be re-written as:

$$\tilde{E} = \frac{E}{x_A} \qquad (14)$$

Thus, measurements of E and x_A for each vesicle in this case allows us to directly determine the value of the Intrinsic FRET, $\tilde{E}$, in each vesicle. Histograms of the measured $\tilde{E}$ are shown throughout the manuscript, such as in Figure 3 in Chapter 1, for example.

1.6. Significance of RTK measurements in this thesis.

The work presented in this thesis provides the first thermodynamic measurements of intact RTKs in plasma membrane derived from mammalian cells. FGFR1, FGFR2, FGFR3, and VEGFR2 were characterized here. Prior to this work, intact RTK thermodynamics and ligand induced structural studies have not been possible in native mammalian membranes. The QI-FRET method, which was utilizaed here in conjuction with plasma membrane derived vesicles, makes biophysical characterization of RTKs possible.

The achievements in this thesis are as follows:

We quantified sequence specific interactions of four different RTKs, and a number of mutants in the plasma membrane over a wide range of concentrations, using RTKs tagged with fluorophores. These donor and acceptor concentrations were determined along with FRET efficiency in order to obtain the donor to acceptor ratio and the total concentrations, dimeric fractions, intrinsic FRET (a structural parameter) and free energy of dimerization. This is the first measurement of the thermodynamics of RTK dimerization.

We extensively characterized the plasma membrane-derived vesicles in terms of their phospholipid content and their utility for study of RTK interactions. Transient transfection in cell based FRET invesitigations results in a large numbers of misfolded fluorescent receptors in inner compartments of mammalian cells. This fluorescence interferes with plasma membrane measurements. Hence, vesicles are ideal for fluorescence based biophysical characterization studies as they are native like and lack cytoplasmic content. Additionaly, using plasma membrane-derived vesicles allowed us to bypass the need for receptor reconstitution in synthetic vesicles. Reconstitution of full lenght RTKs has proved to be extremely challengining and results in improper orientation of the receptors inserted in the bilayer.

All the measrurements performed here accounted for and corrected for proximity FRET or stochastic FRET, which has been previousely verified experimentally. This is in contrasct to previous studies performed in intact cellular membranes, which do not distinguish beween stochastic and sequence specific FRET for membrane protein interactions.

1.7. Dissertation Objectives.

The major objective of this thesis project is to enhance our understanding of RTK function by employing novel FRET-based experimental methods. These methods yield quantitative information about RTK interaction propensities and allow us to monitor structural changes that occur due to ligand binding or due to pathogenic mutations. With this novel methodology, here we investigate if FGF and VEGF receptors can form dimers in the absence of ligand. We study the thermodynamic contributions of the different FGFR and VEGFR domains to dimerization. We investigate the effect of pathogenic mutations on receptor interactions and structure. We characterize the response of the unliganded dimers to ligand binding. The FRET-based measurements are supplemented with biochemical activity assays, to establish a link between RTK dimer stability, RTK dimer structure, and function.

The interactions between the receptors are studied in plasma membrane derived vesicles. Such vesicles are beginning to be used in biophysical research, but have not been characterized thus far. A second objective of this dissertation, therefore, is their characterization. A third objective is to optimize the production of fluorescent proteins, as they are used as calibration standards in the FRET dimerization studies.

Chapter 2. Mechanism of FGFR signal transduction across the plasma membrane

Abstract

Here we demonstrate that the FGF receptors form dimers in the absence of ligand at physiological concentrations, and that the unliganded dimers are phosphorylated. We further demonstrate that the unliganded FGFR dimers undergo structural changes upon ligand binding, The structural changes in response to fgf1 and fgf2 binding are very different, resulting in different phosphorylation of the fgf1 and fgf2-bound dimers. Thus, there exist multiple active ligand-bound states for the FGF receptors. We further show that, upon fgf1 binding, the TM domains in the FGFR3 dimer engage in helix-helix interactions that involve GxxxG-like motifs. Binding of fgf2, however, results in a very different TM structure which is closely packed. This structure ensures the smallest separation between the TM domains and the highest possible FGFR3 phosphorylation, a conclusion which is supported by a strong correlation between TM domain dimer structure and kinase phosphorylation, for wild-type FGFR3 and three FGFR3 mutants. Furthermore, we show that the pathogenic A391E mutation emulates the structural effects of fgf2, trapping FGFR3 in its most active state. This study reveals unexpectedly high structural plasticity of the FGF receptor dimer structure, which enables different biological responses to different ligands. It also uncovers a novel molecular mecahnsim through which FGFR-linked pathologies can arise.

Keywords: Receptor tyrosine kinases, dimerization, intracellular domain, dimer stability

2.1. Introduction

The fibroblast growth factor receptor (FGFR) family includes four receptors that bind 18 ligands called fibroblast growth factors, using heparin as a co-factor (37, 104, 105, 162). The FGF receptors are single-pass membrane proteins, with N-terminal extracellular (EC) domains consisting of three imminoglobulin-like subdomains (D1, D2, and D3), a transmembrane (TM) domain, and an intracellular (IC) domain with tyrosine kinase activity (39, 74, 85). FGFRs transduce biochemical signals via lateral dimerization in the plasma membrane. Although not sufficient, receptor dimerization is required for activation, as it brings the two catalytic domains in close proximity, allowing them to cross-phosphorylate each other on tyrosines in the activation loop (37, 127). This process activates the kinases, which now bind adaptor proteins and phosphorylate cytoplasmic substrates, thus triggering downstream signaling cascades that control cell growth and differentiation (95, 141, 142). The FGF receptors play important roles in all cell types, but are most well known for the critical role that they play in the development of the skeletal system (35). Their many pathogenic mutations are linked to skeletal, cranial, and other developmental abnormalities (74, 151, 161, 162).

Research over the last decade has brought substantial progress in our understanding of FGFR activation, fueled by high resolution structures of isolated FGFR domains (47, 96-98, 102, 115). Yet, while the general principles of FGFR activation are now known, mechanistic knowledge of how the signal is transmitted from the extracellular domains in response to ligand binding to the kinases in the FGFR dimers is incomplete, despite very active research in the field. To gain insight into the process, here we study the dimerization of FGFR1, FGFR2, and FGFR3, as well as the response of these receptors to the ligands fgf1 and fgf2.

2.2. ABREVIATED METHODS

Experiments were performed with CHO cells, cultured as described below. For the FRET experiments, the receptors were tagged with YFP and mCherry on their C-termini. Vesicles were produced from CHO cells using an osmotic stress buffer as previously described (33, 123). Vesicles containing donor and acceptor-labeled receptors were imaged in the confocal microscope, and analyzed with the QI-FRET method, described as a step-by-step protocol in reference (22). The FRET efficiency, the donor concentration and the acceptor concentration were determined using equations (1) through (7) in Supplementary Material. The dimeric fraction, the dimerization constant and the Intrinsic FRET were calculated as decribed in Supplementary Materials, following equations (7) through (10). In the case of 100% dimeric receptors, the experiments yield directy the Intrinsic FRET in each vesicle (see equation 11 in Supplementary Material). Phosphorylation was studied using Western blotting, following protocols given in previous publications (54, 56, 57, 59).

2.2.1. Materials and Methods

The YFP plasmid was received from Dr. M. Betenbaugh (Johns Hopkins University, Baltimore, MD) and the pRSET-mCherry plasmid was obtained from Dr. R.Tsien (University of California, San Diego). The plasmids encoding human wild-type FGFR1 and FGFR2 in the pRK5 vector were received from Dr.M.Mohammadi, NYU. The plasmid encoding human wild-type FGFR3 in the pcDNA3.1(+) vector was a gift from Dr. D. J. Donoghue, UCSD. All primers were purchased from Invitrogen.

For this work, the full length FGFR1 and FGFR2 genes were cloned into the pcDNA 3.1(+) vector. To accomplish this, the genes were first amplified using Polymerase Chain Reaction (PCR) and then each gene was double digested using Hind III and XhoI restriction enzymes and ligated into the pcDNA3.1(+) vector. YFP or mCherry genes were subsequently fused to the C-terminal tail of each receptor via a 3 amino acid (GGS) linker (Figure S1) between the XhoI and XbaI restriction sites in the vector.

Details about the cloning of FGFR3 EC-TM-$(GGS)_5$-YFP and FGFR3 EC-TM-$(GGS)_5$-mCherry into the pcDNA 3.1(+) vector are given elsewhere (Chen et al 2010). For this work, the sequences encoding for the EC and TM domains of FGFR1 and FGFR2 were amplified by PCR, double digested using HindIII and EcoRI restriction enzymes and inserted in place of the FGFR3 EC-TM gene in the FGFR3 EC-TM-$(GGS)_5$-YFP and FGFR3 EC-TM-$(GGS)_5$-mCherry plasmid constructs, to produce the FGFR1 EC-TM-$(GGS)_5$-YFP, FGFR1 EC-TM-$(GGS)_5$-mCherry, FGFR2 EC-TM-$(GGS)_5$-YFP, and FGFR2 EC-TM-$(GGS)_5$-mCherry plasmids.

All the mutant full length FGFR3 constructs were created from the wild-type using QuickChange ® II XL Site-Directed Mutagenesis Kit (Stratagene, CA). These constructs are shown in Figure S2, and are used in the Western blotting experiments.

The A374I-G375I-S378I EC+TM FGFR3 mutant and the L377I-G380I-A391 EC+TM FGFR3 mutant used in the FRET studies were generated from the full-length mutants. The complementary DNA (cDNA) encoding the EC and mutant TM domains was amplified using PCR and was double digested with HindIII and EcoRI. The FGFR2 EC-

TM-$(GGS)_5$-YFP and FGFR2 EC-TM-$(GGS)_5$-mCherry plasmid constructs were also double digested with HindIII and EcoRI enzymes, and ligated with the PCR products.

2.2.2. Cell culture and transfection for FRET experiments

Chinese Hamster Ovary cell (CHO) cells were cultures at 37 ˚C with 5% CO_2 for 24h. Transfection was carried out using Fugene HD transfection reagent (Roche Applied Science), following the manufacturer's protocol. Cells were co-transfected with 3-7 ug of DNA encoding receptors tagged with either YFP or mCherry.

2.2.3. Production of mammalian plasma membrane vesicles

Vesiculation was performed using a chloride salt vesiculation buffer consisting of 200 mM NaCl, 5 mM KCl, 0.5 mM $MgSO_4$, 0.75 mM $CaCl_2$, 100 mM bicine and protease inhibitor cocktail (Complete mini EDTA-free tabs, Roche Applied Science) adjusted to PH of 8.5 (33). CHO cells were rinsed twice with 30% PBS (pH 7.4), and incubated with 1 mL of chloride salt vesiculation buffer overnight at 37 °C. A large number of vesicles were produced after 12 h, and the vesicles were transferred into 4-well Nunc Lab-Tek II chambered coverslips for imaging. Images of vesicles with labeled FGF receptors are shown in Figure S3. Most of the cytoplasm in the vesicles is lost during vesicle production, as attested by the fact that soluble proteins of molecular weight up to 200 kDa are not retained inside the vesicles (paper in preparation).

2.2.4. QI-FRET Image Acquisition

Vesicles were imaged using a Nikon Eclipse confocal laser scanning microscope using a 60× water immersion objective. All the images were collected and stored at a 512 × 512 resolution. Three different scans were performed for each vesicle: (1) excitation at 488 nm, with a 500-530 nm emission filter (donor scan); (2) excitation at 488 nm, with a 565-615 nm emission filter (FRET scan); and (3) excitation at 543 nm, with a 650 nm longpass filter (acceptor scan). Gains of 8.0 were used for all the three scans. The bleaching of the fluorescent proteins was minimized through the use of ND8 filters when excitating with the 488 nm laser, and low pixel dwell time (1.68 μs).

2.2.5. Western blots

CHO cells were cultured in serum-free medium for 24 h following transfection and then treated with lysis buffer (25 mM Tris-HCl, 0.5% Triton X-100, 20mM NaCl, 2 mM EDTA, phosphatase inhibitor and protease inhibitor, Roche Applied Science). Lysates were collected following centrifugation at 15,000 g for 15 min at 4 °C and loaded onto 3–8%NuPAGE®Novex®Tris–Acetatemini gels (Invitrogen, CA). The proteins were transferred onto a nitrocellulose membrane, and blocked using 5% milk in TBS. FGFR total protein levels were assessed using antibodies against FGFR3 (H-100; sc-9007), FGFR2 (H-80; sc-20735) and FGFR1 (H-76; sc-7945) from Santa Cruz Biotechnology. The phosphorylation of the tyrosines in the activation loop of the FGFR kinases was assessed using specific anti-phospho-Tyr antibodies (Tyr653/654; #3471, Cell Signaling Technologies). These antibodies are raised against Tyr653/654 in the activation loop of FGFR1, but are reactive to all FGFR receptors because of their identical activation loop sequences. Anti-phospho-Tyr766 (1E5); (#2544; Cell Signaling Technology) was used to asses FGFR1 phosphorylation at Tyr766. Anti-phospho-Tyr724 (sc-33041; Santa Cruz Biotechnology) was used to detect the phosphorylation of Tyr724 in FGFR3. These antibodies were then followed by anti-rabbit HRP conjugated antibodies (W4011, Promega). The proteins were detected using the Amersham ECL detection system (GE Healthcare).

2.2.6. Activation with fgf1 and fgf2. CHO cells were cultured in normal medium for 24 h following transfection and then starved in serum-free medium for 24 h. 5000 ng/mL of fgf1 or fgf2 (Millipore, MA), were added to the serum-free medium. After incubating for 10 min at 37˚C with ligand, cells were lysed as described above and analyzed using Western blotting.

2.3. Results

2.3.1. Full-length FGF receptors dimerize in the absence of ligand, and unliganded FGFR2 and FGFR3 dimers exist at physiological concentrations.

Unliganded FGFR dimers have been reported in the literature (84). However, the propensities for unliganded dimerization of the FGF receptors have not been measured and are unknown. To fill this knowledge gap, here we characterized the dimerization of full length FGFR1, FGFR2, and FGFR3 in plasma membrane derived vesicles using a FRET-based technique termed "quantitative imaging FRET (QI-FRET)" (22, 23, 114).

To allow FRET detection, the monomeric fluorescent proteins YFP and mCherry (a FRET) pair were attached to the C-termini of full-length FGFR1, FGFR2, and FGFR3 via flexible GGS linkers (see Figure S1). CHO cells were co-transfected with plasmids encoding FGFR1-YFP and FGFR1-mCherry, FGFR2-YFP and FGFR2-mCherry, or FGFR3-YFP and FGFR3-mCherry. After the receptors were expressed on the plasma membrane, the cells were vesiculated using an osmotic stress vesiculation buffer (33, 123). The vesicles were imaged as described previously (23, 122) (see also Figure S3).

The donor concentration, the acceptor concentration, the total receptor concentration, the FRET efficiency, and the receptor dimeric fraction were determined for each vesicle (Figures 1A and B). Eight hundred to 1200 individual plasma membrane-derived vesicles were analyzed for each FGF receptor, and the data for all the vesicles expressing one receptor type were combined to yield dimerization curves for the receptor (Figure 1C).

From the data, we determine: (1) the dimeric receptor fractions for a given receptor concentration (Figure 1C), (2) the dimerization constant K for each receptor (Table 1), and (3) the intrinsic FRET, $\tilde{E}$, for each receptor (Table 1), a structural parameter that depends only on the separation and the orientation of the two fluorescent proteins in the dimer. The dimerization free energies are -4.3 ± 0.2 and -5.4 ± 0.2 kcal/mole and -6.3 ± 0.2 kcal/mole for FGFR1, FGFR2, and FGFR3, respectively, corresponding to two dimensional dissociation constants of 240 to 710 μm^{-2}. The intrinsic FRET values vary between 0.43 and 0.66, corresponding to 48 to 56 Å separation between the fluorescent proteins in the dimers.

The dimerization curves for the three full-length receptors are shown in Figure 1C with the solid lines. To evaluate the biological significance of FGFR unliganded dimerization, we note that typical RTK physiological expression levels are below 100 receptors/μm^2. For these receptor expressions, the binding curves for both FGFR2 and FGFR3 in Figure 1C show substantial dimeric populations. Thus, FGFR unliganded dimers exist in cells under physiological conditions. Furthermore, measurements of phosphorylation in Figure S4 as a function of expression demonstrate that the phosphorylated fraction increases with receptor expression, and thus it trends up similarly to the dimer fraction.

2.3.2. Thermodynamic contributions of FGFR domains to unliganded dimerization

To gain mechanistic knowledge about unliganded dimerization, we investigated how different FGFR domains contribute to the energetics of the process. We created two truncated versions of the receptors. In the first version, the intracellular domains were removed, and the FPs were attached to the TM domains via a $(GGS)_5$ flexible linker (Figure S1). These constructs (termed EC+TM) therefore consisted of the EC domains, the TM domains, flexible linkers, and fluorescent proteins (Figure S1). In the second truncated version, both the IC and EC domains were removed, such that these constructs had the TM domains attached to the fluorescent proteins via flexible $(GGS)_5$ linkers (Figure S1). We then characterized the dimerization of the truncated constructs in plasma membrane derived vesicle using the QI-FRET method. The dimerization curves for the truncated receptors are shown in Figure 2, along with the results for the full-length receptors for comparison. The optimal values for the dimerization constants and the Intrinsic FRET for all the variants are shown in Table 1.

First, we observe that the TM domains have a strong propensity for dimerization, with dimerization free energies varying between -5.2 to -6 kcal/mole (K_{diss} varying between 40 and 156 μm^{-2}). Second, by comparing the stabilities of the two types of truncated receptors (EC+TM and TM), we obtain directly the thermodynamic contribution of the EC domain to FGFR unliganded dimerization, $\Delta\Delta G_{EC}$. For all three FGFRs, the addition of the EC domain decreases the dimerization propensity ($\Delta\Delta G_{EC}$ ranging from 1.4 to 2.3 kcal/mole), and thus the contribution of the EC domain to dimerization is inhibitory.

Third, by comparing the stabilities of the full-length receptors and the truncated receptors without the IC domains, we obtain directly and for the first time the thermodynamic contribution of the IC domain to FGFR unliganded dimerization, $\Delta\Delta G_{IC}$. (Table 1). Surprisingly, we see large differences in $\Delta\Delta G_{IC}$, ranging from zero to ~ -3 kcal/mole. While the contributions of FGFR2 and FGFR3 IC domains are -2.0 and -2.9 kcal/mole, respectively, the contribution of FGFR1 IC domain is practically zero, suggesting that either FGFR1 IC domain does not make contacts that stabilize the full-length FGFR1 dimer, or that the stabilizing contacts are balanced by repulsive ones. We thus conclude that the IC domain contribution is stabilizing, not inhibitory, and it varies substantially for the three receptors

An important finding of this work is that FGFRs form dimers in the absence of the IC domains. It has been proposed previously that the IC domain is required for FGFR dimerization in the absence of ligand (3, 84). Our results directly demonstrate, however, that the IC domain is not necessary for FGF dimerization, but its stabilizing effect is significant for FGFR2 and FGFR3.

2.3.3. Structural changes in FGFR dimers upon fgf1 and fgf2 binding

In the experiments described above, we determined the Intrinsic FRET for all studied dimers, along with the dimerization propensities (Table 1). The value of the Intrinsic FRET contributes to the measured FRET efficiencies, and thus it needs to be determined and accounted for in order to correctly measure the dimerization propensities. Furthermore, the value of the Intrinsic FRET yields information about the distance between the fluorescent proteins in the dimer, thus providing insight into dimer structure. We therefore sought to compare the Intrinsic FRET in the presence and absence of ligand, as a means to follow structural changes on the cytoplasmic side of the receptor upon ligand binding to the extracellular domains. Since the TM domains have been proposed to play a role in FGFR activation (8, 80), we first worked with the truncated EC+TM FGFR constructs, in which the fluorescent proteins were attached to the TM domains via flexible linkers. This way, we could directly monitor possible changes in the structure of the TM domains in the receptor dimers in response to ligand binding.

Experiments were performed at, saturating ligand concentration (5,000 ng/ml), under conditions when the ligand amounts exceed total FGFR amounts by at least two orders of magnitude as previously described (19, 21, 53)), to ensure that all receptor are in the ligand-bound dimeric state (see references (19, 21, 53) for details). In the case of 100% dimeric receptors, the FRET signal depends on (i) the Intrinsic FRET, i.e. the distance and orientation of the fluorescent proteins in the ligand-bound dimers, and (ii) the acceptor fraction, which is measured in each vesicle. The dimerization constant cannot be determined, but the measurements of the Intrinsic FRET at saturating ligand concentrations, allow us to assess structural changes that occur in response to ligand binding.

FRET experiments were performed in the presence of two different ligands, fgf1 and fgf2. For each receptor/ligand pair, 300 to 500 individual plasma membrane-derived vesicles were imaged, one hour after adding 5 μg/ml ligand to the vesicles. Results are shown in Figure S5. The Intrinsic FRET for each vesicle was measured according to equation (11) in Supplementary data, and histograms for these values for each receptor/ligand pair are shown in Figure 3A.

In Figure 3A, we see significant differences between the Intrinsic FRET values measured for fgf1-bound and fgf2-bound FGFR dimers ($p<0.01$). The Intrinsic FRET value in the fgf1-bound state is ~0.55, while the Intrinsic FRET value in the fgf2-bound state is ~0.73.

Assuming random orientation of the fluorophores (justified because they are attached via long linkers), we calculate the distances between the fluorescent proteins (Table 1). In the presence of fgf1, the distance between the fluorescent proteins is about 52 Å (similar to the unliganded case). In the case of fgf2, the distance between the fluorescent proteins is about 44 Å. Since in all cases the attachment of the fluorescent proteins to the TM domain is the same, these differences indicate differences in the separation of the C-termini of the TM domains in the two ligand-bound states. Thus, these experiments yield a direct demonstration of structural differences in FGFR3 TM domain structure in the fgf1- and fgf2- bound cases.

The Intrinsic FRET values in the presence of fgf1 and fgf2 are shown in Table 2, such that these values can be directly compared to the Intrinsic FRET in absence of ligand shown in Table 1. We see that fgf2 binding causes a statistically significant change in Intrinsic FRET, while the change upon fgf1 binding is not statistically significant.

2.3.4. Structural differences in the fgf1 and fgf2 states correlate with phosphorylation levels

To investigate the biological significance of the different structures that we observe in the FRET experiments in the presence of fgf1 and fgf2, we compared the phosphorylation of full-length FGFR1, FGFR2, and FGFR3 at saturating fgf1 and fgf2 concentrations (5 μg/ml) using Western blotting. The architecture of the full-length receptors used in the Western blot experiments is shown in Figure S2. For detection, we used specific anti-FGFR antibodies against the extracellular domains of FGFR1, FGFR2, and FGFR3, as well as anti-phospho-Tyr antibodies that are reactive to phosphorylated tyrosines in the activation loop of the three receptors (anti-phospho-Y653/4) or other tyrosines in the kinase domain. Results are shown in Figures S6 and 3B. We see that tyrosine phosphorylation is higher in the fgf2 bound state for both FGFR1 and FGFR3, as compared to the fgf1 bound state. Interestingly, the Western blot results for FGFR2 reveal the same FGFR2 phosphorylation in the presence and fgf1 and fgf2 (as well as in the absence of ligand, see Figure S6). This finding is surprising, but not entirely unexpected as FGFR2 has been previously described to interact with soluble adaptor proteins which regulate its dimerization and activity (3, 84). The Western blot results are therefore consistent with the findings of two distinct ligand-bound active states, and directly demonstrate that these distinct states exhibit different phosphorylation levels for FGFR1 and FGFR3.

2.3.5. Insights from a high-resolution NMR structure of the isolated FGFR3 TM dimer

The only FGFR TM domain high-resolution dimer structure reported thus far is the FGFR3 TM domain dimer structure (8). In this structure, solved by NMR in micelles, the FGFR3 TM helices form a left-handed dimer, with helix-helix interactions occurring along the entire TM domain. The TM helices are almost parallel to each other, and wrap around each other in a tight closed-packed configuration (see Figure S7).

It can be argued that the TM dimer structure in Figure S7, observed in micelles by NMR, should give the highest intrinsic FRET possible in the FRET experiments, as the two C-termini are tightly packed against each other. The highest Intrinsic FRET observed in our experiments was recorded in the presence of fgf2. These arguments lead us to hypothesize that the isolated FGFR3 TM domain dimer structure in micelles is the same as (or is very similar to) the fgf2-dound dimer structure in plasma membranes.

2.3.6. FGFR3 domain dimer structure in the fgf2 state

To test the hypothesis that the isolated FGFR3 TM domain dimer structure in micelles is the same as (or very similar to) the fgf2-bound dimer structure in plasma membranes, we mutated amino acid residues 377, 380 and 391. These residues were shown to mediate interactions between the TM helices in the NMR structure, based on the recorded inter-helical NOEs (8). The mutations were engineered in the truncated EC+TM construct used in the FRET studies (Figure S1) and in the full-length FGFR3 receptor (Figure S2). The comprehensive FRET characterization of the dimerization of this truncated mutant, in the absence and presence of fgf1 and fgf2, is shown in Figure S8. The Intrinsic FRET values for the truncated mutant, as well as the Western blots that assess the phosphorylation of the full-length mutant are shown in Figure 4, I (in the presence of fgf1 and fgf2), and Figure 5, I (in the absence of ligand). We see that this mutant behaves very differently in the presence of fgf2, as compared to the WT. In particular, the Intrinsic FRET values in the fgf1 and fgf2 states are identical for this mutant, and are the same as the I-FRET value for the WT fgf1 case. Furthermore, the phosphorylation of this mutant in the presence of saturating fgf1 and fgf2 concentrations is also the same, and lower than the phosphorylation of the wild-type in the fgf2 state (see Figure S13). Thus, the engineered mutations in the NMR interface destabilize and abolish the FGFR3 fgf2-bound state, and induce a structural transition to the fgf1 state when fgf2 is bound. This finding is consistent with the hypothesis that the NMR structure and the fgf2-bound TM dimer structures are the same.

FGFR3 TM domain has multiple GxxxG-like motifs that do not participate in the NMR interface, but are believed to be capable of forming a putative alternative dimer interface

(8) in the TM domain dimer. Such GxxxG-like motifs, sometimes called SMALLxxxSMALL motifs, have small amino acids such as Gly, Ala, Thr and Ser in *i*, *i*+4 positions, and are believed to mediate interactions between hydrophobic helices in membranes. To investigate if this GxxxG-like interface pays a role in FGFR3 dimerization, we mutated three glycines in this GxxxG-like interface to virtually eliminate all GxxxG-like motifs (Figure S). The mutations were engineered in the truncated EC+TM construct used in the FRET studies (Figure S7) and in the full-length FGFR3 receptor (Figure S2). The comprehensive characterization of the dimerization of this mutant, in the absence and presence of the fgf ligands, is shown in Figure S9. The Intrinsic FRET values, as well as the measured phosphorylation levels of the full-length mutant from Western blots are shown in Figure 4B, II (in the presence of fgf1 and fgf2), and Figure 5B, II (in the absence of ligand); see also Figure S10. We see that these mutations, which are not expected to impact the NMR structure, do not impact the fgf2 state either. Indeed, both the Intrinsic FRET and the phosphprylation of the GxxxG-like mutants and the wild-type at saturating fgf2 concentrations are the same. This finding lends further support to the hypothesis that the NMR and the fgf2-bound TM dimer structure are similar.

2.3.7. FGFR3 TM domain dimer structure in the fgf1 state

The mutagenesis described above revealed that mutations in the NMR interface have no effect on the Intrinsic FRET value, the distance between fluorescent proteins, and on the phosphorylation in the fgf1-bound state of FGFR3. Thus, the structure of the FGFR3 TM domain dimer in the fgf1-bound state is different from the fgf2-bound state structure, as well as from the NMR TM domain structure. On the other hand, the Intrinsic FRET measured in the fgf1 state is altered when the GxxxG-like interface is mutated (Figure 4), suggesting that these mutations perturb the fgf1 bound structure. Therefore, the FGFR3 TM dimer in the fgf1 state is likely stabilized by helix-helix interactions that involve the GxxxG-like interface.

2.3.8. FGFR3 TM domain dimer structure in the unliganded state

Mutations in both the NMR interface and the GxxxG interface altered the Intrinsic FRET measured in the unliganded state (Figure 5). One way to interpret this unexpected finding is to assume that the TM domain in the unliganded state explores both the fgf1 and fgf2-bound structures. If this is the case, the Intrinsic FRET must be a weighted average of the Intrinsic FRETs between the fgf1 and fgf2-bound states. While we cannot completely exclude this possibility, we note that there are no statistically significant differences in Intrinsic FRET in the unliganded and in the fgf1-bound states (Tables 1 and 2).

A second way to interpret our findings is to postulate that the TM domains can interact through a third helix-helix interface, which involves at least one amino acid from each the two separate sets of mutations. While the mutagenesis could not provide specific structural insights into the unliganded dimer structure, the results strongly suggest that the unliganded dimer structure is different from the fgf1-bound structure, despite having the same Intrinsic FRET, as well as from the fgf2-bound dimer structures. Thus, FGFR3 TM domain dimer can adopt (at least) three structural configurations. Fgf1 binding to the unliganded dimers induces structural changes which do not alter significantly the separation of the fluorescent proteins in the dimer. Fgf2 binding, on the other hand, brings the fluorescent proteins in EC+TM FGFR3 construct closer together.

Our results further suggest that the FGFR3 TM domain may adopt yet another dimer structure in the absence of the EC domain. Indeed, the Intrinsic FRET measured for the EC+TM and TM dimers in the absence of ligand are significantly different for FGFR3, but are the same for FGFR1 and FGFR2 (Table 1). In FGFR3, the fluorescent proteins are closer to each other when the EC domain is deleted, suggesting that the EC domain may push the TM helices apart and thus may interfere with the sequence-encoded interactions between the TM domains.

Next, we performed FRET experiments at saturating ligand concentrations with the three full-length FGF receptors, linked to fluorescent proteins. The values of the Intrinsic FRET measured in the presence of fgf1 and fgf2 are shown in Table S1, together with the values measured in the absence of ligand (i.e. from the experiment in Figure 1). In this case, the structural interpretation of the data is not straight-forward because the fluorescent proteins are attached to the long flexible C-terminal tails (> 50 amino acids) of the full-length receptors. Yet, we see significant changes in Intrinsic FRET upon ligand binding in the case of FGFR1 and FGFR2, consistent with the idea that both fgf1 and fgf2 binding leads to structural changes in the receptor dimers.

2.3.9. Effect of a pathogenic mutation of FGFR3

To further investigate the biological significance of our observations, we studied the pathogenic A391E mutation in the TM domain of FGFR3, a mutation linked to Crouzon syndrome with acanthosis nigricans (94). Previous QI-FRET studies have shown that this mutation stabilizes the unliganded EC+TM FGFR3 dimer by -1.4kcal/mole (122). Intriguingly, the two-parameter fit of the QI-FRET data in the absence of ligand for this mutant yielded a value of 0.70 ± 0.02, the same as the value measured in the fgf2-state for the wild-type (0.72 ± 0.01).

This fact prompted us to investigate further the behavior of the mutant. Using QI-FRET, we characterized the Intrinsic FRET of the A391E EC+TM FGFR3 construct in the presence of saturating fgf1 and fgf2 concentrations. We also characterized the phosphorylation of the full-length mutant in the presence of saturating fgf1 and fgf2 concentrations.

The comprehensive characterization of the dimerization of the A391E pathogenic mutant, in the absence and presence of fgf1 and fgf2, is shown in Figures S11. The Intrinsic FRET values as well as the Western blots that assess the phosphorylation of the mutants in the presence of fgf1 and fgf2 are shown in Figure 6. We see that the Intrinsic FRET values in the fgf1 and fgf2 states are identical for this mutant, and are the same as the I-FRET value for the wild-type fgf2 case (Figure 6A, I). The phosphorylation of the full-length A391E mutant in the presence of saturating fgf1 and fgf2 concentrations are also the same (Figure 6 B, II), and are the same as in the wild-type fgf2-bound state (Figure S13). Thus, the A391E mutation abolishes the fgf1 state, and forces the dimer into the fgf2 state when fgf1 was bound. The mutation also increased the phosphorylation in the presence of fgf1, up to fgf2 levels.

Taken together, published and new data demonstrate that the A391E mutation traps the FGFR3 dimer in the fgf2 state even in the absence of ligand. We thus find that the fgf2 state is stabilized (rather than destabilized) when A391, an amino acid that likely participates in helix-helix contacts in the fgf2 state, is mutated to Glu. This finding can be explained by the formation of a stabilizing hydrogen bond between the mutant Glu and the neighboring helix, an idea which is supported by molecular modeling (82). Once formed, this structure does not change significantly upon binding fgf1 or fgf2. The A391E mutation therefore mimics the action of fgf2 in enforcing a particular dimer structure. Since the fgf2-bound state is the most active one, the A391E mutation leads to increased phosphorylation and thus disregulated signaling and disease.

2.3.10. Correlation between TM dimer structure and receptor phosphorylation

Figures 3 through 6 above show multiple examples of correlations between Intrinsic FRET and phosphorylation levels. In Figure 7A we show the global correlation for wild-type FGFR3 and the three FGFR3 mutants studied here. We see a very strong correlation between Intrinsic FRET and phosphorylation, as measured in our experiments. In Figure 7B we show the correlation between (i) the calculated distance between fluorescent proteins in the dimer and (ii) phosphorylation of the full-length receptor, calculated under the assumption of free fluorescence protein rotation. Again, we see a strong correlation between (i) distance between the fluorescent proteins and (ii) phosphorylation.

2.4. Discussion

2.4.1. Mechanism of FGFR activation.

Here we demonstrate that the FGF receptors form dimers in the absence of ligand at physiological concentrations, and that the unliganded dimers are phosphorylated. We further demonstrate that the unliganded FGFR dimers undergo structural changes upon ligand binding, the structural changes in response to fgf1 and fgf2 binding are very different, resulting in different phosphorylation of the fgf1 and fgf2-bound dimers. These results establish the existence of multiple active ligand-bound states for the FGF receptors.

Upon fgf1 binding, FGFR3 TM domains engage in interactions that involve GxxxG motif. Binding of fgf2, however, results in a very different TM structure which is closely packed. This structure ensures the smallest separation between the TM domains and the highest possible FGFR3 phosphorylation. Thus, fgf2 binding bring the TM domains closer together, as compared to the fgf1 case, and induces maximum kinase phosphorylation. This conclusion is supported by a strong correlation between TM domain dimer structure and kinase phosphorylation, for wild-type FGFR3 and three FGFR3 mutants (Figure 7).

2.4.2. A unified model of RTK activation

Since the discovery of RTKs in the 70s, researchers have been searching for a model that captures the essence of RTK signal transduction across the plasma membrane. The first proposed model was the "diffusion-based" or "canonical" model of RTK activation (39). It postulates that RTKs are monomers in the absence of ligand, but dimerize and cross-phosphorylate/activate each other upon ligand binding. However, recent work has identified unliganded RTK dimers, and thus an alternative model was proposed, the so-called "pre-formed dimer model" (6, 12, 14, 84). In this model, the RTKs are dimeric in the absence of ligand, and ligand binding induces a structural change in the receptor that reorients the catalytic domains for efficient activation. Here we find that FGFR1, FGFR2, and FGFR3 dimerize in the absence of ligand, and they undergo structural changes in response to ligand binding. Thus, they all follow the pre-formed dimer model.

We also see that the dimerization propensities of FGFR1, FGFR2, and FGFR3, are very different (Table 1). This difference is obvious in the dimerization curves in Figure 1 C, which show levels of pre-formed dimers. While significant populations of FGFR2 and particularly FGFR3 exist for receptors concentrations < 100 receptors per micron squared, FGFR1 is predominantly monomeric. Thus, FGFR1 appears to follow the canonical model of activation. Taken together, these results suggest the possibility that the difference between the "canonical" and the "pre-dimerized" mode of activation is not fundamental, but may simply lay in the magnitude of the unliganded dimerization constant. We thus propose that all RTKs may follow a single model of activation, which includes unliganded dimers as intermediates. However, the stability of the unliganded dimers vary significantly and, thus not all receptors exist at pre-formed dimer under physiological conditions.

2.4.3. Interplay of different FGFR domains in dimerization.

Here we measured directly the thermodynamic contributions of the different FGFR domains to unliganded dimerization (Figure 2). These results demonstrate that the deletion of the IC domains decreases the dimerization propensity, with effects varying from negligible to strong (-3 kcal/mole). On the other hand, the deletion of the EC domain increases the dimerization propensity by 1.4 to 2.3 kcal/mole. Thus, the contribution of the IC domain to unliganded dimer stability is generally stabilizing, while the contribution of the EC domain is destabilizing. However, our results further suggest that, at least in the case of FGFR3, these thermodynamic contributions are not completely additive. Indeed, the change in the Intrinsic FRET upon the deletion of the EC domain (Table 1) suggests that the EC domain affects the behavior of the TM domain. Although

FGFR3 TM domains form dimers by themselves, the TM dimer structure and stability may be altered by the presence of the EC domain.

2.4.4. Multiple active RTK dimers

Within the pre-formed dimer model, ligand binding to the extracellular domains induces structural changes that propagate to the kinase domains (4, 6, 36). It has been hypothesized that these structural changes must involve the TM domains, as they connect the two large soluble domains across the membrane. In particular, a change in the separation between the C-termini of the TM domains of about 10 Å has been proposed to occur upon ligand binding for some receptors (8, 9, 42, 67), which in turn is believed to change the distance between the kinase domains, and/or their orientation, and allow for efficient cross-phosphorylation. The experiments presented here provide a direct demonstration that such a structural change occurs in the FGF receptors within the plasma membrane (Tables 1, 2, and S1). Our data demonstrate further that two different structures are adopted by the FGFR TM domain dimers in the fgf1 and fgf2 bound states, and these structures have different biological activities.

Previously, differences in binding strengths for different FGF receptor/ligand pairs have been reported, and these differences have been suggested to underlie the specificity of the biological response of a receptor to a particular ligand (97, 106, 167). Here we further demonstrate differences in structure when different ligands are bound. These structural differences also likely contribute to the specificity of the biological response.

2.4.5. Phosphorylation is correlated with distance between the TM domains.

We discovered here a strong correlation between the Intrinsic FRET (and the distance between the fluorescent proteins in the EC+TM FGFR3 dimer) and the phosphorylation of the receptors (Figure 7). It can be argued that the distance between the fluorescent proteins in our experiments must correlate with the distance between the C-terminal ends of the TM domains in the dimer, at these are the points of attachment of the $(GGS)_5$ linkers. Such a correlation is consistent with our findings that the closed packed NMR structure corresponds to the highest phosphorylation fgf2-bound state. Thus, the activity of the receptor is controlled by the structure of the TM domains. Since the kinase domains are attached to the TM domains in the full-length receptors, our results suggest a correlation between the separation of the kinase domains in the dimer and their phosphorylation. Indeed, fgf2 binding leads to increase in activity over fgf1 by bringing the TM helices closer together in the dimer. However, the receptor itself is not a passive player in the process, as mutations in the receptors can over-ride the effect of the ligand and force it into an alternative structure with aberrant activity.

2.4.6. A new molecular mechanism behind FGFR-linked pathologies

There are many known pathogenic mutations in the FGF receptors, most of them linked to different bone growth disorders (26, 28, 119, 151, 158). Here we uncovered a new mechanism through which FGFR-linked pathologies can arise. In particular, we showed that the A391E mutation mimics the structural effects of fgf2 binding, preventing the dimer from exploring the unliganded and fgf1-bound conformation, and traps it in the most active fgf2 state. This is possible because of the structural plasticity of the FGF receptors, and the multi-faceted mechanism of their activation described here.

	ΔG (kcal/mol)	K_{diss} (μm^{-2})	Intrinsic FRET	d(Å)
Full FGFR1	-4.3 (-4.0 to -4.5)	710 ± 420	0.66 (0.64 to 0.69)	48 ± 1
Full FGFR2	-5.4 (-5.2 to -5.7)	111 ± 44	0.43 (0.41 to 0.44)	56 ± 1
Full FGFR3	-6.3 (-6.0 to -6.8)	24 ± 15	0.55 (0.53 to 0.57)	51 ± 1
ECTM FGFR1	-4.6 (-4.4 to -4.8)	428 ± 145	0.50 (0.46 to 0.55)	53 ± 2
ECTM FGFR2	-3.4 (-3.2 to -3.6)	3235 ± 1100	0.57 (0.51 to 0.64)	51 ± 2
ECTM FGFR3	-3.4 (-3.2 to -3.6)	3235 ± 1100	0.52 (0.46 to 0.57)	52 ± 2
TM FGFR1	-6.0 (-5.7 to -6.3)	40 ± 26	0.50 (0.46 to 0.52)	53 ± 1
TM FGFR2	-5.7 (-5.4 to -6.1)	67 ± 37	0.52 (0.5 to 0.54)	52 ± 2
TM FGFR3	-5.2 (-5.0 to -5.4)	156 ± 54	0.65 (0.64 to 0.67)	48 ± 1

Table 2-1. Parameters describing FGFR unliganded dimerization. Dimerization free energies (dimer stabilities), *ΔG,* two-dimensional dissociation constants K_{diss}, Intrinsic FRET efficiencies $\tilde{E}$, and distance between fluorescent proteins, d, in the dimers. These parameters are obtained from least-square fits of a dimer model to the FRET data. The distance between the fluorescent proteins in the EC+TM FGFR constructs is 51 to 53 Å (highlighted in grey).

	Intrinsic FRET	D(Å)
ECTM FGFR1+fgf1	0.55±0.01	51 ± 1
ECTM FGFR1+fgf2	0.73±0.01	45 ± 1
ECTM FGFR2+fgf1	0.53±0.01	52 ± 1
ECTM FGFR2+fgf2	0.75±0.01	44 ± 1
ECTM FGFR3+fgf1	0.55±0.01	51 ± 1
ECTM FGFR3+fgf2	0.72±0.01	45 ± 1
377I-380I-391I	0.39±0.01	57 ± 1
377I-380I-391I+fgf1	0.52±0.01	52 ± 1
377I-380I-391I+fgf2	0.53±0.01	52 ± 1
374I-375I-378I	0.43±0.01	56 ± 1
374I-375I-378I+fgf1	0.63±0.01	49 ± 1
374I-375I-378I+fgf2	0.74±0.01	45 ± 1
A391E+fgf1	0.75±0.01	44 ± 1
A391E+fgf2	0.78±0.01	43 ± 1

Table 2-2. Intrinsic FRET efficiencies $\tilde{E}$, measured in the presence of saturating fgf1 and fgf2 concentrations for the truncated EC+TM FGFR constructs. In the fgf1 state, the measured distance between the fluorescent proteins is 51 to 52 Å (highlighted in grey). In the fgf2 state, the measured distance between the fluorescent proteins is 43 to 45 Å (highlighted in yellow).

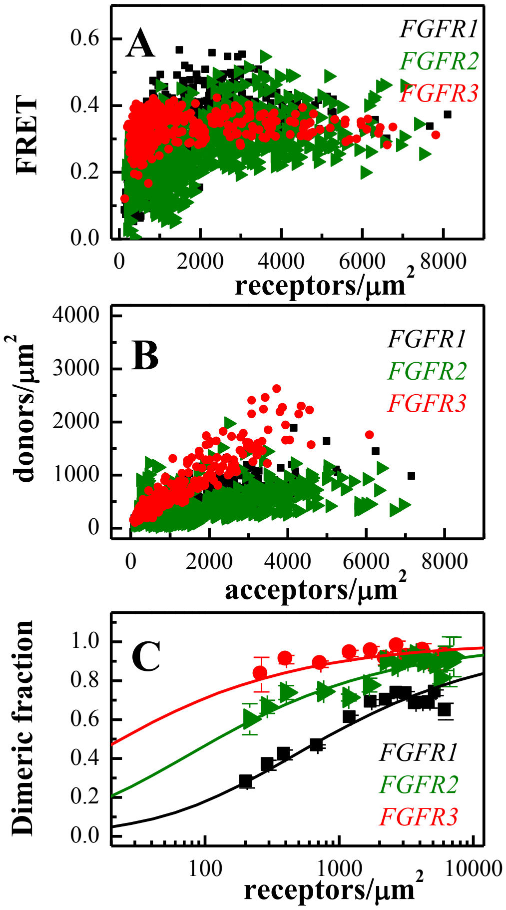

Figure 2-1. (A) Measured FRET as a function of receptor concentration, for the three full-length receptors. Every data point represents a single vesicle (B) The donor concentration is plotted as a function of the acceptor concentration, for each vesicle. (C) Dimeric fraction as a function of total receptor concentrations. The solid line is the dimerization model, plotted for the optimized dimerization constants in Table 1.

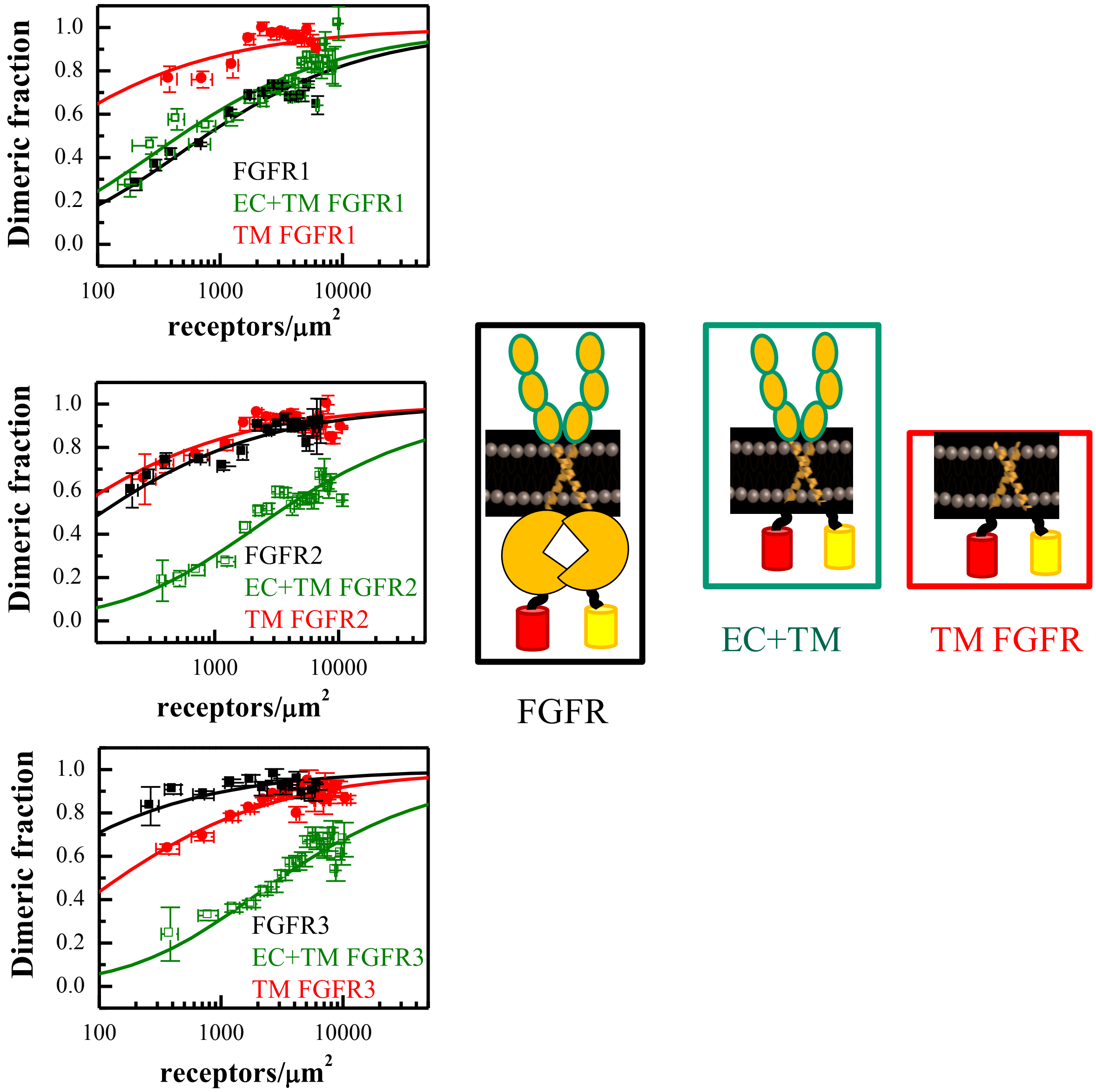

Figure 2-2. Dimerization curves for the full-length receptors (black), truncated receptors that lack the IC domain and thus contain only the EC and TM domains (olive), and the TM domains only (red). Data for EC+TM FGFR3 and TM FGFR3 are from (124). The measured dimeric fractions are binned and are shown with the symbols, along with the

standard errors. The solid lines are the best fits of a monomer-dimer equilibrium model to the data. These data demonstrate that the TM domains have a very strong propensity for dimerization. The EC domains, on the other hand, inhibit dimerization. The contribution of the IC domains is favorable, but it varies from zero to -3 kcal/mole for the three receptors.

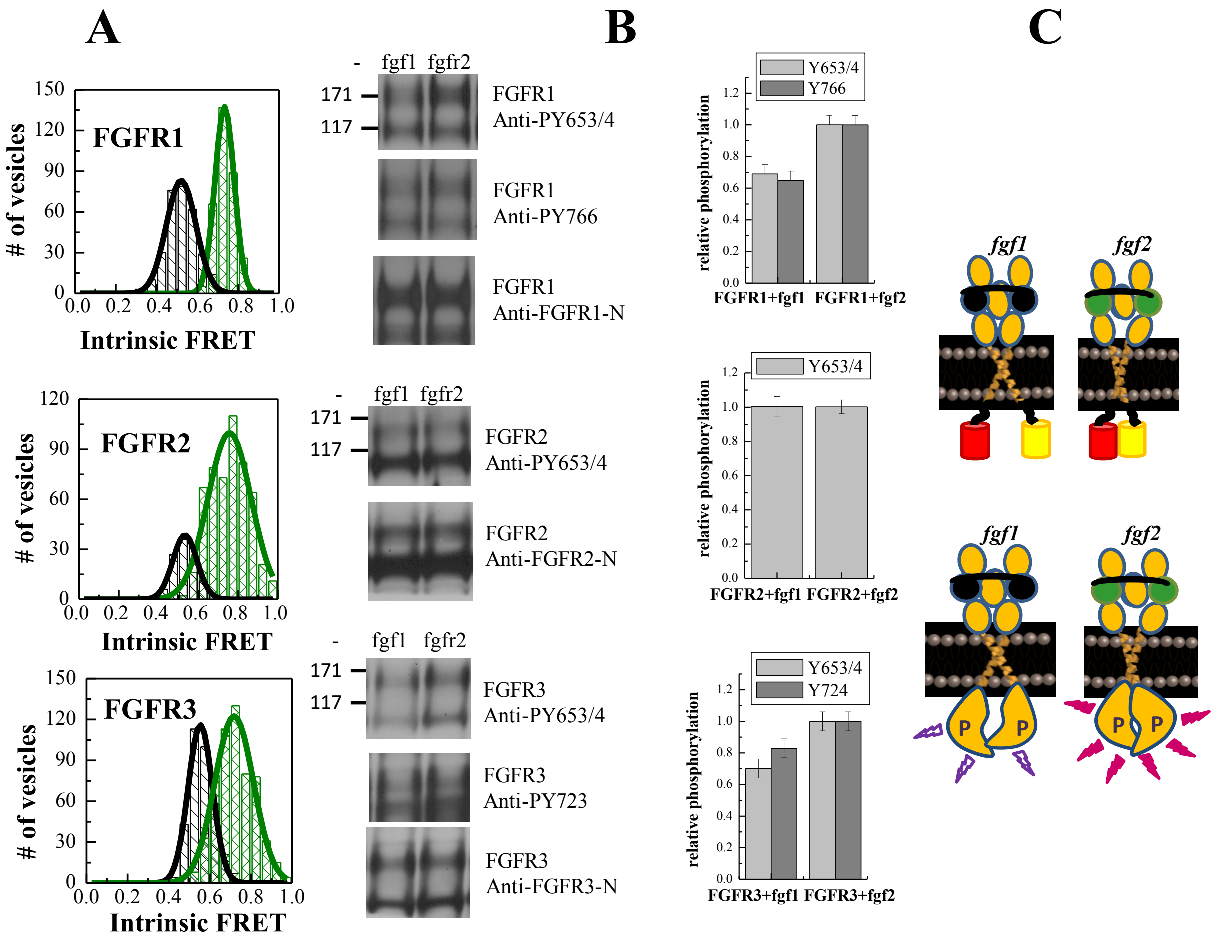

Figure 2-3. FRET and Western blot results for wild-type FGFR1, FGFR2, and FGFR3. (A). Intrinsic FRET values, measured for the three FGF EC+TM receptors in the presence of saturating fgf1 and fgf2 concentrations. The Intrinsic FRET is a measure of the separation between the fluorescent proteins in the dimer. Two different Intrinsic FRET values were measured for fgf1 and fgf2 (see also Supplementary Figure S5). Therefore, the binding of these two ligands to the extracellular domains of the receptors leads to different separation of the fluorescent proteins on the cytoplsmic side of the membrane. (B). Western blots, reporting on the phosphorylation of the full-length receptors in the presence of saturating concentrations of fgf1 and fgf2. Expression of the receptors was probed with anti-FGFR1, anti-FGFR2, and anti-FGFR3 antibodies to the extracellular domains of the three receptors. Phosphorylation was assays using antibodies against phosphorylated tyrosines in the activation loop of the three kinases (anti-phospho-Y653/4) or other phosphorylated tyrosine residues (Y766 in FGFR1 and Y723 in FGFR3). Two bands are observed for all receptors. The top bands are the fully glycosylated mature receptors that reside primarily in the plasma membrane. Only the top bands are used to quantify phosphorylation. Phosphorylation was calculated by dividing the intensities of the anti-phospho-Y bands to the intensities of the anti-receptor bands. Relative phosphorylation is reported with respect to the fgf2 case. There is a statistically significant difference between the phosphorylation in response to fgf1 and fgf2 for FGFR1 and FGFR3. (D) Graphical representation of the findings that the fgf1-bound and fgf2-bound states are structurally and functionally distinct.

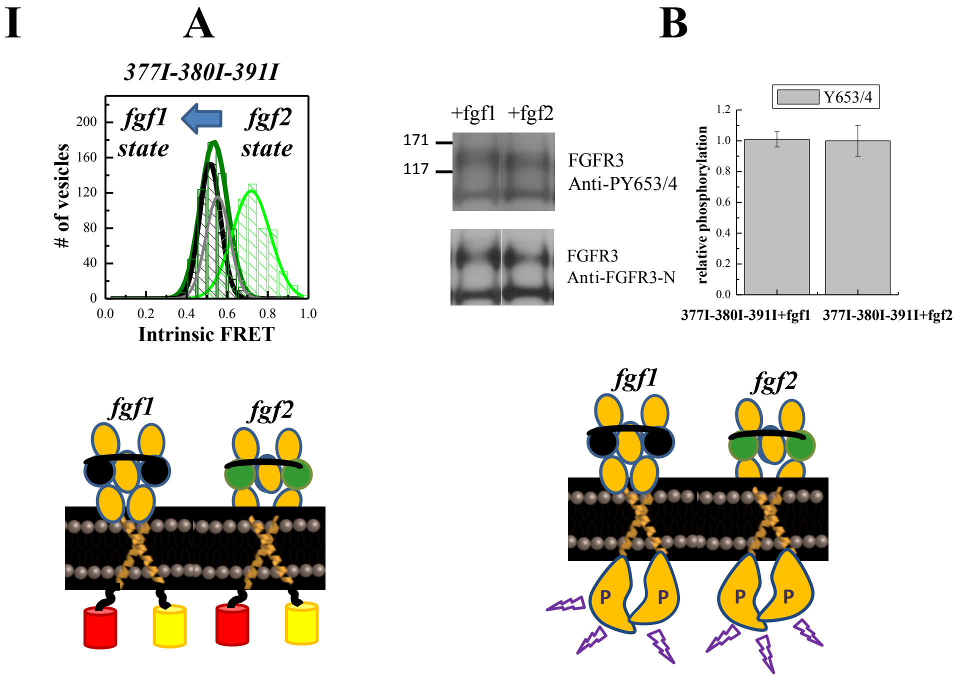

DEAGSVYAGI**L**SY**G**VGFFLFILVV**A**AVTLCRLR
377 380 391

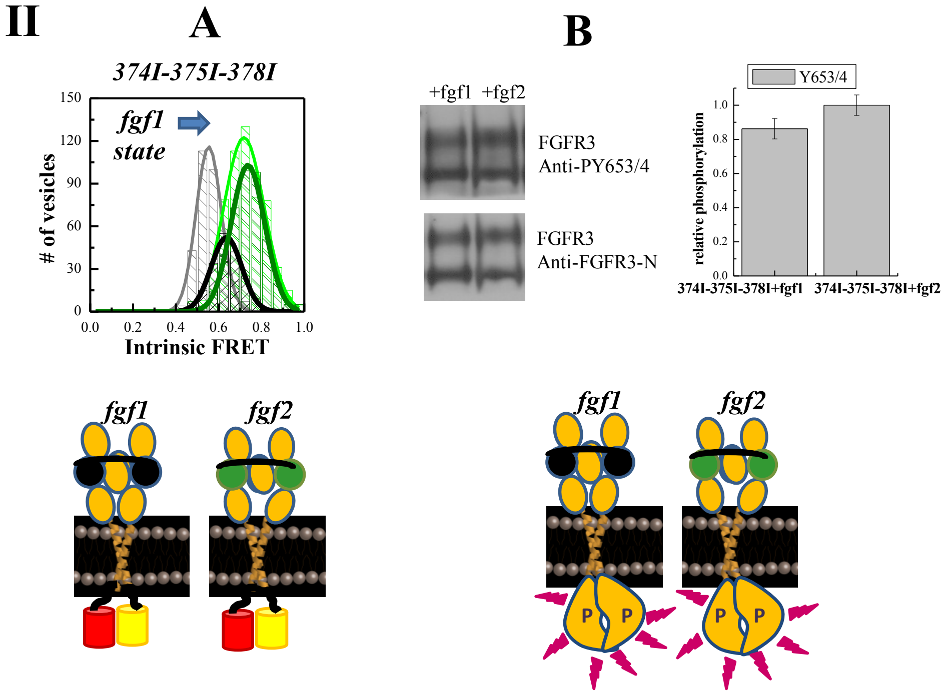

DEAGSVYAGILSYGVGFFLFILVVAAVTLCRLR
374,5 378

Figure 2-4. Insights into the fgf1-bound and fgf2-bound FGFR3 dimer structures in the plasma membrane, based on mutagenesis that is guided by a high resolution NMR structure of the isolated FGFR3 TM domain in micelles ((8), see Figure S7). (I) Data for the 377I-380I-391I mutant in the presence of saturating of fgf1 and fgf2 concentrations. The 377I-380I-391I mutations were engineered to destabilize the FGFR3 dimer structure, solved for the isolated TM domain in micelles (see Figure S7B). (II) Data for the 374I-375I-378I mutant in the presence of saturating fgf1 and fgf2 concentrations. The 374I-375I-338I mutations were engineered to destabilize a putative alternative dimer structure not observed in the NMR experiments, mediated by GxxxG-like motifs (see Figures S7C and S7D). (A) Intrinsic FRET values, measured for the truncated EC+TM FGFR3 mutants. The histograms of measured Intrinsic FRET values in single vesicles for the wild-type are shown in grey for the fgf1 case and in green for the fgf2 case. The histograms for the mutants are shown in black in the presence of fgf1 and in olive in the presence of fgf2. In the presence of the 377I-380I-391I mutations (I), the Intrinsic FRET values measured in the presence of fgf2 shift such that they overlap with the fgf1 wild-type case. In the presence of the 374I-375I-378I mutations (II), the Intrinsic FRET values measured in the presence of fgf1 move towards the fgf1 wild-type case. (B) Western blots showing expression of the full length 374I-375I-378I and 374I-375I-378I mutants, as assayed by anti-FGFR3 antibodies, and phosphorylation of the tyrosines in the activation loop, as assayed by the anti-phospho-Y653/4 antibodies. The quantification of the Western blot results demonstrates the phosphorylation of the two mutants is similar in the fgf1 and fgf2-bound case. Thus, the 374I-375I-378I mutations abolish the fgf2 state and the 374I-375I-378I mutations abolish the fgf1 state.

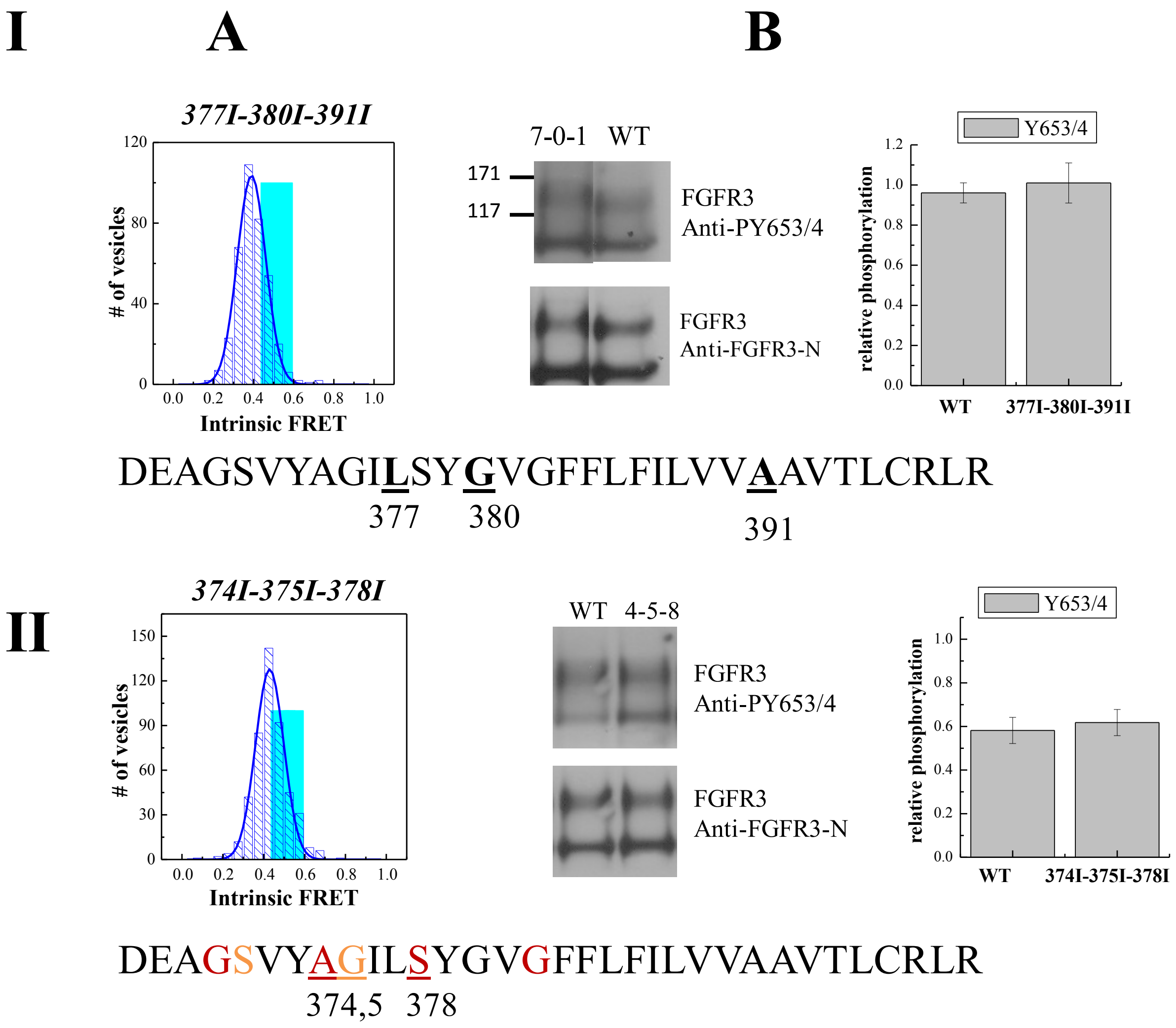

Figure 2-5. The unliganded FGFR3 dimer structure, based on mutagenesis, guided by the high resolution structure of the isolated FGFR3 TM domain in micelles (8). (I). Data for the 377I-380I-391I mutant in the absence of ligand. The 377I-380I-391I mutations were engineered to destabilize the FGFR3 dimer structure, solved for the isolated TM domain in micelles. (II) Data for the 374I-375I-378I mutant in the absence of ligand. The 374I-375I-338I mutations were engineered to destabilize a putative alternative dimer structure,

mediated by GxxxG motifs. (A). Blue Gaussian: Intrinsic FRET measured for the constitutively dimeric EC+TM 377I-380I-391I (I) and 374I-375I-338I (II) mutants in the absence of ligand (see Supplemental Figures S8 and S9). Cyan bar: Intrinsic FRET for the wild-type, obtained by fitting the FRET data to a dimerization model (Table 1). The Intrinsic FRET decreases due to both mutations, suggesting that the fluorescent proteins in the dimer move way from each other due to the mutations. (B) Western blot data, reporting on the phosphorylation of the full-length mutants as compared to the wild-type. The phosphorylation of the wild-type and the mutants is the same, despite the increased dimerization due to the mutations.

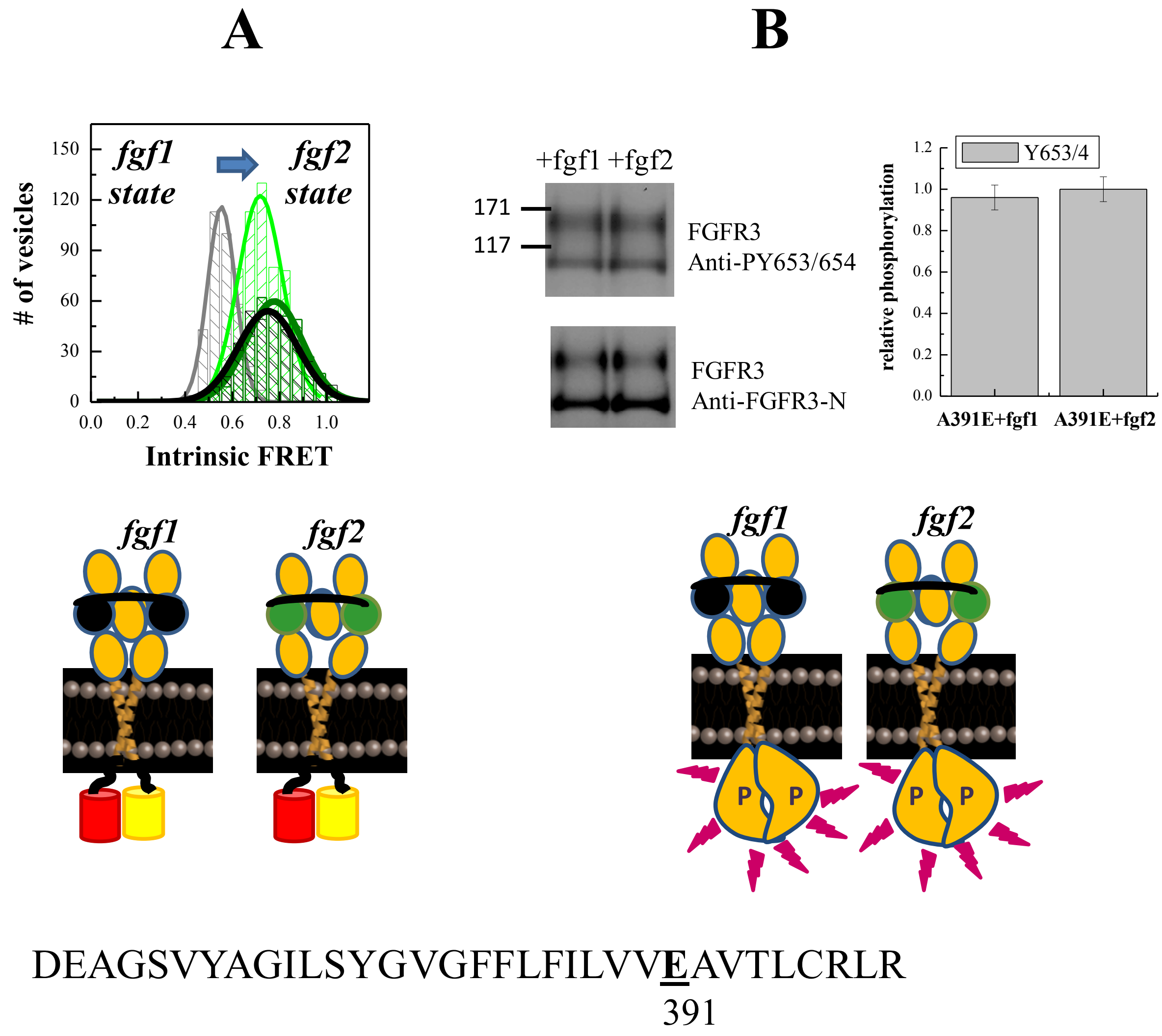

Figure 2-6. Effect of the pathogenic A391E FGFR3 mutation on dimer structures in the fgf1 and fgf2 states. The A391E mutation is the genetic cause for Crouzon syndrome with acanthosis nigricans, a cranial abnormality. (A) Intrinsic FRET values, measured for the A391E EC+TM mutant in the presence of saturating concentrations of fgf1 and fgf2. The histograms for the wild-type are shown in grey in the presence of fgf1 and green in the presence of fgf2. The histograms for the mutants are shown in black in the presence of fgf1 and olive in the presence of fgf2. In the presence of the A391E

mutations, the Intrinsic FRET values measured in the presence of fgf1 shift such that they overlap with the fgf2 wild-type case. Thus, the A391E mutation abolished the fgf1 state. (B) Western blots showing expression, as assayed by anti-FGFR3 antibodies, and phosphorylation of the tyrosines in the activation loop, as assayed by anti-phospho-Y653/4 antibodies. Also shown is the quantification of the Western blot results; only the top bands of fully-glycosylated receptors are quantified. The phosphorylation of the A391E mutant is identical in the fgf1 and fgf2 states, and is the same as the phosphorylation of the wild-type in the fgf2 state (see Figure S13). The A391E mutation increases the phosphorylation in the fgf1 state to fgf2-state levels.

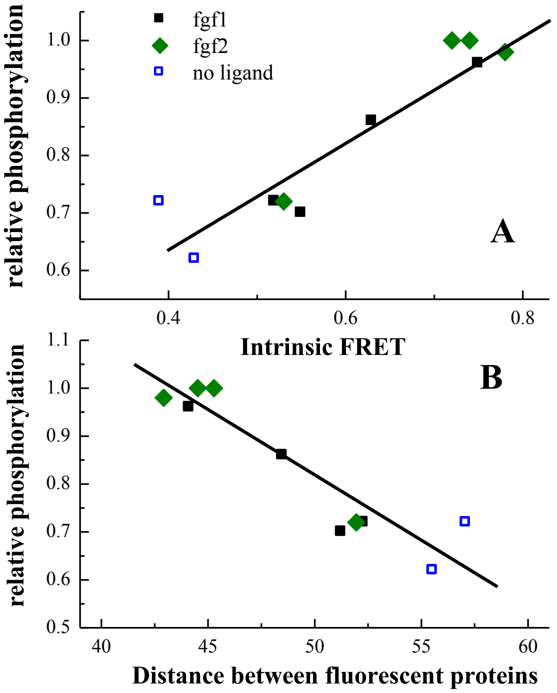

Figure 2-7. Correlation between Intrinsic FRET and phosphorylation, for FGFR3 and the three studied FGFR3 mutants. Only results for constitutive dimer are included. The

phosphorylation of the wild-type in the fgf2-bound state is assigned a value of 1, and all other measured phosphorylation levels are scaled accordingly using the data in Figure S13. There is a strong correlation between the two measured quantities ($p<0.0001$). (B) Strong correlation between the distance between fluorescent proteins in the EC+TM FGFR3 constructs and full-length FGFR3 phosphorylation.

	Intrinsic FRET	D(Å)
FGFR1	0.66 ± 0.03	48 ± 1
FGFR1+fgf1	0.57 ± 0.01	51 ± 1
FGFR1+fgf2	0.58 ± 0.01	50 ± 1
FGFR2	0.43 ± 0.02	56 ± 1
FGFR2+fgf1	0.55 ± 0.01	51 ± 1
FGFR2+fgf2	0.69 ± 0.01	46 ± 1
FGFR3	0.55 ± 0.02	51 ± 1
FGFR3+fgf1	0.59 ± 0.01	50 ± 1
FGFR3+fgf2	0.59 ± 0.01	50 ± 1

Table S1(2-3). Intrinsic FRET, measured for the full-length receptors in the absence and presence of ligand. In this case, the fluorescent proteins are attached to the long flexible C-terminal tails of the full-length receptors (which vary in sequence and length), complicating direct structural interpretation of the data. Yet, we see significant changes in Intrinsic FRET upon ligand binding for FGFR1 and FGFR2, consistent with the idea that both fgf1 and fgf2 binding leads to structural changes in the receptor dimers.

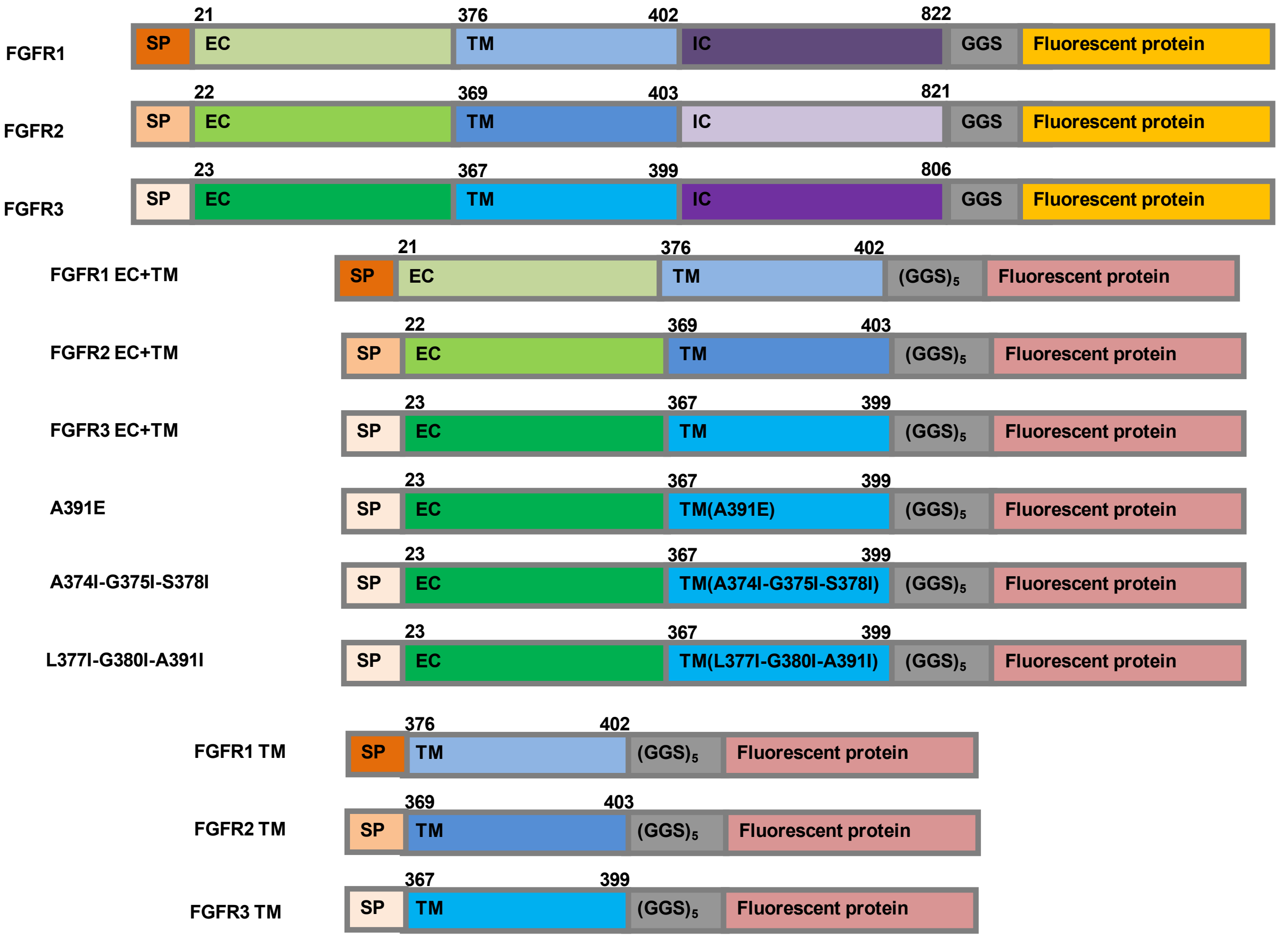

Figure S1(2-8). The plasmid constructs used in the FRET experiments. SP: signal peptide, EC: extracellular domain, FGFR3 TM domain: (DEAGSVYAG ILSYGVGFFLFILVVAAVTLCRLR), IC: intracellular domain, FP: Fluorescent protein, either YFP or mCherry (a FRET pair). The full-length receptors had fluorescent proteins attached to their C-termini via a flexible GGS linker. The truncated receptors had the intracellular domain substituted with a fluorescent protein, which was attached to the TM domain via a longer flexible $(GGS)_5$ linker.

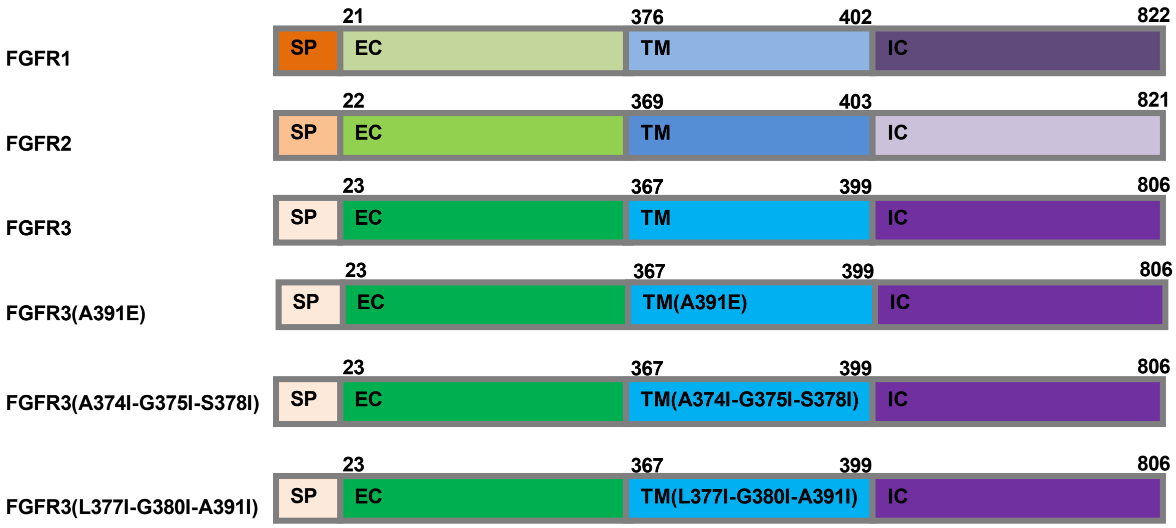

Figure S2 (2-9). The plasmid constructs used in Western blot experiments.

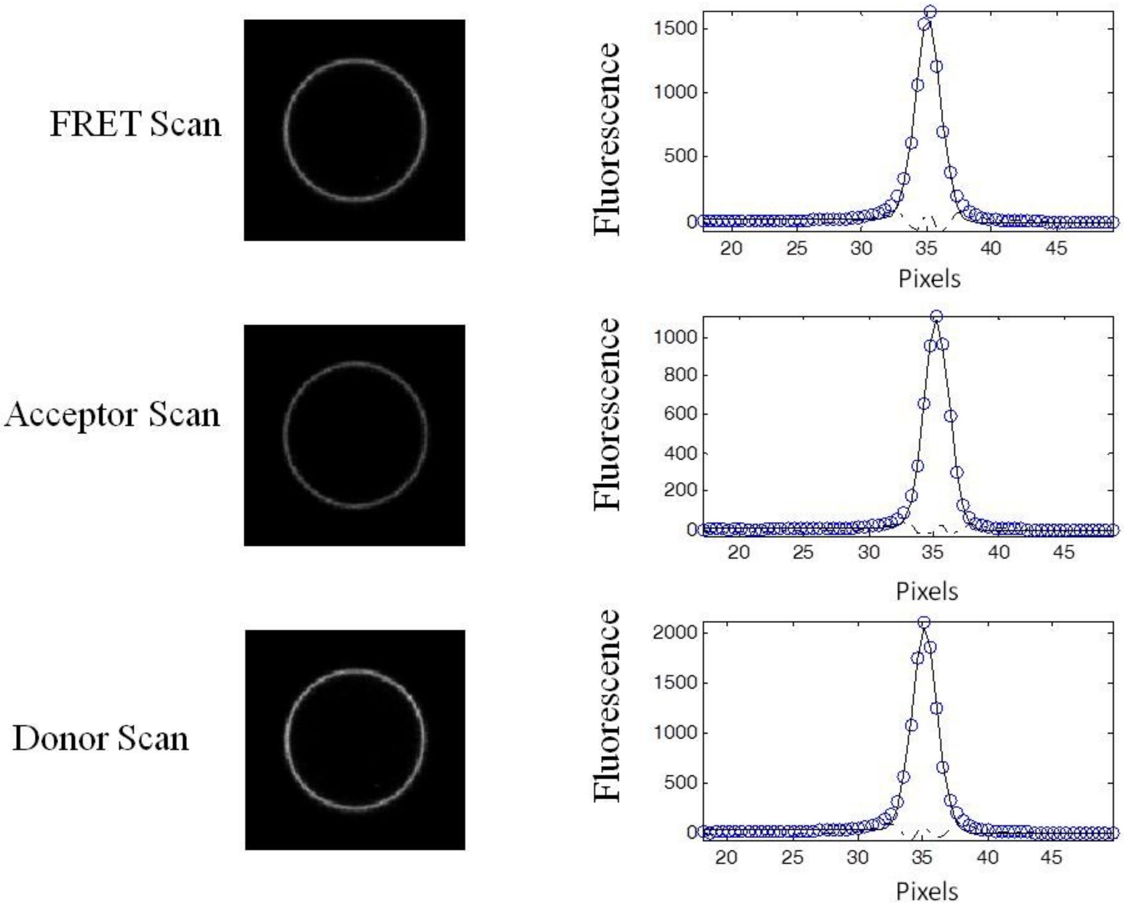

Figure S3 (2-10). One vesicle, imaged in the FRET, acceptor, and donor channels. A Gaussian function (black line) was fitted to the fluorescence intensity across the membrane (blue symbols) after correcting for background fluorescence. The residuals from the fits are shown with the dashed lines.

Figure S4 (2-11). Relative phosphorylation of mature FGFR1 in the absence of ligand, as a function of FGFR1 expression. (A) Western blot results. Varying levels of receptor expression were achieved by varying the amount of plasmid used for transfection from 0.25 µg to 2 µg. (B) The ratios of phospho-staining to receptor staining intensities were calculated and scaled with respect to the results from the first lane (2 µg of DNA). Only the top bands containing the mature fully glycosylated FGFR1 were included in the quantification. The relative phosphorylation increases with receptor expression, as predicted by the dimer model and by the law of mass action.

Figure S5 (2-12). FRET efficiencies, donor concentrations and acceptor concentrations, measured for the wild-type EC+TM FGF receptors. Each data point represents a single vesicle.

Figure S6 (2-13). Phosphorylation of FGFR1, FGFR2, and FGFR3, characterized via Western blotting. Lane "CHO": no transfection; Lane "-": no ligand; Lane "fgf1": 5 μg/ml fgf1; Lane "fgf2": 5 μg/ml fgf2.

Figure S7 (2-14). FGFR3 TM domain structure in micelles, solved by NMR (8). (A) The solved structure is tightly packed. (B) The amino acids L377, G380, and A391 mediate the helix-helix contacts in the structure, based on inter-helical NOEs that were measured experimentally. We mutated these three amino acids to Ile in order to disrupt this "NMR interface". (C) Amino acids A374, G375 and S378 participate in several GxxxG-like motifs (also known as SMALLxxxSMALL motifs), known to mediate TM helix dimerization, but do not play a role in helix packing in the NMR structure (8). These GxxxG motifs have been proposed to stabilize a putative alternative FGFR3 TM dimer structure (8). Here we mutated A374, G375 and S378 in order to disrupt this putative dimer interface. (D) Amino acids A374, G375 and S378 face predominantly lipids in the NMR structure.

Figure S8 (2-15). FRET data for the EC+TM FGFR3 (L377I-G380I-A391I) mutant

Figure S9 (2-16). FRET data for the EC+TM FGFR3 (A374I-G375I-S378I) mutant.

Figure S10 (2-17). Phosphorylation of the L377I-G380I-A391I and A374I-G375I-S378I mutants, characterized via Western blotting. Lane “WT”: wild-type FGFR3, no ligand; Lane “M“: mutant, no ligand; Lane “+fgf1”: mutant + 5 μg/ml fgf1; Lane “+fgf2”: mutant + 5 μg/ml fgf2.

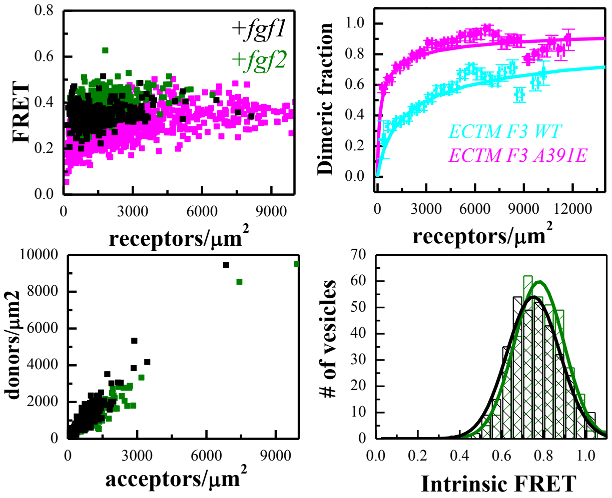

Figure S11 (2-18). FRET data for the A391E EC+TM FGFR3 mutant. The A391E mutation is the genetic cause for Crouzon syndrome with acanthosis nigricans. Data in the absence of ligand are from (JM paper).

391

DEAGSVYAGILSYGVGFFLFILVV**E**AVTLCRLR

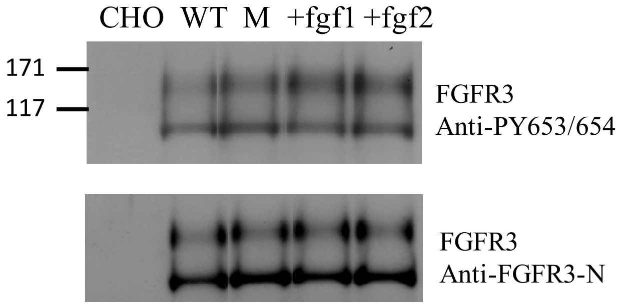

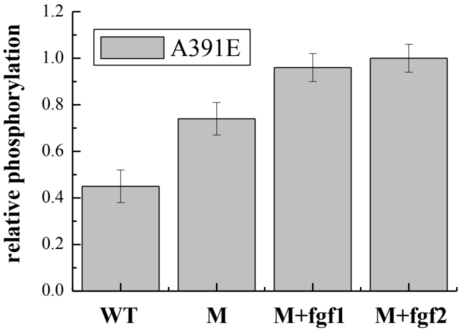

Figure S12 (2-19). Phosphorylation of the pathogenic A391E mutant, characterized via Western blotting. Lane “CHO”: no transfection; Lane “WT”: wild-type FGFR3, no ligand; Lane “M“: mutant, no ligand; Lane “+fgf1”: mutant + 5 μg/ml fgf1; Lane “+fgf2”: mutant + 5 μg/ml fgf2.

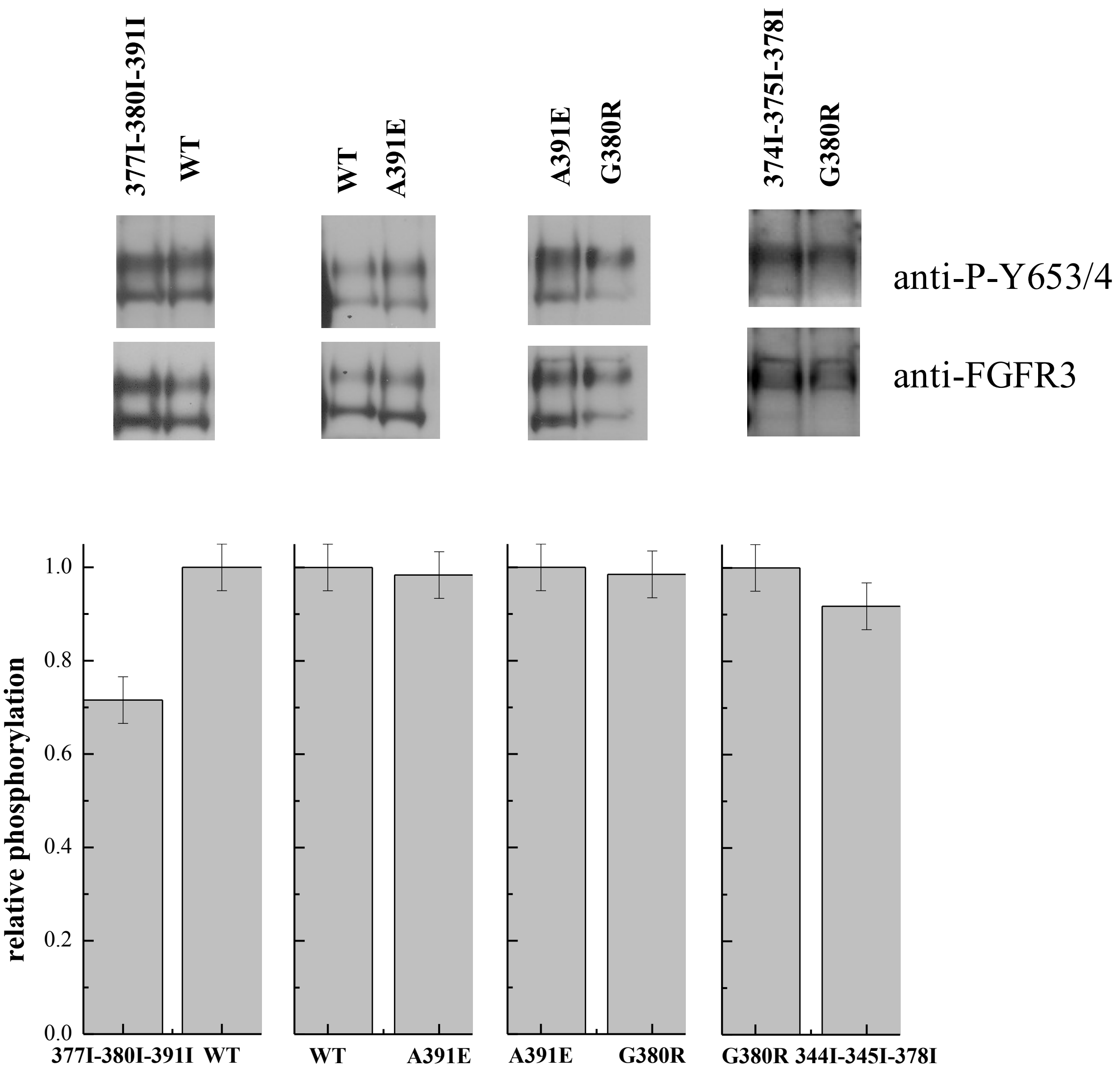

Figure S13 (2-20). Relative phosphorylation of wild-type FGFR3 and the FGFR3 mutants studied here, in the presence of saturating fgf2 concentrations. The relative phosphorylation was calculated as the ratio of anti-phospho band staining intensity divided by the anti-receptor staining intensity. Only the fully glycosylated mature FGFR3 top bands are included in the calculation. Shown are pair-wise comparisons for receptors run on the same gel, with one of the receptors in each pair assigned a value of 1.

Chapter 3. Mechanism of VEGFR2 signal transduction across the plasma membrane

Abstract

Here we demonstrate that VEGFR2 forms dimers in the absence of ligand, and that these dimers undergo a structural change upon binding the ligands VEGF-A_{121}, VEGF-A_{165}, VEGF-C and VEGF-D. The structural change entails a movement of the transmembrane domain C-termini away from each other, and correlates with receptor activation. Furthermore, we show that the pathogenic C482R mutation resembles the structural effects of the ligand, trapping VEGFR2 in its most active state. Investigations with three other VEGFR mutants reveal that mutations can easily alter the structures and stabilities of both unliganded and liganded VEGFR2 dimers, sometimes with profound functional consequences. Our results challenge the current paradigm that VEGFR dimerization and activation occur only in response to ligand binding. They establish that unliganded VEGFR2 dimers are an important intermediate in the process of VEGF signal transduction across the plasma membrane.

Keywords: VEGFR, vegf, angiogenesis, receptor tyrosine kinase, unliganded dimerization, dimer stability

3.1. Introduction

Angiogenesis, the development of new blood vessels from pre-existing ones, is critically important for embryogenesis, organ development, and wound healing (100, 116) (1). Angiogenesis is also tightly linked to cancer, as the growth of all solid tumors require the recruitment of new blood vessels to supply nutrients (87, 150). Thus, a therapy that inhibits angiogenesis would be applicable to many human cancers. In addition, a therapy that promotes angiogenesis could be used to restore blood supply to ischemic tissues in heart disease and in stroke.

Angiogenesis is predominantly regulated by the ligands and receptors of the vascular endothelial growth factor (VEGF) signaling network (41, 72, 92, 103, 135). Of the three receptors, VEGFR2 is the primary regulator of endothelial cell proliferation and migration (46, 146), VEGFR-2 is expressed in virtually all human vascular endothelial cells, and is overexpressed in many solid tumors (139, 164). There is a correlation between cancer survival and VEGFR-2 signaling, as aggressive cancerous phenotypes correlate with enhanced signaling (18). Thus, VEGFR2 is recognized as an attractive therapeutic target.

VEGFR2 is a receptor tyrosine kinase (RTK), and conducts biochemical signals via lateral dimerization in the membrane. Like all RTKs, VEGFR has four domains: an extracellular (EC), a transmembrane (TM) domain, and an intracellular (IC) domain composed of a juxtamembrane (JM) domain, a kinase domain, and a tail (Figure 1) and an intracellular catalytic (IC) domain. The EC domain of VEGFR is large, consisting of seven immuloglobulin-like (Ig-like) domain, termed D1 (at the N-terminus) to D7 (closest to the membrane). VEGFR2 binds to, and is activated by the ligand VEGF-A, as well as the processed forms of VEGF-C and VEGF-D. The binding affinity of VEGFR2 is highest for VEGF-A, and the signaling through the VEGF-A/VEGFR2 complex is considered the most angiogenic signaling pathway (41, 72, 92, 103, 135).

Many aspects of VEGFR2 dimerization and activation are not well understood, and this lack of knowledge is one bottleneck in the development of targeted VEGFR2 therapies. In the RTK field, currently is no consensus model of RTK signal transduction across the plasma membrane. Instead, two models are most often discussed in the literature. The first is the "diffusion-based" or "canonical" model, in which RTKs are monomers in the absence of ligand, and dimerize only upon ligand binding. Ligand-driven dimerization brings the two catalytic domains into close proximity, allowing for their efficient cross-phosphorylation. The second model is the "pre-formed dimer model", in which the receptors are dimeric in the absence of ligand, and ligand binding induces a structural change that reorients the catalytic domain to allow for efficient cross-phosphorylation. The difference between the two models lies in the absence and presence of unliganded dimers. High resolution structures for VEGF/VEGFR complexes revealed that extracellular D2 and D3 are involved as ligand binding pocket (13, 78).

While unliganded dimers have been described for some RTKs, it not known which model adequately describes the activation of most RTKs. The "diffusion-based" or "canonical" model of RTK activation, is the model used in textbooks and in highlighting drug development efforts by pharmaceutical companies. Unliganded VEGFR dimers have not been reported in the literature, and thus (by default) their activation is assumed to follow the canonical model. Though various domains in the extracellular region have been investigated for their role in ligand-dependent and ligand-independent VEGFR2 dimerization. Domains 4 and 7 of VEGFR2 are implicated in homotypic contacts of the receptor in the presence of ligand (65, 71, 120).

Here we study the behavior of the VEGFR2 receptor in the absence of ligand, and the response of the receptor to VEGFA121, VEGFA165, VEGF C and VEGF D, in the presence of missense and domain replacement mutations in order to gain insights into the mechanism of VEGFR2 activation.

3.2. Materials and Methods

The YFP plasmid was received from Dr. M. Betenbaugh (Johns Hopkins University, Baltimore, MD) and the pRSET-mCherry plasmid was obtained from Dr. R.Tsien (University of California, San Diego). All of the truncated plasmid constructs used for mammalian expression were constructed with pcDNA 3.1(+) vector (Invitrogen). The full length VEGFR2 (KDR) and V769E and C342R mutants were constructed in pBE vector. The full length (D4→D5) and (D7→D6) were constructed in pLib and pc5Frt vectors respectively. All primers were purchased from Invitrogen.

To generate VEGFR2-(GGS)-mCherry and VEGFR2-(GGS)-YFP, MluI restriction site was created in the multiple cloning site of the pBE vector which had full length human VEGFR2 (KDR) insert. The cDNAs encoding YFP and mCherry were then amplified using Polymerase Chain Reaction (PCR) and double digested with MluI and XhoI. The double digested YFP and mCherry cDNAs were then ligated to the C-terminus of digested pBE-VEGFR cDNA.

The sequence encoding for the EC and TM domains of VEGFR2 were amplified by PCR, double digested using HindIII and EcoRI restriction enzymes and inserted into $(GGS)_5$-

YFP and (GGS)$_5$-mCherry pcDNA3.1(+) vectors containing a flexible 15 amino acids GGS linker and YFP or mCherry fluorophores, to produce VEGFR2 EC-TM-(GGS)$_5$-YFP, VEGFR2 EC-TM-(GGS)$_5$-mCherry plasmids.

The V769E and C482R mutant full length VEGFR2 constructs (VEGFR2$_{V769E}$, VEGFR2$_{C482R}$), VEGFR2 EC-TM$_{V769E}$-(GGS)$_5$-YFP, VEGFR2 EC-TM$_{V769E}$-(GGS)$_5$-mCherry, VEGFR2 EC-TM$_{C482R}$-(GGS)$_5$-YFP, VEGFR2 EC-TM$_{C482R}$-(GGS)$_5$-mCherry plasmids were created using QuickChange ® II XL Site-Directed Mutagenesis Kit (Stratagene, CA).

The VEGFR2$_{D4\rightarrow D5}$ was generated by replacing domain 4 of VEGFR2 with domain 5 of VEGFR1. The VEGFR2$_{D7\rightarrow D6}$ construct was created by replacing domain 7 of VEGFR2 with domain 6 of VEGFR1 (detailed in (65)).

The VEGFR2$_{D7\rightarrow D6}$ was generated by replacing domain 7 of VEGFR2 with domain 6 of VEGFR1. The VEGFR2$_{D7\rightarrow D6}$ construct was created by replacing domain 7 of VEGFR2 with domain 6 of VEGFR1 (detailed in (65)).

To construct VEGFR2 EC-TM$_{D4\rightarrow D5}$-(GGS)$_5$-YFP and VEGFR2 EC-TM$_{D4\rightarrow D5}$-(GGS)$_5$-mCherry plasmids, cDNA encoding EC-TM$_{D4\rightarrow D5}$ was amplified from VEGFR2$_{D4\rightarrow D5}$ plasmid construct. This cDNA was then double digested with HinIII and EcoRI. The digested cDNA was then ligated with pcDNA3.1(+)-(GGS)$_5$-YFP or pcDNA3.1(+)-(GGS)$_5$-mCherry double digested with Hind III and EcoRI.

To construct VEGFR2 EC-TM$_{D7\rightarrow D6}$-(GGS)$_5$-YFP and VEGFR2 EC-TM$_{D7\rightarrow D6}$-(GGS)$_5$-mCherry plasmids, cDNA encoding EC-TM$_{D7\rightarrow D6}$ was amplified from VEGFR2$_{D7\rightarrow D6}$ plasmid construct. This cDNA was then double digested with HinIII and EcoRI. The digested cDNA was then ligated with pcDNA3.1(+)-(GGS)$_5$-YFP or pcDNA3.1(+)-(GGS)$_5$-mCherry double digested with Hind III and EcorI.

To generate VEGFR2 TM-(GGS)$_5$-YFP, VEGFR2 TM-(GGS)$_5$-mCherry plasmids, the sequence encoding the TM domain of VEGFR2 (GAQEKTNLE**IIILVGTAVIAMFFWLLLVII**LRTVKR) was amplified using PCR. This cDNA was then double digested with HindIII and EcoRI and ligated with digested pcDNA3.1(+)-(GGS)$_5$-YFP or pcDNA3.1(+)-(GGS)$_5$-mCherry.

3.2.1. Cell culture and transfection

Chinese Hamster Ovary cell (CHO) cells were cultures at 37 ˚C with 5% CO_2 for 24h. Transfection was carried out using Fugene HD transfection reagent (Roche Applied Science), following the manufacturer's protocol. Cells were cotransfected with 3-7 ug of DNA encoding VEGFR2-YFP and VEGFR2-mCherry constructs. Cells were vesiculated 24 h post transfection as described below. We have not observed staining for VEGFR2 (via Western blots) in the above cells unless transfected.

3.2.2. Production of mammalian plasma membrane vesicles

Vesiculation was performed using a chloride salt vesiculation buffer (33) consisting of of 200 mM NaCl, 5 mM KCl, 0.5 mM $MgSO_4$, 0.75 mM $CaCl_2$, 100 mM bicine and protease inhibitor cocktail (Complete mini EDTA-free tabs, Roche Applied Science) adjusted to PH of 8.5. CHO cells were rinsed twice with 30% PBS (pH 7.4), and incubated with 1 mL of chloride salt vesiculation buffer overnight at 37 °C. A large number of vesicles were produced after 12 h, and the vesicles were transferred into 4-well Nunc Lab-Tek II chambered coverslips for imaging.

In the past, we have observed that when we express soluble fluorescent proteins in cells and we vesiculate with this procedure, the fluorescent proteins are not found within the vesicles, suggesting that at least some of the cytoplasmic content is lost during vesicle production.

3.2.3. Treatment with VEGF. CHO cells were cultured in normal medium for 24 h following transfection for 24 h. The cells were then vesiculated with osmotic stress buffer overnight. The vesicles (1 mL) were collected in one well of a 4 chambered slide and treated with 2500 ng/mL of VEGF-A_{121}, VEGF-A_{165} (Cell Signaling Technologies), VEGF-C and VEGF-D (PeproTech, USA) were added to the serum-free medium. After incubating for 1 h at room temperature with ligand, the vesicles were imaged using a Nikon confocal microscope.

3.2.4. QI-FRET Image Acquisition

Vesicles were imaged using a Nikon Eclipse confocal laser scanning microscope using a 60× water immersion objective. All the images were collected and stored at a 512 × 512 resolution. Three different scans were performed for each vesicle: (1) excitation at 488 nm, with a 500-530 nm emission filter (donor scan); (2) excitation at 488 nm, with a 565-615 nm emission filter (FRET scan); and (3) excitation at 543 nm, with a 650 nm longpass filter (acceptor scan). Gains of 8.0 were used for all the three scans. The bleaching of the fluorescent proteins was minimized through the use of ND8 filters when excitation with the 488 nm laser, and low pixel dwell time (1.68 μs).

3.2.5. QI-FRET data Analysis: Methodology and Protocol

The QI-FRET method has been described previously (22, 81).

3.2.6. Western blots

CHO cells were starved in serum-free medium for 24 h following transfection and then treated with lysis buffer (25 mM Tris-HCl, 0.5% Triton X-100, 20mM NaCl, 2 mM EDTA, phosphatase inhibitor and protease inhibitor, Roche Applied Science). Lysates were collected following centrifugation at 15,000 g for 15 min at 4 °C and loaded onto 3–8%NuPAGE®Novex®Tris–Acetatemini gels (Invitrogen, CA). The proteins were transferred onto a nitrocellulose membrane, and blocked using 5% milk in TBS. VEGFR2 total protein levels were assessed using antibody against VEGFR2 (55B11; Cell Signaling Technologies) or anti-HA tag (ab9134; abcam). Phosphotyrosine levels were assessed using Phospho-VEGFR2 receptor antibody (Tyr1054/1059; #3817, Cell Signaling Technologies). The endogenous VEGF-A levels were detected by staining with anti-VEGF-A antibody (PA1080, Boster Biological Technology Co, USA).This was followed by anti-rabbit HRP conjugated (W4011, Promega) and Goat anti-rat (sc-2006, Santa Cruz Biotechnology) HRP conjugated antibodies. The proteins were detected using the Amersham ECL detection system (GE Healthcare).

3.2.7. Cross-linking Experiments. Following a 24h starvation, CHO cells expressing full length VEGFR2, EC+TM VEGFR2 WT were subjected to cell surface cross-linker and lysed for western blotting. The cells transfected with full length VEGFR2, EC+TM VEGFR2 WT were incubated with 2 mM membrane impermeable crosslinker BS^3 (Pierce) for 30 min at room temperature. The cells transfected with TM VEGFR2 WT and TM VEGFR2 V769E were incubated with 2 mM membrane permeable crosslinker EGS (Pierce) for 60 min at room temperature. All samples were quenched in 20 mM Tris-HCl for 15 min. After one rinse with ice-cold PBS, the cells were lysed and the receptors were detected using Western blotting. Following the cross-linking and PBS washes, the cells were then treated with lysis buffer (25 mM Tris-Cl, 0.5% TritonX-100, 20 mM NaCl, 2 mM EDTA, 2 mM Na_3VO_4 and protease inhibitor, Roche Applied Science). The lysates were collected following centrifugation at 15,000 g for 15 minutes at 4^{o}C and loaded onto 3–8% NuPAGE® Novex® Tris-Acetate mini gels (Invitrogen, CA). The proteins in the gels were transferred simultaneously onto a nitrocellulose membrane, and blocked using 5% milk in TBS. VEGFR2 total protein levels were probed with antibodies against VEGFR2 (#2479; Cell Signaling Technology) and anti-HA tag (ab9134; abcam), followed by HRP conjugated antibodies anti-Rabbit (W4011, Promega) and Goat anti-rat (sc-2006, Santa Cruz Biotechnology) respectively. The membranes were incubated with substrate (Amersham ECL Plus™ Western Blotting Detection Reagent) for 2 minutes. The x-ray film was exposed for 3 minutes.

3.3. Results

3.3.1. Full-length VEGFR2 dimerizes in the absence of ligand

VEGFR2 can dimerize in the absence of ligand. Unliganded dimers have been reported for other RTKs (84, 86), and they have been shown to play an important biological role by potentiating the response of the receptor to ligand. Unliganded VEGFR dimers has not been investigated in the literature, and thus (by default) VEGFR2 activation is assumed to be canonical. To characterize the unliganded dimerization of full-length VEGFR2, we used a FRET method that gives quantitative dimerization propensities of RTKs (22). Measurements were performed in plasma membrane derived vesicles using the QI-FRET method as previously described. These experiments were designed such that receptor concentrations varied over one to two orders of magnitude, and the concentrations of the receptors are measured in the plasma membrane-derived vesicles, along with FRET efficiencies. Thus, we can assess if the data is described by a dimerization model, calculate dimeric fractions, and dimerization free energies.

Plasmids encoding for full-length VEGFR2 linked to fluorescent proteins at the C-terminus were constructed as shown in Materials and Methods. CHO cells were co-transfected with plasmids encoding for VEGFR2-YFP and VEGFR2-mCherry. CHO cells do not express VEGFR2 or VEGFA (Figure 3), and thus the CHO cell line is appropriate for these experiments. After VEGFR2 was expressed and trafficked to the plasma membrane, the cells were vesiculated by applying osmotic stress as described. Each vesicle was imaged, and FRET efficiencies, donor concentration, and acceptor concentration were determined for each vesicle. The measured FRET efficiency for each vesicle is shown as a function of acceptor concentration in Figure 1 (red solid symbols). With the solid line, we show the so-called proximity FRET which occurs due to random approach of donors and acceptors, in the absence of specific FRET. This contribution has been characterized in detail in previous work. We see that FRET significantly exceeds the proximity FRET values, indicative of specific interactions.

The donor versus the acceptor concentration and the corrected FRET as a function of total concentration in each vesicle are plotted in Figure 1. The FRET data are then used to determine both the dimer stabilities (ΔG) and I-FRET as discussed in Supplemental Material. The dimer stabilities are a quantitative measure of the dimerization propensity. The measured I-FRET value depends on the dimer structure, in particular on the distance and orientation of the fluorescent proteins in the dimer. The values are given in Table 1.

In Figure 1D we show the averaged dimeric fractions as well as the dimerization curve for full-length VEGFR2.

The dimerization free energy is -6.1 kcal/mole. To evaluate the significance of dimerization, we examined the dimerization curves for physiological VEGFR2 expression levels. VEGFR2 expression levels have been reported as 10^4 to 10^5 per cell, corresponding to 10 to 100 receptors per square microns. We note that over this expression range expressions, 30% to 60% of full-length VEGFR2 are predicted to be dimeric. These data demonstrate that VEGFR2 has a strong dimerization propensity and thus does not follow the canonical activation model, contrary to popular belief.

3.3.2. VEGFR2 is autophosphorylated in the absence of ligand

To further investigate if VEGFR2 can dimerize in the absence of ligand, we performed cross-linking experiments as described in Materials and Methods, using Western blotting. A cross-linked dimeric band for full-length VEGFR2 was observed in these experiments, confirming the FRET results that VEGFR2 can dimerize in the absence of ligand.

Some RTKs have been shown to form phosphorylated dimers in the absence of ligand. To learn if VEGFR can be phosphorylated in the absence of ligand, we measured the phosphorylation full-length VEGFR2 receptors in the absence of ligand. We probed the phosphorylation of the tyrosines in the activation loop of the VEGFR2 kinase using anti-P-Y1054/Y1059 antibodies. Experiments were performed after starving for 24 hours, to remove any traces of growth factors. This fact, and the fact that CHO cells do not produce VEGF (Figure 3), allowed us to investigate the phosphorylation of unliganded VEGFR2 dimers. The blots, shown in Figure 2, demonstrate tyrosine phosphorylation in the absence of ligand. The results in Figure 2 support the idea that VEGFR2 dimerizes and is at least partially phosphorylated in the absence of ligand.

3.3.3. The extracellular domain inhibits VEGFR2 dimerization. The intracellular domain is not required for dimerization but significantly stabilizes VEGFR2 dimers.

To understand how the unliganded dimer is stabilized, we asked how the three different VRGFR2 domains (EC, TM, and IC) contribute to the stability of the unliganded dimers. To answer this question, we performed experiments with two truncated VEGFR2 constructs, one lacking the IC domain (a EC+TM construct) and one lacking both the EC and IC domains (a TM construct). The TM construct includes the VEGFR2 signal peptide (to be cleaved), VEGFR2 TM domain, a $(GGS)_5$ flexible linker, and fluorescent proteins. The EC+TM construct also includes the VEGFR2 EC domain (see Figure 1B). The results for these two constructs are shown in Figure 1 with the olive and black symbols, and in Table 1.

From Figure 1d, we see that: (i) the isolated TM domain forms dimers (dimer stability ΔG = -4.5 kcal/mole). (ii) the EC domain inhibits dimerization ($\Delta\Delta G$ = +1.1 kcal/mole), such that the stability of the EC+TM dimer is reduced to -3.4 kcal/mole. (ii) The IC domains stabilize the dimer by -2.7 kcal/mole. Thus, we show that the EC domain inhibits unliganded VEGFR2 dimerization, while the TM and IC domains promote dimerization (i.e. stabilize unliganded dimers).

The results show that the TM and EC+TM constructs exhibit the same I-FRET value (I-FRET ≈ 0.61). The latter finding suggests that the addition of the EC domain does not alter the separation of the C-termini of the TM domains in the dimer. On the other hand, the I-FRET values are distinctly different when the kinase domain is present, as expected, reflecting the difference in the attachment of the fluorescent proteins to the full-length and truncated receptors.

Previous results (Figure S2A from (90)) agree with our results. These previous findings show that phosphorylation of VEGFR dramatically increased upon removal of the EC domain (phosphorylation of full VEGFR2 compared to TM+IC).

3.3.4. Bound ligand causes a structural change in the receptor. VEGF-A_{121}, VEGF-A_{165}, VEGF-C and VEGF-D induce similar structural change in the VEGFR2 dimer.

The idea of a structural change in RTK dimers upon ligand binding is a key concept in the pre-formed dimer model. According to this paradigm, the unliganded dimers lack full activity because the kinase domains are not positioned optimally with respect to each other. Upon ligand binding, there is a structural change in the extracellular domain that propagates to the kinase domain. The TM domain can be expected to play a key role in this process, as it mediates the connection between the two soluble domains. However, structural changes are very challenging to detect directly in the native plasma membrane due to experimental limitations. Experiments in the RTK literature often utilize isolated RTK domains, and there are NO high resolution full-length RTK dimer structures. Thus, structural changes are difficult to capture experimentally even in model systems. For some RTKs, a large change in the separation between the C-termini of the TM domain has been proposed to occur upon ligand binding. We therefore asked if the VEGFR ligands can induce a change in the separation of the TM domain C-termini. To answer this question, we compared the I-FRET values for the EC+TM constructs in the absence of ligand and in the presence of 3 ligands.

In the absence of ligand, the Intrinsic FRET is obtained via two parameter fits as in Figure 1 (solid black squares), and the I-FRET value is 0.61, corresponding to separation between the proteins of 49 ± 1Å. In the presence of high ligand concentrations, when all receptors become 100% liganded dimers, the measured FRET signal does not depend on the concentrations of the receptors. We therefore preformed the FRET experiments in the presence of ligands at very high concentrations (2.5 μg/ml). The goal here was to ensure that the receptors are in the liganded dimeric state, such that the measured FRET signal depends only on the distance and orientation of the fluorescent proteins and on the donor-to-acceptor ratio (and not on dimerization).

Data are shown in Figure 4. Consistent with expectation, the FRET efficiency does not depend on receptor concentration, suggesting that the dimeric fraction becomes 100% for all receptor concentrations. In the case of 100 % (constitutive dimerization) all the FRET experiments measure the value of the intrinsic FRET, after correcting for different donor-to-acceptor ratios. Figure 5 shows the distribution of the I-FRET values, which is about 0.42 corresponding to a separation between the proteins of 56 ± 2 Å.

Thus, we see that ligand binding changes the value of I-FRET for the EC+TM construct from 0.61 to 0.42. This change in I-FRET demonstrates that ligand binding leads to a structural change, suggesting that the fluorescent proteins become further apart in the dimer (illustrated in Figure 5). VEGF-A, VEGF-C and VEGF-D has been shown to induce the same activation which is consistent with the same structural changes we observe here.

3.3.5. The C482R mutation induces ligand-independent constitutive dimerization. The mutant unliganded dimer is similar to liganded wild-type dimers.

The C482R mutation in D5 of VEGFR2 is implicated in infantile hemangiomas, characterized by disorganized angiogenesis in infants. It was identified in cultured hemangioma endothelial cells from two out of 9 subjects investigated in the study (11). It is believed that this mutation leads to constitutive VEGFR signaling, through a mechanism that involved VEGFR2-mediated control over VEGFR1 expression (66). However, the effect of the mutation on VEGFR2 dimerization has not been investigated. Yet, mutations of Cysteines in RTK extracellular domains have been suggested to affect receptor dimerization. Therefore, we asked whether the C482R mutation might affect dimerization in the absence of ligand, as well as the dimer structure in the liganded state. With this goal in mind, we examined the unliganded dimerization of the mutant. The dimeric fraction did not depend on the concentration, similarly to the case when ligand was present, suggesting a constitutive dimer (Figure 6). Furthermore, the I-FRET value is exactly the same as measured in the presence of ligand. Thus, this mutation leads to constitutive dimerization of the VEGFR2 receptor, and the unliganded mutant dimer has the same structure as the liganded wild-type dimer. Thus, this mutation seems to emulate the effect of ligand. Further proof for this behavior comes from the fact that the addition of ligand does not alter dimerization (Figure 6). This finding is consistent with the idea that the mutant is dimeric, and that the unliganded mutant dimer adopts the liganded wild-type structure, prior to ligand binding. Importantly, Western blots under reducing and non-reducing conditions, shown in Supplementary data, show that disulfide bond formation does not play a role in dimer stabilization.

To investigate if VEGFR2 C482R is capable of ligand binding, we added saturating amount of VEGF121-Alexa Fluor to CHO vesicles expressing EC-TM-VEGFR2$_{C482R}$-(GGS)$_5$-YFP. As Figure 6 (right) demonstrates, the mutant receptor was fully capable of binding VEGF.

3.3.6. The V769E mutation causes a structural change in the isolated TM domain dimer, but stabilizes the dimer when the EC domain is present.

The phosphorylation of VEGFR2 increases upon ligand binding. We found that the liganded VEGFR2 structure is characterized by larger separation between the C-termini of the TM domains. Thus, it appears that kinase auto-phosphorylation activity is higher for larger separation between these C-termini. To further examine this relationship, we characterized mutants with different phosphor-tyrosine activities as compared to wild-type in the presence of ligand, and investigate if these mutants will give different I-FRET as compared to the wild-type. One such mutant is the V769E mutant, carrying a valine to glutamic acid substitution in its TM domain. The phosphorylation of the V769E mutant in the presence of VEGF121 is decreased when compared to wild type VEGFR2 (Figure S3 from (90)), however the activity of the V769E mutant is not different from VEGFR2 in the absence of ligand.

We performed experiments with the EC+TM and TM VEGFR2 constructs that carry the V769E mutation in the TM domain. In the absence of ligand, the dimer was more stable than the wild-type. Such dimer stabilization has been observed for other glutamic acid mutants in RTK TM domains, and can be interpreted as dimer stabilization die to the formation of E-mediated hydrogen bonds. The I- FRET value that we obtained is similar, suggesting that this hydrogen bond does not perturb the structure of the unliganded dimer. The I-FRET value in the presence of ligand, however, is distinctly different, and has a value of 0.54 (Figure 7). This is smaller than in the case of the liganded wild-type dimer, consistent with the connection between (i) distance between C-termini of the TM domains and (2) phosphorylation.

3.3.7. The D7(VEGFR2)→D6(VEGFR1) mutation affects ligand-independent and ligand-dependent dimerization, yet VEGFR2 is capable of binding to VEGFA$_{121}$. The D4(VEGFR2)→D5(VEGFR1) mutation completely inactivates VEGFR.

Studies in the literature have focused on mapping out possible contacts that stabilize the active ligand-bound state of the receptor. Electron microscopy (120) and small-angle solution scattering (71) studies of ECD of VEGFR2 in the presence of VEGF demonstrated that contacts occur between D7 and D4 subunits predominantly. Furthermore, a crystal structure of the D7 VEGFR2 dimer rvealed direct D7-D7 contacts (165). Thus, the current structural model postulates that the ligand-bound EC domain dimer is stabilized by ligand binding to D2 and D3, as well direct receptor-receptor contacts, specifically D4-D4 and D7-D7 contacts (120). These D4-D4 and D7-D7 contacts are believed to be essential as they establish the relative positioning of the receptors in the dimer, and ultimately affect the positioning of the kinase domains with respect to each other. Consistent with this view, changes in sequence within the putative contacts regions have been linked to decrease in receptor activity.

Here we sought to directly investigate if the liganded dimer is affected if the D4-D4 and D7-D7 contacts are disturbed. With this goal in mind, we examined two mutants in which D4 and D7 are not present. We reasoned that if the contacts between these domains indeed establish the active structure, we will obtain a value for I-FRET that is different from the wild-type. We therefore created EC+TM constructs that had the following substitutions D7(VEGFR2)→D6(VEGFR1) and D4(VEGFR2)→D5(VEGFR1).

We characterized the dimerization of the mutants in the presence and absence of ligand. The results are shown in Figures 8 and 9. Figure 8 demonstrates that the replacement of D7 of VEGFR2 with D6 of VEGFR1 affects both unliganded and liganded dimerization (data in open magenta and solid blue respectively). The measured FRET was not consistent with the dimerization model, suggesting the possibility of formation of higher order oligomers for this mutant.

Upon ligand addition, the FRET data overlapped with measurements in the absence of ligand. Thus, the dimerization was not changed in the presence of ligand. We therefore assessed the ligand binding capability of the mutant in the plasma membrane derived vesicles. As shown in figure 8 (right), VEGFA121 binds to $\text{VEGFR}_{\text{D7}\rightarrow\text{D6}}$, as observed in fluorescent microscopy experiments. This work suggests that ligand binds to the mutant oligomers, but does not stabilize these oligomers. The ligand does not induce a transition to a liganded dimer, either.

The results for ECTM $\text{VEGFR2}_{\text{D4}\rightarrow\text{D5}}$ construct are shown in Figure 9. This mutant forms dimers with slightly higher propensity compared to wild type VEGFR2. However, the dimer structure appears to be quite different from the wild-type, as suggested by the very high I-FRET observed for this mutant. Furthermore, upon ligand addition, we observed no change in the FRET data for this mutant, either. Unlike the D7 mutant, this mutant did not bind ligand (see Figure 9). We interpret this finding as a demonstration that the D4→D5 mutation induced a transition to a completely different dimer structure that is not observed for the wild-type. This novel structure does not bind ligand and does respond to it, and can be considered analogous to the "inactivated" third state of channels. This view is consistent with prior results of (65), which showed that this mutation of domain 4 completely inactivates the receptor.

3.4. Discussion

VEGFR2 is believed to exist in a monomeric form in the absence of ligand, and to follow the canonical model of ligand-induced dimerization and activation. Using a quantitative FRET-based assay that is specifically designed to probe receptor dimerization in the plasma membrane, we demonstrated that full-length VEGFR2 forms dimers in the absence of ligand. We further showed that VEGFR2 unliganded dimers are partially phosphorylated, using Western blotting. Both dimerization and phosphorylation increase with receptor expression, suggesting that they are correlated. Unliganded dimers have been previously observed for other RTKs, such as EGFR and FGFR. Thus, VEGFR2 shares a mode of activation with RTKs from different families.

The QI-FRET methodology can monitor structural changes in the cytoplasmic portion of the dimer in response to ligand binding to the extracellular domain. Here, the QI-FRET experiments directly demonstrated that ligand binding induces a structural change in the VEGFR2 dimer, in the plasma membrane. Since VEGFR2 TM domain has been previously suggested to play an active role in establishing the ligand-bound dimer structure, the experiments were performed with a truncated VEGFR2 construct in which the FPs were attached via a flexible (GGS)5 linker directly to the C-termini of the TM domain. Upon ligand binding, the Intrinsic FRET decreased from 0.61 to 0.42, corresponding to an increase in separation between the fluorescent proteins in the dimer from 49 to 56 Å. Thus, ligand binding increased the separation between the C-termini of VEGFR2 TM domains.

The phosphorylation of all VEGFR2 tyrosines is known to increase upon ligand addition. Therefore, the increase in separation between the C-termini of the TM domains correlates with an increase in phosphorylation. A similar mechanism of activation has been proposed for EGFR; the large separation between EGFR TM C-termini in the ligand-bound state is believed to create the space needed for the assembly of the active kinase dimer. However, the structural change observed for VEGFR2 upon VEGF binding is the opposite to the one observed for FGFR upon fgf2 binding. Thus, while a ligand-induced structural change seems to be a general principle of RTK activation, the exact nature of the change can be quite different for different receptors.

The significance of the ligand-bound state is highlighted by our results for the C482R VEGFR mutant, identified in infant hemangiomas. We showed that this mutant forms a constitutive dimer even in the absence of ligand. Since this mutation eliminates a cysteine and thus results in an unpaired cysteine, we expected that the mutant dimer is stabilized by a disulfide bond. The comparison of the Western blot results under reducing and non-reducing conditions, however, were identical, suggesting that this is not the case. The Intrinsic FRET measured for the mutant in the absence of ligand was the same as the

Intrinsic FRET measured for the WT in the presence of ligand. Thus, the C482R mutation forced the unliganded dimer into the WT liganded state, mimicking the effect of ligand.

Questions arise as to whether VEGFR2 dimers can exist in other configurations that are different from the unliganded and liganded states observed for the WT. Insights came from studies of the V769E mutant. The Intrinsic FRET for the mutant dimer in the presence of ligand is 0.54, a value that is not observed for the WT. The V769E mutation therefore destabilized the liganded state and induced a transition to a new dimer configuration. Thus, the VEGFR2 dimer exhibits a high degree of plasticity.

The plasticity of the VEGFR2 dimer is further confirmed by our results for the D4 and D7 mutants. The D4 mutant formed a dimer with very high intrinsic FRET, 0.82, corresponding to tightly packed TM C-termini. This state is structurally different from both the unliganded and liganded WT states, and is not capable of binding ligands. The D7 substitution induced a transition into yet another structural state. This mutant formed an oligomer, not a dimer, even in the absence of ligand. Unlike the D4 dimer, the D7 oligomer was capable of binding VEGFR. Yet, ligand binding neither stabilizes the D7 oligomer, nor altered its structure.

Previously, the decreased activation of D4 and D7 mutants upon ligand addition was interpreted as an indication that D4-D4 and D7-D7 contacts position the two receptors in the dimer correctly with respect to each other in the ligand-bound state. With the help of the QI-FRET methodology we demonstrated that, in fact, the D4 and D7 domain substitutions affected the unliganded state. VEGF either failed to bind to the altered structure (in the case of the D4 mutant), or failed to induce a transition to the liganded state (in the case of the D7 mutant). Thus, our work highlights the importance of the unliganded state as an intermediate in VEGFR2 signal transduction.

Based on our results, it can be argued that the inhibition of unliganded VEGFR2 dimers, in parallel to VEGFR2 liganded dimers, may be a new useful therapeutic strategy. With such future applications in mind, we sought new insight into the unliganded VEGFR2 dimer state. Here we measured the contributions of the different VEGFR2 domains to unliganded dimerization. First, we showed that VEGFR2 intracellular domain has a large favorable contribution to unliganded dimerization. Thus, targeting the interactions between VEGFR2 intracellular domains can significantly decrease unliganded VEGFR2 dimer populations. Second, we demonstrated that the contribution of the entire VEGFR2 EC domain to unliganded dimerization is inhibitory. One way to interpret this finding is to assume that the EC domains do not interact, and inhibit unliganded dimerization due to steric hindrance. This interpretation, however, is difficult to rationalize in view of our finding that the substitution of D4 and D7 significantly alters the unliganded state. It is thus possible that D4-D4 and D7-D7 interactions stabilize the unliganded VEGFR2 dimers, while other domains in the extracellular portion of the receptor have inhibitory contributions to unliganded dimerization.

Over-all, this work establishes the existence and the significance of VEGFR2 unliganded dimers. Very little is known about these dimers, and their high resolution structures are unknown. Future studies of these dimers will be required in order to arrive at complete mechanistic understanding of VEGFR signaling.

Figures

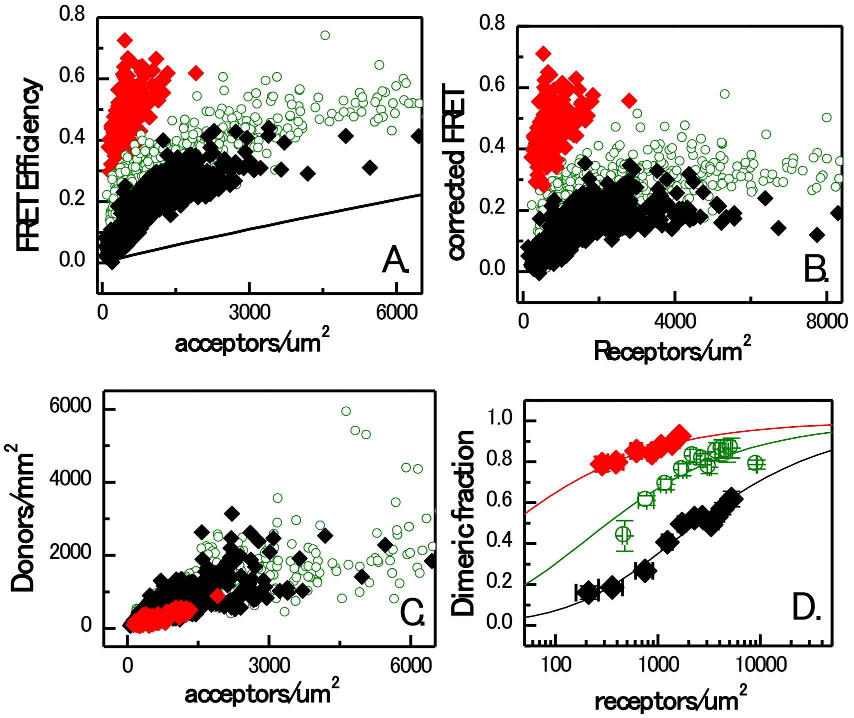

FRET Efficiency
0.8
0.6
0.4
0.2
0.0
0
3000
6000
acceptors/um^2
A.
corrected FRET
0.8
0.6
0.4
0.2
0.0
0
4000
8000
Receptors/um^2
B.
Donors/mm^2
6000
4000
2000
0
0
3000
6000
acceptors/um^2
C.
Dimeric fraction
1.0
0.8
0.6
0.4
0.2
0.0
100
1000
10000
receptors/um^2
D.

Figure 3-1. FRET data describing VEGFR2 dimerization. (A) FRET efficiencies as a function of acceptor concentration for full length VEGFR2 (solid red diamonds), EC-TM VEGFR2 (solid black diamonds), and TM VEGFR2 (open olive circles). A schematic of these receptor constructs is shown in Figure S1. (B) FRET efficiencies corrected for stochastic FRET. (C) Donor to acceptor values plotted for the three constructs. (D). Dimeric fractions versus total receptor concentrations, for the full-length VEGFR2 (red solid diamonds), EC+TM VEGFR2 (black solid diamonds), and the TM domains only (olive, open circles). The measured dimeric fractions are binned and are shown with the symbols, along with the standard errors. The solid lines are the best fits of a monomer-dimer equilibrium model to the data. These data demonstrate that the TM domains have a very strong propensity for dimerization. The EC domains, on the other hand, inhibit dimerization. The contribution of the IC domains is favorable (Table 1).

Variant	ΔG (kcal/mol)	Ẽ	Distance between fluorophores (Å)
Full length VEGFR2	-6.1 ± 0. 4	0.82 ± 0.06	41 ± 3
Wild Type EC+TM VEGFR2	-3.4 ± 0. 2	0.61 ± 0.05	49 ± 1
WT+VEGF A 121	-	0.45 ± 0.08	56 ± 2
WT+VEGF A 165	-	0.43 ± 0.09	56 ± 2
WT+VEGF C	-	0.43 ± 0.09	56 ± 2
WT+VEGF D	-	0.43 ± 0.09	56 ± 2
WT TM	-4.8 ± 0. 2	0.61 ± 0.05	49 ± 1
V769E TM	-4.8 ± 0. 2	0.78 ± 0.02	43 ± 1
D7 MUT	-	-	-
D7 MUT+VEGF 121	-	-	-
D4 MUT	-4.7(+0.5,-0.3)	0.82 (+0.1, -0.08)	41(+4,-3)
D4 MUT+VEGF 121	-4.7(+0.5,-0.3)	0.82 (+0.1, -0.08)	41(+4,-3)
C482R MUT	-	0.45 ± 0.08	56 ± 2
C482R MUT+VEGF 121	-	0.45 ± 0.08	56 ± 2
V769E ECTM MUT	-4.2 ± 0. 2	0.61 ± 0.05	49 ± 1
V769E ECTM MUT+VEGF 121	-	0.54±0.05	52± 1

Domain	$\Delta\Delta G_{IC}$	$\Delta\Delta G_{EC}$
VEGFR2	-2.7	1.4

Table 3-1. Dimerization free energies (dimer stabilities) ΔG and Intrinsic FRET efficiencies $\tilde{E}$, obtained from least-square parameter fits to the FRET data for full-length and truncated constructs that lack the IC domain (EC+TM) and both EC and IC (TM only).

[a]95% confidence intervals

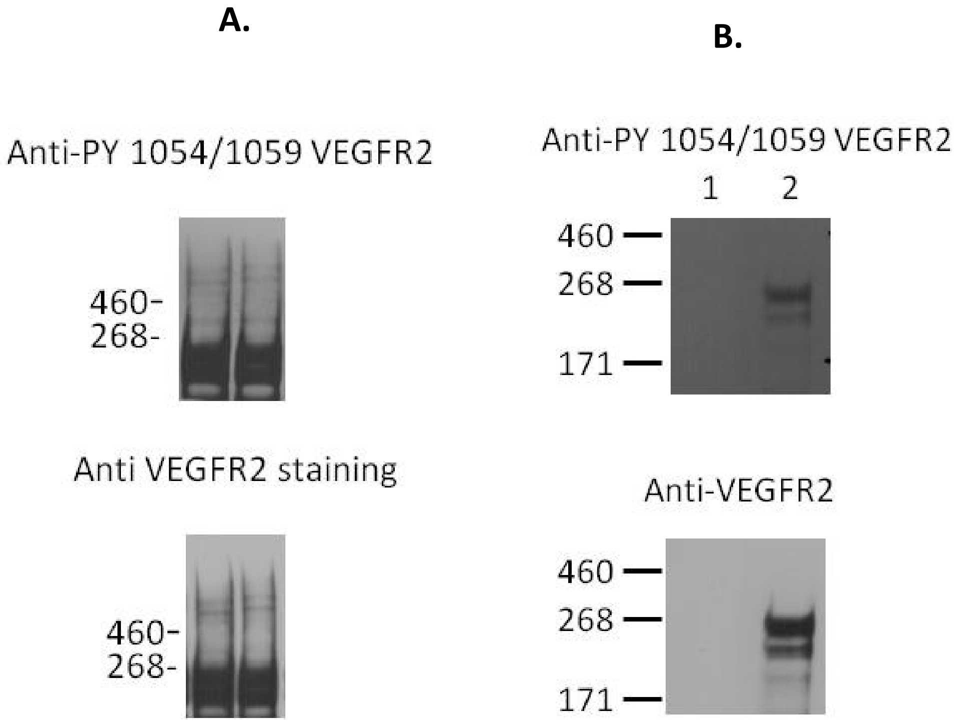

Figure 3-2. VEGFR2 cross-linking and phosphorylation in CHO cells. **(A)** BS3 cross-linking of CHO cells expressing VEGFR2. Cells were starved for 24 hours to ensure there was no ligand present. Staining with anti-VEGFR2 antibodies shows the presence of a glycosylated monomer band at MW ~ 240 kDa and glycosylated dimer band at MW ~ 480 kDa. These results support the FRET results in Fig. 1 that VEGFR2 forms ligand-independent dimers in the plasma membrane. **(B)** Western blots showing the expression and activation of full-length VEGFR2 in CHO cells in the absence of ligand, when a range of μg of DNA was used for transfection (Lane 2). The expression of the three receptors is probed with anti-VEGFR2 antibody. The phosphorylation of tyrosines in the activation loop of the three receptors is probed with anti-p-1054/1059 antibodies. We see antibody staining in all cases, suggesting that the probed tyrosines are phosphorylated in the absence of ligand. We did not observe VEGFR2 staining in CHO cells unless transfected (Lane 1)

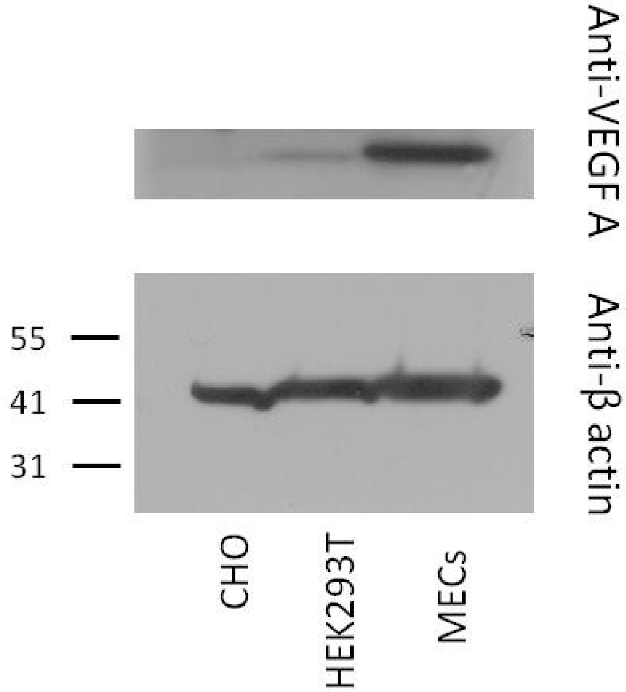

Figure 3-3. CHO, HEK293T and MEC (microvascular endothelial) cells stained for VEGF-A. The results show that CHO cells do not express VEGF-A endogenously.

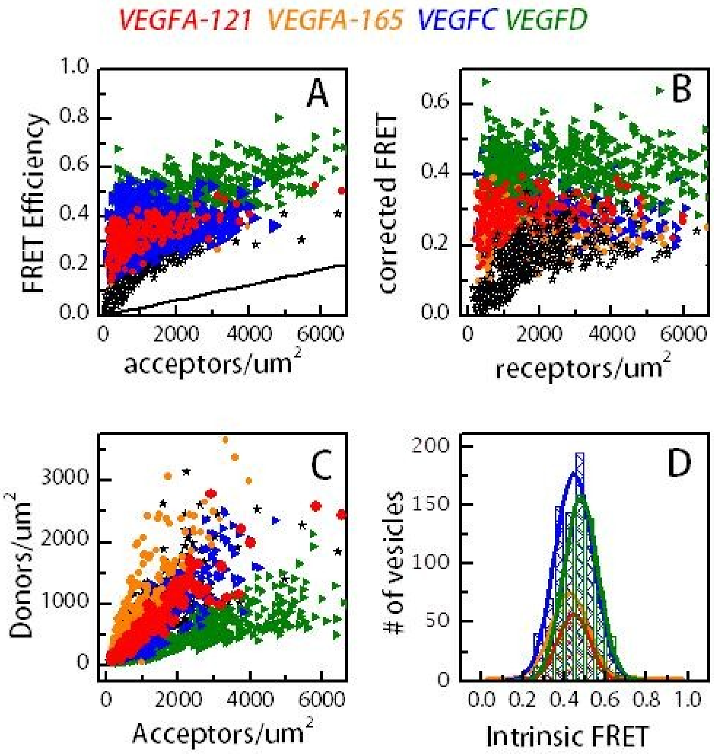
VEGFA-121 VEGFA-165 VEGFC VEGFD
A
FRET Efficiency
1.0
0.8
0.6
0.4
0.2
0.0
0
2000
4000
6000
acceptors/um^2
B
corrected FRET
0.6
0.4
0.2
0.0
receptors/um^2
C
Donors/um^2
3000
2000
1000
Acceptors/um^2
D
# of vesicles
200
150
100
50
0.0 0.2 0.4 0.6 0.8 1.0
Intrinsic FRET

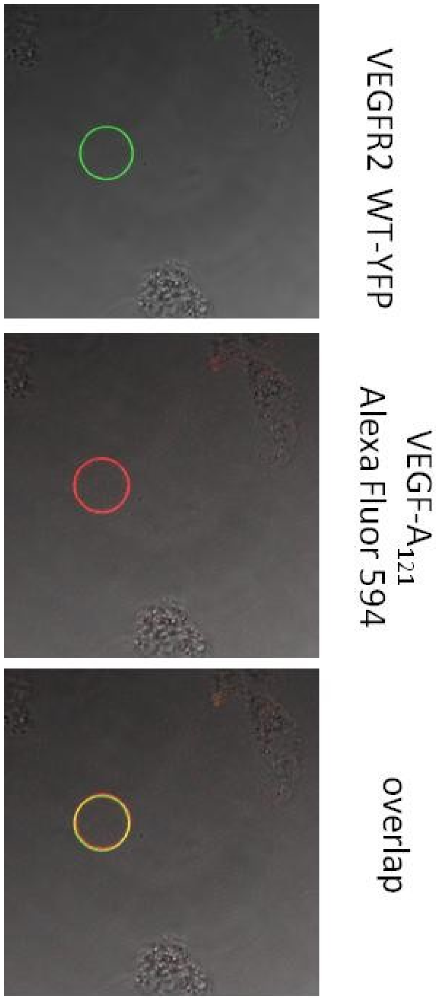
VEGFR2 WT-YFP
VEGF-A$_{121}$
Alexa Fluor 594
overlap

Figure 3-4. Left: (A) FRET efficiency measured as a function of acceptor concentration for EC+TM VEGFR2, in the absence of ligand and in the presence of VEGF-A121, VEGFA-165, VEGF C or VEGF D. The proximity FRET contribution is shown as solid line. **(B)** FRET values, were corrected for stochastic FRET contributions. **(C)** Donor concentrations plotted against acceptor concentrations for unliganded and liganded EC+TM VEGFR2. **(D)** Intrinsic FRET values, measured for the three EC+TM receptors in the presence of saturating concentrations of VEGF-A_{121}, VEGF-A_{165}, VEGF-C and VEGF-D. **Right:** confocal images showing VEGF-A_{121}-Alexa Fluor 594 binding to EC-TM-VEGFR2-$(GGS)_5$-YFP CHO vesicles.

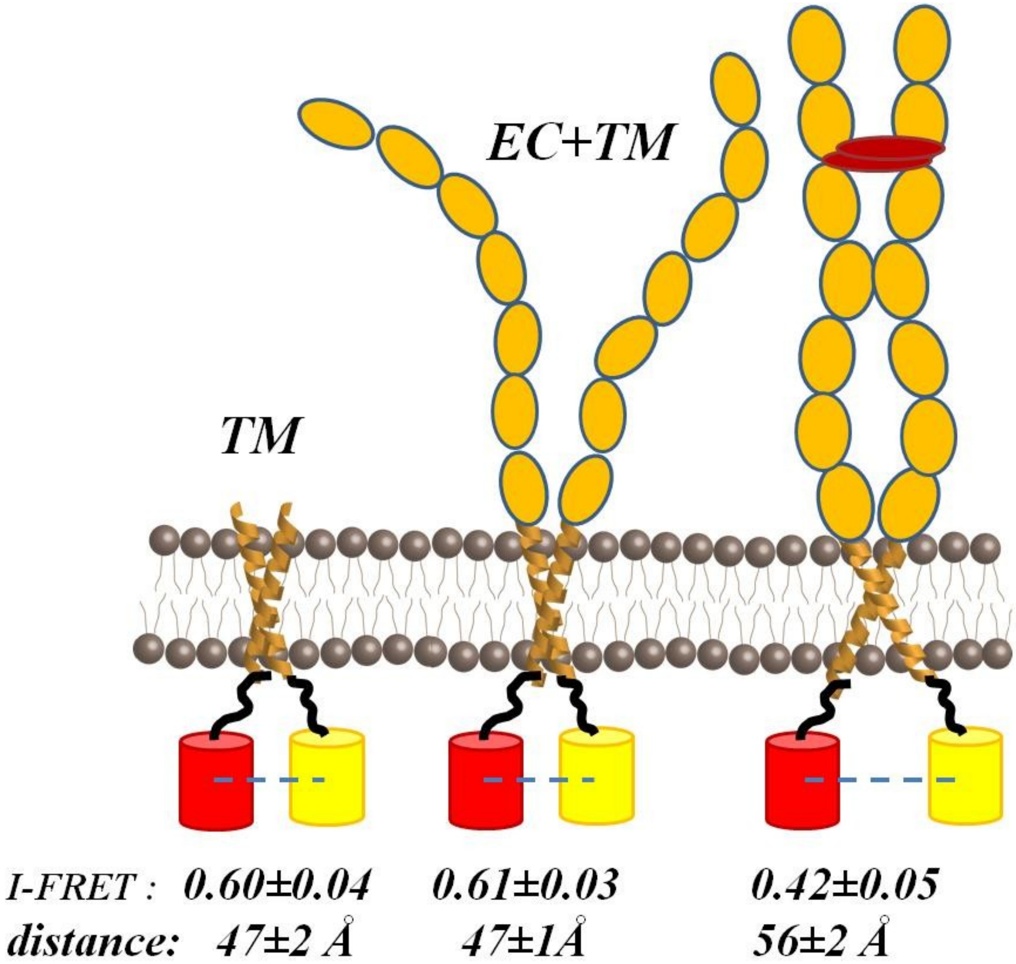

Figure 3-5. The model of VEGFR2 dimerization and activation based on our experiments.

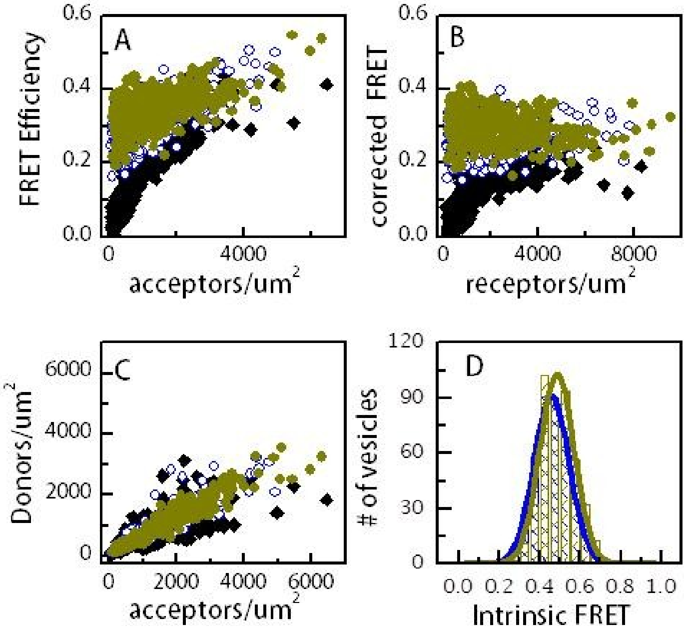
A
FRET Efficiency
0.0
0.2
0.4
0.6
0
4000
acceptors/um^2
B
corrected FRET
0.0
0.2
0.4
0.6
0
4000
8000
receptors/um^2
C
Donors/um^2
0
2000
4000
6000
0
2000
4000
6000
acceptors/um^2
D
# of vesicles
0
30
60
90
120
0.0
0.2
0.4
0.6
0.8
1.0
Intrinsic FRET

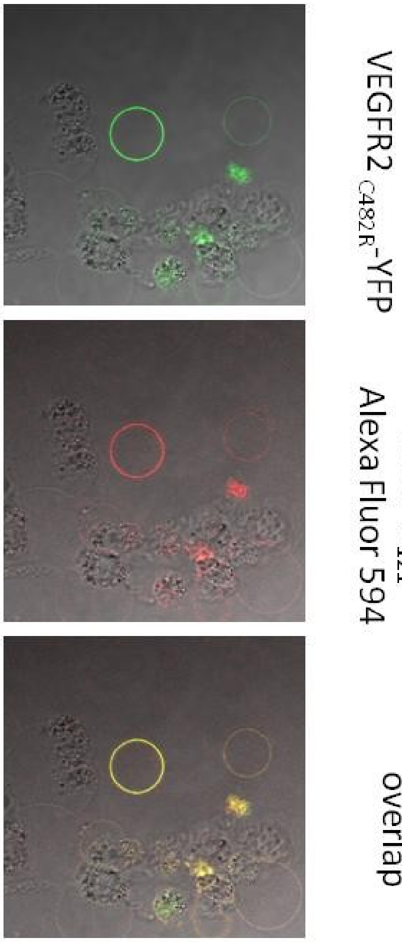
VEGFR2$_{C482R}$-YFP
VEGF-A$_{121}$
Alexa Fluor 594
overlap

Figure 3-6. Left: FRET data comparing the dimerization of wild-type in the absence of ligand (black), the C482R mutant in the absence of ligand (blue) and the C482R mutant in the presence of ligand (dark yellow). **(A)** Measured FRET efficiencies in single plasma membrane derived vesicles. **(B)** Corrected FRET. **(C)** Measured donor versus acceptor concentrations in each vesicle. The measured FRET for the mutant does not depend on concentration, demonstrating that the mutant is a constitutive dimer in the presence and absence of ligand **(D)** Histograms of measured FRET efficiencies for the mutant, revealing Intrinsic FRET values of ~ 0.42. **Right:** Confocal images of VEGF-A$_{121}$-Alexa Fluor 594 binding to EC-TM-VEGFR2$_{C482R}$-(GGS)$_5$-YFP CHO vesicles.

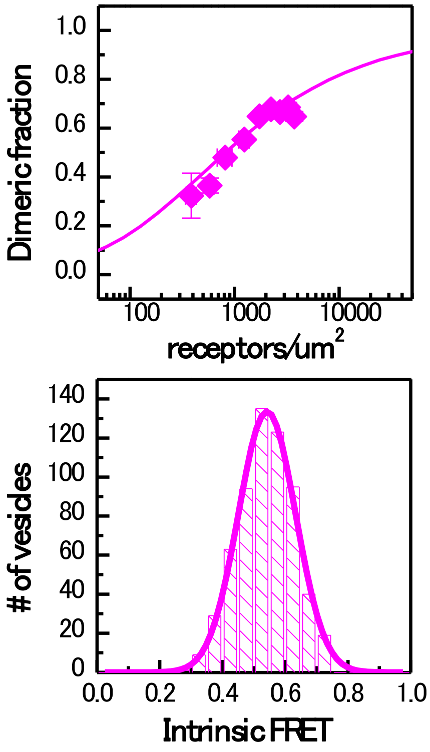

Figure 3-7. Results for the V769E mutant. (A) Dimeric Fractions in the absence of ligand. The solid line is the fit of the dimerization model to the data. The dimerization constant and the Intrinsic FRET values, obtained in the fit, are shown in Table 1. (B) Histograms of I-FRET values measured in single vesicles in the presence of ligand. The average values are shown in Table 1.

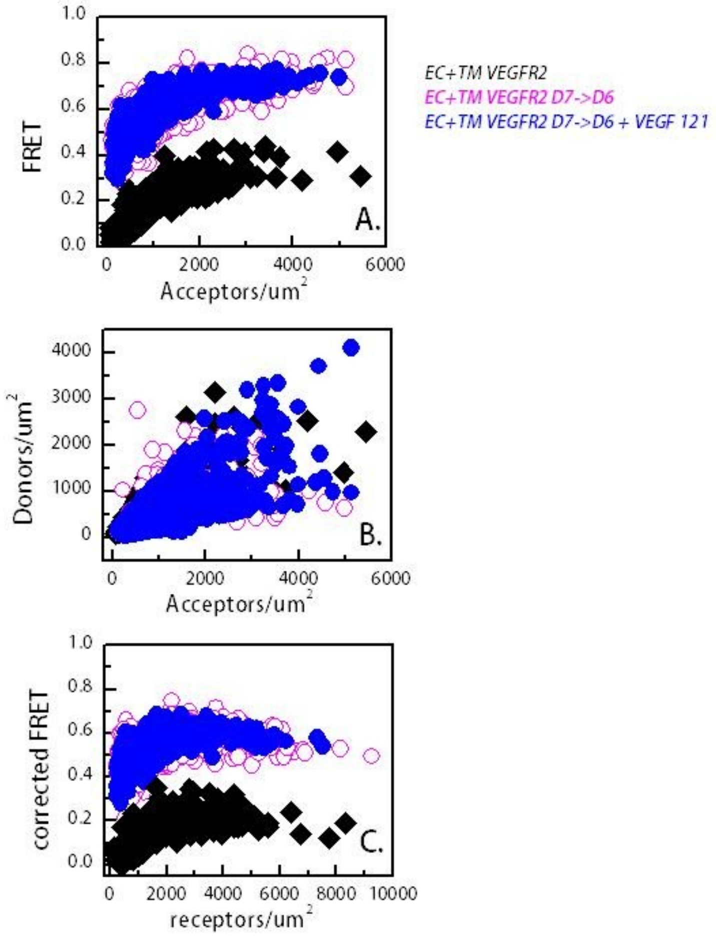
1.0
0.8
0.6
0.4
0.2
0.0
FRET
0
2000
4000
6000
Acceptors/um^2
A.
EC+TM VEGFR2
EC+TM VEGFR2 D7->D6
EC+TM VEGFR2 D7->D6 + VEGF 121
4000
3000
2000
1000
0
Donors/um^2
0
2000
4000
6000
Acceptors/um^2
B.
1.0
0.8
0.6
0.4
0.2
0.0
corrected FRET
0
2000
4000
6000
8000
10000
receptors/um^2
C.

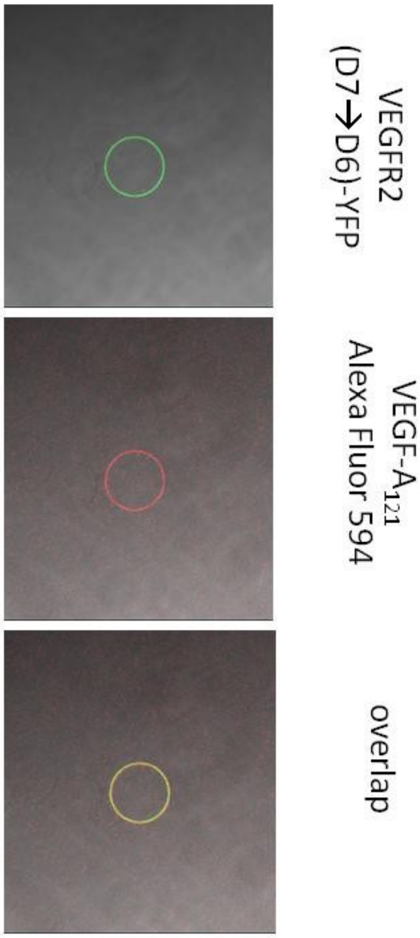
VEGFR2
(D7→D6)-YFP
VEGF-A$_{121}$
Alexa Fluor 594
overlap

Figure3- 8. Left: (A) FRET efficiency plotted as a function of acceptor concentration for WT EC+TM and D7→D6 ECTM VEGFR2. (B) Donor concentration plotted against acceptor concentration for each vesicle. (C) Raw FRET was corrected for random FRET contribution. The FRET dta do not fit the dimerization model, suggesting that the D7→D6 (VEGFR1) substitution results in the formation of an oligomeric complex. **Right:** The mutant VEGFR2 is capable of VEGF121-Alexa Fluor 594 binding.

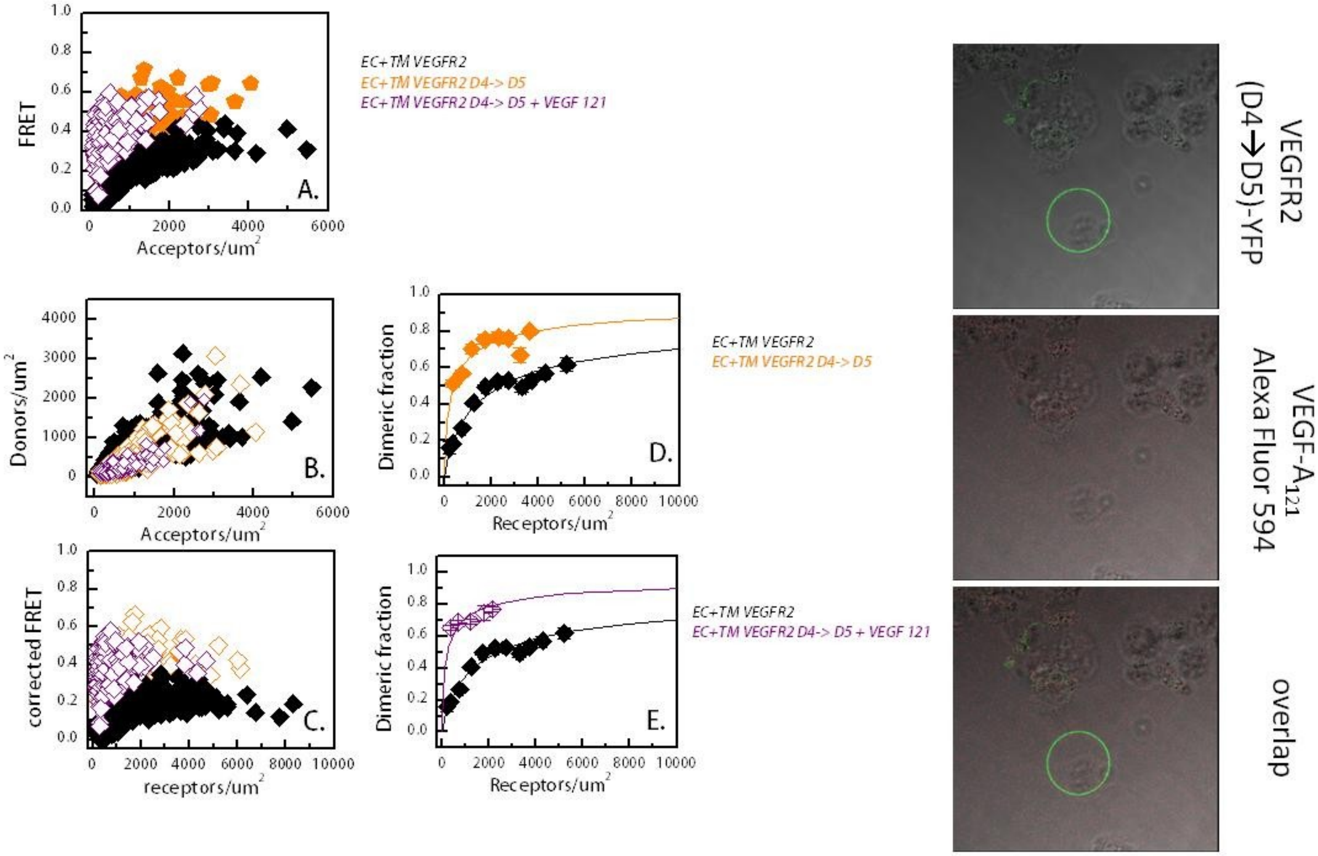

Figure 3-9. Left: (A) FRET efficiency plotted as a function of acceptor concentration for WT EC+TM and D4→D5 ECTM VEGFR2. (B) Donor concentration plotted against acceptor concentration for each vesicle. (C) Raw FRET was corrected for random FRET contribution. D4→D5 (VEGFR1) mutation results in formation of a slightly more stable dimer than wild type VEGFR2. (D) Dimeric fraction versus receptor concentration for the wild-type and the mutant (E). Dimeric fraction versus receptor concentration for the wild-type and the mutant in the presence of ligand. **Right:** the mutant VEGFR2 is not capable of ligand binding, as evident from the lack of binding of VEGF121-Alexa Fluor 594 to vesicles expressing ECTM-VEGFR2 $_{D4\rightarrow D5}$-YFP.

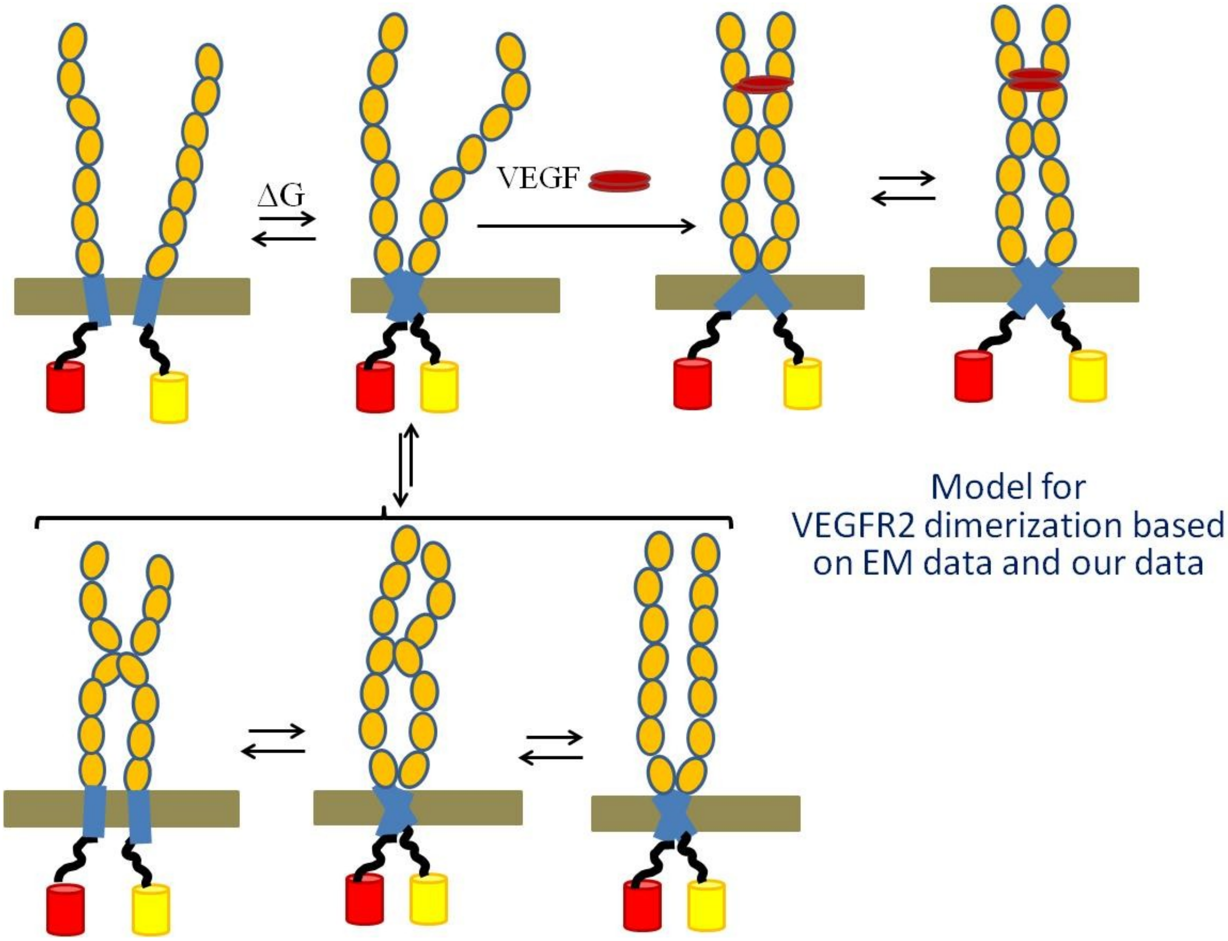

Figure 3-10. Our proposed dimerization model for VEGFR, based on our experiments only the above scenarios are possible on the plasma membrane. This corrects/refines models offered by previous studies based on VEGFR2 TM domain or EC domain interaction only, as well as electron microscopy images of the EC domain (65, 120).

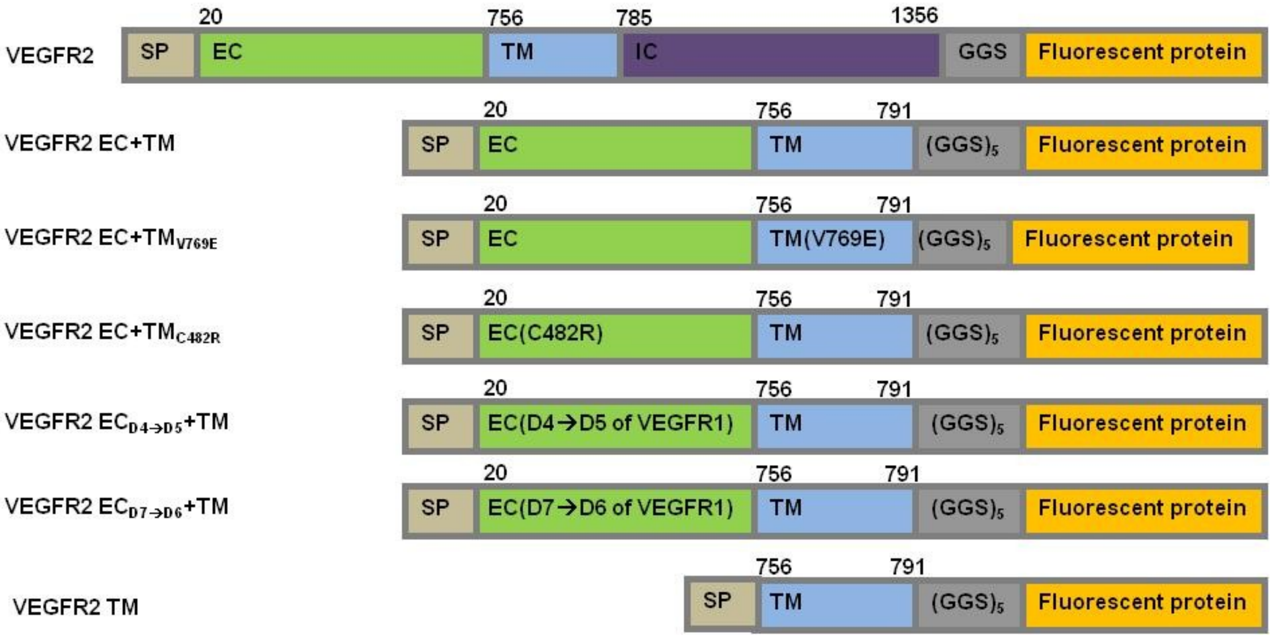

Figure S1(3-11). The constructs used in the FRET experiments. The full-length receptors had fluorescent proteins attached to their C-termini via a flexible GGS linker. The truncated receptors had the intracellular domain substituted with a fluorescent protein, which was attached to the TM domain via a longer flexible $(GGS)_5$ linker. SP: signal peptide, EC: extracellular domain, TM: transmembrane domain. Fluorescent protein was either YFP or mCherry. Amino acid residue numbers are shown above the constructs.

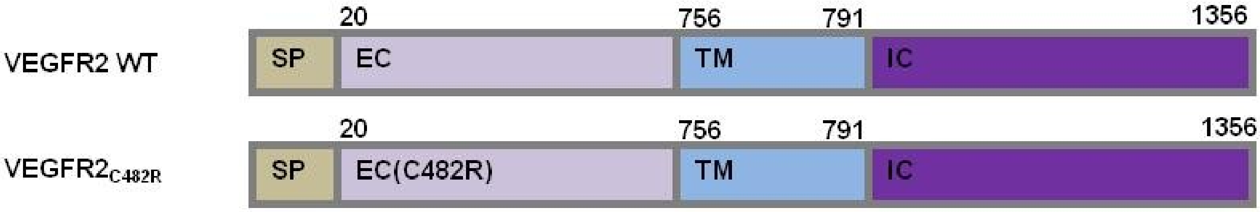

Figure S2(3-12). The plasmid construct used for western blotting measurements.

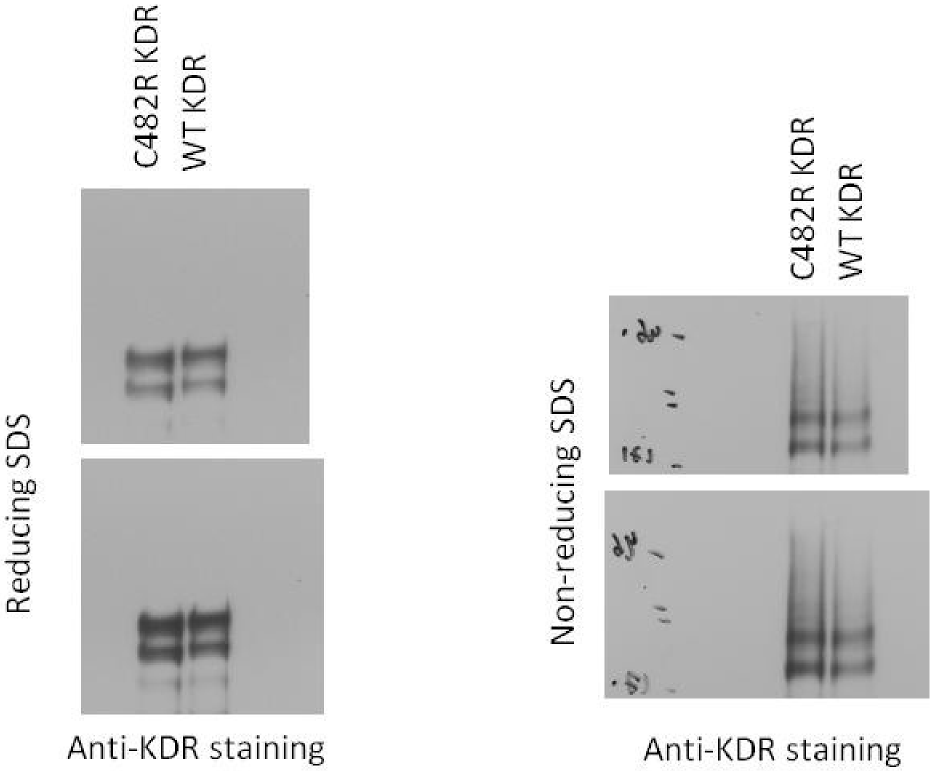

Figure S3(3-13). Left: reduced SDS PAGE and Right: Non-reduced SDS PAGE for WT and C482R VEGFR2 followed by western blot staining demonstrates that the constitutive dimerization as a result of C342R mutation is not due to cysteine linked disulfide bonds.

Chapter 4. FGFR3 unliganded dimer stabilization by the juxtamembrane domain

Abstract

Receptor Tyrosine Kinases (RTKs) conduct biochemical signals upon dimerization in the membrane plane. While RTKs are generally known to be activated in response to ligand binding, many of these receptors are capable of forming unliganded dimers that are likely important intermediates in the signaling process. All 58 RTKs consist of an extracellular domain, a transmembrane (TM) domain, and an intracellular domain which includes a juxtamembrane (JM) sequence and a kinase domain. Here we investigate directly the effect of the JM domain on unliganded dimer stability of FGFR3, a receptor that is critically important for skeletal development. The data suggest that FGFR3 unliganded dimers are stabilized by receptor-receptor contacts that involve the JM domains. The contribution is significant, as it is similar in magnitude to the stabilizing contribution of a pathogenic mutation and the repulsive contribution of the extracellular domain. Furthermore, we show that the effects of the JM domain and a TM pathogenic mutation on unliganded FGFR3 dimer stability are additive. We observe that the JM-mediated dimer stabilization occurs when the JM domain is linked to FGFR3 TM domain and not simply anchored to the plasma membrane. These results point to a coordinated stabilization of the unliganded dimeric state of FGFR3 by its JM and TM domains via a mechanism that is distinctly different from the case of another well studied receptor, EGFR.

4.1. Introduction

Receptor tyrosine kinases (RTKs) are membrane proteins that control cell proliferation, differentiation, survival and migration (85, 159). They are thus implicated in many pathologies, including tumorigenesis, cancer progression, and developmental abnormalities (48, 159). The basic architecture of all RTKs consists of a ligand-binding extracellular (EC) domain, a single transmembrane domain and an intracellular portion composed of a juxtamembrane (JM) sequence, and a kinase domain (39, 76). The activation of RTKs requires that they dimerize in the plasma membrane, an event that brings the two kinase domains in close proximity and leads to their phosphorylation (126). This is followed by the phosphorylation of additional tyrosine residues in the intracellular domains, which triggers the recruitment of adaptor proteins, and the initiation of intracellular signaling cascades (37, 127, 168).

While the general principles of RTK activation are now well established, we still lack comprehensive mechanistic understanding of this process, despite very active research in the field. In the "canonical" model of RTK activation (39), RTKs are monomers in the absence of ligand, but dimerize and cross-phosphorylate/activate each other upon ligand binding. However, recent work has identified unliganded dimers for many RTKs (36, 84, 86, 91, 134), and thus an alternative "pre-formed dimer" model of RTK activation was proposed in which the RTKs are dimeric in the absence of ligand, and ligand binding induces a structural change in the dimer that reorients the catalytic domains for efficient activation (6, 56, 80). Activation may be therefore viewed as a thermodynamic change of state, i.e. a transition from an unliganded dimeric state which lacks full activity, to the fully active liganded dimeric state (56).

Recent studies of EGFR, the most widely researched RTK, has suggested that its JM domain is critical for establishing the distinct structural features of the liganded and unliganded states, and for the transition between the two states (4, 36, 67). In particular, while the liganded state is stabilized by direct N-terminal JM-JM contacts, in the unliganded state the JM domain interacts with membrane lipids and does not engage in stabilizing contacts (4, 36). Intriguingly, the behavior of EGFR JM domain appears to be impacted by the lateral interactions between the TM domains, via a mechanism that is not completely understood (36).

Here we investigate the role of the JM domain of another RTK, FGFR3, in stabilizing the unliganded state. We also study the coordination of FGFR3 JM and TM domains in the absence of ligand. Many developmental abnormalities have been linked to disregulated unliganded FGFR3 dimerization (20, 53, 58, 64, 83, 94, 151), but the physical interactions that stabilize the unliganded FGFR3 dimer are not completely known. Here we make direct measurements of the effect of the JM domain on dimer stabilization, within and out of the context of the FGFR3 dimer. The results show that the FGFR3 JM domain, unlike the EGFR JM domain, plays an active role in stabilizing the unliganded FGFR3 dimers, in coordination with FGFR3 TM domain.

4.2. EXPERIMENTAL METHODS

The YFP plasmid was a gift from Dr. M. Betenbaugh (Johns Hopkins University, Baltimore, MD) and pRSET-mCherry was obtained from Dr. R. Tsien (University of California, San Diego). The plasmid encoding human wild-type FGFR3 was a gift from Dr. D. J. Donoghue (University of California, San Diego). All primers were purchased from Invitrogen.

22 different gene constructs, inserted into the multiple cloning site of pcDNA3.1(+) between HindIII and XbaI (Table 1) were used in this study. The cloning procedures for FGFR3 TM-$(GGS)_5$-YFP, FGFR3 TM-$(GGS)_5$-mCherry, FGFR3 EC-TM-$(GGS)_5$-YFP, FGFR3 EC-TM-$(GGS)_5$-mCherry, GpA-$(GGS)_5$-YFP and GpA-$(GGS)_5$-mCherry, FGFR3 EC-TM_{A391E}-$(GGS)_5$-YFP, and FGFR3 EC-TM_{A391E}-$(GGS)_5$-mCherry have been described previously(22, 23, 122). All constructs included the signal peptide of FGFR3 (MGAPACALALCVAVAIVAGASS) at the N-terminus.

To create the FGFR3 EC-TM-JM-YFP and FGFR3 EC-TM-JM-mCherry plasmids, the AsiSi site before $(GGS)_5$ in FGFR3 EC-TM-$(GGS)_5$-YFP and FGFR3 EC-TM-$(GGS)_5$-mCherry was mutated to a BsrGI site. The FGFR3 EC-TM-$(GGS)_5$-YFP and FGFR3 EC-TM-$(GGS)_5$-mCherry plasmid constructs containing the BsrGI site were then double digested using BsrGI and AgeI restriction enzymes. The complementary DNA (cDNA) encoding the JM domain of FGFR3 was amplified using Polymerase Chain Reaction (PCR), double digested with BsrGI and AgeI and ligated with FGFR3 EC-TM-$(GGS)_5$-YFP and FGFR3 EC-TM-$(GGS)_5$-mCherry that have been digested with the BsrGI and AgeI restriction enzymes.

To create the FGFR3 EC-TM-JM_{60}-YFP and FGFR3 EC-TM-JM_{60}-mCherry plasmid constructs, a XhoI site in the JM sequence of FGFR3 was utilized to double digest EC-TM-JM_{60} using Hind III and XhoI. This cDNA was then inserted into the multiple cloning sites in the pcDNA3.1(+) vector plasmids encoding YFP and mCherry between the HindIII and XhoI sites.

To generate GpA-$(GGS)_2$-JM-YFP and GpA-$(GGS)_2$-JM-mCherry, a BsrGI site was first created at the 7th Glycine position in the $(GGS)_5$ linker sequence in the GpA-$(GGS)_5$-YFP and GpA-$(GGS)_5$-mCherry sequences. The cDNA encoding the JM domain of FGFR3 together with YFP or mCherry was then amplified from FGFR3 EC-TM-JM-YFP and FGFR3 EC-TM-JM-mCherry using PCR, and double digested with the BsrGI and XbaI restriction enzymes. The JM-YFP/mCherry digested cDNA was then ligated into the pCDNA-GpA-TM-$(GGS)_5$ vector which has been double digested with BsrGI and XbaI.

The A391E mutation was generated in the FGFR3 EC-TM-JM_{60}-YFP and FGFR3 EC-TM-JM_{60}-mCherry plasmid sequences using a QuickChange ® II XL Site-Directed Mutagenesis Kit (Strategene, CA).

The GpA-$(GGS)_2$-YFP/mCherry and GpA-$(GGS)_3$-YFP/mCherry plasmid constructs were created from GpA-$(GGS)_5$-YFP/mCherry. The GpA-$(GGS)_2$ and GpA-$(GGS)_3$ cDNAs were amplified using PCR. The GpA-$(GGS)_5$-YFP/mCherry plasmids were double digested with HindIII and AsiSI restriction enzymes. The amplified GpA-$(GGS)_2$ and GpA-$(GGS)_3$ cDNAs were then double digested with HindIII and AsiSI and ligated with the double digested GpA-$(GGS)_5$-YFP/mCherry cDNAs.

4.2.1. Cell culture and transfection

Chinease Hamster Ovary (CHO) cells were a kind gift of Dr. M. Betenbaugh (Johns Hopkins University, Baltimore, MD). The cells were cultured at 37 C with 5% CO_2 for 24h. Transfection was carried out using Fugene HD transfection reagent (Roche Applied Science), following the manufacturer's protocol. Cells were co-transfected with total of 4-5 ug total DNA encoding YFP and mCherry tagged constructs.

4.2.2. Production of mammalian plasma membrane vesicles

Vesiculation was performed as described previously(33). CHO cells were rinsed twice with 30% PBS (pH 7.4), and incubated with 1 mL of chloride salt vesiculation buffer overnight at 37 °C. The vesiculation buffer consisted of 200 mM NaCl, 5 mM KCl, 0.5 mM $MgSO_4$, 0.75 mM $CaCl_2$, 100 mM bicine and protease inhibitor cocktail (Complete mini EDTA-free tabs, Roche Applied Science) adjusted to PH of 8.5. A large number of vesicles were produced after 1.5 h, and the vesicles were transferred into 4-well Nunc Lab-Tek II chambered coverslips for imaging.

4.2.3. Fluorescence Image Acquisition. Vesicles were imaged using a Nikon Eclipse confocal laser scanning microscope using a 60× water immersion objective. All the images were collected and stored at a 512 × 512 resolution. Three different scans were performed for each vesicle: (1) excitation at 488 nm, with a 500-530 nm emission filter (donor scan); (2) excitation at 488 nm, with a 565-615 nm emission filter (FRET scan); and (3) excitation at 543 nm, with a 650 nm longpass filter (acceptor scan). Gains of 8.0 and pixel dwell time of 1.68 μs were used for the three scans. To minimize the bleaching of fluorescent proteins, ND8 filters were used during excitation with the 488 nm laser.

The imaged vesicles exhibited uniform fluorescence intensities (see Figure 2), which allowed us to determine the concentrations of the fluorescent proteins in the membrane using solutions of purified YFP and mCherry solutions of known concentration as described in(125). The fluorescent protein solutions were prepared as described in (125). They were imaged in the microscope using the same settings used for vesicle imaging, to allow direct comparison of solution and vesicle intensities.

Each vesicle was analyzed using a Matlab® program to determine the fluorescence intensity across the membrane(23, 81), which was fitted to a Gaussian function and the background intensity was approximated as an error function (see Figure 2). The donor, acceptor, and FRET intensities for each vesicle were used to determine (i) the donor concentration, (ii) the acceptor concentration, and (iii) the FRET efficiency in each vesicle as described in detail elsewhere (23, 81) and in Supplementary Material.

4.2.4. QI-FRET DATA ANALYSIS IN BRIEF

Please refer to ref.(22) for a step-by-step detailed protocol.

Each vesicle co-expressing FGFR-YFP and FGFR-mCherry was imaged in the donor, acceptor and FRET channels, yielding the fluorescence intensities, I_D, I_{FRET}, and I_A (see Figure 2). The acceptor concentrations in each vesicle, C_A , is calculated according to:

$$C_A = \frac{I_A}{i_A} \tag{1}$$

The sensitized emission of the acceptor in each vesicle is determined as:

$$I_{SEN} = I_{FRET} - \beta_A I_A - \beta_D I_D \tag{2}$$

The donor intensity in the absence of the acceptor $I_{D,corr}$, and the donor concentrations (C_D) are calculated as:

$$I_{D,corr} = I_D + G_F I_{SEN} \tag{3}$$

$$C_D = \frac{I_{D,corr}}{i_D} \tag{4}$$

The FRET efficiency, E, is calculated using eq.5:

$$E = 1 - \frac{I_D}{I_{D,corr}} \tag{5}$$

and is corrected for the so-called “by-stander FRET” that one would expect if there were no specific protein interactions, but donors and acceptors approached each other by chance within distances of 100 Å or so (the reader is referred to a detailed discussion in ref.(70)). FRET due to sequence-specific dimerization E_D is proportional to the fraction of receptors in the dimeric state:

$$\frac{E_D}{x_A} = f_D \widetilde{E} \tag{7}$$

x_A is the acceptor fraction. The proportionality constant $\widetilde{E}$ is the “Intrinsic FRET”, the FRET efficiency in a dimer containing a donor and an acceptor. This is a purely structural parameter, which depends only on the separation and the orientation of the two fluorescent proteins in the dimer, but not on the dimerization propensity.

Based on the law of mass action, the dimeric fraction can be written as a function of the total receptor concentration, *T*, and the dimerization constant *K* according to equation 8.

$$f_D = \frac{1}{T}\left(T - \frac{1}{4K}\left(\sqrt{1+8TK} - 1\right)\right) \tag{8}$$

Substituting equation (8) into (7), we obtain:

$$\frac{E_D}{x_A} = \frac{1}{T}\left(T - \frac{1}{4K}\left(\sqrt{1+8TK} - 1\right)\right)\widetilde{E} \tag{9}$$

We use equation (9) to fit the measured ED/xA while optimizing for the two adjustable parameters: the dimerization constant *K*, and the intrinsic FRET Ẽ. The free energy of dimerization (dimer stability) is calculated according to:

$$\Delta G = -RT \ln(K) \tag{10}$$

4.3. SECONDARY STRUCTURE PREDICTIONS

Secondary structures of FGFR3 and EGFR JM domains were evaluated using the program JPRED: **http://www.compbio.dundee.ac.uk/www-jpred.**

The underlined amino acids in FGFR3 JM domain are predicted to have β-sheet propensities. No helical segments are predicted for FGFR3. For EGFR, a helical segment is predicted (underlined and bold), which has been shown to interact with lipids in the unliganded state and not participate in dimerization(4, 36).

FGFR3:

^{400}SPPKKGLGSPTVHKISRFPLKRQVSLESNASMSSNTPLVRIARLSSGEGPTLANV
SELELPADPKWELSRAR^{472}

EGFR:

^{669}RRRH**IVRKRTLRRLLQ**ERELVEPLTPSGEAPNQALLRILKETE^{711}

4.4. RESULTS

4.4.1. The substitution of an unstructured linker with the FGFR3 JM domain stabilizes FGFR3 dimers in the absence of ligand.

Previously, we have shown that the FGFR3 construct EC-TM-$(GGS)_5$-YFP/mCherry (Table 1), in which the intracellular domain has been substituted with a fluorescent protein attached via a $(GGS)_5$ linker, forms dimers in mammalian plasma membrane derived vesicles in the absence of ligand (23). The $(GGS)_5$ linker has been shown to be unstructured and to behave like a random coil (38). Here we substituted this 15-residue flexible linker with the 72 amino acid long JM domain of FGFR3 (see Figure 1) and we asked how this substitution affects dimerization. To answer this question we measured and compared the dimerization of EC-TM-$(GGS)_5$-YFP/mCherry and EC-TM-JM-YFP/mCherry in plasma membrane derived vesicles from CHO cells.

In these experiments, CHO cells were first co-transfected with plasmids encoding either EC-TM-JM-YFP and EC-TM-JM-mCherry or EC-TM-$(GGS)_5$-YFP and EC-TM-$(GGS)_5$-mCherry. After the receptors were produced and trafficked to the plasma membrane, the cells were induced to form plasma membrane derived vesicles using an osmotic stress method described recently(33). The dimerization of the two FGFR3 constructs was characterized with a FRET-based method termed QI-FRET as described previously(22). The FRET experiments were performed with a laser-scanning confocal microscope, imaging a thin slice through the equator of each vesicle (see Figure 2). For each receptor, 600 to 1000 individual plasma membrane-derived vesicles were imaged and analyzed with the QI-FRET method which yields (i) the donor concentration, (ii) the acceptor concentration, and (iii) the FRET efficiencies in each vesicle. The total receptor concentration and the dimeric receptor fraction were calculated in each vesicle, and data from many vesicles were combined to yield dimerization curves (Figure 3).

The QI-FRET methodology has been published as a detailed step-by-step protocol(22), and the reader is referred to this protocol for details. In addition, basic concepts behind the QI-FRET method are briefly outlined in Supplemental Material to this manuscript (see also Figure 2 for an illustration of vesicle image processing).

Unique aspects of the methodology are: (i) we design our experiments such that receptor concentrations are varied over a wide range, and (ii) we independently measure donor and acceptor concentrations in the plasma membranes, along with FRET efficiencies. Thus, we can assess if the data is described by a dimerization model, calculate dimeric fractions, and predict dimeric fractions for receptor concentrations that are not experimentally accessible. From the data, we determine (i) the dimerization constant, **K,** and the dimer stability, or the dimerization free energy **$\Delta G = -RT \ln K$** and (ii) the purely structural parameter "Intrinsic FRET", $\tilde{E}$(22). The measured Intrinsic FRET value depends on the dimer structure, in particular on the distance and orientation of the fluorescent proteins in the dimer. Most importantly, this is a parameter that affects the measured FRET efficiencies, and it needs to be determined and accounted for in order to correctly measure K and the dimer stability ΔG. The Intrinsic FRET value $\tilde{E}$ is a means to compare structures and follow large-scale structural perturbations.

The FRET efficiencies measured the two FGFR3 constructs are shown in Figure S1, where each data point represents a single vesicle. The donor concentration in each vesicle is also shown in Figure S1 versus the acceptor concentration in the same vesicle. Thus, each vesicle contains different concentrations of donors and acceptors, and different total receptor concentrations. From the FRET efficiencies and the donor to acceptor ratio in Figure S1 and following the step-by step QI-FRET protocol (22), we obtain the dimerization curves shown in Figure 3, as well as the dimerization constant K and Ẽ shown in Table 1.

In Figure S1, the FRET efficiencies appear higher in the presence of the JM domain, suggesting that the dimerization is higher when the JM domain is present. After accounting for the effect of Ẽ, in Figure 3 we show that the dimeric fraction is higher in the presence of the JM domain. The dimerization free energy changes from -3.4 kcal/mole to -5.4 kcal/mole upon the substitution of the unstructured linker with the JM domain. Thus, this substitution increases the stability of the FGFR3 dimer by $\Delta\Delta G_{JM}$ = -2 kcal/mole.

4.4.2. The interplay of FGFR3 domain interactions

To understand the interplay of the different domains in FGFR3 unliganded dimerization, next we studied how the dimerization of the FGFR3 construct studied above changes when the EC domains were deleted. Specifically, we worked with (a) a FGFR3 construct containing the TM domain, the JM domain, and fluorescent proteins (TM-JM-YFP/mCherry) and (b) a FGFR3 construct containing the TM domain, a 15 amino acid flexible $(GGS)_5$ linker, and fluorescent proteins (TM-$(GGS)_5$-YFP/mCherry), see Figure 1. The dimerization results for the two proteins are shown in Figure S2 and Figure 4.

For TM-$(GGS)_5$-YFP/mCherry, we measure unliganded dimer stability of -5.2 kcal/mole (Figure 4), which is higher than the stability in the presence of FGFR3 EC domain. Comparison of the stabilities of the EC+TM and TM dimers (-3.4 and -5.2 kcal/mole, respectively), demonstrates that the deletion of the EC domain stabilizes the dimer by 1.8

kcal/mole, with the positive sign indicating that the contribution is inhibitory. This result is similar to our previous measurements in vesicles produced via chemical vesiculation using formaldehyde and DTT (129-131), which yielded ~1 kcal/mole for the inhibitory EC domain contribution(23).

In Figure S2, the FRET efficiency for TM-JM-YFP/mCherry construct does not depend on the concentrations, which suggests that the construct is 100% dimer over the concentration range we study. In this case, the exact values of K and $\Delta\Delta G_{JM}$ cannot be determined. However, the data demonstrate that the stability of the FGFR3 TM dimer is increased by at least -1.5 kcal/mol in the presence of the JM domain.

The data in Figures 3 and 4 suggest that the substitution of the unstructured linker with the JM domain stabilizes the FGFR3 dimer by -2 kcal/mole, while the EC domain inhibits dimerization by 1.8 kcal/mole. In other words, the stabilizing effect of the JM domain cancels the inhibitory contribution of the EC domain in the FGFR3 unliganded dimer.

4.4.3. The $(GGS)_5$ linker does not contribute significantly to dimerization.

The $(GGS)_5$ linker has been previously assumed to have a negligible effect on protein interactions as it is thought to be long enough to allow for flexibility and to prevent significant steric overlap between the fluorescent proteins in the dimer (22, 38). Here, we sought experimental support for this assumption.

We reasoned that if the linker affects dimerization, for instance due to the overlap of the random coil radii of the two linkers, or due to the steric clash of the fluorescent proteins, its contribution will depend on its length. We therefore compared the interactions between TM helices when the fluorescent proteins were attached to 6, 9, and 15 amino acid long linkers. To address this question in a most general context, we performed the experiments with the TM helix of glycophorin A (GpA), a well-characterized sequence that is traditionally used as a model in transmembrane helix dimerization studies (63, 77). In particular, we characterized the dimerization of GpA TM domain when the fluorescent proteins are connected via $(GGS)_2$, $(GGS)_3$, and $(GGS)_5$ linkers (see Figure 1). Dimerization results for the three constructs are shown in Figure S7, Figure 5, and in Table 1. The length of the linker had no effect on GpA dimer stability. The dimerization curves in Figure 5 are essentially identical, as also shown by the resulting dimerization free energies in Table 1. Furthermore, the value of the Intrinsic FRET, $\tilde{E}$, is the same for GpA-$(GGS)_3$-YFP/mCherry and GpA-$(GGS)_5$-YFP/mCherry (0.52). The value of $\tilde{E}$ is somewhat lower for GpA-$(GGS)_2$-YFP/mCherry (0.41), which may be indicative of restrictions in mobility of the fluorescent proteins when attached to the shortest linker.

Overall, these data support the idea that the $(GGS)_5$ linker does not contribute measurably to the stabilization of TM dimers. Thus, the $\Delta\Delta G_{JM}$ contribution that we measure above represents the stabilizing contribution of the JM domain.

4.4.4. Tethering the JM domain to the membrane does not lead to stabilizing interactions

The behavior of the JM domain of EGFR has been shown to depend on the TM domain(4, 36). To test if the FGFR3 JM domain has inherent stabilizing interactions that arise simply from membrane tethering, we attached the JM domain to the unrelated GpA TM domain via a short, flexible $(GGS)_2$ linker (GpA-$(GGS)_2$-JM-YFP/mCherry, see Figure 1). The role of GpA in this experiment was to anchor the protein to the plasma membrane and bring the two JM domains into close proximity upon dimerization. The role of the $(GGS)_2$ linker was to decouple the JM domain from the GpA helices, since the GpA and FGFR3 dimer structures are different, and the cytoplasmic ends of the dimeric helices have different separations.

We compared the dimerization of the GpA-$(GGS)_2$-JM-YFP/mCherry and GpA-$(GGS)_5$-YFP/mCherry constructs. The results for these two constructs are shown in Figure S4, Figure 6 and in Table 1. There is no difference in the dimerization of the two constructs. Thus, the effect of the substitution of the $(GGS)_5$ linker with $(GGS)_2$-JM was negligible. The JM domains therefore engaged in stabilizing contacts only when attached to the TM domain of FGFR3 in the appropriate context, but not when closely tethered to the membrane via a short, flexible $(GGS)_2$ linker on a different TM domain. Thus, the behavior of FGFR3 JM domain in our experiments depends on the details of the TM domain dimer. In FGFR3, the two domains seem to act in synergy to stabilize the dimeric form.

4.4.5. The interactions between the JM domains occur within the N-terminal part of the JM sequence.

In EGFR, direct JM-JM contacts in the liganded state occur in the N-terminal portion of the JM domain (4, 67). Here we asked whether, similarly, the N-terminal end of the FGFR3 JM domain might be responsible for the JM-mediated stabilization of the FGFR3 unliganded dimers. In particular, we investigated if the removal of a C-terminal segment from the JM segment will decrease FGFR3 dimer stability in the absence of ligand. We thus shortened the JM domain by 12 residues, using a convenient restriction site in the DNA sequence encoding the JM domain. We then measured the dimerization of the construct EC-TM-JM_{60}-YFP/mCherry containing the shorter 60 amino acid JM sequence. Results are shown in Figure S5, Figure 7 and in Table 1. The dimer stabilities for EC-TM-JM_{60}-FP and EC-TM-JM-FP are the same, demonstrating that the C-terminal 12 amino acid segment of the JM domain does not participate in JM-JM stabilizing interactions. Furthermore, the value of the intrinsic FRET, $\tilde{E}$, is somewhat higher in the case of the shorter linker (0.7 versus 0.57, see Table 1). This suggests that the distance between the FPs may be shorter in the dimer when the JM domain is shorter (46 Å versus 51 Å, assuming free fluorophore rotation), a finding which is consistent with the idea of JM-JM interactions occurring within the N-terminal part of the JM domain, close to the membrane.

4.4.6. FGFR3 JM domain stabilizes the A391E FGFR3 dimer

Previously, we have characterized the dimerization of FGFR3 in the presence of the A391E mutation which causes a craniosynostosis, Crouzon syndrome with acanthosis nigricans (94). We have shown that the mutation stabilizes the unliganded FGFR3 dimer by -1.4 kcal/mole in plasma membrane derived vesicles produced with the DTT/formaldehyde vesiculation buffer (122). Here we asked if the substitution of the $(GGS)_5$ linker with the JM domain will alter the stability of the pathogenic A391E dimer. We therefore engineered the A391E mutation into the ECTM-JM_{60}-FP sequence and then measured and compared the dimerization of EC-TM_{A391E}-$(GGS)_5$-YFP/mCherry and EC-TMA391E-JM_{60}-FP in vesicles produced with the osmotic stress method. Results are shown in Figure S6, Figure 8 and in Table 1. The mutation stabilized the FGFR3 dimer by -1.4 kcal/mole, consistent with previous results(122), and the JM domain stabilizes the A391E mutant dimer by an additional -1.8 kcal/mole. The latter is within experimental error of the contribution of the JM domain in the wild-type protein. Thus, the contributions of the A391E pathogenic mutation in the TM domain and of the JM domain to dimer stability are additive.

4.5. DISCUSSION

4.5.1. Goals and findings of this study

Our long term goal is to understand the roles of the different RTK domains in RTK unliganded dimerization. Here we focus on FGFR3 JM domain, and we find that it stabilizes the unliganded FGFR3 dimer. The contribution is significant, when compared to the contribution of other FGFR3 domains. For instance, the JM contribution completely cancels the inhibitory contribution of FGFR3 EC domain. Furthermore, the magnitude of the stabilizing effect is similar to the effect of a pathogenic FGFR3 mutation, and the two effects are additive. These comparisons suggest that the stabilizing effect that we measure here is likely important for FGFR3 biological function.

Interestingly, the JM domain stabilizes the dimer only when it is attached to FGFR3 TM domain (Figures 3 and 4). On the other hand, simply anchoring of the JM domain to the membrane does not potentiate JM-JM interactions (Figure 5). These findings suggest that the TM and the JM domains in FGFR3 work synergistically to stabilize the unliganded FGFR3 dimer.

4.5.2. Experimental approach

Studies of the effect of different RTK domains on RTK dimer stability have been challenging, as the interactions of interest occur within the two dimensional space of the plasma membrane. Soluble isolated domains are sometimes produced and studied in solution, but results acquired for the three dimensional case cannot be extrapolated to two dimensions (49, 147). This is why, here we used a methodology that allowed us to directly explore the thermodynamics of RTK dimerization in plasma membrane derived vesicles.

The QI-FRET method that we use here has been described previously(22). Yet, this work required significant improvements in experimental protocols as in this case we compared the dimerization of RTK constructs that utilized different attachments of the fluorescent proteins. Thus, no *a-priori* assumptions could be made about changes in dimer structure and the Intrinsic FRET, $\tilde{E}$, upon the incorporation of the JM domain. Instead, all the data were subjected to two parameter fits which yielded the values of $\tilde{E}$ along with the values of the dimerization constant K and the dimer stability ΔG. These fits were possible because the RTK concentrations in our experiments spanned ~ two orders of magnitude, an improvement of ~ one order of magnitude over our previous work. In particular, we were able to decrease the lowest accessible receptor concentration by a factor of ~5, while increasing the maximum expression levels by a factor of ~2. Additionally, for this project we used vesicles that are produced using an osmotic stress method (33), and thus were not exposed to DTT and formaldehyde which may introduce perturbations in RTK interactions.

4.5.3. Comparison with EGFR

Previously, we have shown that the substitution of EGFR JM domain with an unstructured $(GGS)_{10}$ sequence has no effect on unliganded EGFR dimerization(55). Thus, in the EGFR case the JM domain does not stabilize the dimer in the absence of ligand, a behavior that is very different from the behavior that we observe here. This prompted us to seek differences in sequence characteristics of the FGFR3 and EGFR JM domains. We used the web-based program JPRED to evaluate the propensity of FGFR3 JM domain for folding into secondary structure (see Supplemental data). The FGFR3 sequence was predicted to be mainly unstructured, with low beta sheet content but no helical content. On the other hand, EGFR JM domain has a short alpha-helical segment close to its N-terminus which has been implicated in the interactions of EGFR JM domain with lipids in the absence of ligand(4). Thus, the differences in JM domain secondary structures may underlie the difference in behavior.

The activity of all RTKs is often modeled after the mode of activation of the extensively studied EGFR. Yet, it is not clear if the lessons learned about EGFR are directly transferable to other RTKs. For instance, there are distinct differences in the activation mode of the kinases from different RTK families(76). Here we further show that the behavior of FGFR3 JM domain is distinctly different from EGFR JM domain, which engages in JM-JM stabilizing contacts only upon ligand binding. These results reinforce the idea that different families of RTKs have evolved different mechanisms of dimerization and activation, and thus all the 58 RTKs merit in-depth investigation.

4.5.4. Implications

There is evidence in the literature that unliganded FGFR dimers are important for FGFR biological function(84). Unliganded FGR dimers are phosphorylated, and this basal phosphorylation has been suggested to “prime” the kinases for rapid activation upon ligand binding (6, 84). Furthermore, FGFR mutations have been shown to cause disease by specifically increasing unliganded dimerization (24, 119, 157). For instance, the G380R mutation in FGFR3, which causes the most common form of human dwarfism, increases ligand-independent FGFR3 dimerization and phosphorylation, without having a significant effect on FGFR3 phosphorylation in the presence of ligand (55).

Within the "pre-formed dimer" model of RTK activation, the transition from unliganded to liganded dimers can be considered as a thermodynamic change of state (56). Thus, unliganded dimers are an intermediate in the activation process. When unliganded dimers are present, the response of the pre-formed dimers to ligand is not limited by the diffusion of the receptors in the plasma membrane and is thus faster. As a result, there is interest in understanding the unliganded dimer state, with the long-term goal of understanding RTK activation.

This work yields new knowledge about the unliganded FGFR3 state by demonstrating that FGFR3 JM domain plays an important role in unliganded dimer stabilization. The biological significance of our observations comes from the fact that the JM contribution is similar in magnitude to the effect of pathogenic mutations that stabilize the FGFR3 dimers, and is additive. Furthermore, the effect opposes and cancels the inhibitory contribution of the EC domain.

Since RTKs are implicated in many human cancers and developmental abnormalities, new strategies are being sought to inhibit their dimerization and activation. And because the unliganded FGFR3 dimer is an activation intermediate, its destabilization could be a viable therapeutic strategy. The significant stabilization of FGFR3 unliganded dimers by the JM domains suggests that JM-mediated interactions could be a novel target.

	ΔG (kcal/mol)	$\Delta\Delta G_{JM}$ (kcal/ mol)	Intrinsic FRET, Ẽ	D(Å)
FGFR3 EC-TM-$(GGS)_5$-FP	-3.4 (-3.2 to -3.6)		0.52(0.46 to 0.57)	52.42 (50.7 to 54.6)
FGFR3 EC-TM-JM-FP	-5.4 (-5, to -6)	-2	0.57(0.53 to 0.61)	50.7 (49.3 to 52.1)
FGFR3 EC-TM-JM_{60}-FP	-5.3 (-5,-5.9)	-1.9	0.7(0.66 to 0.74)	46.1 (44.6 to 47.6)
FGFR3 TM-$(GGS)_5$-FP	-5.2 (-5.0 to -5.4)		0.65(0.64 to 0.67)	47.9 (47.2 to 48.2)
FGFR3 TM-JM_{60}-FP	100% dimer-	> -1.5	0.38±0.01	57.6 (56.6 to 58.6)
GpA-$(GGS)_5$-FP	-5.3 (-5,-5.4)		0.52(0.5 to 0.54)	52.4 (51.7 to 53.1)
GpA-$(GGS)_3$-FP	-5.2 (-5,-5.4)		0.53(0.52 to 0.55)	52.0 (51.4 to 52.4)
GpA-$(GGS)_2$-FP	-5.4 (-5.2,-5.6)		0.41(0.39 to 0.43)	56.5 (55.7 to 57.2)
GpA-$(GGS)_2$-JM-FP	-5.3 (-5,-5.9)	0	0.54(0.52 to 0.57)	51.7 (50.7 to 52.4)
FGFR3 EC-TM_{A391E}-$(GGS)_5$-FP	-4.8 (-4.5 to -5.0)		0.72(0.68 to 0.74)	45.4 (44.6 to 46.85)
FGFR3 EC-TM_{A391E}-JM_{60}-FP	-6.6 (-6.2 to -8.9)	-1.8	0.83(0.8 to 0.86)	40.8 (42.2 to 39.2)

Table 4-1. Dimer stabilities and Intrinsic FRET for the proteins studies here. Shown are optimal values and 95% confidence intervals. Ẽ is the value of the Intrinsic FRET, which depends on the distance between the fluorescent proteins and on their mobility within the dimer. Average distance between the fluorescent proteins (D) is calculated under the assumption of free fluorescent protein rotation, which may not be correct in all cases.

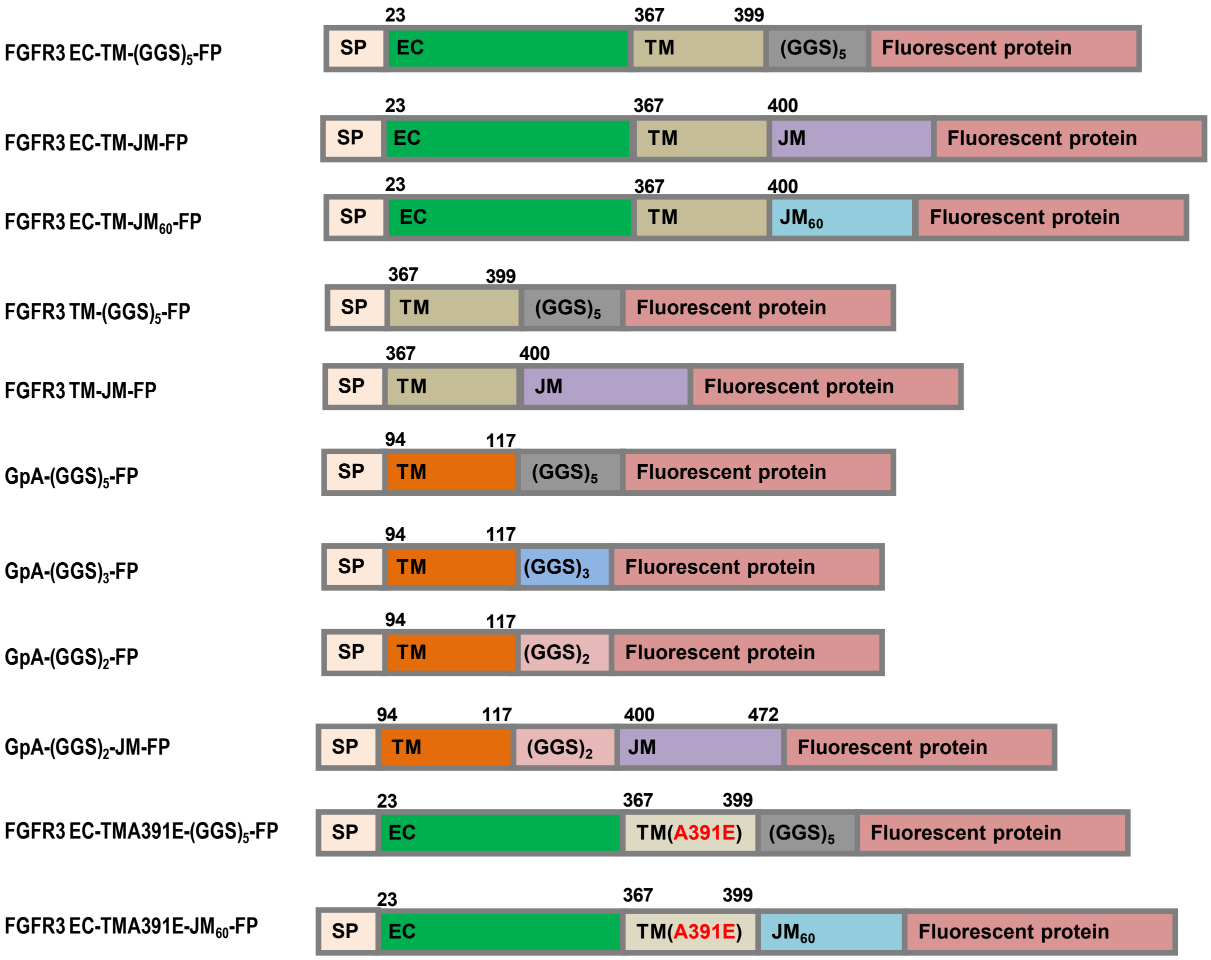

Figure 4-1. The plasmid constructs used in the FRET experiments. SP: FGFR3 signal peptide (**MGAPACALALCVAVAIVAGASS)**, EC: extracellular domain, FGFR3 TM domain: (DEAGSVYAG ILSYGVGFFLFILVVAAVTLCRLR), GpA TM domain: (LIIFGVMAGVIGTILLISYGIRRL), FGFR3 JM domain: (S PPKKGLGSPT VHKISRFPLK RQVSLESNAS MSSNTPLVRI ARLSSGEGPT LANVSELELP ADPKWELSRAR), FGFR3 JM_{60} (S PPKKGLGSPT VHKISRFPLK RQVSLESNAS MSSNTPLVRI ARLSSGEGPT LANVSELEL), FP: Fluorescent protein, either YFP or mCherry (a FRET pair).

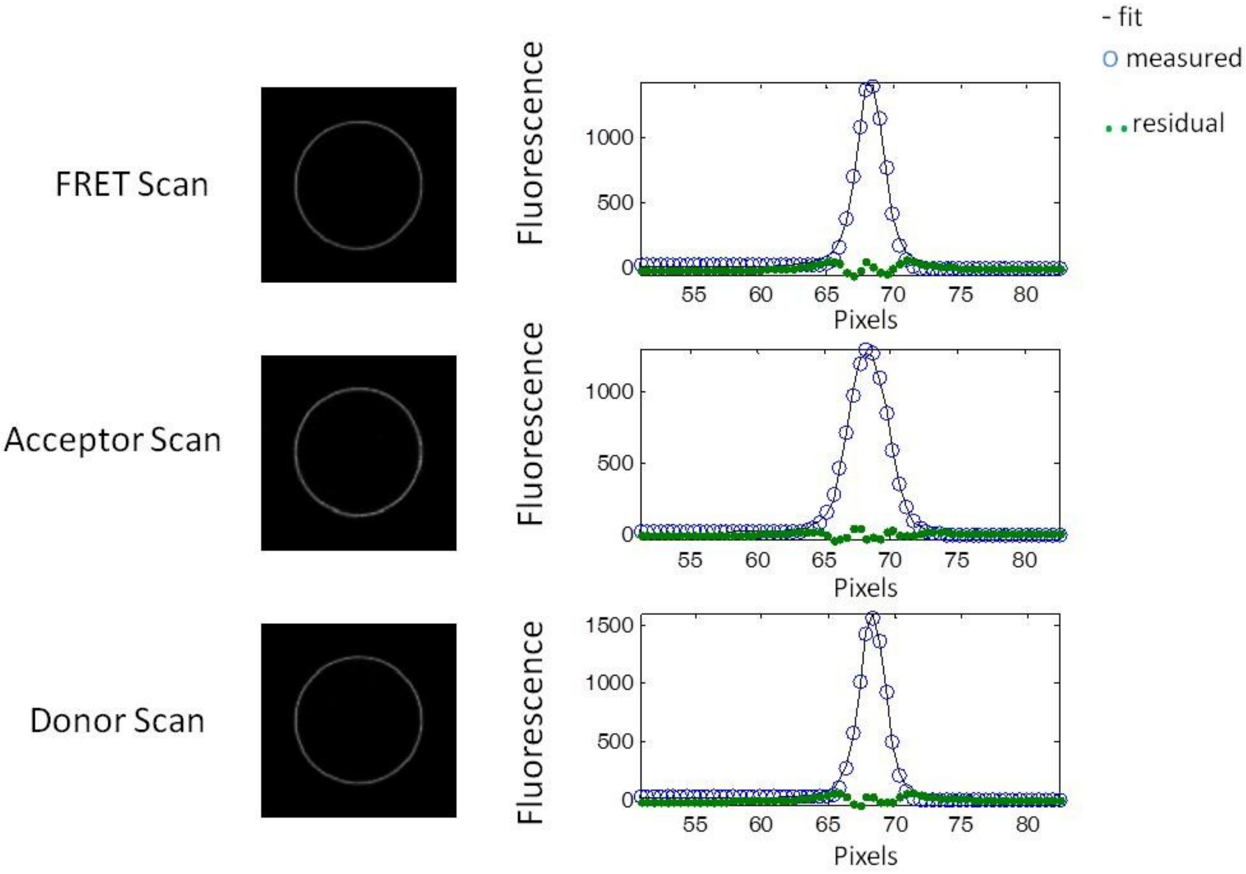

Figure 4-2. A vesicle, imaged and analyzed in the FRET, acceptor, and donor channels. Images were acquired with a Nikon laser scanning confocal microscope. The images are analyzed with a Matlab code that has been discussed in detail in a previous publication (22). The intensity across the membrane (open blue symbols) is fit to a Gaussian (solid line) after background correction. The green dotted line is the residual from the fit.

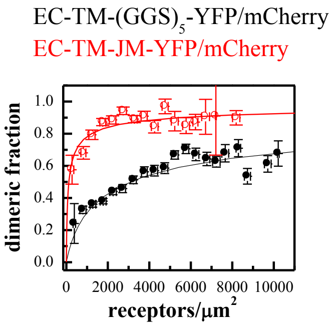

Figure 4-3. Dimerization curves for EC-TM-(GGS)$_5$-YFP/mCherry and EC-TM-JM-YFP/mCherry. The dimer that contains the JM domain is more stable.

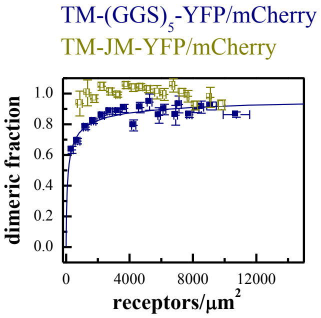

Figure 4-4. Dimerization curves for TM-(GGS)$_5$-YFP/mCherry and TM-JM-YFP/mCherry. The dimer that contains the JM domain is more stable.

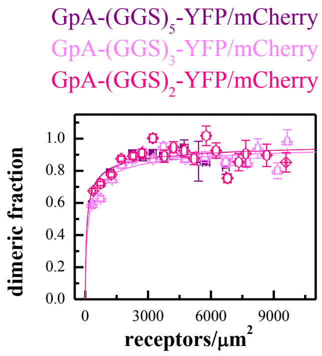

Figure 4-5. Dimerization curves for three Glycophorin A TM helix constructs in which the fluorescent proteins are attached to the TM helix via different length linkers. The linker length does not affect dimer stability.

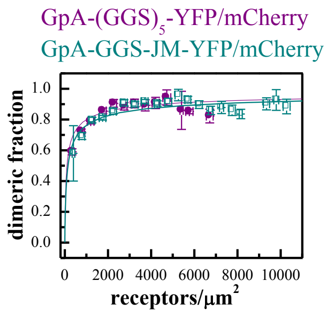

Figure 4-6. Dimerization curves for GpA-(GGS)$_5$-YFP/mCherry and GpA-(GGS)2-JM-YFP/mCherry. The two dimers are equally stable.

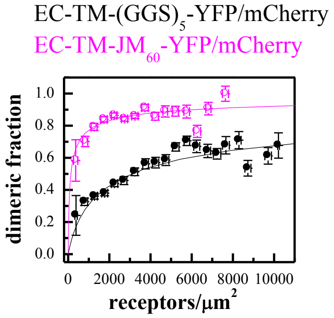

Figure 4-7. Dimerization curves for EC-TM-$(GGS)_5$-YFP/mCherry and EC-TM-JM_{60}-YFP/mCherry. The shorter JM domain stabilizes the dimer to the same extent as the full-length JM domain (see Figure 3 and Table 1).

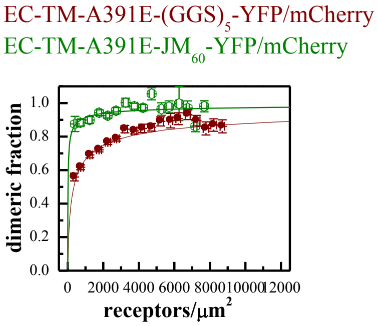

Figure 4-8. Dimerization curves for and EC-TMA391E-$(GGS)_5$-YFP/mCherry and EC-TMA391E-JM_{60}-YFP/mCherry. The A391E mutation is the genetic cause for Crouzon syndrome with acanthosis nigricans. The JM domain stabilizes the mutant dimer.

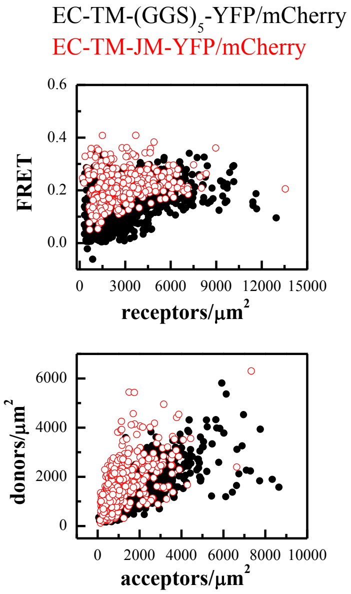

Figure S1(4-9).

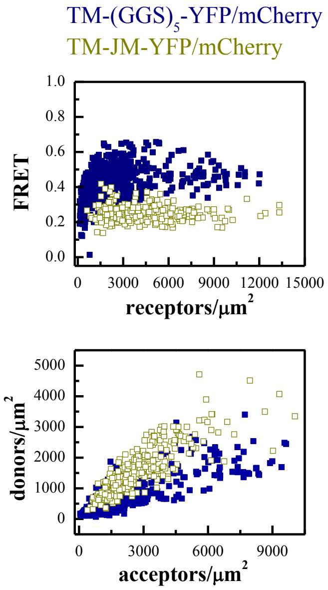

Figure S2(4-10).

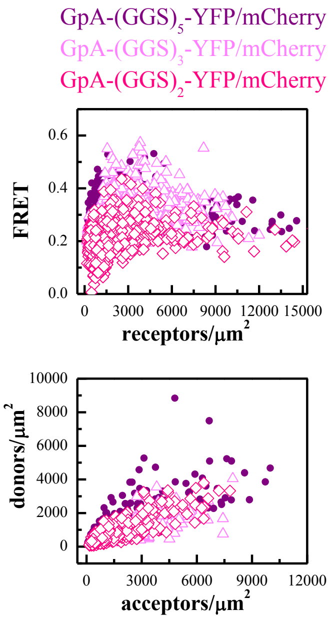

Figure S3(4-11).

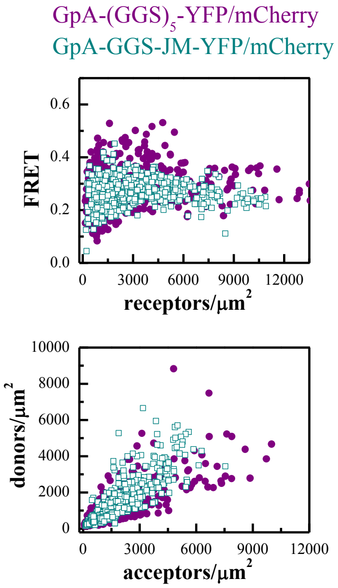

Figure S4(4-12).

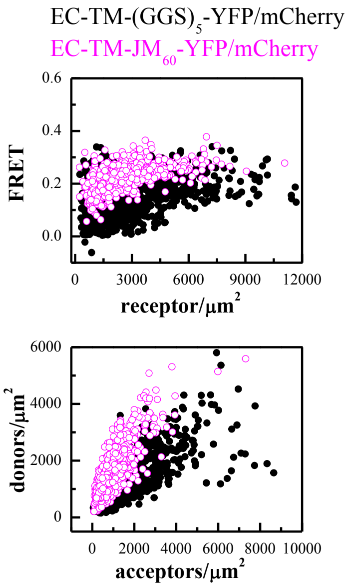

Figure S5 (4-13).

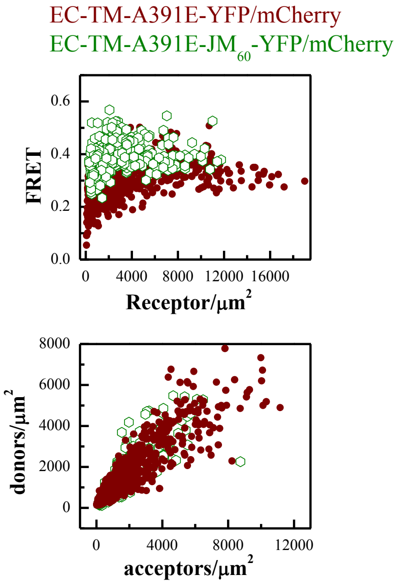

Figure S6(4-14).

Chapter 5. Strong inter-molecular disulfide linked dimers caused by mutations of key intramolecular Cysteines in FGF receptors

Abstract

FGF receptors play crucial roles in embryonic and adult development. Missense mutations in FGFR1, 2 and 3 are linked to a wide array of skeletal disorders. Many of these mutations are in cysteines of receptor Ig domains, which form intrachain disulfide bonds. Here we investigated how pathogenic mutations of key cysteines in FGFR structure affect dimerization and activation of the receptors. In particular we quantify the effect of the pathogenic cysteine mutations on FGFR1, 2 and 3 dimer stability. We show that the FGFR1/C178S, FGFR2/C342R and FGFR3/C228R from disulfide linked dimers of various strengths in the absence of ligands even at physiological concentrations. The mutations increase dimer stability substantially with FGFR2 C342R and FGFR3 C228R forming the strongest (constitutive) dimers. We further show that these mutations induce a structural change in unliganded FGF receptor dimer.

Keywords: Receptor tyrosine kinases, dimerization, cysteine, skeletal disorders, disulfide bond, dimer stability

5.1. Introduction

Fibroblast growth factor receptors (FGFR1-4) comprise a family of transmembrane tyrosine kinases which bind with high affinity to 22 distinct FGF ligands in humans. FGFRs play a key role in the regulation of cell differentiation, migration, proliferation and apoptosis. They are critically required for embryonic development, lung morphogenesis, osteogenesis and limb bud development. It has been established that FGFRs homodimerize in the absence of ligands (3, 84, 155). This ligand-independent dimerization induces receptor phosphorylation at a basal level resulting in low activity of the receptor. Mutations in FGFR genes (for example over sixty mutations only in FGFR2) are associated with pathologies such as skeletal disorders and various forms of cancer (110, 151). Interestingly, somatic mutations found in cancers are identical to germline mutations which cause skeletal abnormalities such as Crouzon syndrome (CS), Apert syndrome (AS) and Pfieffer syndrome (PS)(153). One example is the A391E mutation in FGFR3, identified as a somatic mutation in bladder cancers (152, 153) but also found in individuals with CS with Acanthosis nigricans. Other cases include gain or loss of a cysteine residue in FGFR1, FGFR2 and FGFR3. Examples of such mutations are Arg248Cys, Ser249Cys, Gly370Cys, Ser371Cys, and Tyr373Cys in FGFR3, associated with Thanatophoric dysplasia (TD) where a single amino acid is substituted with a cysteine (2, 27, 151). Other examples of pathogenic cysteine mutations are C178S in FGFR1, C342R in FGFR2, and C228R in FGFR3.

The phenotypes due to FGFR cysteine mutations have been linked to high activity or loss of activity of the receptors. However, the physico-chemical basis for the behavior of these mutants remains unknown. This lack of basic knowledge is a major obstacle for drug discoveries, as the goal is to target specific mutant FGFR complexes and not wild type FGFR dimers, in various skeletal diseases and cancers.

Here we investigate the effect of cysteine mutations in FGFR1 (C178S), FGFR2 (C342R) and FGFR3 (C228R) on the dimerization and activation of these receptors. These mutations disrupt intramolecular disulfide bonds in Ig domains. We aimed to study the effect of these cysteine mutations on the stability and structure of the unliganded dimer. We found that mutations of these critical cysteines result in increased propensity for dimerization in the absence of fgf ligands, likely due to the formation of disulfide bonds between unpaired cysteines in the Ig-like domains. The mutations also induce structural changes in the intracellular domains of the receptor dimers and hence, alter the activity of the receptors.

Here we approached the problem using the QI-FRET method, which allowed us to measure the dimerization propensity and the Intrinsic FRET for the mutant receptor dimers. The measurements were carried out in plasma membrane vesicles derived from CHO cells (33). The dimerization constant, K, and the Intrinsic FRET, $\tilde{E}$, were parameters which were obtained from a two parameter fitting to the measured dimeric fractions. The intrinsic FRET monitors structural changes by reporting on the distance between the fluorescent proteins (FRET pair).

5.2. Materials and Methods. The YFP plasmid was received from Dr. M. Betenbaugh (Johns Hopkins University, Baltimore, MD) and the pRSET-mCherry plasmid was obtained from Dr. R.Tsien (University of California, San Diego). The plasmids encoding human wild-type FGFR1 and FGFR2 in the pRK5 vector were received from Dr.M.Mohammadi, NYU. The plasmid encoding human wild-type FGFR3 was a gift from Dr. D. J. Donoghue, UCSD. All of the plasmids used for mammalian expression were constructed with pcDNA 3.1(+) vector (Invitrogen). All primers were purchased from Invitrogen.

The cloning procedure for wild type full length human FGFR1, FGFR2 and FGFR3 in pcDNA3.1(+) vector have been described previously (Sarabipour and Hristova FGFR 2015). Cloning of FGFR1-(GGS)-YFP, FGFR1-(GGS)-mCherry, FGFR2-(GGS)-YFP, FGFR2-(GGS)-mCherry, FGFR3-(GGS)-YFP and FGFR3-(GGS)-mCherry is described in detail in (Sarabipour et al FGFR 2015). Detailed cloning procedure for FGFR3 EC-TM-$(GGS)_5$-YFP, FGFR3 EC-TM-$(GGS)_5$-mCherry is described in (Chen et al 2010), FGFR1 EC-TM-$(GGS)_5$-YFP, FGFR1 EC-TM-$(GGS)_5$-mCherry, FGFR2 EC-TM-$(GGS)_5$-YFP, FGFR2 EC-TM-$(GGS)_5$-mCherry is described in (Sarabipour and Hristova FGFR 2015).

For this work, we created 12 plasmid constructs by creating missense mutations in full length and truncated FGFR1, FGFR2 and FGFR3 (Figure 1). We created C228R mutation in FGFR3 EC-TM-$(GGS)_5$-YFP, FGFR3 EC-TM-$(GGS)_5$-mCherry, FGFR3-(GGS)-YFP and FGFR3-(GGS)-mCherry plasmid constructs. We introduced C342R into FGFR2 EC-TM-$(GGS)_5$-YFP, FGFR2 EC-TM-$(GGS)_5$-mCherr, FGFR2-(GGS)-YFP and FGFR2-(GGS)-mCherry plasmid constructs. Finally we created C178S mutation in FGFR1 EC-TM-$(GGS)_5$-YFP, FGFR1 EC-TM-$(GGS)_5$-mCherry, FGFR1-(GGS)-YFP and FGFR1-(GGS)-mCherry plasmid constructs using QuickChange ® II XL Site-Directed Mutagenesis Kit (Stratagene, CA).

5.2.1. Cell culture and transfection. Chinese Hamster Ovary cell (CHO) and Human Embryonic Kidney (HEK) 293 T cells were cultures at 37 ˚C with 5% CO_2 for 24h. Transfection was carried out using Fugene HD transfection reagent (Roche Applied Science), following the manufacturer's protocol. Cells were cotransfected with 3-7 ug of DNA encoding either (i) pcDNA-FGFR1-YFP and pcDNA-FGFR1-mCherry, (ii) pcDNA-FGFR2-YFP and pcDNA-FGFR2-mCherry, or (iii) pcDNA-FGFR3-YFP and pcDNA-FGFR3-mCherry. Cells were vesiculated 24 h post transfection as described below. We have not observed staining for FGFR1, 2 or 3 (via Western blots) in the CHO and HEK293T cells unless transfected.

5.2.2. Production of mammalian plasma membrane vesicles. Vesiculation was performed using a chloride salt vesiculation buffer consisting of of 200 mM NaCl, 5 mM KCl, 0.5 mM $MgSO_4$, 0.75 mM $CaCl_2$, 100 mM bicine and protease inhibitor cocktail (Complete mini EDTA-free tabs, Roche Applied Science) adjusted to PH of 8.5. (33). CHO cells were rinsed twice with 30% PBS (pH 7.4), and incubated with 1 mL of chloride salt vesiculation buffer overnight at 37 °C. A large number of vesicles were produced after 12 h, and the vesicles were transferred into 4-well Nunc Lab-Tek II chambered coverslips for imaging. Images of vesicles with labeled FGF receptors are shown in Figure S1. Most of the cytoplasm in the vesicles is lost during vesicle production, as attested by the fact that soluble fluorescent proteins are not retained inside the vesicles (Sarabipour et al 2015, lipids).

5.2.3. QI-FRET Image Acquisition. Vesicles were imaged using a Nikon Eclipse confocal laser scanning microscope using a 60× water immersion objective. All the images were collected and stored at a 512 × 512 resolution. Three different scans were performed for each vesicle: (1) excitation at 488 nm, with a 500-530 nm emission filter (donor scan); (2) excitation at 488 nm, with a 565-615 nm emission filter (FRET scan); and (3) excitation at 543 nm, with a 650 nm longpass filter (acceptor scan). Gains of 8.0 were used for all the three scans. The bleaching of the fluorescent proteins was minimized through the use of ND8 filters when exciting with the 488 nm laser, and low pixel dwell time (1.68 μs).

5.2.4. QI-FRET data Analysis: Methodology and Protocol. The quantitative imaging FRET method

5.2.5. Western blots. CHO and HEK293T cells were starved in serum-free medium for 24 h following transfection and then treated with lysis buffer (25 mM Tris-HCl, 0.5% Triton X-100, 20mM NaCl, 2 mM EDTA, phosphatase inhibitor and protease inhibitor, Roche Applied Science). Lysates were collected following centrifugation at 15,000 g for 15 min at 4 °C and loaded onto 3–8%NuPAGE®Novex®Tris–Acetatemini gels (Invitrogen, CA). The proteins were transferred onto a nitrocellulose membrane, and blocked using 5% milk in TBS. The expression of the receptors was probed with anti-FGFR antibodies. FGFR total protein levels were assessed using antibodies against FGFR3 (H-100; sc-9007), FGFR2 (H-80; sc-20735) and FGFR1 (H-76; sc-7945) from Santa Cruz Biotechnology. Phosphotyrosine levels were assessed using Phospho-FGF receptor antibodies (Tyr653/654; #3471, Cell Signaling Technologies) which is raised against residues surrounding Tyr653/654 FGFR1 but the corresponding sequence is the same for FGFR2 and FGFR3. So this antibody detects endogenous levels of all three FGF receptors only when phosphorylated at Tyr653/654. This was followed by anti-rabbit

HRP conjugated antibodies (W4011, Promega). The proteins were detected using the Amersham ECL detection system (GE Healthcare).

5.3. Results & Discussion

Figure 1 shows the general structure of FGF receptors and the location of the cysteine mutations investigated in this chapter.

5.3.1. FGFR1 C178S. The C178S mutation in Ig-like D1 of FGFR1 is associated with Kallman syndrome. The pediatric phenotype of this syndrome includes severe ear anomalies (hypoplasia or agenesis of the external ear), failure to start puberty, infertility and complete lack of sense of smell. It occurs in 1 in 10,000 men and 1 in 50,000 women (166). To investigate the effect of this mutation on FGFR1 dimerization, we created the C178S mutation in FGFR1, which has been tagged with YFP or mCherry as a FRET pair (Figure S1). Dimerization was studied in plasma membrane vesicles using QI-FRET, a methodology which allows measurements of dimerization propensities and structural changes. The two constructs FGFR1$_{C178S}$-YFP and FGFR1C178S-mCherry were co-expressed in CHO cells. Twenty four hours after transfection, the cells were treated with chloride salt buffer overnight at 37˚C to induce shedding of plasma membrane vesicles bearing the receptors. Vesicles were collected in 4 chambered slides and imaged in a confocal laser scanning microscope (22). Each vesicle was imaged in 3 scans: (i) a donor scan giving the fluorescence of the FRET donor, YFP, when excited directly (ii) a FRET scan giving the fluorescence of the acceptor fluorophore, mCherry, when excited indirectly by energy transfer from the donor (iii) an acceptor scan which gives the fluorescence of the acceptor when excited directly. The intensity of each vesicle image was quantified using a Matlab program as described previously (22). Using the intensity values and parameters obtained from calibrations performed with purified solutions of YFP and mCherry, the donor concentration, the acceptor concentration and the FRET efficiencies were obtained for each vesicle. Figure 1 (I) shows (A) the FRET efficiency as a function of total receptor (donor labeled + acceptor labeled) concentration, (B) donor versus acceptor concentrations and (C) dimeric fractions as a function of total receptor concentration for wild type FGFR1 and the C178S FGFR1 mutant. A monomer-dimer equilibrium model with two adjustable parameters, the dimerization constant K and the intrinsic FRET efficiency $\tilde{E}$ was fitted to the data in Figure 2 (IA), yielding the optimal K and $\tilde{E}$ values for the receptors. Then, each data set in Figure 2 was divided by the optimal $\tilde{E}$ to obtain the dimeric fraction in each vesicle as a function of the total receptor concentration in the vesicles. Then, the dimeric fractions for similar receptor concentrations were averaged within bins of width 500 receptors/μm^2. Along with these data, the theoretical dimeric fraction is plotted for each receptor for the optimal value of K determined in the fit. The results demonstrate that the C178S mutation modestly increases the dimerization propensity of FGFR1 by -1.2 kcal/mol (Table 1).

The QI-FRET method allows us to calculate distances between fluorescent proteins and thus monitor structural changes which occur within the receptor dimers due to mutations. As shown in Table 1, The Intrinsic FRET value for C178S FGFR1 dimers was measured as 0.7±0.02 and was the same as the Intrinsic FRET value for the wild-type FGFR1 dimers (0.66±0.02). Thus, the C178S mutation did not change the distance between the fluorescent proteins in the FGFR1 dimer.

In the full length receptors, the fluorophores are attached to the C-terminal tail at the end of the intracellular domain (plasmid constructs shown in Fig S1), which are flexible. Thus, it is possible that structural changes are not detected, although they occur. We have shown in Chapter 1 that the structure of the transmembrane domain can be monitored when this domain is directly attached to fluorescent proteins via a flexible linker. In order to monitor possible structural changes which may be propagated from the extracellular domain to the TM domain, we deleted the intracellular domains of wild-type FGFR1 and the C178S mutant and replaced it with a flexible $(GGS)_5$ 15 amino acid linker attached to YFP or mCherry. The results for EC-TM FGFR1 and EC-TM $FGFR1_{C178S}$ are shown in Fig.2 (II). The mutation increases the dimerization propensity of truncated FGFR1 by -0.7 kcal/mol, an effect that is even smaller than in the case of the full-length receptor. The Intrinsic FRET measured showed that the C178S mutation induces a structural change by moving the TM domain C-termini of FGFR1 closer to each other (Intrinsic FRET = 0.68) compared to wild-type EC-TM FGFR1 (Intrinsic FRET = 0.5). Over-all, the data show that the effect of this mutation on dimerization is modest, and that the mutation induces a structural change in the dimer.

We probed the nature of the C178S dimer by non-reducing SDS gel followed by Western blot staining for FGFR1. The schematic of the plasmid constructs used for western blotting experiments is shown in Figure S2. As shown in figure 3, $FGFR1_{C178S}$ and EC-TM $FGFR1_{C178S}$ form dimers on a non-reducing gel, but not on a reducing gel, demonstrating the formation of inter-molecular disulfide bonds by the unpaired cysteines. We further probed the activation of the C178S FGFR1 mutant. Figure 3 demonstrates that the C178S mutation results in a loss of function in FGFR1, as evident from the reduced intensity of the anti-pY653/654 bands for the C178S FGFR1 mutant compared to wild-type FGFR1.

5.3.2. FGFR2 C342R. The C342R mutation in the Ig-like D3 of FGFR2 is observed in individuals with Crouzon Syndrome (CS), Jackson-Weiss syndrome (JWS), and Antley-Bixler-like syndrome (ABS2) (69, 73, 75, 93, 107-110, 117, 118, 121, 149). Crouzon syndrome is characterized by premature fusion of one or several skull sutures (craniosynostosis), and has an incident rate of 1 in 2500 individuals. If untreated, the abnormal skull growth may result in impaired cerebral blood flow, impaired vision, impaired hearing and central nervous system problems (60). The JWS phenotype is characterized by foot abnormalities, the PS phenotype is characterized by short fingers and soft-tissue syndactyly, and the ABS2 phenotype is characterized by craniofacial and limb abnormalities (50, 94, 107, 121). The mutation C342R disrupts the C278-C342 intramolecular disulfide bond.

We measured the dimerization of wild-type FGFR2 and the C342R FGFR2 mutant in CHO cell-derived plasma membrane vesicles. Each data point in Figure 4 represents a vesicle. Figure 4 (I) shows the FRET efficiency as a function of total receptors/μm^2 for FGFR2 and $FGFR_{C342R}$. The dimeric fraction measured for $FGFR2_{C342R}$ is 100%, indicative of formation of constitutive dimers. The Intrinsic FRET value for wild-type FGFR2 was measured as 0.43±0.02 while the Intrinsic FRET value for the C342R FGFR2 mutant was 0.55±0.02. Thus, the C342R mutation is responsible for a conformational change in FGFR2 dimers which propagated from the EC domain to the tyrosine kinase domain and the C-terminal tail of the receptor.

We further measured the dimerization propensity of the EC-TM FGFR2 constructs. Figure 4 (II) shows the FRET efficiency and dimeric fractions for ECTM-FGFR2 and ECTM-FGFR2$_{C342R}$ as a function of total receptor concentration. The EC-TM FGFR2 dimer stability was -3.4 kcal/mole while the ECTM-FGFR2$_{C342R}$ formed constitutive dimers (Figure 4 II).

Unlike the C178S mutation in FGFR1, the C342R mutation in FGFR2 strongly stabilized the unliganded dimer. The mutation also induces a structural change in FGFR2 dimer by shifting the Iintrinsic FRET value from 0.57 to 0.72.

Consistent with the FRET results, Figure 5 demonstrates that in all cases the mutant FGFR2 monomer band completely shifts to a dimer in non-reducing gels, indicating strong disulfide bond formation between the mutant receptors. Thus, in conclusion, the mutation disrupts the C278-C342 intramolecular disulfide bond and disrupts the structure of the FGFR2 dimer, as evident from the change in the Intrinsic FRET value. The mutant favors the formation of an inter molecular disulfide bond as evident from the non-reduced SDS PAGE results (Figure 5).

5.3.3. FGFR3 C228R. Colorectal cancer is the most common type of intestinal cancer with 140,000 cases each year in the United States alone, according to the National Cancer Institute. The C228R mutation in Ig-like D2 of FGFR3 is a somatic mutation found in human colorectal carcinoma (50). The mutation disrupts one of the three intramolecular disulfide bonds in D2 (they occur between C61-C109, C176-C228 and C275-C339). To investigate the effect of the C228R mutation on FGFR3 dimerization, we generated the mutation in full length FGFR3 tagged with YFP or mCherry, as well as in the truncated EC-TM FGFR3 constructs. The results of the FRET experiments are shown in Fig 6.

We next performed FRET experiments with the full-length and the truncated EC-TM FGFR2 constructs. The increase in stability due to the mutation in EC-TM FGFR3 is -2.3 kcal/mol (Figure 6 II, Table 1). The increase in full length FGFR3 dimerization was even higher and the receptor forms constitutive (100%) dimers (Figure 6 I). Similarly to the FGFR2 C342R mutation and unlike the FGFR1 C178S mutation, the FGFR3 C228R mutation strongly contributes to receptor dimerization. The mutation induced a structural change in full-length FGFR3, shown by the Intrinsic FRET value of 0.63 (compared to Intrinsic FRET=0.55 for WT FGFR3, Table 1). This structural change was also observed for the EC-TM FGFR3 C228R construct with an Intrinsic FRET value of 0.69 (compared to Intrinsic FRET of 0.51 for WT EC-TM FGFR3).

We assessed the dimerization of FGFR3 C228R and EC-TM FGFR3 C228R using reducing and non-reducing SDS PAGE. Figure 7 A shows that FGFR3 C228R formed disulfide linked dimers in non-reducing SDS, but the receptor migrated as monomer only in the reduced SDS PAGE (Figure 7B), suggesting that disulfide bonds stabilize the dimers. Similarly, the EC-TM FGFR3 C228R formed cysteine linked dimers in the non-reducing environment (Figure 7C) but not in reducing one (Figure 7D).

When assessing phosphorylation of FGFR3 C228R, we found that the mutant receptor was mainly expressed in its unglycosylated form in HEK293T cells (Figure 7E). However, the receptor was phoshphorylated at key tyrosine residues (Y653/654), and thus active.

5.4. Conclusion

Here we measured the difference in dimerization between wild type FGFR1 and C178S FGFR1, wild type FGFR2 and C342R FGFR2, wild type FGFR3 and C228R FGFR3 in plasma membrane-derived vesicles of CHO cells. We investigated these mutations in full length and truncated receptors.

Cysteine mutations are extremely challenging to study by crystallography due to the oxidative conditions required for the formation of disulfide bonds. Here we used a quantitative FRET methodology and we observed modest to strong dimer stabilization as a result of the FGFR1 C178S, FGFR2 C342R and FGFR3 C228R mutations. We probed the nature of dimer formation by non-reducing SDS gels followed by Western blots and FGFR staining. The results demonstrated formation of disulfide bonds due to the three mutations. Finally, we probed the activation of wild type and mutant FGFRs and we found that the FGFR1 C178S mutation results in loss of function and that the FGFR3 C228R mutant is highly phosphorylated as an unglycosylated receptor inside the cell.

Figures

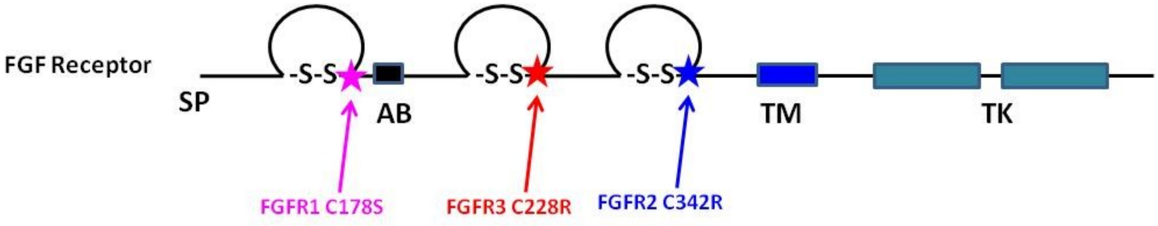

Figure 5-1. Schematic of FGF receptor structure and location of the three mutations investigated here.

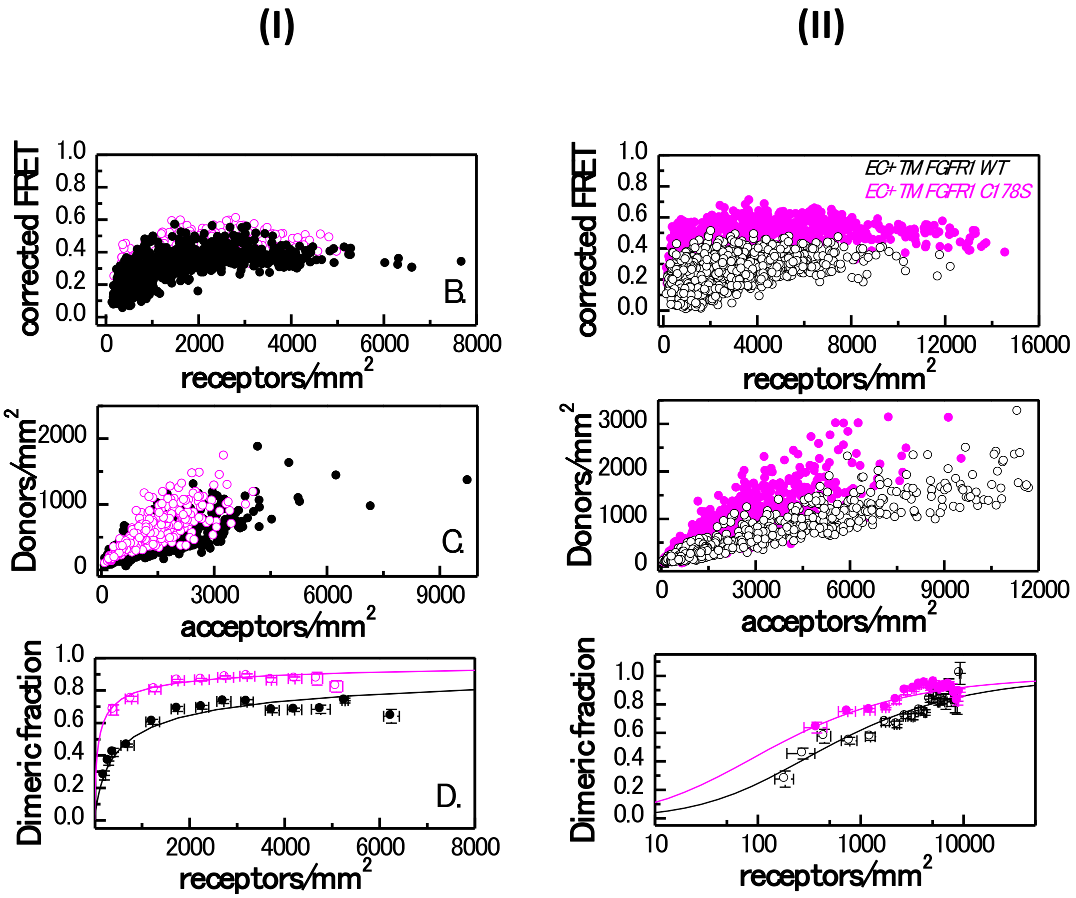

Figure 5-2. (I) FRET results for wild type FGFR1 (solid black circles) and C178S FGFR1 (open magenta circles). Each data point represents a vesicle. Donor versus acceptor concentration in each vesicle. DNA ratios in transfections varied from 1:2 to 1:5, and the acceptor concentration exceeds the donor concentration in all cases. This difference in expression is necessary in our experiments because of the different quantum yields of the donor (0.61) and the acceptor (0.22), and is fully accounted for in the data analysis. (II) FRET results for EC+TM wild type FGFR1 (open black circles) and C178S FGFR1 (solid magenta circles). C178S results in a modest increase ((0.7 kcal/mol for EC-TM), (1.2 kcal/mol for full length) higher stability for FGFR dimers).

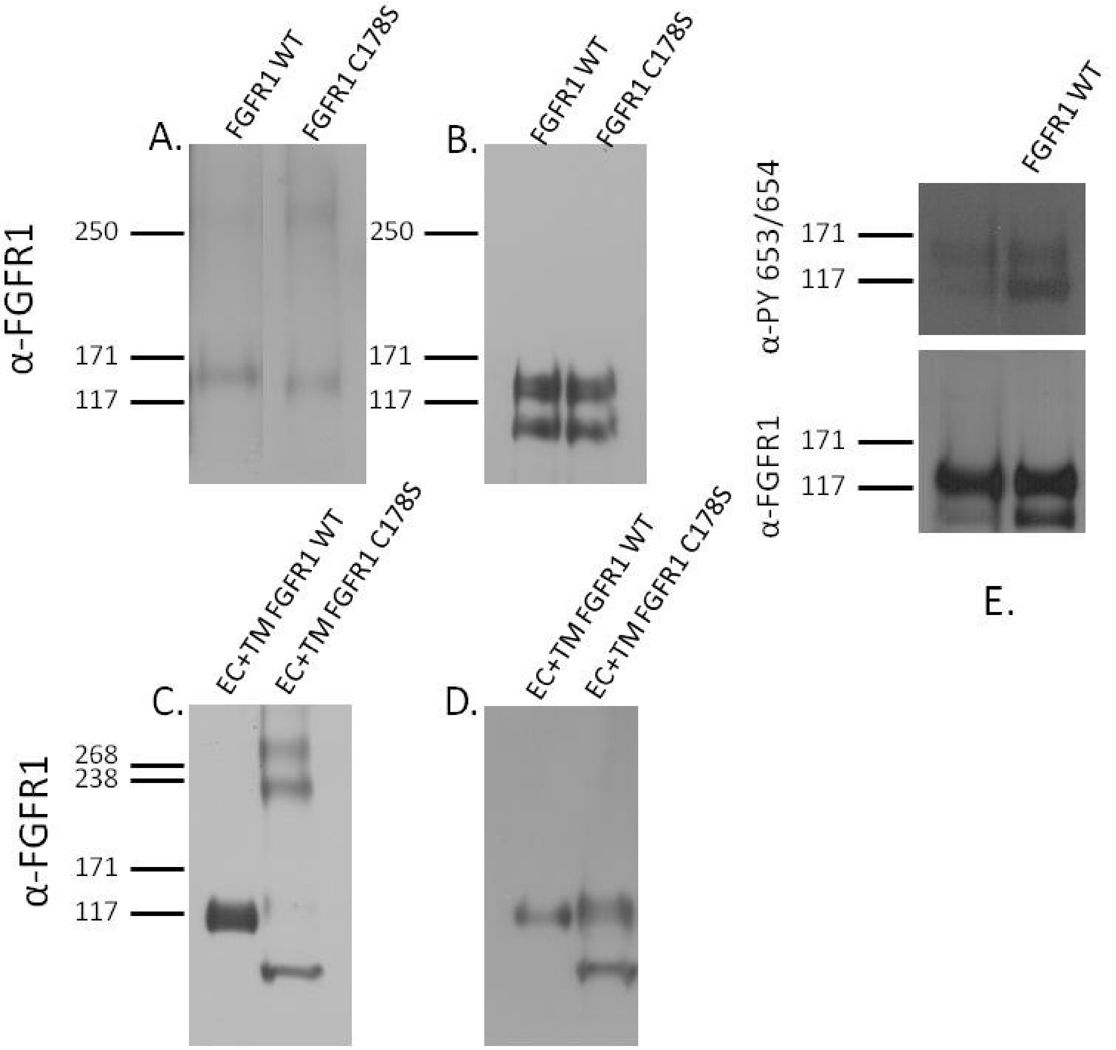

Figure 5-3. Anti-FGFR1 staining of (A) non-reducing and (B) reducing western blots for wild type and C178S FGFR1. Anti-FGFR1 staining of (C) non-reducing and (D) reducing western blots for wild type and C178S EC+TM FGFR1. (E) Anti-pY 653/654 staining revealed that C178S mutation results in FGFR1 loss of activation.

	ΔG (kcal/mol)	$\Delta\Delta G_{MUT}$(kcal/mol)	Ẽ	d(Å)
ECTM FGFR1 WT	-4.6(-4.4 to -4.8)		0.5(0.46 to 0.55)	53.1(51.4 to 54.6)
ECTM FGFR2 WT	-3.4(-3.2 to -3.6)		0.57(0.51 to 0.64)	50.68(48.3to 52.8)
ECTM FGFR3 WT	-3.4(-3.2 to -3.6)		0.52(0.46 to 0.57)	52.42(50.7 to 54.6)
ECTM FGFR1 C178S	-5.3(-5.2 to -5.4)	-0.7(-0.6 to -0.8)	0.68(0.66 to 0.7)	46.8 (46.1 to 47.6)
ECTM FGFR2 C342R	100% dimer	-	0.72 (0.71,0.73)	45.4 (45 to 46.1)
ECTM FGFR3 C228R	-5.7(-5.6 to -5.8)	-2.3	0.69(0.7 to 0.72)	46.8 (46.1 to 47.6)
Full FGFR1 WT	-4.3 (-4.0 to -4.5)		0.66 (0.64 to 0.69)	47.56 (46.5 to 48.3)
Full FGFR2 WT	-5.4(-5.2 to -5.7)		0.43(0.41 to 0.44)	55.67(55.3 to 56.4)
Full FGFR3 WT	-6.3(-6.0 to -6.8)		0.55(0.53 to 0.57)	51.4(50.7 to 52.1)
Full FGFR1 C178S	-5.5(-5.3 to -5.7)	-1.2 (-1.2 to -1.3)	0.7(0.68 to 0.72)	46.1 (45.4 to 46.8)
Full FGFR2 C342R	100% dimer	-	0.55(0.54 to 0.56)	51.4 (51 to 51.7)
Full FGFR3 C228R	100% dimer	-	0.63(0.62 to 0.64)	48.6 (48.2 to 48.9)

Table 5-1. Dimerization free energies (dimer stabilities) *ΔG* and Intrinsic FRET efficiencies $\tilde{E}$, obtained from least-square parameter fits to the FRET data for wild type and mutant full-length and truncated constructs that lack the IC domain (EC+TM).

[a] 95% confidence intervals

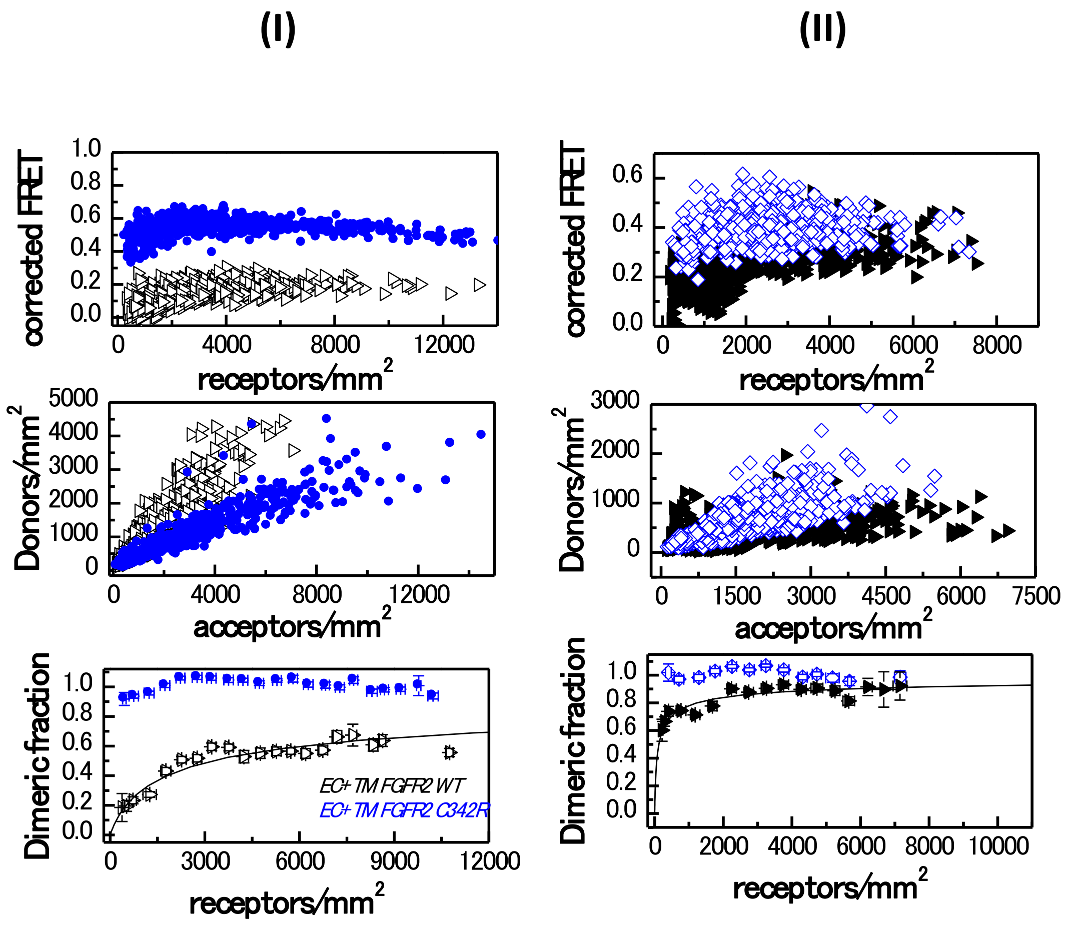

Figure 5-4. (I) FRET results for wild type FGFR2 (solid black triangles) and C342R FGFR2 (open blue diamonds). Each data point represents a vesicle. (II) FRET results for EC+TM wild type FGFR2 (open black triangles) and C342R FGFR2 (solid blue diamonds).

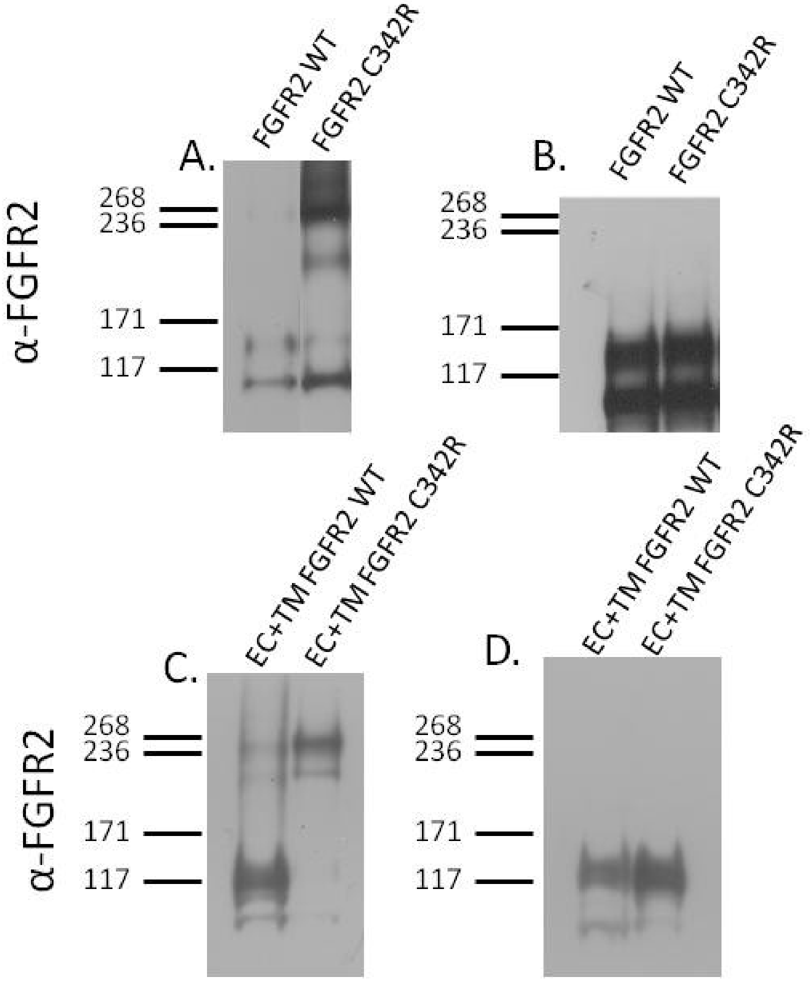

Figure 5-5. Anti-FGFR2 staining of (A) non-reducing and (B) reducing western blots for wild type and C342R FGFR2. Anti-FGFR2 staining of (C) non-reducing and (D) reducing western blots for wild type and C342R EC+TM FGFR2.

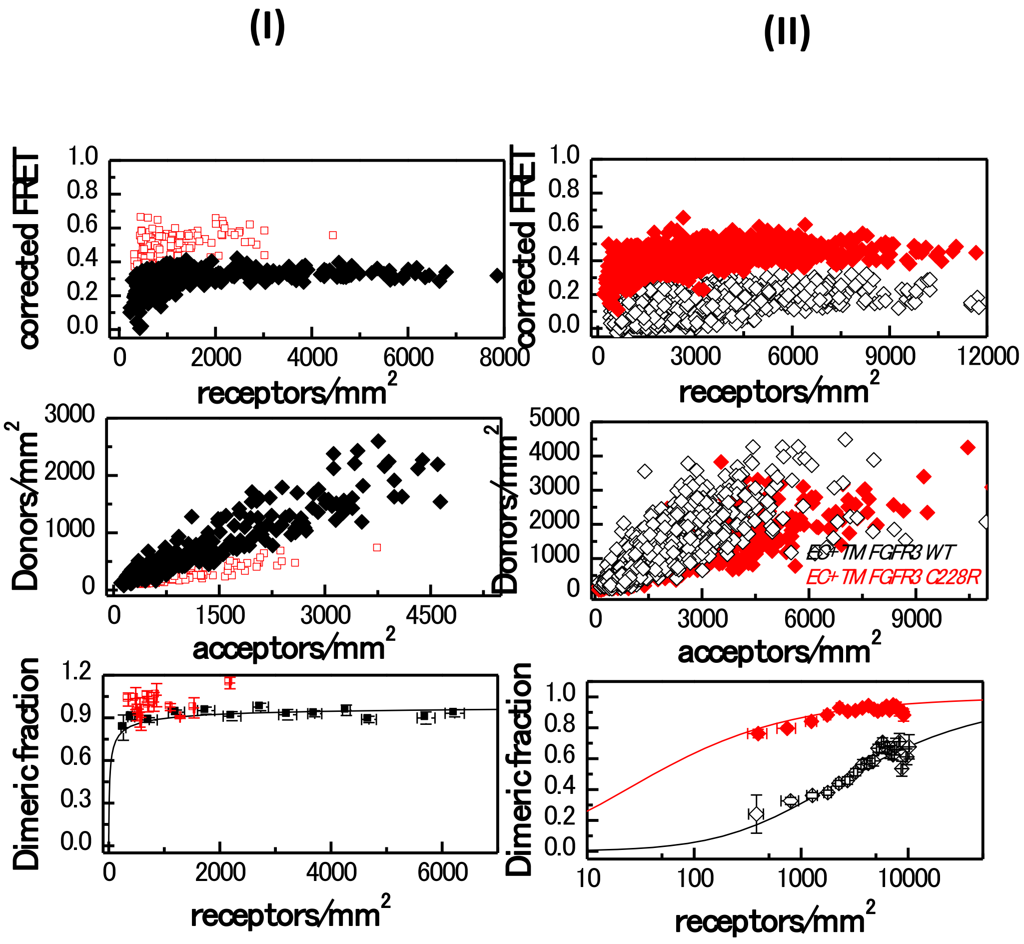

Figure 5-6. (I) FRET results for wild type FGFR3 (solid black diamonds) and C228R FGFR3 (open red squares). Each data point represents a vesicle. (II) FRET results for EC+TM wild type FGFR3 (open black diamonds) and C228R FGFR3 (solid red diamonds).

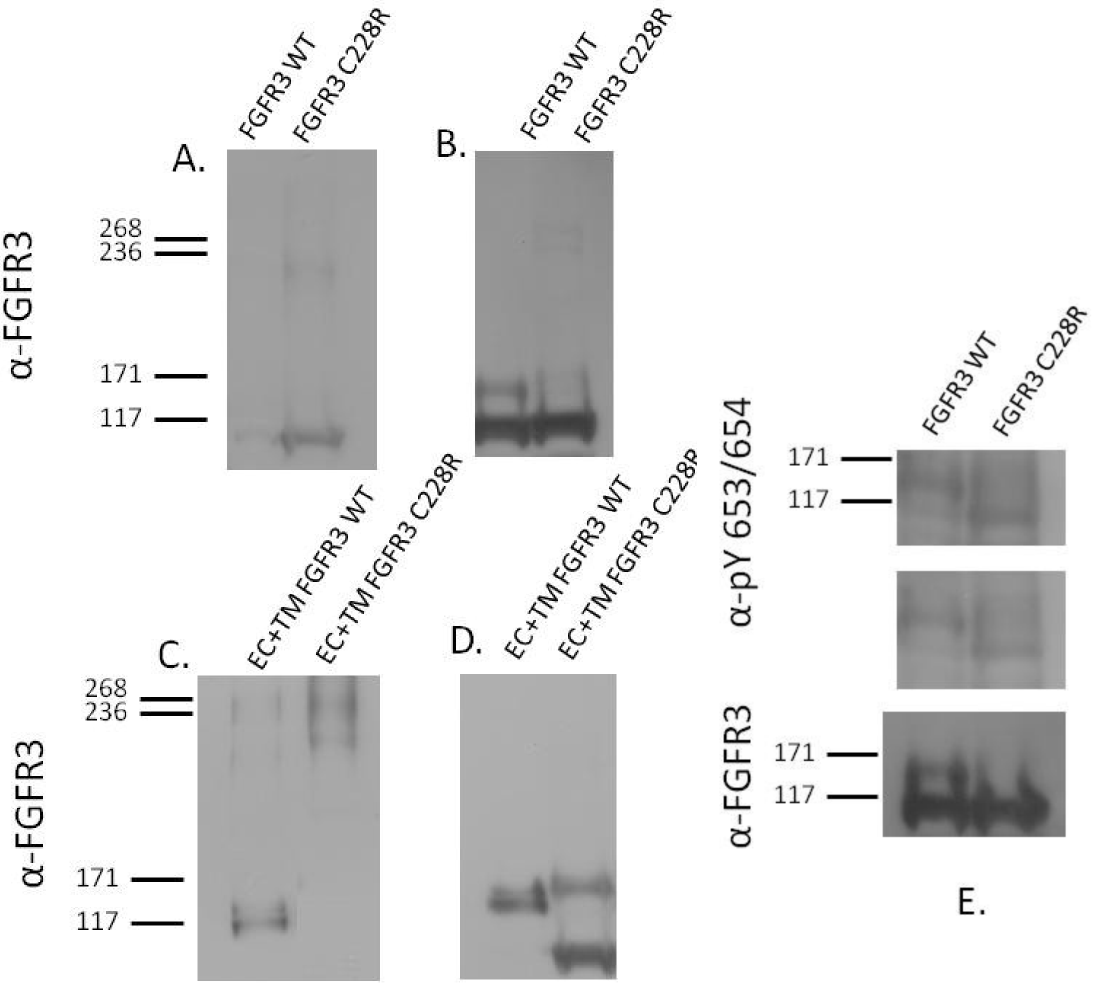

Figure 5-7. Anti-FGFR3 staining of (A) non-reducing and (B) reducing western blots for wild type and C228R FGFR3 in HEK293T cells. Anti-FGFR1 staining of (C) non-reducing and (D) reducing western blots for wild type and C228R EC+TM FGFR3 in CHO cells.(E) A large amount of FGFR3 C228R is unglycosylated (glycosylation deficient), but highly phosphorylated inside the HEK293T cell.

FGFR1
21
376
402
822
SP
EC
TM
IC
GGS
Fluorescent protein
FGFR2
22
369
403
821
SP
EC
TM
IC
GGS
Fluorescent protein
FGFR3
23
367
399
806
SP
EC
TM
IC
GGS
Fluorescent protein
FGFR1$_{C178S}$
21
376
402
822
SP
EC (C178S)
TM
IC
GGS
Fluorescent protein
FGFR2$_{C342R}$
22
369
403
821
SP
EC (C342R)
TM
IC
GGS
Fluorescent protein
FGFR3$_{C228R}$
23
367
399
806
SP
EC (C228R)
TM
IC
GGS
Fluorescent protein

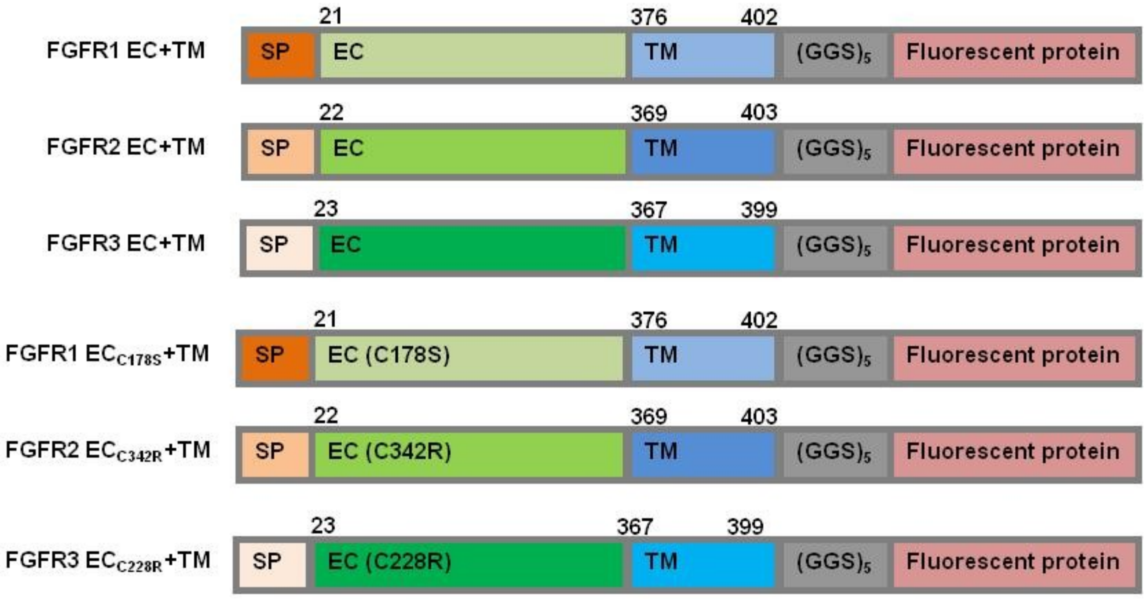

FGFR1 EC+TM
21
376
402
SP
EC
TM
$(GGS)_5$
Fluorescent protein
FGFR2 EC+TM
22
369
403
SP
EC
TM
$(GGS)_5$
Fluorescent protein
FGFR3 EC+TM
23
367
399
SP
EC
TM
$(GGS)_5$
Fluorescent protein
FGFR1 EC$_{C178S}$+TM
21
376
402
SP
EC (C178S)
TM
$(GGS)_5$
Fluorescent protein
FGFR2 EC$_{C342R}$+TM
22
369
403
SP
EC (C342R)
TM
$(GGS)_5$
Fluorescent protein
FGFR3 EC$_{C228R}$+TM
23
367
399
SP
EC (C228R)
TM
$(GGS)_5$
Fluorescent protein

Figure S1(5-8). Plasmid constructs used for the FRET experiments. The full-length receptors had fluorescent proteins attached to their C-termini via a flexible GGS linker. The truncated receptors had the intracellular domain substituted with a fluorescent protein, which was attached to the TM domain via a longer flexible $(GGS)_5$ linker. SP: signal peptide, EC: extracellular domain, TM: transmembrane domain. Fluorescent protein was either YFP or mCherry. Amino acid residue numbers are shown above the constructs.

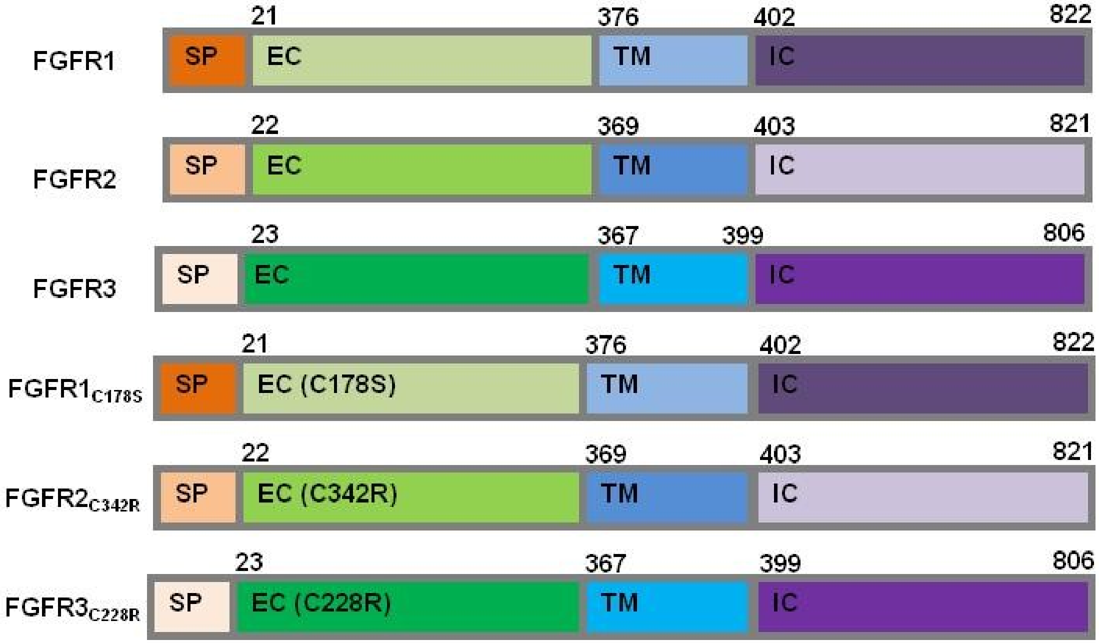

Figure S2(5-9). Plasmid constructs used for the Western blot experiments. Amino acid residue numbers are shown above the constructs.

Chapter 6. Analytical characterization of plasma membrane-derived vesicles produced via osmotic and chemical vesiculation

Abstract

Plasma membrane-derived vesicles are being used in biophysical and biochemical research as a simple, yet native-like model of the cellular membranes. Here we report on the characterization of vesicles produced via two different vesiculation methods. The first one is a recently developed method which utilizes chloride salts to induce osmotic vesiculation. The second one is a well established chemical vesiculation method which uses DTT and formaldehyde. We show that these two vesiculation methods lead to small but statistically significant differences in lipid composition. Highly significant differences were observed, however, in the degree of incorporation of a membrane receptor and in the degree of retention of soluble cytosolic proteins within the vesicles. Thus, in general, vesicles produced via osmotic and chemical means cannot be considered equivalent models of the cellular membrane, even when derived from the same cell pool.

6.1. Introduction

The cellular plasma membrane, a complex assembly of lipids and proteins, plays a critical role in cell physiology (31, 88, 143, 148). The membrane provides the barrier, and mediates the communication, between the cell and its environment. The processes that occur in the plasma membrane, such as ion conduction, nutrients uptake, and signal transduction, are critical for cell function (10, 39, 99, 160). It is often difficult, however, to study these processes in the plasma membrane of living cells, and thus biophysicist and biochemists often rely on model membrane systems. One such model system is plasma membrane-derived vesicles, which bud off cells in response to external stress (33, 129). These vesicles are derived from the native cellular membrane, and are thus more native-like than vesicles made of synthetic lipids. They are increasingly used in studies of lipid-lipid, lipid-protein and protein-protein interactions, and have yielded new knowledge about lipid domains and receptor interactions in the membrane (22, 34, 79, 114, 154). Often, however, they are not well characterized in terms of their lipid and protein content.

The most widely used vesiculation method, developed in the 1960s, utilizes the chemicals formaldehyde and dithiothreitol (DTT) to stress the cells and to induce an apoptosis-like response (129-131). Vesicles can be produced with this method from a variety of mammalian cells including human embryonic kidney (HEK) 293T cells, Chinese hamster ovary (CHO) cells, A431 human epidermoid carcinoma cells, 3T3 fibroblasts, endothelial cells, a variety of other cancer cells, and macrophages (5, 61, 123, 129-132, 154). These vesicles have been used widely in the literature to study lipid domains, but concerns may arise in some cases due to the presence of DTT, a reducing agent, as well as formaldehyde, a molecular cross-linker. Thus, an alternative vesiculation method, which utilizes osmotic stress rather than chemicals, was recently developed (33). In this method, vesiculation is induced by incubating cells with a buffer which contains high concentration of chloride salts. This osmotic method has been used to produce vesicles from CHO and A431 cells, in the absence of DTT and formaldehyde. The overall appearance of the vesicles produced with the osmotic stress method and the DTT/formaldehyde method is very similar (33), and both vesicle preparations have been used successfully in studies of protein interactions in membranes (123).

Here we sought to characterize and compare the vesicles produced by chemical and osmotic vesiculation and to identify differences that might exist between the two types of vesicles. In particular, we characterized and compared A431 chloride salt vesicles and A431 DTT/formaldehyde vesicles. As a control, we also characterized CHO DTT/formaldehyde vesicles, with the goal of comparing differences due to vesiculation method and differences due to cell type.

6.2. Materials and Methods

6.2.1. Cell culture and vesiculation. Chinese hamster ovary (CHO) and A431 cells were cultured in T75 flasks. These cells were vesiculated at 70% confluency using a DTT/formaldehyde buffer (129) or a chloride salt osmotic buffer (33).

6.2.2. Vesicle lipid pelleting. Centrifugation was performed at 125xg, 4 ˚C to pellet the cell debris. A second centrifugation was performed at 25000xg for 45 minutes at 4 ˚C to pellet the vesicles. The supernatant was discarded.

6.2.3. Liquid chromatography mass spectrometric (LC-MS) analysis of lipids and cholesterol. Three independent samples were prepared for each vesicle type. After pelleting**,** lipids and cholesterol were extracted as described previously using a modified Bligh/Dyer procedure, spiked with appropriate internal standards (17), and analyzed using a 6490 Triple Quadrupole LC-MS system (Agilent Technologies, Santa Clara, CA). Glycerophospholipids and sphingolipids were separated with normal-phase HPLC as described before (17), with a few changes. An Agilent Zorbax Rx-Sil column (inner diameter 2.1 x 100 mm) was used under the following conditions: mobile phase A (chloroform:methanol:1 M ammonium hydroxide, 89.9:10:0.1, v/v) and mobile phase B (chloroform:methanol:water:ammonium hydroxide, 55:39.9:5:0.1, v/v); 95% A for 2 min, linear gradient to 30% A over 18 min and held for 3 min, and linear gradient to 95% A over 2 min and held for 6 min. Sterols and glycerolipids were separated with reverse-phase HPLC using an isocratic mobile phase as before (17) except with an Agilent Zorbax Eclipse XDB-C18 column (4.6 x 100 mm).

Quantification of lipid species was accomplished using multiple reaction monitoring (MRM) transitions (17) in conjunction with referencing of appropriate internal standards: PA 14:0/14:0, PC 14:0/14:0, PE 14:0/14:0, PG 15:0/15:0, PI 16:0/16:0, PS 14:0/14:0, BMP 14:0/14:0, APG 14:0/14:0, LPC 17:0, LPE 14:0, LPI 13:0, Cer d18:1/17:0, SM d18:1/12:0, dhSM d18:0/12:0, GalCer d18:1/12:0, GluCer d18:1/12:0, LacCer d18:1/12:0, D_7-cholesterol, CE 17:0, MG 17:0, 4ME 16:0 diether DG, D_5-TG 16:0/18:0/16:0 (Avanti Polar Lipids, Alabaster, AL).

6.2.4. Thin layer chromatography. The pelleted plasma membrane vesicles were resuspended in distilled water. The solution was dried in a rotory evaporator and the lipids were extracted using the Folch method with chloroform:methanol:distilled water (2:1:1 (v/v)) at room temperature (43). The extracts were dried under a stream of N_2 gas and resuspended in a chloroform: methanol mixture (2:1 (v/v)). One dimensional thin layer chromatography (TLC) was used to analyze the lipid content. Whatman flexible silica gel G plates were spotted with solutions containing the extracted lipids, as well as the following lipid standards: 1-palmitoyl-2-deoyl-sn-glycerol-3-phosphocholine

(POPC), 1-palmitoyl-2-deoyl-sn-glycerol-3-phospho-L-Serine (POPS), 1-palmitoyl-2-deoyl-sn-glycerol-3-phosphoethanolamine (POPE), Sphingomyelin (from Porcine brain), and cholesterol (Avanti Polar Lipids Inc). The plates were then placed in a chamber with a chloroform: methanol:7-N NH_4OH (65:27:5 (v/v)) solution to separate the different lipid components. After separation, the lipid components were visualized in iodine vapor.

6.2.5. ^{31}P NMR phospholipid analysis. Vesicle pellets were resuspended in distilled water. The solution was dried in a rotory evaporator and the lipids were extracted using the Folch method with chloroform:methanol:distilled water (2:1:1 (v/v)) at room temperature (43). The extracts were dried under a stream of N_2 gas and resuspended in a chloroform: methanol mixture (2:1 (v/v)). 20-30 mg of lipid extracts from each vesicle type was sent to Avanti Polar Lipids Analytical Services for ^{31}P NMR analysis. A Bruker Avance™ III 400 mHz with a 5 mm BBFO Probe NMR spectrometer was used to characterize the phospholipid composition of the samples dissolved in 1 mL of detergent.

6.2.6. Annexin V binding to plasma membrane derived vesicles. Vesicles were incubated for 1 hour with fluorescein-conjugated Annexin V using the LI2004 Annexin V detection kit (Molecular Probes). Images were recorded in a Nikon confocal microscope.

6.2.7. Plasmids for vesicle content leakage assays. The wild type human fibroblast growth factor receptor 2 (FGFR2) plasmid was a gift from Dr. Moosa Mohammadi (NYU). The FGFR2-mCherry plasmid was constructed by fusing mCherry to the C-terminus of full length FGFR2. The plasmid encoding 1-phosphatidylinositol 4,5-bisphosphate phosphodiesterase delta-1-GFP (Plcδ1-PH-GFP) was obtained from Dr. Tamas Balla (NIH). The plasmids encoding Intersectin II-GFP, 1-phosphatidylinositol

4,5-bisphosphate phosphodiesterase gamma-1-GFP (Plcɣ-GFP) and Protein kinase C theta-GFP (PKCϴ-GFP) were a kind gift from Dr. Christoph Wuelfing (University of Bristol). The Growth factor receptor-bound protein 2-Venus (Grb2-Venus) plasmid was a gift from Dr. Jin Zhang (Johns Hopkins). The VVVVVV (Venus x 6) plasmid was purchased from Addgene (courtesy of Dr. Steven Vogel, NIH).

6.2.8. Western blot analysis of EGFR in A431 vesicles. The vesicle pellets were lysed with lysis buffer (25 mM Tris-HCl, 0.5% Triton X-100, 20mM NaCl, 2 mM EDTA, phosphatase inhibitor and protease inhibitor, Roche Applied Science). The lysates were loaded onto 3–8% NuPAGE®Novex®Tris–Acetatemini gels (Invitrogen, CA). The proteins were transferred onto a nitrocellulose membrane, and blocked using 5% milk in TBS. EGFR was detected with anti-EGFR receptor antibodies (2232s, Cell Signaling Technology USA), followed by anti-rabbit HRP conjugated antibodies (W4011, Promega). The proteins were visualized with the Amersham ECL detection system (GE Healthcare) as described previously (53, 54).

6.2.9. EGF-Rhodamine binding to EGFR in A431 vesicles. Vesicles were incubated with 1ug/mL of Epidermal Growth Factor - Tetramethylrhodamine Conjugate (E3481, Molecular Probes) for 1h, and were then imaged in the confocal microscope.

6.3. Results

6.3.1. Different methods of vesicle production lead to small, but statistically significant differences in cholesterol and lipid composition. We first compared the lipid and cholesterol content of the three types of vesicles used in this study: A431 chloride salt vesicles, A431 DTT/formaldehyde vesicles, and CHO DTT/formaldehyde vesicles using liquid chromatography-mass spectrometry (LC-MS). Three independent samples were prepared for each type of vesicle preparation. The vesicles were pelleted and the lipids were extracted as described in Materials and Methods. The LC-MS results, shown in Figure 1, report on the relative abundance of cholesterol and lipids in the three vesicle preparations. We found that the three types of vesicles contain significant amounts of free cholesterol (FC), phosphatidylcholine (PC), sphingomyelin (SM), phosphatidylethanolamine (PE), phosphatidylserine (PS) and phosphatidylinositol (PI). Other substantial lipids are dhSM, PCe, PEp and LPC in A431 DTT/formaldehyde vesicles, Cer, dhSM, PCe, PEp and LPC in A431 chloride salt vesicles, DG, GM3, dhSM, PCe, PEp and LPC in CHO DTT/formaldehyde vesicles (see abbreviations in Figures 1).

The mole % of free cholesterol in the three vesicle preparations is 33.5 ± 0.1, 30.0 ± 1.4, and 22.5 ± 2 for A431 chloride salt, A431 DTT/formaldehyde, and CHO DTT/formaldehyde vesicles, respectively.–There is no statistically significant difference between the free cholesterol mole% in A431 chloride salt and A431 DTT/formaldehyde vesicles ($p = 0.092$), based on a two-tailed t-test. However, there is a statistically significant difference between A431 DTT/formaldehyde vesicles and CHO DTT/formaldehyde vesicles ($p = 0.023$).

Figure 2 compares the lipid content of the three vesicle preparations. As expected, the major lipid component in the three vesicle preparations is PC. There is a statistically significant difference between PC mole % in A431 chloride salt vesicles (43.8 ± 0.8 mole %) and A431 DTT/formaldehyde vesicles (51.0 ± 1.4 mole %) ($p = 0.014$). On the other hand, the PC levels in A431 DTT/ formaldehyde vesicles are not different from CHO DTT/ formaldehyde levels (55.5 ± 3.1mole %) ($p =0.34$).

The SM content in the A431 chloride salt vesicles, A431 DTT/formaldehyde vesicles, and CHO DTT/formaldehyde vesicles is 7.2 ± 0.6 mole %, 7.7 ± 0.6 mole %, and 9.6 ± 0.5 mole % respectively. No statistical differences are observed between SM mole % in A431 chloride salt and A431 DTT/ formaldehyde vesicles ($p = 0.25$), or between A431 DTT/formaldehyde and CHO DTT/formaldehyde vesicles ($p = 0.6$). Similarly, PI mole % is not significantly different in the three vesicle types.

PS content was 5.9 ± 0.6 mole % in A431 chloride salt vesicles, 6.5 ± 0.4 mole % in A431 DTT/formaldehyde vesicles, and 3.5 ± 0.1 mole % in CHO DTT/ formaldehyde vesicles. The PS content was different in A431 DTT/ formaldehyde and in CHO DTT/ formaldehyde vesicles ($p = 0.0009$) but not in A431 DTT/ formaldehyde and A431 chloride salt vesicles. Similarly, the PE content was similar in the two types of A431 vesicles, but different in the A431 and CHO vesicles.

Monosialodihexosylganglioside 3 (GM3) levels were not statistically different in A431 chloride salt vesicles (0.3 mole %) and in A431 DTT/formaldehyde vesicles (0.3 mole %) ($p=0.15$), but were significantly different when comparing A431 DTT/formaldehyde (0.3 mole %) and CHO DTT/formaldehyde (2.0 mole %) vesicles. This difference was most likely due to differences in cellular membrane composition, as GM3 has been previously reported in the plasma membranes of intact CHO cells (156), but not in A431 cells (112).

Overall, the LC-MS results (see Fig S1 for complete results) demonstrated that all vesicle preparations contain all the major lipids known to exist in plasma membranes of intact cells. While there were some statistically significant differences between lipids in A431 chloride salt vesicles and A431 DTT/formaldehyde vesicles, these differences appeared only in two lipid components, namely PC and plasmalogen phosphatidylethanolamine

(PEp). On the other hand, significant differences were observed between free cholesterol, CE, GM3, dhSM, PE, PEp and PS levels when comparing A431 DTT/formaldehyde and CHO DTT/formaldehyde vesicles, due to differences in cell type.

The lipid composition of the three types of vesicles was further studied using Thin Layer Chromatography (TLC) and ^{31}P NMR. The TLC results, presented in Figure S2, show that cholesterol, PC, SM, PE, PS and PI are present in all vesicle types. We also used the Avanti analytical services to characterize the lipid composition of A431 chloride salt vesicles and A431 DTT/formaldehyde vesicles with ^{31}P NMR (spectra shown in Figure S3). The analysis identified PC, PE, PI, PS, SM and LPE as the major species in the A431 chloride salt vesicles, and PC, PE, PI, PS, SM, LPE and LPC in the A431 DTT/formaldehyde vesicles (Fig 3).

Overall, ^{31} P NMR and TLC results are in agreement with the LC-MS results, since they identified the same major lipids as the LC-MS experiments. They further confirmed that PC is the major phospholipid component in all vesicle preparations.

6.3.2. Vesicles bind annexin V, independent of production method. It is known that plasma membrane vesicles form as a result of cell stress which induces an apoptotic response (130, 131). Under stress, the cellular membrane loses some of its asymmetry, as PS, which is found in the cytoplasmic leaflet of intact cells, becomes exposed on the cell surface. As a result, the plasma membrane derived-vesicles are expected to have PS on their outer surfaces. Annexin V, which binds specifically to PS, is therefore expected to bind to the vesicles (101). Here we asked whether we can detect differences in Annexin V binding to the A431 chloride salt vesicles, A431 DTT/formaldehyde vesicles, and CHO DTT/formaldehyde vesicles. We thus incubated the vesicles with fluorescently labeled Annexin V. Fluorescence images, captured in the confocal microscope, are shown in Figure 4. We did not detect obvious differences in Annexin V binding, based on recorded pixel intensities. Thus, it appears that there are no measurable differences in PS exposure to Annexin V due to production method. In these experiments, no Annexin V binding was observed to intact, non-apoptotic, un-vesiculated cells, which served as control.

6.3.3. Cytoplasmic proteins are not retained in vesicles produced via osmotic vesiculation. In our prior work, we have shown that soluble fluorescent proteins, expressed in CHO cells, fill the DTT/formaldehyde vesicles (81). In the course of the current work we noticed, however, that the fluorescent proteins are not retained within chloride salt vesicles. To further investigate this phenomenon, we studied the retention of several soluble cytoplasmic proteins of different molecular weight, within the vesicles. We labeled the membranes of cells and vesicles using Fibroblast Growth Factor Receptor-(FGFR2)-mCherry, a fluorescently tagged membrane protein.

Figure 5 shows the results for Grb2-Venus (molecular weight ~60 kDa). In these experiments, CHO cells were co-transfected with plasmids encoding for FGFR2-mCherry and Grb2-Venus. After expression, FGFR2-mCherry was located on the membane, while Grb2 filled the cytoplasm. After vesiculation, Grb2-Venus (molecular weight ~60 kDa) was not found inside CHO chloride salt vesicles, but was found inside the CHO DTT/formaldehyde vesicles. We next performed experiments with proteins of higher molecular weight, PKCΘ-GFP (MW~120 kDa), Venusx6 (MW~160 kDa), Intersectin II-GFP (MW~170 kDa), and PLCɣ-GFP (MW~210 kDa). These are all soluble proteins that reside in the cytoplasm of intact cells (Figure S4, B-F). As shown in Figures S6-S8 and

Figure 6, none of these proteins were found inside the vesicles produced with the osmotic stress method.

In Figure 6, we see that PLCɣ-GFP (MW~210 kDa) associates with the plasma membrane in cells when FGFR2-mCherry is present because it specifically interacts with it. Despite binding to FGFR2 in cells, however, PLCɣ-GFP was not found in the choloride salt vesicles (Figure 6). This likely occurs because, upon vesiculation, PLCɣ-GFP reaches a new equilibrium with the aqueous sample volume which is effectively infinite.

To confirm that transient interactions with the membrane do not lead to soluble protein retention in the chloride salt vesicles, we also worked with Plc□1-PH domain-GFP (MW~45 kDa), which is known to bind to PIP2 in cells. As seen in Figure S6, Plc□1-PH domain-GFP is not retained inside the chloride salt vesicles, either. All above experiments lead us to conclude that the chloride salt vesicles, unlike the DTT/formaldehyde vesicles, are ghost vesicles that lack cytoplasmic content.

6.3.4. EGFR incorporates very efficiently in chloride salt vesicles, but not in DTT/formaldehyde vesicles. Vesicles are derived from the plasma membranes of cells, and are thus expected to contain membrane proteins, not only lipids. However, it is not known if the incorporation of membrane proteins in the vesicles in affected by the method of vesicle production. Since A431 cells are known to express the epidermal growth factor receptor (EGFR) endogenously at high levels (15, 16, 52), we sought to compare the amount of EGFR in the A431 vesicles produced with the two methods using Western blotting.

After vesiculation, we loaded identical amounts of total protein on the gel, and we visualized EGFR using anti-EGFR antibodies as described in Materials and Methods. The results are shown in Figure 7. While we see intense anti-EGFR bands in vesicles produces with the osmotic stress method, we see very weak anti-EGFR staining in the vesicles produces with the DTT/formaldehyde method. This finding suggests that EGFR is not efficiently incorporated in the vesicles during DTT/formaldehyde vesiculation, but is efficiently incorporated during osmotic vesiculation.

To assess the functionality of EGFR in the two types of vesicles, we investigated if the incorporated EGFR is capable of binding its ligand, EGF. The vesicles were therefore incubated with fluorescently labeled EGF (EGF-Rhodamine), see Figure 8. We observed that a large fraction (~50-90%) of the A431/chloride salt vesicles was labeled. On the other hand, only a small fraction of the A431 DTT/formaldehyde vesicles (~5%) bind EGF-Rhodamine. This finding is consistent with the observation that EGFR is not incorporated efficiently in the DTT/formaldehyde vesicles. Yet, EGF-Rhodamine binding in Figure 8 suggests that the receptors in the two types of vesicles are capable of ligand binding.

6.4. Discussion

Here we characterized and compared A431 vesicles produced by two different methods: osmotic vesiculation with chloride salts and chemical vesiculation using DTT and formaldehyde. We also characterized CHO DTT/formaldehyde vesicles. The goal of these experiments was to understand how differences due to production method compare with differences due to cell type.

Here we uncovered small but statistically significant differences in lipid composition, particularly in PC and PEp content, due to production method. On the other hand, statistically significant differences in FC, CE, dhSM, GM3, PE, PEp and PS were observed in A431 and CHO vesicles produced with the same chemical vesiculation method. Thus, differences in cholesterol and lipid content due to production method are quite modest, and smaller than differences due to cell type.

We further demonstrated that the vesiculation method affects the efficiency of incorporation of the membrane protein EGFR into the vesicles. In particular, EGFR incorporates easily into A431 chloride salt vesicles but is much less efficiently incorporated into DTT/formaldehyde vesicles. Yet, prior work has demonstrated that other membrane proteins such as GPA, Neu, and FGFR3 readily incorporate in DTT/formaldehyde vesicles (22, 23, 113, 114, 122). Thus, the incorporation efficiency of a membrane protein into the vesicles depends both on the production method and on the identity of the membrane protein itself.

The most striking difference between chloride salt and DTT/formaldehyde vesicles is in the degree of retention of soluble proteins inside the vesicles. While soluble proteins are retained within the DTT/formaldehyde vesicles, soluble proteins of molecular weight up to 210 kDa are not found inside the chloride salt vesicles. An explanation of this finding may be that formaldehyde cross-links cellular components and thus helps with the retention of soluble proteins in the cytoplasm.

Overall, we find that plasma membrane-derived vesicles produced by osmotic and chemical vesiculation are not identical models of the cellular membrane. We therefore propose that parallel biophysical characterization of membrane proteins in the two types of vesicles may be highly advantageous in some cases. Thus far, the interactions between TM helices have been characterized in the two types of vesicles and have been shown to be similar (33, 123). Soluble proteins, however, may interact with full-length membrane proteins and modulate their behavior. While such effects are difficult to quantify in live cells, they could be assessed by quantifying differences in membrane protein interactions in different vesicle preparations, in the presence and absence of soluble proteins.

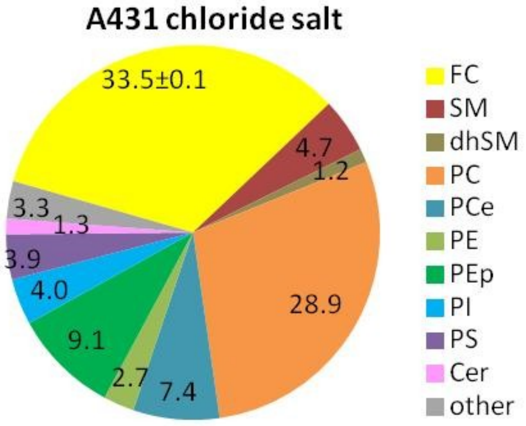
A431 chloride salt

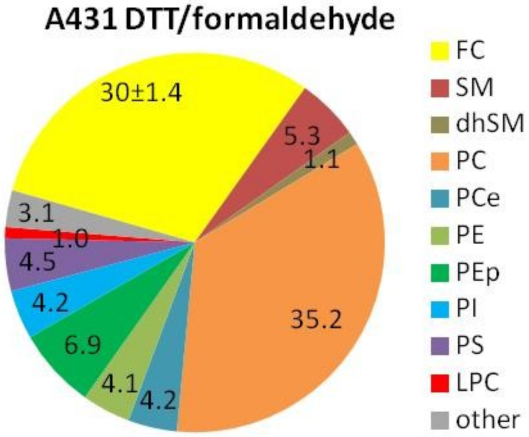
A431 DTT/formaldehyde

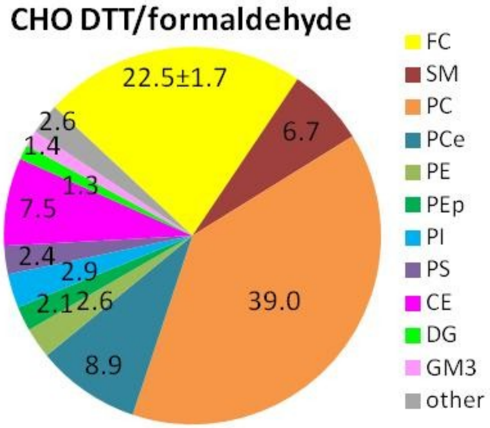
CHO DTT/formaldehyde

Figure 6-1. Cholesterol and lipid composition of A431 chloride salt vesicles, A431 DTT/formaldehyde vesicles, and CHO DTT/formaldehyde vesicles, determined by LC-MS. Three independent samples were analyzed for each vesicle preparation. FC: free cholesterol; SM: sphingomyelin; PC: phosphatidylcholine; PCe: ether phosphatidylcholine; PE: phosphatidylethanolamine; PEp: plasmalogen phosphatidylethanolamine; PI: phosphatidylinositol ; PS: phosphatidylserine; CE: cholesteryl ester; DG: diacylglycerol, Cer: ceramide; GM3: monosialodihexosylganglioside 3; dhSM: dihydrosphingomyelin; PA: phosphatidic acid; LPC: lysophosphatidylcholine. Cholesterol is significantly different between A431 and CHO vesicles.

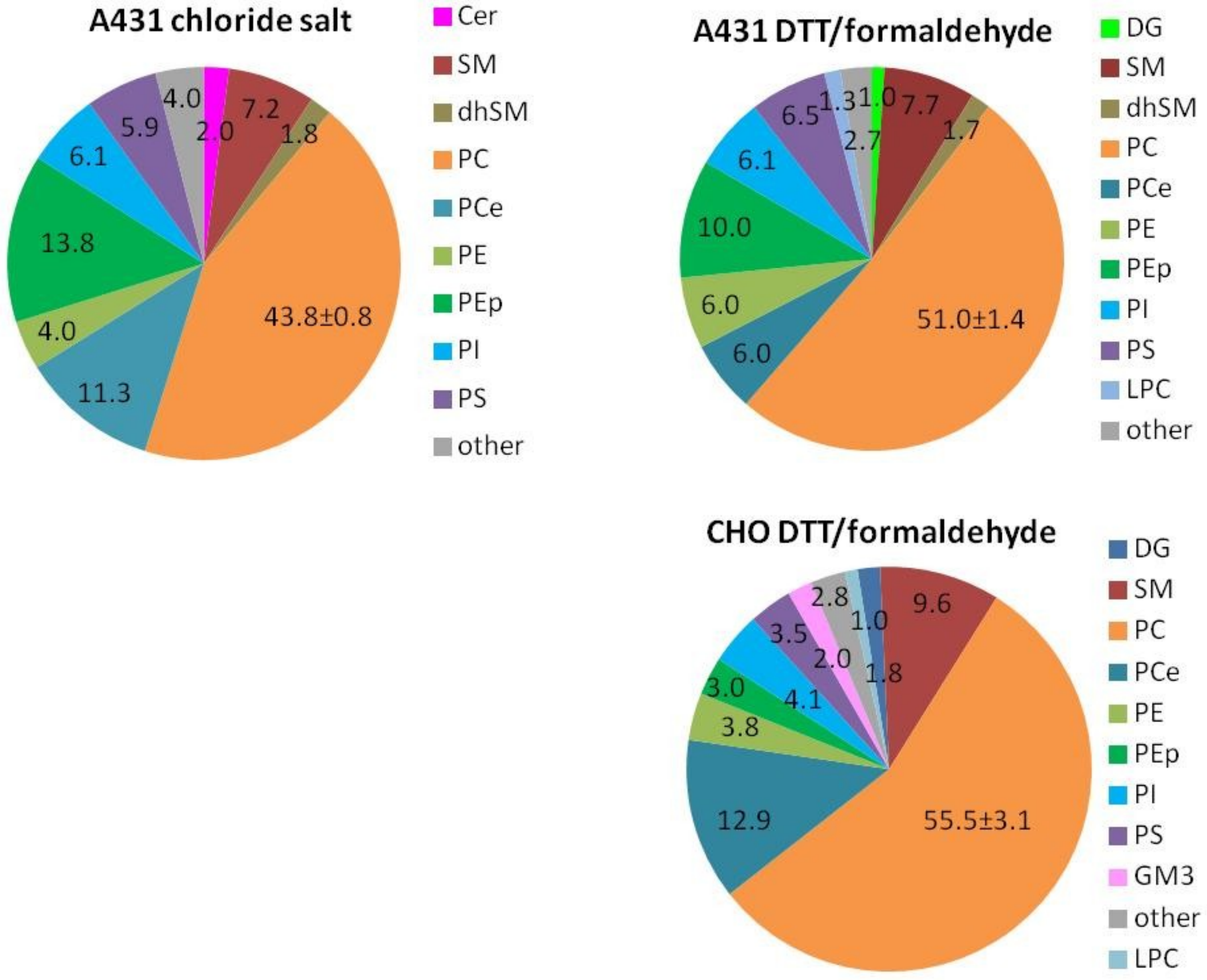
A431 chloride salt

A431 DTT/formaldehyde

CHO DTT/formaldehyde

Figure 6-2. Lipid composition of A431 chloride salt vesicles, A431 DTT/formaldehyde vesicles, and CHO DTT/formaldehyde vesicles, calculated by re-scaling the LC-MS data shown in Figure 1. The major lipid component is PC, and there is a statistically significant difference between PC abundance in A431 vesicles produced with the two methods (DTT/formaldehyde and chloride salt). There are also significant differences in PEp abundance. Comparing A431 DTT/formaldehyde and CHO DTT/formaldehyde samples, statistically significant differences are observed between PE, PS, GM3, dhSM, and PEp levels.

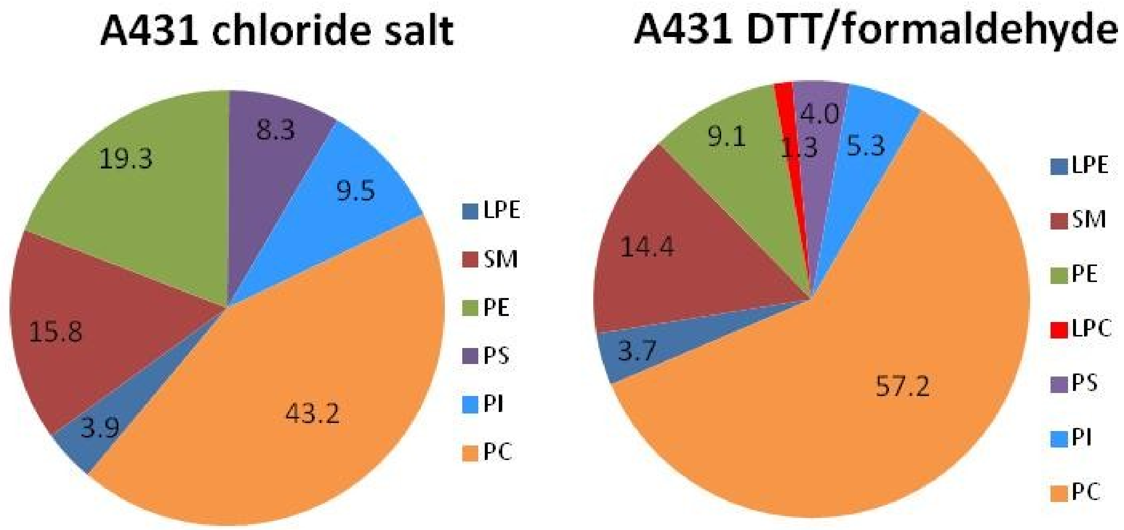
A431 chloride salt

A431 DTT/formaldehyde

Figure 6-3. Phospholipid content of the vesicles, from ^{31}P NMR experiments performed by Avanti Polar Lipids Analytical Services (see Figure S2 for spectra). Single samples were analyzed for each vesicle preparation. Qualitatively, the results are in agreement with the results in Figure 2, with PC being the most abundant phospholipid in the two samples.

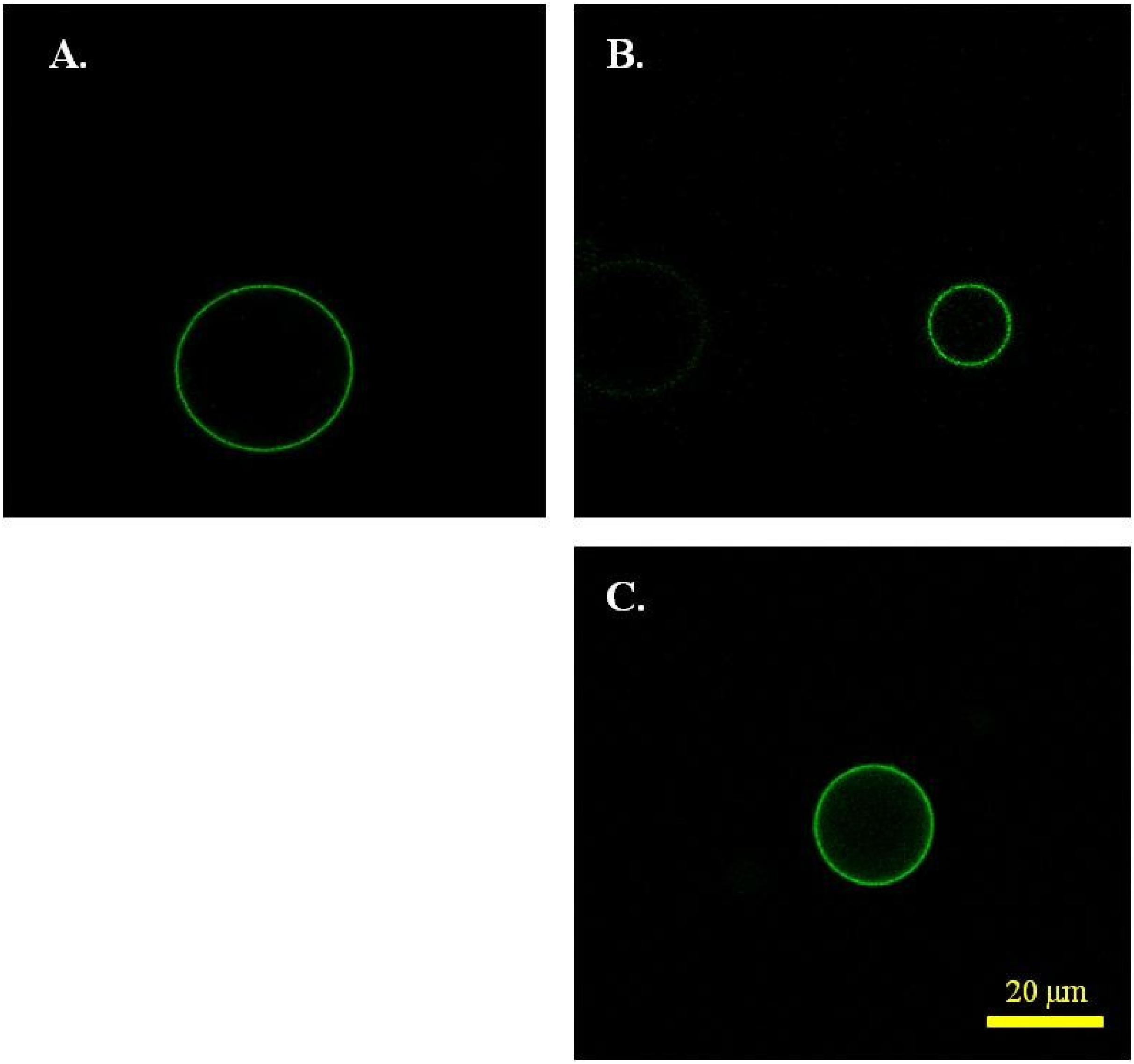

Figure 6-4. Annexin V binding to (A) A431 chloride salt vesicles, (B) A431 DTT/formaldehyde vesicles, and (C) CHO DTT/formaldehyde vesicles. No statistical significant differences in Annexin V binding were observed between the three vesicle preparations.

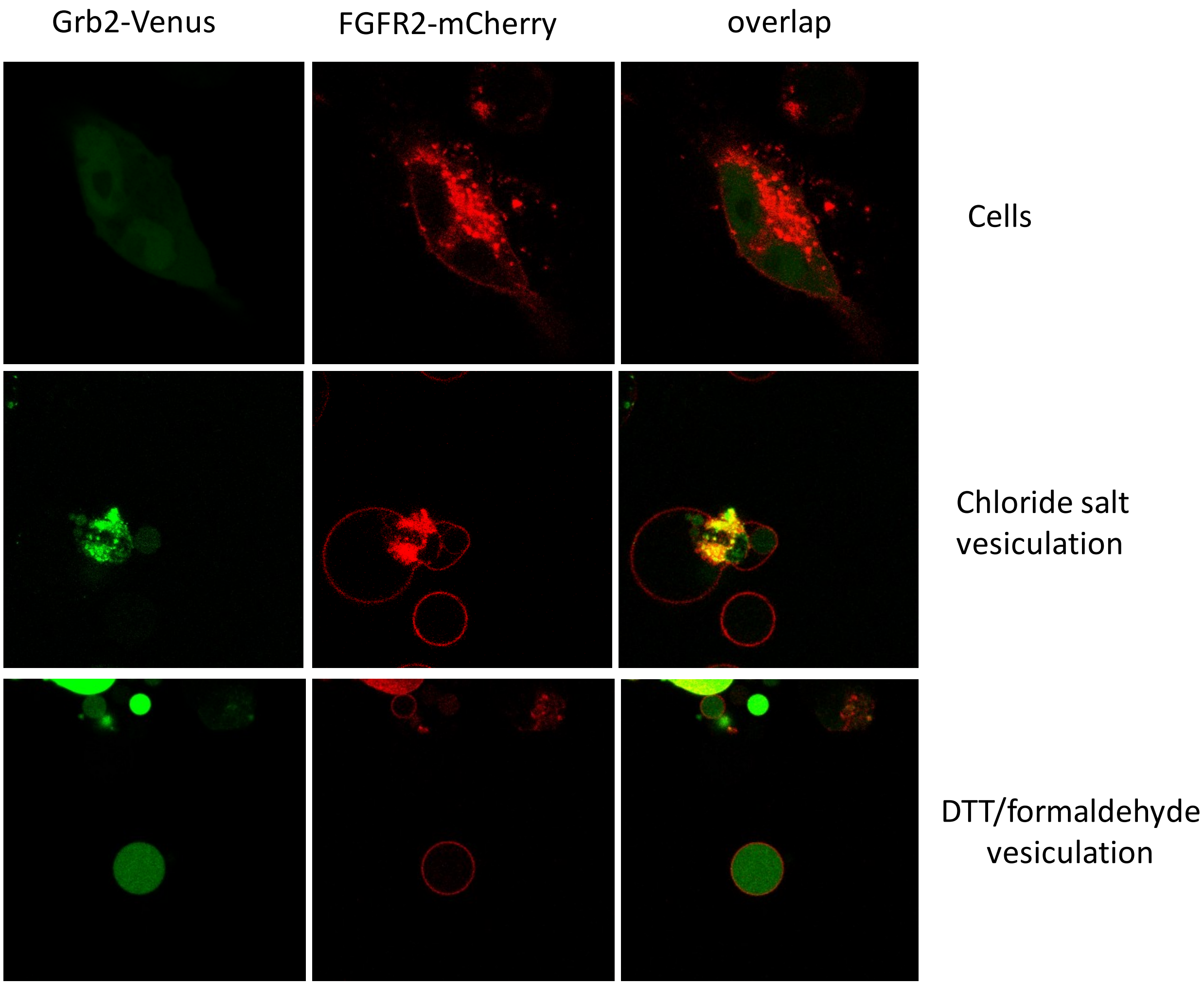

Figure 6-5. Top panel: Chinese Hamster Ovary (CHO) expressing Grb2-Venus (MW ~ 60 kDa) and FGFR2-mCherry. Middle panel: Grb2-Venus (MW ~ 60 kDa) is not retained in CHO chloride salt vesicles. Bottom panel: Grb2-Venus is retained in DTT/formaldehyde vesicles.

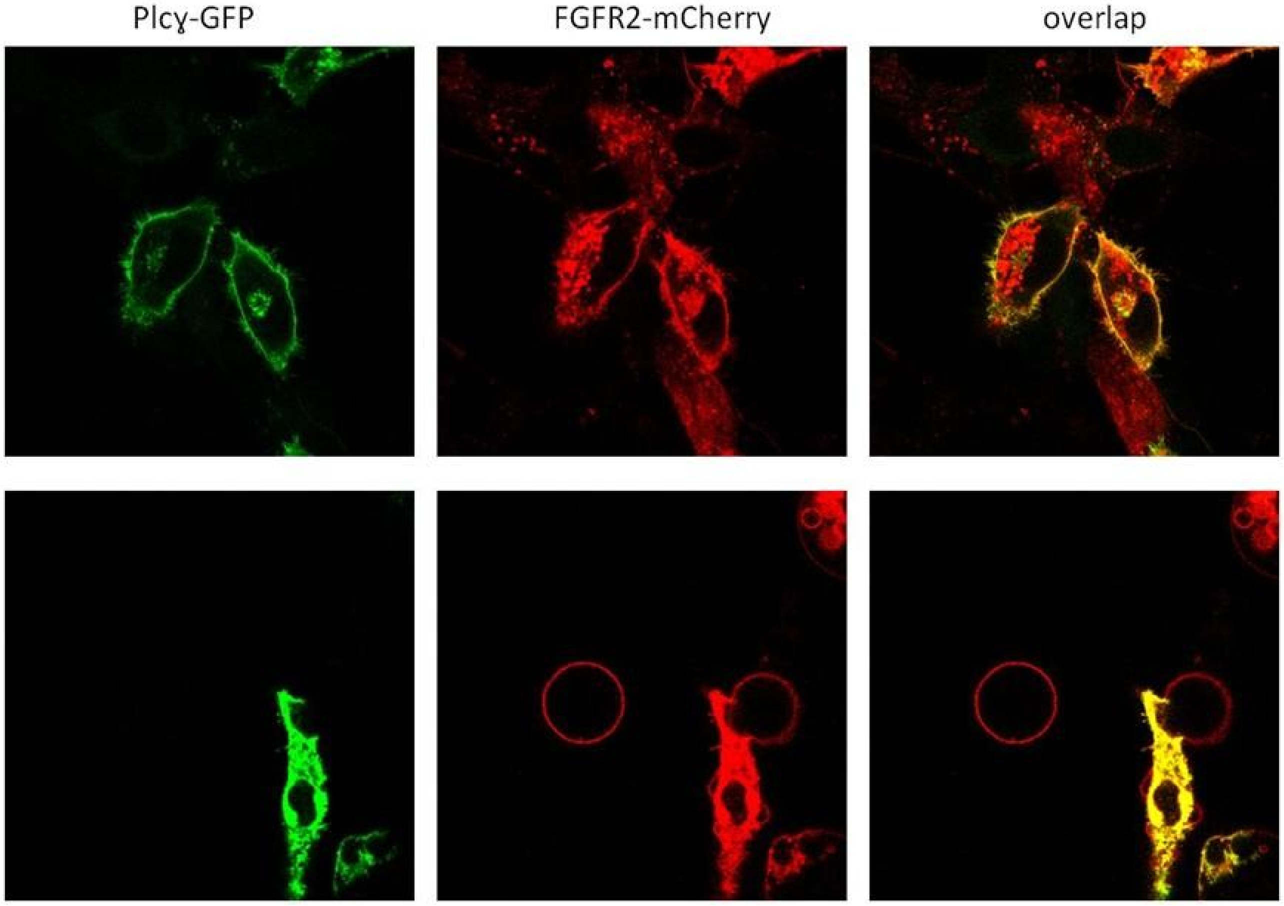

Figure 6-6. Top panel: CHO cells expressing Plcɣ-GFP and FGFR2-mCherry. Bottom panel: Plcɣ-GFP (MW ~ 210 kDa) is not retained in CHO chloride salt vesicles.

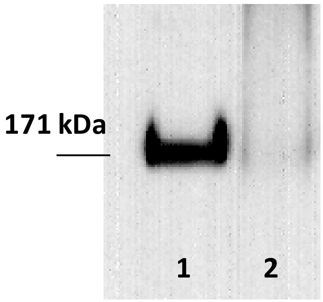

Figure 6-7. Western blots staining for endogenous Epidermal Growth Factor Receptor (EGFR) in A431 vesicles. After vesicle lysis, identical amounts of total protein were loaded on the gel, and EGFR bands were visualized using anti-EGFR antibodies as described in Materials and Methods. **Lane 1:** A431 chloride salt vesicles. **Lane 2:** A431 DTT/formaldehyde vesicles.

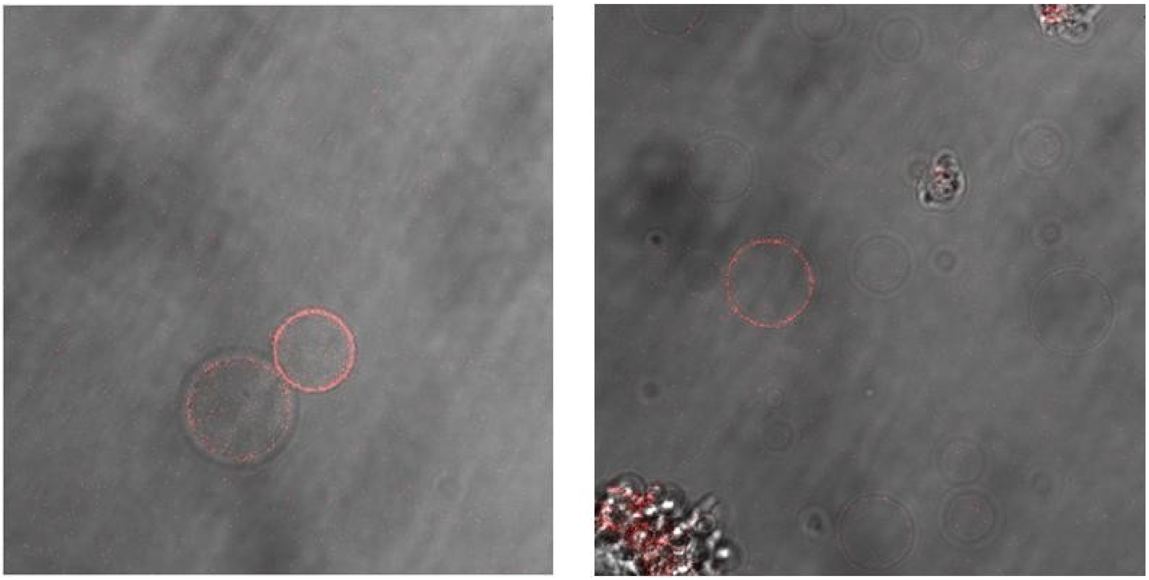

Figure 6-8. EGF-Rhodamine binding to A431 vesicles. Left: A341 chloride salt vesicles; Right: A431 DTT/formaldehyde vesicles.

A.

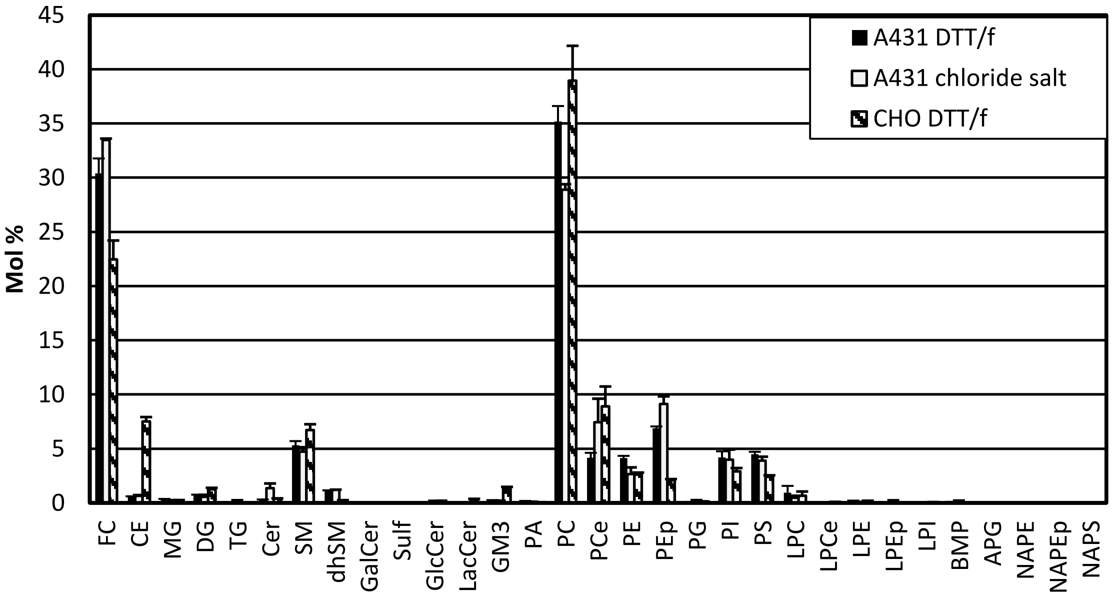

45
40
35
30
25
20
15
10
5
0
Mol %
A431 DTT/f
A431 chloride salt
CHO DTT/f
FC
CE
MG
DG
TG
Cer
SM
dhSM
GalCer
Sulf
GlcCer
LacCer
GM3
PA
PC
PCe
PE
PEp
PG
PI
PS
LPC
LPCe
LPE
LPEp
LPI
BMP
APG
NAPE
NAPEp
NAPS

B.

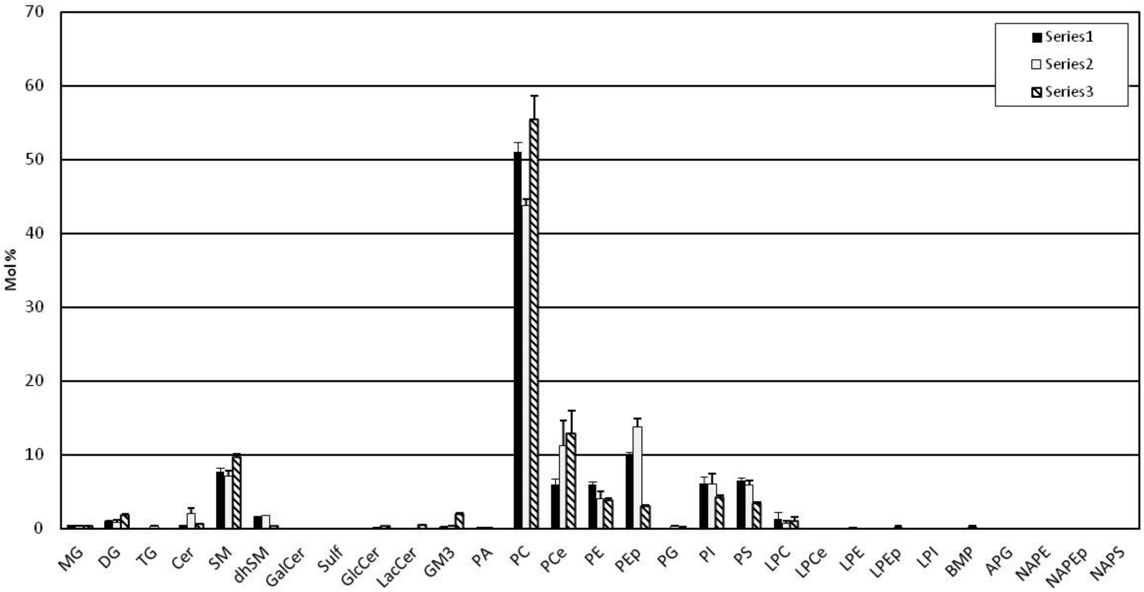

70
60
50
40
30
20
10
0
Mol %
Series1
Series2
Series3
MG
DG
TG
Cer
SM
dhSM
GalCer
Sulf
GlcCer
LacCer
GM3
PA
PC
PCe
PE
PEp
PG
PI
PS
LPC
LPCe
LPE
LPEp
LPI
BMP
APG
NAPE
NAPEp
NAPS

Figure S1(6-9). High Performance Liquid Chromatography Mass Spectrometry (LC-MS) results for A431 chloride salt vesicles, A431 DTT/formaldehyde vesicles, and CHO DTT/formaldehyde vesicles. (A) Cholesterol and lipids. (B) Lipids only. FC: free cholesterol; SM: sphingomyelin; PC: phosphatylcholine; PCe: ether phosphatidylcholine; PE: phosphatidylethanolamine; Pep: plasmalogen phosphatidylethanolamine; PI: phosphatidylinositol ; PS: phosphatidylserine; CE: cholesteryl ester; DG: diacylglycerol, Cer: ceramide; GM3: Monosialodihexosylganglioside 3; dhSM: dihydrosphingomyelin; PA: phosphatidic acid; LPC: lysophosphatidylcholine; LPE: Lysophosphatidylethanolamine.

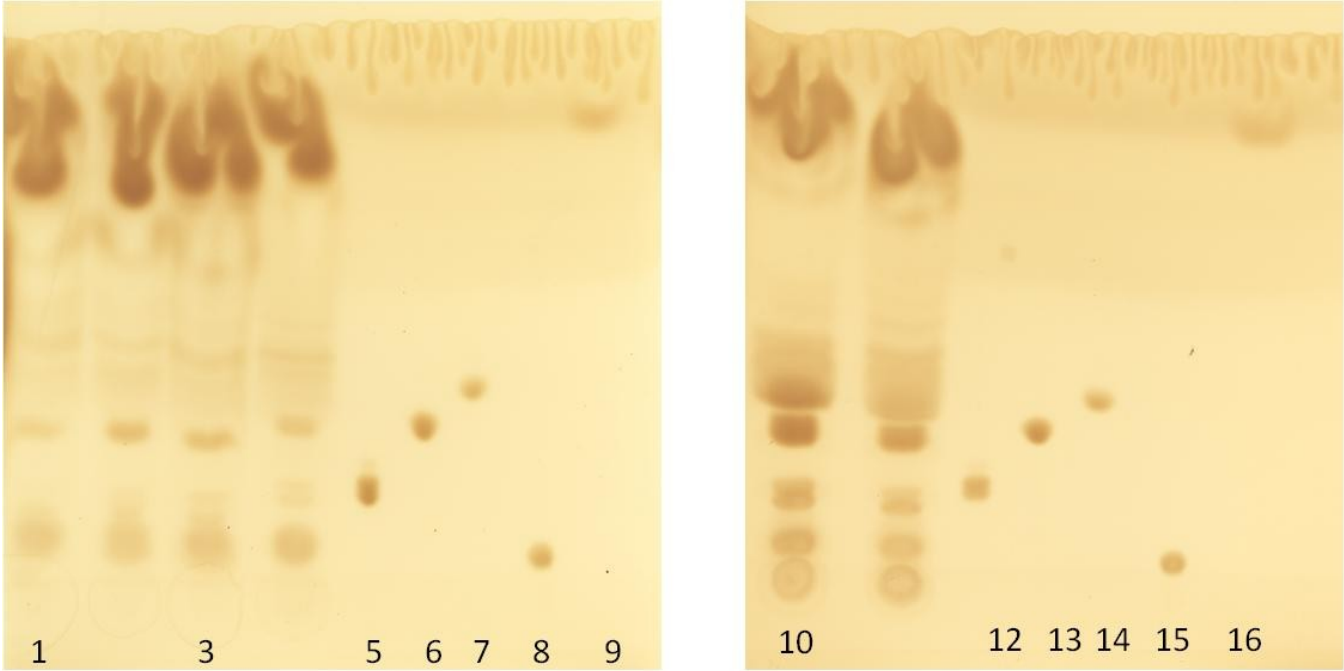

Figure S2(6-10). Thin-layer chromatogram of lipid extracts from different vesicle preparations. **Lane 1:** CHO, DTT/formaldehyde method. **Lane 3:** A431, DTT/formaldehyde method. **Lane 5:** Sphingomyelin (SM1 and SM2). **Lane 6:** Phoshatidylcholine (PC), **Lane 7:** Phoshatidylethanolamine (PE). **Lane 8:** Phoshatidylserine (PS). **Lane 9:** Cholesterol (CL). **Lane 10:** A431, chloride salt osmotic method. **Lane 12:** Sphingomyelin (SM1 and SM2). **Lane 13:** Phoshatidylcholine (PC), **Lane 14:** Phoshatidylethanolamine (PE). **Lane 15:** Phoshatidylserine (PS). **Lane 16:** Cholesterol (CL). **Thin layer chromatography results for lipid extracts from the three types of vesicles.** Qualitatively, the results support the MS-LC data, as the TLC analysis identifies PC, PE, PS, SM, and Cholesterol.

A.

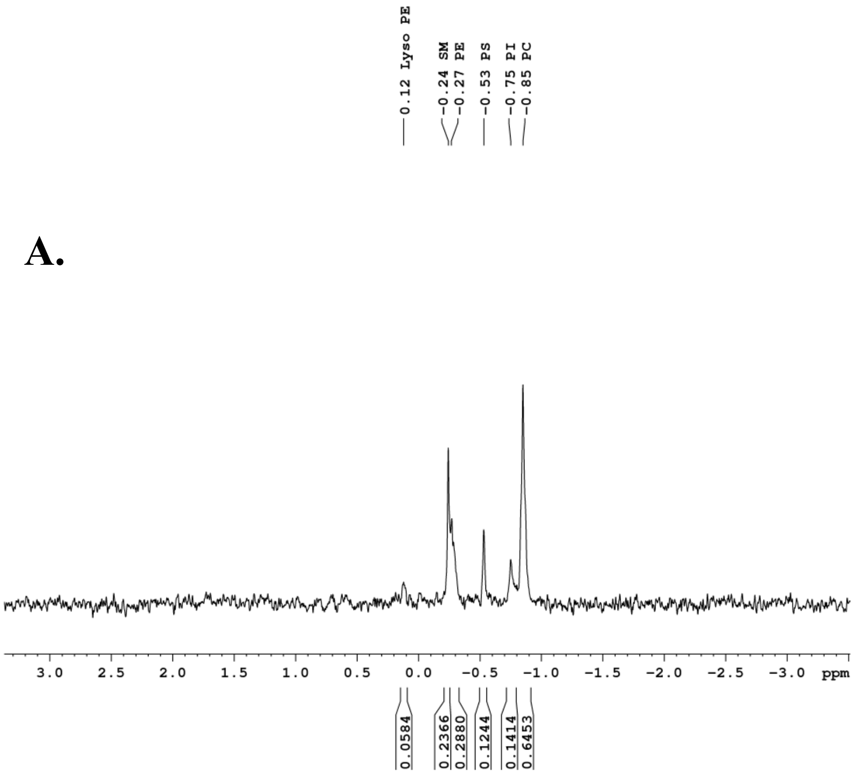

0.12 Lyso PE
-0.24 SM
-0.27 PE
-0.53 PS
-0.75 PI
-0.85 PC
3.0
2.5
2.0
1.5
1.0
0.5
0.0
-0.5
-1.0
-1.5
-2.0
-2.5
-3.0
ppm
0.0584
0.2366
0.2880
0.1244
0.1414
0.6453

B.

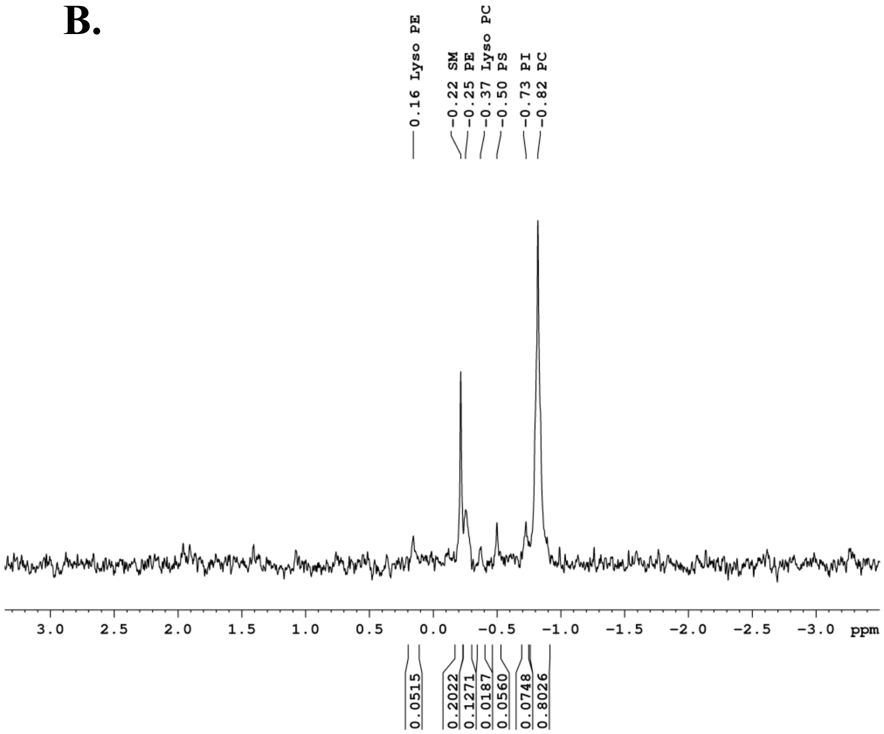

0.16 Lyso PE
-0.22 SM
-0.25 PE
-0.37 Lyso PC
-0.50 PS
-0.73 PI
-0.82 PC
3.0
2.5
2.0
1.5
1.0
0.5
0.0
-0.5
-1.0
-1.5
-2.0
-2.5
-3.0
ppm
0.0515
0.2022
0.1271
0.0187
0.0560
0.0748
0.8026

Figure S3(6-11). ^{31}P NMR spectra (acquired by Avanti Polar Lipids Analytical Services) for (A) A431 chloride salt vesicles sample and (B) A431 DTT/formaldehyde vesicle sample.

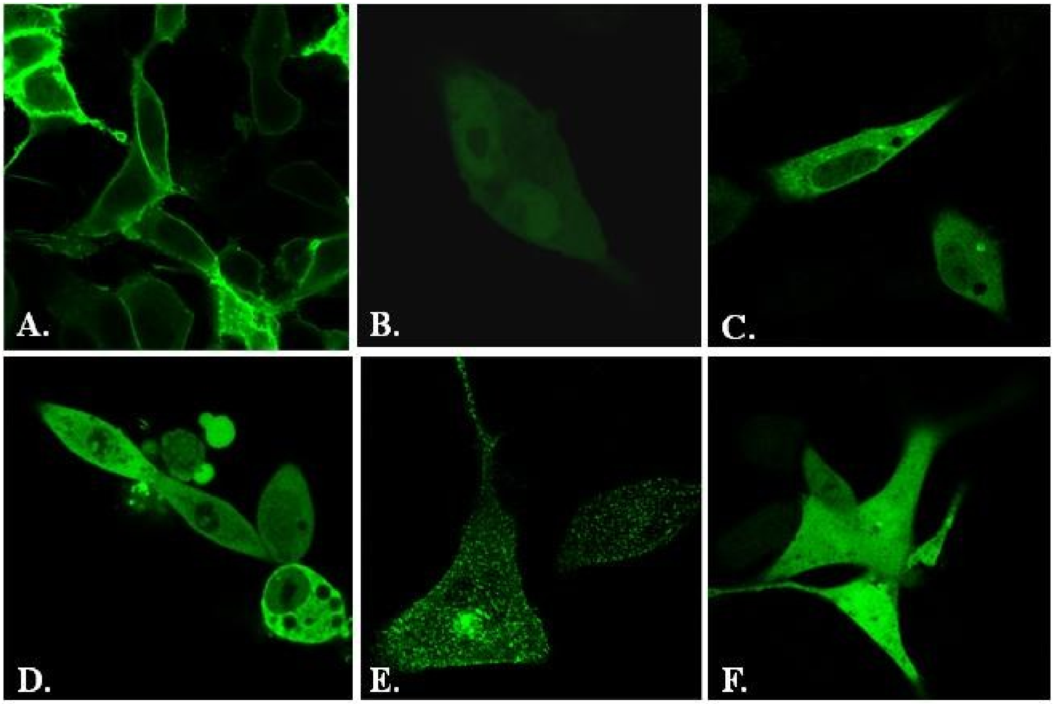

Figure S4(6-12). CHO cells expressing the soluble cytoplasmic proteins used in the leakage assays: **(A)** Plcδ1-PH-GFP (MW~45 kDa), **(B)** Grb2-Venus (MW~60 kDa), **(C)** PKCϴ-GFP (MW~120kDa), **(D)** Venusx6 (MW~160 kDa), **(E)** Intersectin II-GFP (MW~ 170 kDa) and **(F)** Plcɣ-GFP (MW~210 kDa).

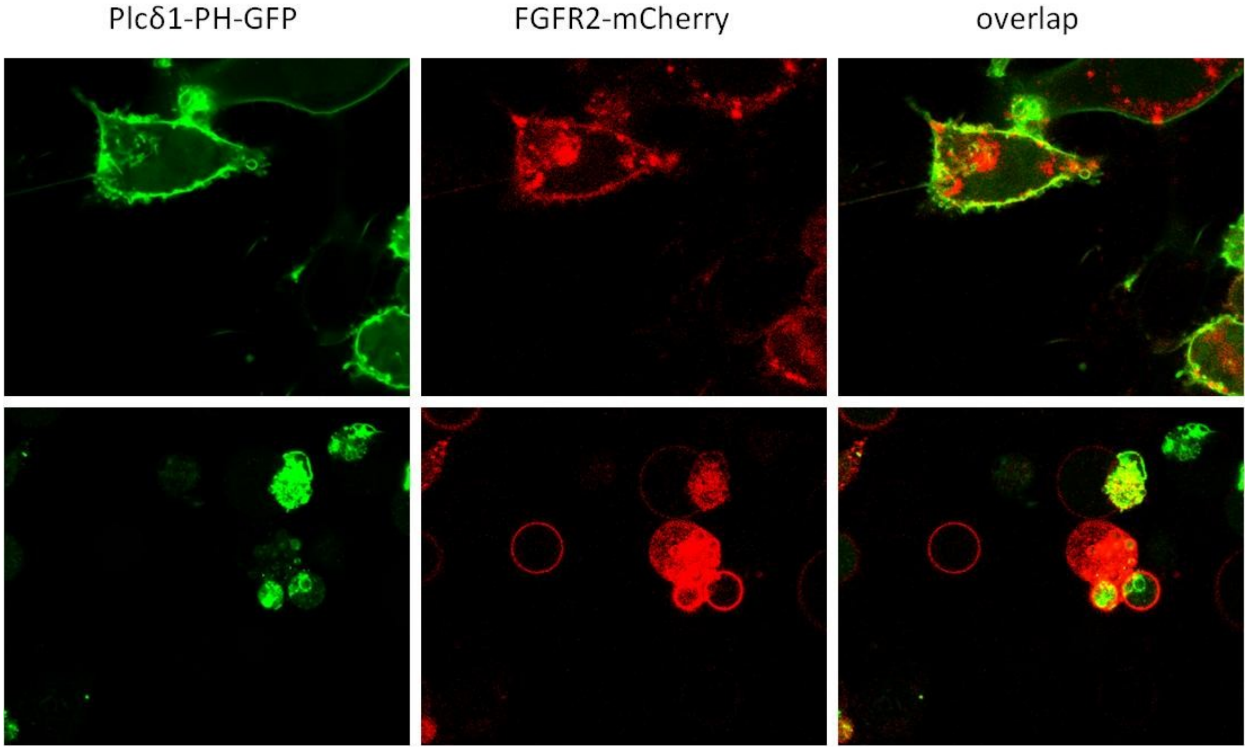

Figure S5(6-13). Top panel: Chinese Hamster Ovary (CHO) cells co-expressing FGFR2-mCherry and Plcδ1-PH-GFP. Bottom panel: Plcd1-PH-GFP (MW~45 kDa) in not retained inside CHO chloride salt vesicles.

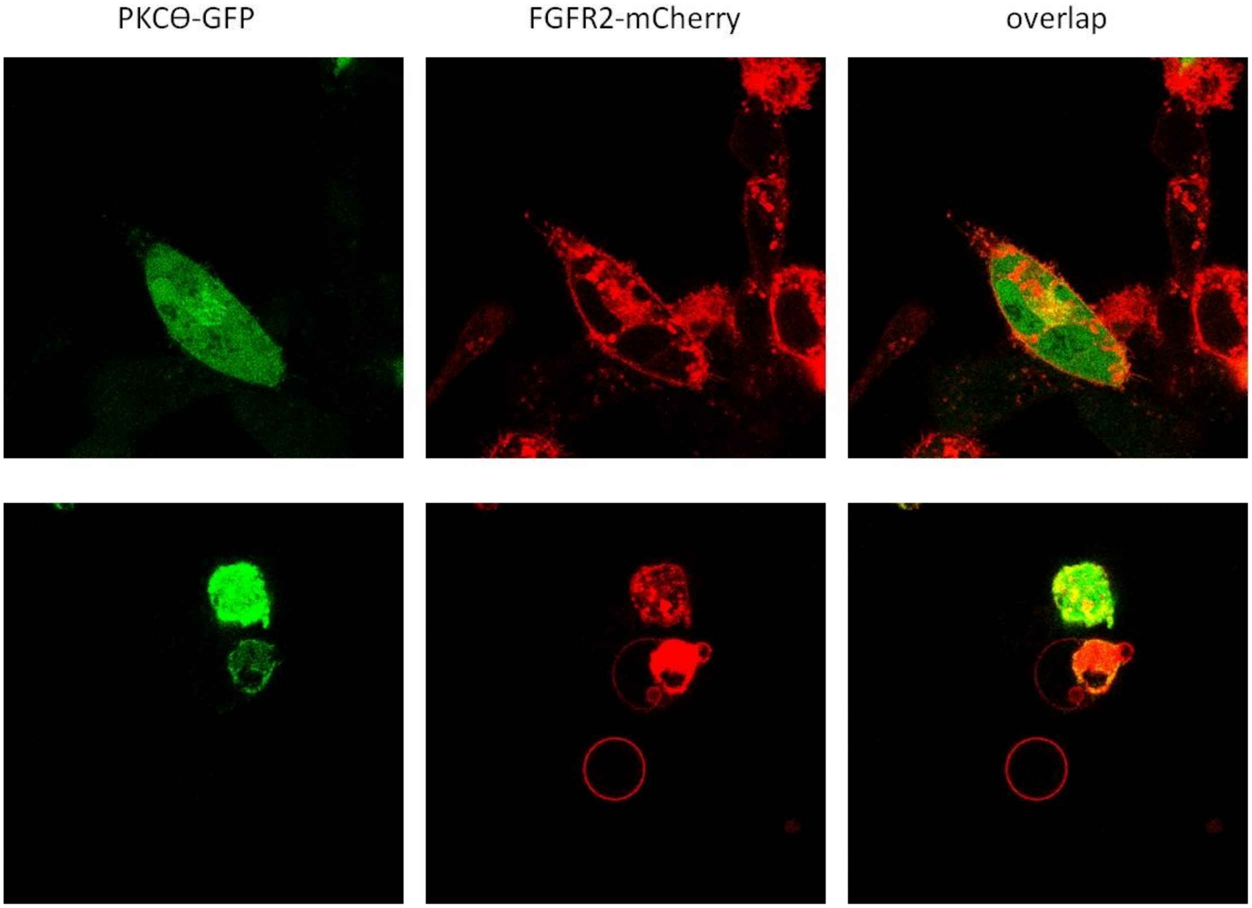

Figure S6(6-14). Top panel: CHO cells co-expressing PKCΘ-GFP and FGFR2-mCherry. Bottom panel: PKCΘ-GFP (MW~ 120kDa) is not retained inside CHO chloride salt vesicles.

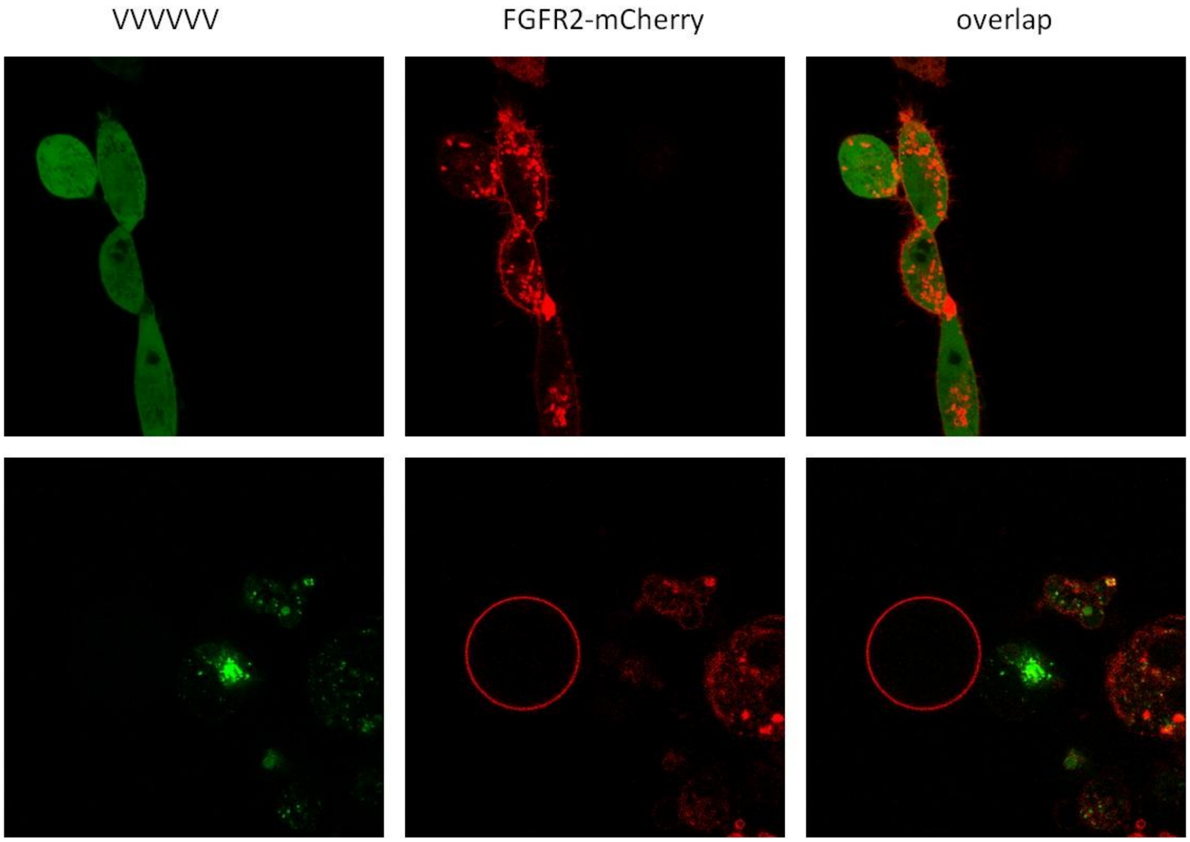

Figure S7(6-15). Top panel: Chinese Hamster Ovary (CHO) co-expressing VVVVVV (Venus x 6) and FGFR2-mCherry. Bottom panel: Venus x 6 (MW~ 160kDa) is not retained in CHO chloride salt vesicles.

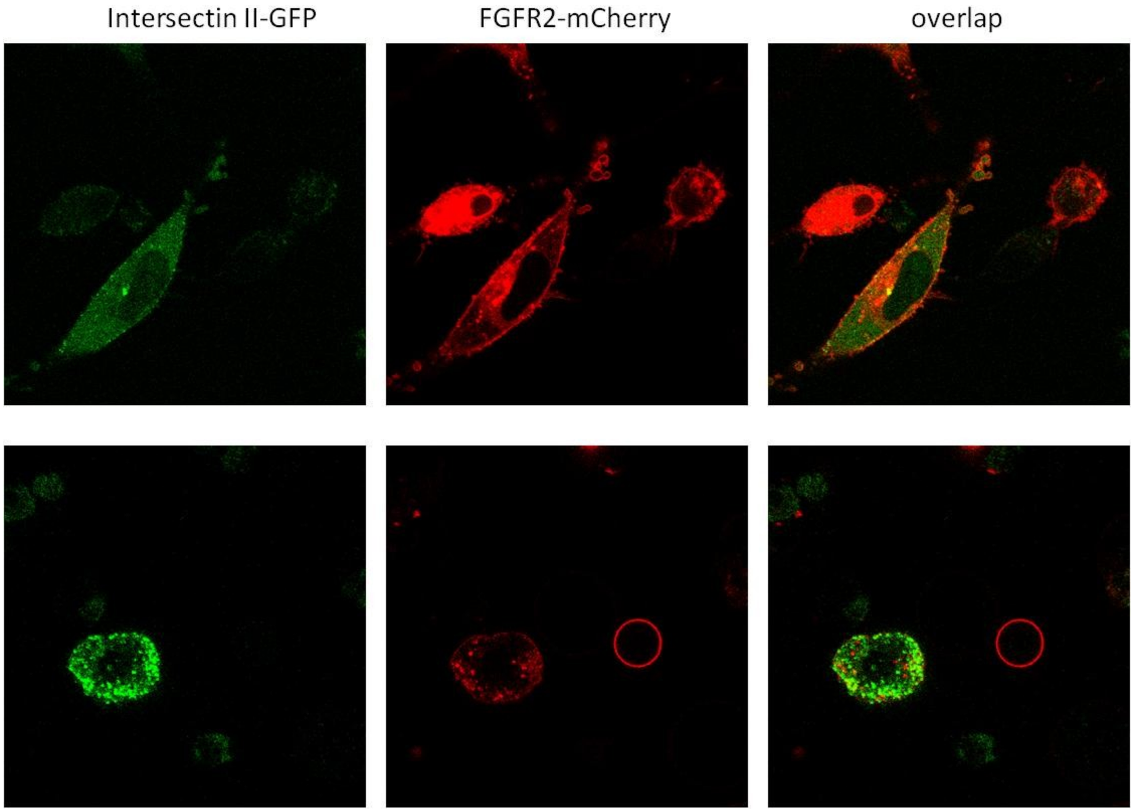

Figure S8(6-16). Top panel: CHO cells co-expressing Intersectin II-GFP and FGFR2-mCherry. Bottom panel: Intersectin II-GFP (MW~ 170kDa) is not retained inside CHO chloride salt vesicles.

Chapter 6. Un-induced high-yield bacterial expression of fluorescent proteins

Abstract

Here we introduce a fast, cost-effective, and highly efficient method for production of soluble fluorescent proteins from bacteria. The method does not require optimization, and does not utilize IPTG induction. The method relies on un-induced expression in the BL21-gold (DE3) strain of *E.coli* and yields large amounts (up to 0.4 µmoles) of protein from a 250 mL culture. This method is much simpler than published methods, and can be used to produce any fluorescent protein that is needed in biomedical research.

Keywords: Fluorescent protein, gene expression, protein production, high-yield, FRET, His-Tag, *E. coli.*

Fluorescent proteins are widely used as reporters of molecular localization and molecular interactions in cells or in model systems. Quantitative fluorescence spectroscopic techniques, including Förster Resonance Energy Transfer (FRET)-based methods, often rely on calibrations that utilize purified solutions of soluble fluorescent proteins of known concentrations (22, 25, 45, 81, 138). The production of such proteins from *E.coli* has traditionally relied on extensive and time consuming optimization of bacterial cultures, followed by optimization of Isopropyl β-D-1-thiogalactopyranoside (IPTG) induction of protein expression (111). These production methods, however, are never guaranteed to work, even after many laborious optimization steps. Fluorescent proteins from commercial sources are very expensive, and an efficient and cost-effective method of fluorescent protein production will be of great utility to the researchers in the field. Here we report on such a method, which can be used for the production of any soluble fluorescent protein. The method is based on the un-induced expression of fluorescent proteins in a strain of *E.coli,* BL21-Gold (DE3). It does not require optimization, and does not utilize IPTG. The yield of the method matches or surpasses the best optimized scenarios for IPTG-induced protein yields.

We have expressed and purified four different fluorescent proteins using this new method. The genes encoding for these fluorescent proteins were cloned into a commonly used and commercially available bacterial vector (pRSETB). The pRSETB-mCherry plasmid was a gift from Dr. R. Tsien (University of California, San Diego, CA), and was used without further manipulation. The yellow fluorescent protein (YFP) plasmid was a gift from Dr. M. Edidin (Johns Hopkins University, Baltimore, MD). The GFP2 gene was received from Dr. V. Raicu (University of Wisconsin, Milwaukee, WI) and the mTurquoise gene was a gift from Dr. P. Park (Case Western Reserve University, Cleveland, OH). The cDNA for all four proteins encoded a start codon, an N-terminal His-tag (6xHistidine) sequence, and the gene for the fluorescent protein. To produce pRSETB-YFP, pRSETB-GFP2, and pRSETB-mTurquoise, the fluorescent protein cDNA was inserted between the BamHI and Hind III sites within the multiple cloning site of the pRSETB vector (which encodes for the PT7 promoter, pUC origin and Ampicillin resistance genes, and a stop codon at the 3’ end). All the plasmids were sequenced using the T7 forward and T7-term primers by Genewiz, Inc., and were subsequently used for *E. coli* transformation.

In commonly used procedures, small cultures of bacteria are first optimized for protein expression before moving to large cultures (89, 111). To do so, small cultures of LB media (~ 5mL) are inoculated with a bacterial glycerol stock from a previous culture, or with a freshly transformed *E. coli* colony. These cultures are then incubated at 37˚C for different time periods to yield different optical densities (as measured in a UV-Vis spectrometer). The bacterial expression of fluorescent proteins is then induced by adding various amounts of IPTG. The expression time is varied to find the optimal conditions that ensure the highest yield of fluorescent proteins (usually assessed by SDS-PAGE). Once the optimum conditions are identified for the small culture, a large culture (100mL to 1L) is initiated and protein expression is induced with IPTG at the optimum optical density (Figure 1). Over the past few years we have attempted to use this procedure to produce large quantities of fluorescent proteins. Although we were successful several times, we also encountered many challenges. The optimization procedure was time-consuming and the yields were often very low, despite many optimization steps. Furthermore, the optimization did not always translate from small to large culture, and the reproducibility was low. In addition, the optimal optical density and IPTG concentration were different for each type of fluorescent protein and thus separate optimization procedures were required for each protein. Lastly, the *E.coli* glycerol stocks stored from previous bacterial cultures did not express the proteins under any of the optimized conditions.

We discovered, however, that fluorescent proteins are produced in BL21-Gold (DE3) cells without IPTG induction via un-induced expression that does not require optimization. BL21-Gold (DE3) Competent Cells (Agilent Technologies) are integral to this method of production, as other strains of *E. coli* did not prove suitable for high levels of un-induced expression. The *E.coli* cells were transformed with YFP, mCherry, GFP2, and mTurquoise-encoding plasmid DNA according to the manufacturer's protocol. The bacteria were grown in LB growth media containing 100 µg/mL Ampicillin salt (Sigma Aldrich). We inoculated 250-300mL of LB media with a freshly transformed bacterial colony and cultured it for 18-22 hours at 37˚C. To our amazement, we found that at the end of this long period of time visibly large quantities of the fluorescent proteins were produced without any IPTG addition. This was obvious from the change in the color of the LB media into the color of the fluorescent protein. The exact harvesting time within the 18-22 hour time window was not critical, unlike the stringent time requirements of common protocols.

To purify the fluorescent proteins, the intact cells were pelleted using a Beckman Coulter centrifuge at 9000 rpm, 14 minutes, 4˚C. The pellet was visibly colored (intense purple for mCherry (Figure 2B) and bright yellow to bright green for YFP, mTurquoise and GFP2). The intense color was an indication of successful fluorescent protein production and very high protein yields which we have never observed using the established protocols. The pellets could be stored at -20C or immediately lysed using Bugbuster® Master Mix (Invitrogen) with added protease inhibitor cocktail (complete mini EDTA-free tabs, Roche Applied Science). The lysate was gently agitated for 20 minutes at room temperature before centrifugation. Centrifugation was performed at 13000 rpm, at a temperature of 4˚C, for 20 minutes. The supernatant of the bacterial lysate, which contained the fluorescent proteins, was collected and the fluorescent proteins were purified by nickel affinity chromatography. The column was filled with 2 mL of nickel-NTA Agarose resin (5Prime), which was pre-equilibrated in 50 mM NaH_2PO_4 and 0.5 M NaCl at pH 8.0. The lysate was added to the column in portions and equilibrated for 30-60 minutes after each lysate addition. A wash buffer (50 mM NaH_2PO_4,0.5 M NaCl, pH 8.0 with 20 mM Imidazole PH 6.0) was applied to the column three times, followed by an elution buffer (50 mM NaH_2PO_4, 0.5 M NaCl, pH 8.0 with 250 mM Imidazole PH 6.0) to collect the purified fluorescent protein fractions. Upon the completion of elution, the collected protein solution was passed through a 0.22 μm filter and the stock solutions (Figure 3) were stored at 4 °C. The concentration was measured by collecting the absorption spectra using a UV-Vis spectrometer (Cary 50, Varian). The yields measured for the different fluorescent proteins ranged from 0.02 μmoles to 0.4 μmoles, purified from a 250 mL culture. The fluorescent proteins produced from a single trial were sufficient to use in tens of imaging experiments for calibration purposes.

While we do not understand the exact mechanism behind this un-induced mass protein production, the critical step in the protocol is the long, 18-22h incubation time. The phenomenon that we observe here is likely similar to the so-called “auto-induction” reported previously (51, 144). It has been suggested that this auto-induction is caused by small amounts of lactose (usually present in yeast extract), and can be inhibited by the presence of glucose (144). To test if glucose inhibits fluorescent protein production, we prepared three cultures from freshly transformed colonies and added 1mg/mL glucose after 6h and 12h of shaking. In addition, we prepared a culture where we added 500 mg/mL of glucose after 1h of shaking. In all these cases, after 22h we still observed high levels of fluorescent protein expression (Figure 2). Therefore, the glucose did not suppress significantly the production of fluorescent proteins in the absence of IPTG.

The spectral properties of the purified fluorescent proteins were recorded in a fluorometer. Figure 4 shows the excitation and emission spectra of each of the four fluorescent proteins that were produced and purified as described above. The resulting excitation and emission spectra were identical to the ones reported in the literature (81, 133). Therefore, this method provides a quick, high-yield production route for any soluble fluorescent protein that is needed for imaging purposes in biophysical research.

Figures

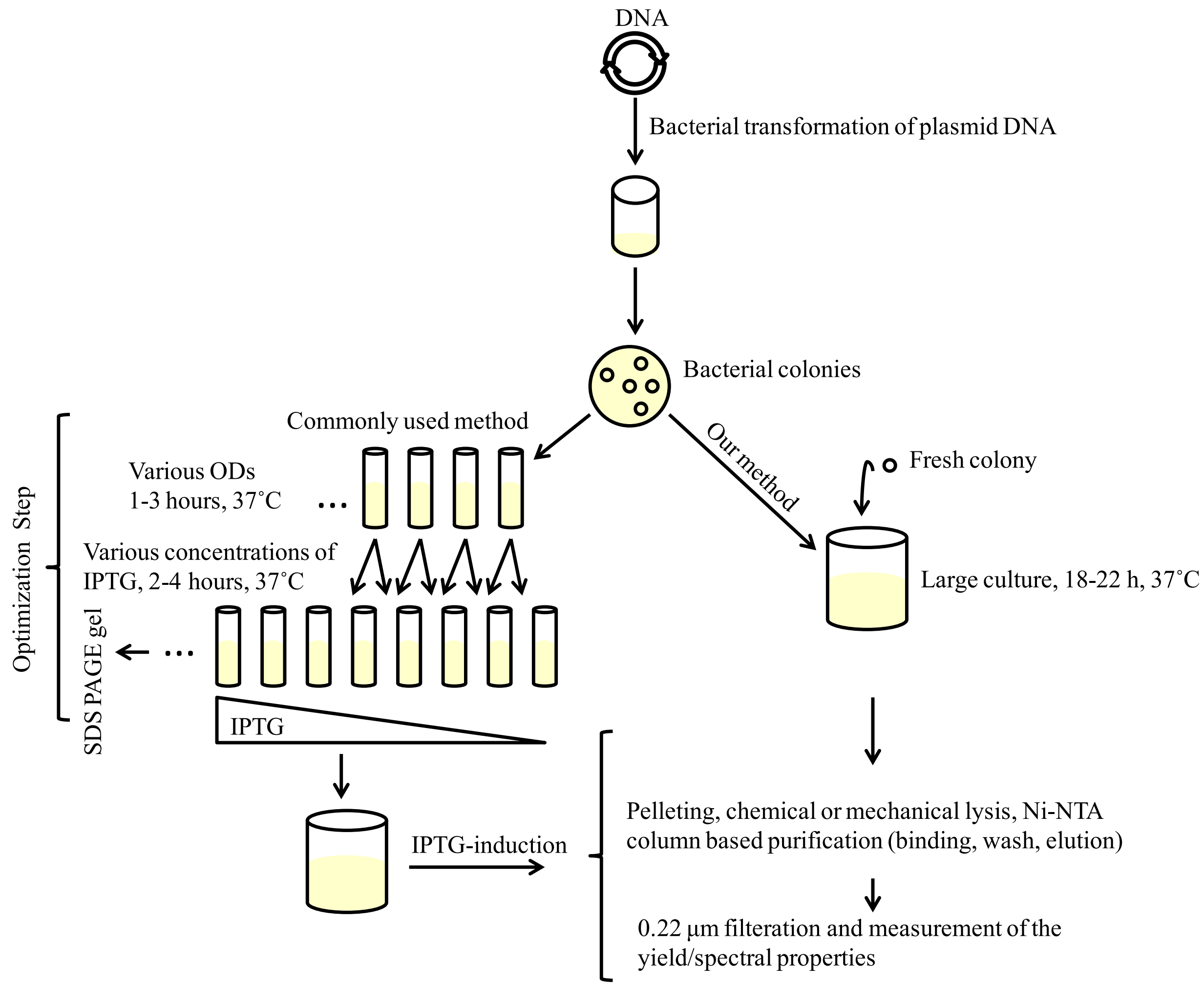

Figure 7-1. Protocols for fluorescent protein expression *in E. coli*. The commonly used method is on the left. Our new method is on the right.

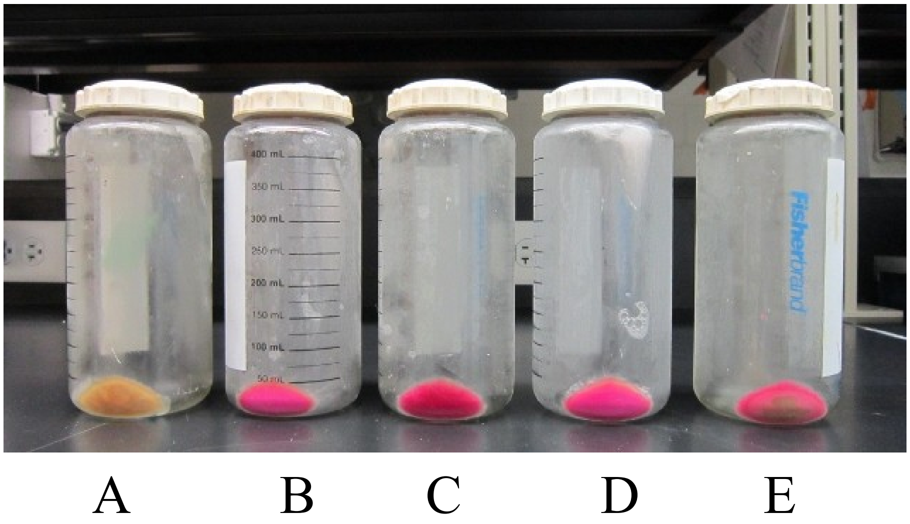

Figure 7-2. The mCherry pellet. (A) IPTG-induced culture; (B) un-induced culture; (C) un-induced culture, 1 mg/mL glucose added after 6h; (D) un-induced culture, 1mg/mL glucose added after 12h; (E) un-induced culture, 500 mg/mL glucose added after 1h.

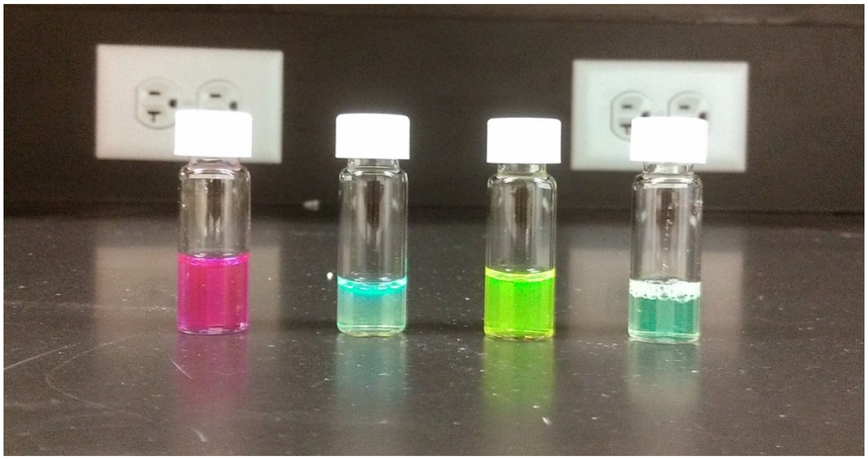

Figure 7-3. Purified stocks of fluorescent proteins in phosphate saline buffer. From left to right: mCherry, mTurquoise, YFP and GFP2 solutions.

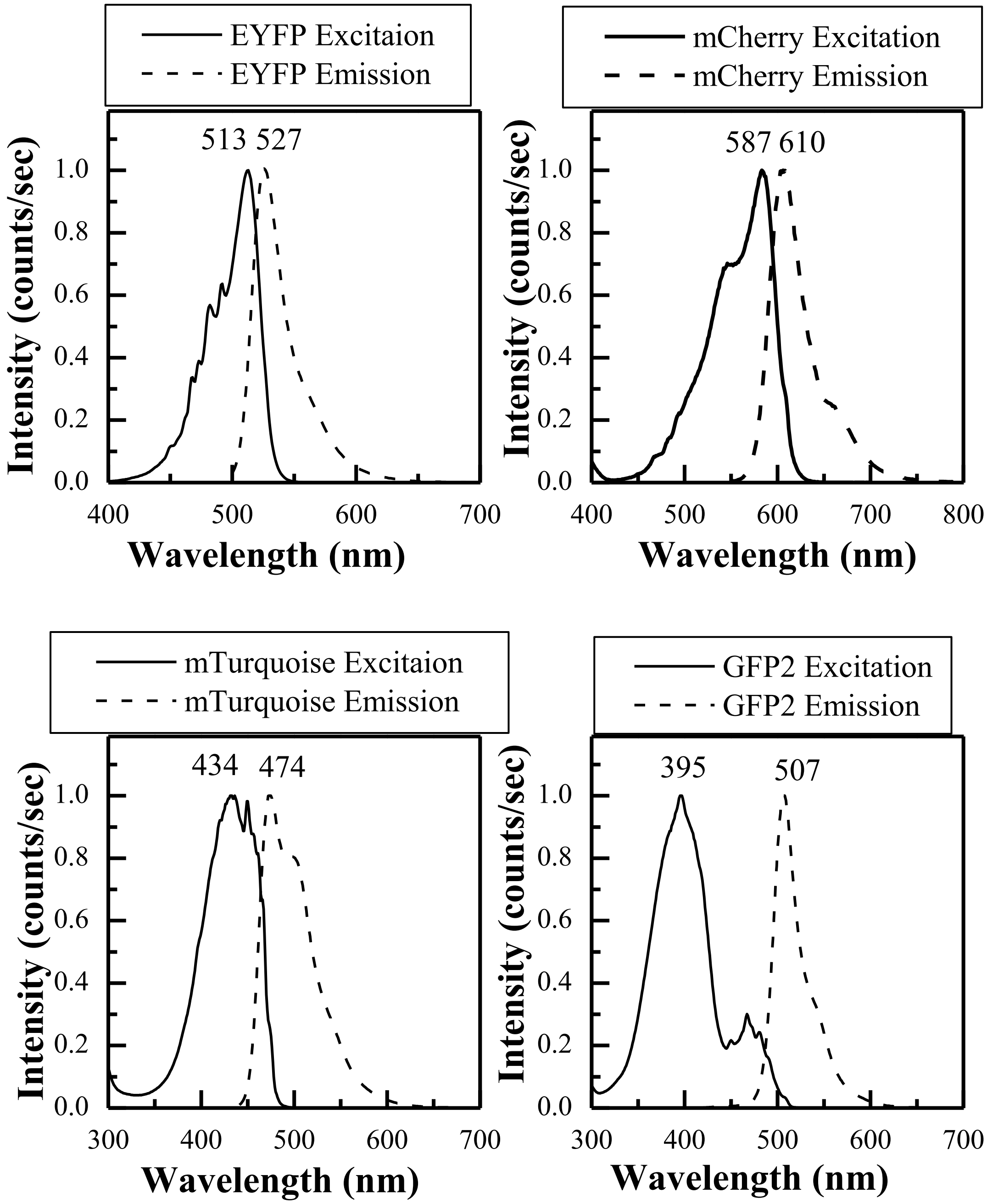

Figure 7-4. Excitation and emission spectra of the produced fluorescent proteins: EYFP, mCherry, GFP2 and mTurquoise. The emission and excitation maxima (in nm) are also shown. Spectra are identical to the ones reported in the literature (133).

Conclusions

One of the objectives of this thesis was to understand ligand-independent FGFR and VEGFR2 dimerization. In Chapter 1, the QI-FRET methodology was utilized as a direct dimerization assay to quantify FGFR1, FGFR2 and FGFR3 interactions in plasma membrane-derived vesicles. In this work, the vesicles were produced from mammalian cells expressing FGFRs tagged with YFP or mCherry as a FRET pair. 500-1000 vesicles were imaged for each receptor and analyzed. By fitting the data to a dimerization model, the free energy of dimerization (ΔG) and the intrinsic FRET (I-FRET), which depends on the distance between the fluorescent proteins in the dimers, were calculated. The results demonstrated that although the three receptors belong to the same RTK family, they possess different propensities for ligand-independent dimerization. The extrapolation of the dimerization curves to concentrations below 100 rec/μm^2 revealed that FGFR2 and FGFR3 form dimers even at low physiological concentrations. Similarly, the results presented in Chapter 2 demonstrated that VEGFR2 has a strong propensity for dimerization in the absence of ligands even at low physiological concentrations.

A second goal for this thesis was to investigate the effect of bound ligand on FGFR and VEGFR2 dimerization and dimer structure. Our measurements demonstrated that both FGF and VEGF receptors form constitutive dimers when treated with high concentrations of fgfs and vegfs, respectively. Next, we monitored the effect of ligand binding on the structure of the transmembrane domain dimers of the receptors, using truncated versions in which the fluorescent proteins were attached to the TM domains. The results in Chapter 1 demonstrated that fgf1-bound and fgf2-bound FGFR dimers have different structures. The fgf1-bound structure is characterized by larger distance between the C-termini of the TM domains. In the fgf2-bound structure, the C-termini of the TM domains are closer together. We further showed that the phosphorylation of FGFR1 and FGFR3 is higher in the fgf2-bound state than in the fgf1 state, thus establishing the biological significance of these new structural findings.

In Chapter 2 we also investigated if different VEGFs (VEGFA121, VEGFA165, VEGF C and VEGF) induce structural changes upon binding to VEGFR2 dimers. We found that all four ligands induce structural changes, but there were no measurable differences between the ligand-bound structures. Furthermore, while fgf2 binding to FGFR dimers brought the C-termini of FGFR TM domains closer together, VEGF binding to VEGFR2 pushed the C-termini of VEGFR2 TM domains further apart. Thus, the ligand induced a structural change for all studied receptors, but the nature of the change was different for the two receptor families.

In Chapter 3 of the thesis we investigated the role of the juxtamembrane domain of FGFR3 in unliganded dimerization. We demonstrated that the JMD stabilizes FGFR3 unliganded dimers. We further demonstrated that the TMD and the JMD work synergistically in dimer stabilization. Indeed, merely anchoring the JMD to the plasma membrane via a different TM sequence (the one of GpA) did not increase GpA dimer stability.

In Chapter 4, we investigated the role of three cysteine pathogenic mutations in the extracellular domains of the FGF receptors, on receptor dimerization and function. The FGFR1 C178S mutation is in domain D1, and is linked to Kallman syndrome. The FGFR2 C342R mutation is in domain D3, and is linked to Crouzon and Pffiefer syndromes. The FGFR3 C228R mutation is in domain D2 and in found in colorectal cancer. Our results demonstrated that all three mutations stabilized FGFR dimers to varying degrees, with C342R FGFR2 and C228 FGFR3 forming the strongest dimers. Using non-reducing and reducing SDS PAGE, we demonstrated that inter-molecular disulfide bonds play a role in the stabilization of C178S FGFR1, C342R FGFR2 and C228R FGFR3 dimers.

In Chapter 5, we characterized the plasma membrane derived vesicles used in the dissertation. A range of analytical techniques demonstrated the existence of key phospholipid components of mammalian plasma membranes in CHO and A431 vesicles. We showed that the different vesiculation methods have a small but statistically significant effect on lipid composition. We further showed that soluble cytoplasmic proteins leak out of the vesicles used in our studies.

Finally, in Chapter 6, we describe a fast and effective method for purification of fluorescent proteins from bacteria. These proteins are necessary for calibration purposes in the QI-FRET methodology and in other quantitative imaging techniques used in biophysical research.

The dissertation sheds new light on the molecular mechanism of FGFR and VEGFR signal transduction across the plasma membrane. Unlike many traditional biophysical and biochemical methods, the QI-FRET methodology provides a direct quantitative assay for studies of receptor dimerization in the plasma membrane. The method enables us to directly obtain the following four parameters over a range of RTK concentrations: (i) concentrations of RTK dimers, (ii) concentrations of RTK monomers, (iii) total RTK concentrations and (iv) FRET efficiencies. These parameters are then sufficient to calculate dimerization propensities in quantitative terms.

The QI-FRET method was used here in conjunction with plasma membrane-derived vesicles. These vesicles are a simple homogeneous model of the plasma membrane, allowing us to focus on the physical interactions between the receptors. Now that the plasma membrane-derived vesicles are characterized, they will likely continue to be a useful model system in biomembrane research. They offer a major advantage over other model systems because diverse membrane proteins can be studied without the need for their purification and reconstitution.

Overall, our results demonstrate the power of quantitative methods in RTK research. They provide new knowledge about RTK signal transduction across the plasma membrane, and establish the biological significance of unliganded RTK dimers. As unliganded dimers are implicated in cancers arising due to RTK overexpression, we hope that this new knowledge, in the long term, will help guide the search for new therapies.

Reference List

1. Adams, R. H., and K. Alitalo. 2007. Molecular regulation of angiogenesis and lymphangiogenesis. Nature Reviews Molecular Cell Biology 8: 464-478

2. Adar, R., E. Monsonego-Ornan, P. David, and A. Yayon. 2002. Differential activation of cysteine-substitution mutants of fibroblast growth factor receptor 3 is determined by cysteine localization. Journal of Bone and Mineral Research 17: 860-868

3. Ahmed, Z., C. C. Lin, K. M. Suen, F. A. Melo, J. A. Levitt, K. Suhling, and J. E. Ladbury. 2013. Grb2 controls phosphorylation of FGFR2 by inhibiting receptor kinase and Shp2 phosphatase activity. J. Cell Biol. 200: 493-504

4. Arkhipov, A., Y. B. Shan, R. Das, N. F. Endres, M. P. Eastwood, D. E. Wemmer, J. Kuriyan, and D. E. Shaw. 2013. Architecture and Membrane Interactions of the EGF Receptor. Cell 152: 557-569

5. Baumgart, T., A. T. Hammond, P. Sengupta, S. T. Hess, D. A. Holowka, B. A. Baird, and W. W. Webb. 2007. Large-scale fluid/fluid phase separation of proteins and lipids in giant plasma membrane vesicles. Proceedings of the National Academy of Sciences of the United States of America 104: 3165-3170

6. Belov, A. A., and M. Mohammadi. 2012. Grb2, a Double-Edged Sword of Receptor Tyrosine Kinase Signaling. Science Signaling 5

7. Blume-Jensen, P., and T. Hunter. 2001. Oncogenic kinase signalling. Nature 411: 355-365

8. Bocharov, E. V., D. M. Lesovoy, S. A. Goncharuk, M. V. Goncharuk, K. Hristova, and A. S. Arseniev. 2013. Structure of FGFR3 Transmembrane Domain Dimer: Implications for Signaling and Human Pathologies. Structure

9. Bocharov, E. V., K. S. Mineev, P. E. Volynsky, Y. S. Ermolyuk, E. N. Tkach, A. G. Sobol, V. V. Chupin, M. P. Kirpichnikov, R. G. Efremov, and A. S. Arseniev. 2008. Spatial structure of the dimeric transmembrane domain of the growth factor receptor ErbB2 presumably corresponding to the receptor active state. J. Biol. Chem. 283: 6950-6956

10. Bockaert, J., A. Dumuis, L. Fagni, and P. Marin. 2004. GPCR-GIP networks: A first step in the discovery of new therapeutic drugs? Current Opinion in Drug Discovery & Development 7: 649-657

11. Boye, E., M. Jinnin, and B. R. Olsen. 2009. Infantile hemangioma: challenges, new insights, and therapeutic promise. J. Craniofac. Surg. 20 Suppl 1: 678-684

12. Brewer, M. R., S. H. Choi, D. Alvarado, K. Moravcevic, A. Pozzi, M. A. Lemmon, and G. Carpenter. 2009. The Juxtamembrane Region of the EGF Receptor Functions as an Activation Domain. Molecular Cell 34: 641-651

13. Brozzo, M. S., S. Bjelic, K. Kisko, T. Schleier, V. M. Leppanen, K. Alitalo, F. K. Winkler, and K. Ballmer-Hofer. 2012. Thermodynamic and structural description of allosterically regulated VEGFR-2 dimerization. Blood. 119: 1781-1788

14. Burgess, A. W., H. S. Cho, C. Eigenbrot, K. M. Ferguson, T. P. J. Garrett, D. J. Leahy, M. A. Lemmon, M. X. Sliwkowski, C. W. Ward, and S. Yokoyama. 2003. An open-and-shut case? Recent insights into the activation of EGF/ErbB receptors. Molecular Cell 12: 541-552

15. Carpenter, G., and S. Cohen. 1979. Epidermal Growth-Factor. Annu. Rev. Biochem. 48: 193-216

16. Carpenter, G., L. King, and S. Cohen. 1979. Rapid Enhancement of Protein-Phosphorylation in A-431 Cell-Membrane Preparations by Epidermal Growth-Factor. J. Biol. Chem. 254: 4884-4891

17. Chan, R. B., T. G. Oliveira, E. P. Cortes, L. S. Honig, K. E. Duff, S. A. Small, M. R. Wenk, G. H. Shui, and G. Di Paolo. 2012. Comparative Lipidomic Analysis of Mouse and Human Brain with Alzheimer Disease. J. Biol. Chem. 287: 2678-2688

18. Chatterjee, S., L. C. Heukamp, M. Siobal, J. Schottle, C. Wieczorek, M. Peifer, D. Frasca, M. Koker, K. Koenig, L. Meder, D. Rauh, R. Buettner, J. Wolf, R. A. Brekken, B. Neumaier, G. Christofori, R. K. Thomas, and R. T. Ullrich. 2013. Tumor VEGF:VEGFR2 autocrine feed-forward loop triggers angiogenesis in lung cancer (vol 123, pg 1732, 2013). Journal of Clinical Investigation 123: 3183

19. Chen, F., C. Degnin, M. B. Laederich, A. W. Horton, and K. Hristova. 2011. The A391E mutation enhances FGFR3 activation in the absence of ligand. Biochimica et Biophysica Acta-Biomembranes **1808**: 2045-2050

20. Chen, F., S. Sarabipour, and K. Hristova. 2013. Multiple Consequences of a Single Amino Acid Pathogenic RTK Mutation: The A391E Mutation in FGFR3. PLoS ONE 8: e56521

21. Chen, F. H., and K. Hristova. 2011. The Physical Basis of FGFR3 Response to fgf1 and fgf2. Biochemistry 50: 8576-8582

22. Chen, L., L. Novicky, M. Merzlyakov, T. Hristov, and K. Hristova. 2010. Measuring the Energetics of Membrane Protein Dimerization in Mammalian Membranes. J. Am. Chem. Soc. 132: 3628-3635

23. Chen, L., J. Placone, L. Novicky, and K. Hristova. 2010. The extracellular domain of fibroblast growth factor receptor 3 inhibits ligand-independent dimerization. Science Signaling 3: ra86

24. Chen, L. I., M. K. Webster, A. N. Meyer, and D. J. Donoghue. 1997. Transmembrane domain sequence requirements for activation of the p185(c-neu) receptor tyrosine kinase. J. Cell Biol. 137: 619-631

25. Chiu, C. S., E. Kartalov, M. Unger, S. Quake, and H. A. Lester. 2001. Single-molecule measurements calibrate green fluorescent protein surface densities on transparent beads for use with 'knock-in' animals and other expression systems. Journal of Neuroscience Methods 105: 55-63

26. Cohen, M. M. 1997. Short-limb skeletal dysplasias and craniosynostosis: What do they have in common? Pediatric Radiology 27: 442-446

27. Cohen, M. M. 1998. Achondroplasia, hypochondroplasia and thanatophoric dysplasia: clinically related skeletal dysplasias that are also related at the molecular level. International Journal of Oral and Maxillofacial Surgery 27: 451-455

28. Cohen, M. M. 2002. Some chondrodysplasias with short limbs: Molecular perspectives. American Journal of Medical Genetics 112: 304-313

29. Colvin, J. S., B. A. Bohne, G. W. Harding, D. G. Mcewen, and D. M. Ornitz. 1996. Skeletal overgrowth and deafness in mice lacking fibroblast growth factor receptor 3. Nat. Genet. 12: 390-397

30. Colvin, J. S., R. P. Green, J. Schmahl, B. Capel, and D. M. Ornitz. 2001. Male-to-female sex reversal in mice lacking fibroblast growth factor 9. Cell 104: 875-889

31. Coskun, U., and K. Simons. 2010. Membrane rafting: From apical sorting to phase segregation. FEBS Lett. 584: 1685-1693

32. Cross, M. J., and L. Claesson-Welsh. 2001. FGF and VEGF function in angiogenesis: signalling pathways, biological responses and therapeutic inhibition. Trends Pharmacol. Sci. 22: 201-207

33. Del Piccolo, N., J. Placone, L. He, S. C. Agudelo, and K. Hristova. 2012. Production of plasma membrane vesicles with chloride salts and their utility as a cell membrane mimetic for biophysical characterization of membrane protein interactions. Anal. Chem. 84: 8650-8655

34. Del Piccolo, N., J. Placone, and K. Hristova. 2015. Effect of Thanatophoric Dysplasia Type I Mutations on FGFR3 Dimerization. Biophys. J. 108: 272-278

35. Deng, C., A. Wynshaw-Boris, F. Zhou, A. Kuo, and P. Leder. 1996. Fibroblast growth factor receptor 3 is a negative regulator of bone growth. Cell 84: 911-921

36. Endres, N. F., R. Das, A. W. Smith, A. Arkhipov, E. Kovacs, Y. J. Huang, J. G. Pelton, Y. B. Shan, D. E. Shaw, D. E. Wemmer, J. T. Groves, and J. Kuriyan.

2013. Conformational Coupling across the Plasma Membrane in Activation of the EGF Receptor. Cell 152: 543-556

37. Eswarakumar, V. P., I. Lax, and J. Schlessinger. 2005. Cellular signaling by fibroblast growth factor receptors. Cytokine Growth Factor Rev. 16: 139-149

38. Evers, T. H., E. M. W. M. van Dongen, A. C. Faesen, E. W. Meijer, and M. Merkx. 2006. Quantitative understanding of the energy transfer between fluorescent proteins connected via flexible peptide linkers. Biochemistry 45: 13183-13192

39. Fantl, W. J., D. E. Johnson, and L. T. Williams. 1993. Signaling by Receptor Tyrosine Kinases. Annu. Rev. Biochem. 62: 453-481

40. Feldman, B., W. Poueymirou, V. E. Papaioannou, T. M. Dechiara, and M. Goldfarb. 1995. Requirement of Fgf-4 for Postimplantation Mouse Development. Science 267: 246-249

41. Ferrara, N., H. P. Gerber, and J. LeCouter. 2003. The biology of VEGF and its receptors. Nature Medicine 9: 669-676

42. Fleishman, S. J., J. Schlessinger, and N. Ben-Tal. 2002. A putative molecular-activation switch in the transmembrane domain of erbB2. Proceedings of the National Academy of Sciences of the United States of America 99: 15937-15940

43. Folch, J., M. Lees, and G. H. Sloan Stanley. 1957. A simple method for the isolation and purification of total lipides from animal tissues. J. Biol. Chem. 226: 497-509

44. Forster, T. 1948. Intermolecular energy migration and fluorescence. Annalen der Physik 2: 55-75

45. Gerena-Lopez, Y., J. Nolan, L. Wang, A. Gaigalas, A. Schwartz, and E. Fernandez-Repollet. 2004. Quantification of EGFP expression on molt-4 T cells using calibration standards. Cytometry Part A 60A: 21-28

46. Gerhardt, H., M. Golding, M. Fruttiger, C. Ruhrberg, A. Lundkvist, A. Abramsson, M. Jeltsch, C. Mitchell, K. Alitalo, D. Shima, and C. Betsholtz. 2003. VEGF guides angiogenic sprouting utilizing endothelial tip cell filopodia. J. Cell Biol. 161: 1163-1177

47. Goetz, R., and M. Mohammadi. 2013. Exploring mechanisms of FGF signalling through the lens of structural biology. Nat. Rev. Mol. Cell Biol. 14: 166-180

48. Grandis, J. R., and J. C. Sok. 2004. Signaling through the epidermal growth factor receptor during the development of malignancy. Pharmacology & Therapeutics 102: 37-46

49. Grasberger, B., A. P. Minton, C. DeLisi, and H. Metzger. 1986. Interaction Between Proteins Localized in Membranes. Proceedings of the National Academy of Sciences of the United States of America 83: 6258-6262

50. Greenman, C., P. Stephens, R. Smith, G. L. Dalgliesh, C. Hunter, G. Bignell, H. Davies, J. Teague, A. Butler, S. Edkins, S. O'Meara, I. Vastrik, E. E. Schmidt, T. Avis, S. Barthorpe, G. Bhamra, G. Buck, B. Choudhury, J. Clements, J. Cole, E. Dicks, S. Forbes, K. Gray, K. Halliday, R. Harrison, K. Hills, J. Hinton, A. Jenkinson, D. Jones, A. Menzies, T. Mironenko, J. Perry, K. Raine, D. Richardson, R. Shepherd, A. Small, C. Tofts, J. Varian, T. Webb, S. West, S. Widaa, A. Yates, D. P. Cahill, D. N. Louis, P. Goldstraw, A. G. Nicholson, F. Brasseur, L. Looijenga, B. L. Weber, Y. E. Chiew, A. Defazio, M. F. Greaves, A. R. Green, P. Campbell, E. Birney, D. F. Easton, G. Chenevix-Trench, M. H. Tan, S. K. Khoo, B. T. Teh, S. T. Yuen, S. Y. Leung, R. Wooster, P. A. Futreal, and M. R. Stratton. 2007. Patterns of somatic mutation in human cancer genomes. Nature 446: 153-158

51. Grossman, T. H., E. S. Kawasaki, S. R. Punreddy, and M. S. Osburne. 1998. Spontaneous cAMP-dependent derepression of gene expression in stationary phase plays a role in recombinant expression instability. Gene 209: 95-103

52. Haigler, H., J. F. Ash, S. J. Singer, and S. Cohen. 1978. Visualization by Fluorescence of Binding and Internalization of Epidermal Growth-Factor in Human Carcinoma Cells A-431. Proceedings of the National Academy of Sciences of the United States of America 75: 3317-3321

53. He, L., W. A. Horton, and K. Hristova. 2010. The physical basis behind achondroplasia, the most common form of human dwarfism. J. Biol. Chem. **285**: 30103-30114

54. He, L., and K. Hristova. 2008. Pathogenic activation of receptor tyrosine kinases in mammalian membranes. J. Mol. Biol. 384: 1130-1142

55. He, L., and K. Hristova. 2012. Consequences of replacing EGFR juxtamembrane domain with an unstructured sequence. Sci. Rep. 2: 854

56. He, L., and K. Hristova. 2012. Physical-chemical principles underlying RTK activation, and their implications for human disease. Biochim. Biophys. Acta 1818: 995-1005

57. He, L., W. C. Wimley, and K. Hristova. 2011. FGFR3 heterodimerization in achondroplasia, the most common form of human dwarfism. J. Biol. Chem. 286: 13272-13281

58. He, L. J., C. Serrano, N. Niphadkar, N. Shobnam, and K. Hristova. 2012. Effect of the G375C and G346E Achondroplasia Mutations on FGFR3 Activation. PLoS ONE 7

59. He, L. J., N. Shobnam, and K. Hristova. 2011. Specific inhibition of a pathogenic receptor tyrosine kinase by its transmembrane domain. Biochimica et Biophysica Acta-Biomembranes 1808: 253-259

60. Hirsch, J. F., D. Renier, and C. Sainterose. 1982. Intracranial-Pressure in Craniostenosis. Monographs in Paediatrics 15: 114-118

61. Holowka, D., and B. Baird. 1983. Structural Studies on the Membrane-Bound Immunoglobulin E-Receptor Complex .1. Characterization of Large Plasma-Membrane Vesicles from Rat Basophilic Leukemia-Cells and Insertion of Amphipathic Fluorescent-Probes. Biochemistry 22: 3466-3474

62. Holt, J. A., G. Z. Luo, A. N. Billin, J. Bisi, Y. Y. McNeill, K. F. Kozarsky, M. Donahee, D. Y. Wang, T. A. Mansfield, S. A. Kliewer, B. Goodwin, and S. A. Jones. 2003. Definition of a novel growth factor-dependent signal cascade for the suppression of bile acid biosynthesis. Genes & Development 17: 1581-1591

63. Hong, H., and J. U. Bowie. 2011. Dramatic destabilization of transmembrane helix interactions by features of natural membrane environments. J. Am. Chem. Soc. 133: 11389-11398

64. Horton, W. A., J. G. Hall, and J. T. Hecht. 2007. Achondroplasia. Lancet 370: 162-172

65. Hyde, C. A., A. Giese, E. Stuttfeld, S. J. Abram, D. Villemagne, T. Schleier, H. K. Binz, and K. Ballmer-Hofer. 2012. Targeting extracellular domains D4 and D7 of vascular endothelial growth factor receptor 2 reveals allosteric receptor regulatory sites. Mol. Cell. Biol. 32: 3802-3813

66. Jinnin, M., D. Medici, L. Park, N. Limaye, Y. Q. Liu, E. Boscolo, J. Bischoff, M. Vikkula, E. Boye, and B. R. Olsen. 2008. Suppressed NFAT-dependent VEGFR1 expression and constitutive VEGFR2 signaling in infantile hemangioma. Nature Medicine 14: 1236-1246

67. Jura, N., N. F. Endres, K. Engel, S. Deindl, R. Das, M. H. Lamers, D. E. Wemmer, X. W. Zhang, and J. Kuriyan. 2009. Mechanism for Activation of the EGF Receptor Catalytic Domain by the Juxtamembrane Segment. Cell 137: 1293-1307

68. Kalinina, J., K. Dutta, D. Ilghari, A. Beenken, R. Goetz, A. V. Eliseenkova, D. Cowburn, and M. Mohammadi. 2012. The Alternatively Spliced Acid Box Region Plays a Key Role in FGF Receptor Autoinhibition. Structure 20: 77-88

69. Ke, R., X. Yang, C. Tianyi, M. Ge, J. Lei, and X. Mu. 2015. The C342R Mutation in FGFR2 Causes Crouzon Syndrome With Elbow Deformity. J. Craniofac. Surg. 26: 584-586

70. King, C., S. Sarabipour, P. Byrne, D. J. Leahy, and K. Hristova. 2014. The FRET signatures of non-interacting proteins in membranes: simulations and experiments. Biophys. J. 106: 1309-1317

71. Kisko, K., M. S. Brozzo, J. Missimer, T. Schleier, A. Menzel, V. M. Leppanen, K. Alitalo, T. Walzthoeni, R. Aebersold, and K. Ballmer-Hofer. 2011. Structural analysis of vascular endothelial growth factor receptor-2/ligand complexes by small-angle X-ray solution scattering. FASEB J. 25: 2980-2986

72. Koch, S., S. Tugues, X. Li, L. Gualandi, and L. Claesson-Welsh. 2011. Signal transduction by vascular endothelial growth factor receptors. Biochem. J. 437: 169-183

73. Kress, W., H. Collmann, M. Busse, B. Halliger-Keller, and C. R. Mueller. 2000. Clustering of FGFR2 gene mutations inpatients with Pfeiffer and Crouzon syndromes (FGFR2-associated craniosynostoses). Cytogenet. Cell Genet. 91: 134-137

74. L'Horte, C. G. M., and M. A. Knowles. 2005. Cell responses to FGFR3 signaling: growth, differentiation and apoptosis. Experim. Cell Res. 304: 417-431

75. Lajeunie, E., S. Heuertz, V. El Ghouzzi, J. Martinovic, D. Renier, M. Le Merrer, and J. Bonaventure. 2006. Mutation screening in patients with syndromic craniosynostoses indicates that a limited number of recurrent FGFR2 mutations accounts for severe forms of Pfeiffer syndrome. European Journal of Human Genetics 14: 289-298

76. Lemmon, M. A., and J. Schlessinger. 2010. Cell Signaling by Receptor Tyrosine Kinases. Cell 141: 1117-1134

77. Lemmon, M. A., H. R. Treutlein, P. D. Adams, A. T. Brünger, and D. M. Engelman. 1994. A dimerization motif for transmembrane alpha-helices. Nature Struct. Biol. 1: 157-163

78. Leppanen, V. M., M. Jeltsch, A. Anisimov, D. Tvorogov, K. Aho, N. Kalkkinen, P. Toivanen, S. Yla-Herttuala, K. Ballmer-Hofer, and K. Alitalo. 2011. Structural determinants of vascular endothelial growth factor-D receptor binding and specificity. Blood. 117: 1507-1515

79. Levental, I., M. Grzybek, and K. Simons. 2011. Raft domains of variable properties and compositions in plasma membrane vesicles. Proceedings of the National Academy of Sciences of the United States of America 108: 11411-11416

80. Li, E., and K. Hristova. 2006. Role of receptor tyrosine kinase transmembrane domains in cell signaling and human pathologies. Biochemistry 45: 6241-6251

81. Li, E., J. Placone, M. Merzlyakov, and K. Hristova. 2008. Quantitative measurements of protein interactions in a crowded cellular environment. Anal. Chem. 80: 5976-5985

82. Li, E., M. You, and K. Hristova. 2006. FGFR3 dimer stabilization due to a single amino acid pathogenic mutation. J. Mol. Biol. 356: 600-612

83. Li, Y., K. Mangasarian, A. Mansukhani, and C. Basilico. 1997. Activation of FGF receptors by mutations in the transmembrane domain. Oncogene 14: 1397-1406

84. Lin, C. C., F. A. Melo, R. Ghosh, K. M. Suen, L. J. Stagg, J. Kirkpatrick, S. T. Arold, Z. Ahmed, and J. E. Ladbury. 2012. Inhibition of Basal FGF Receptor Signaling by Dimeric Grb2. Cell 149: 1514-1524

85. Linggi, B., and G. Carpenter. 2006. ErbB receptors: new insights on mechanisms and biology. Trends in Cell Biology 16: 649-656

86. Low-Nam, S. T., K. A. Lidke, P. J. Cutler, R. C. Roovers, van Bergen en Henegouwen PM, B. S. Wilson, and D. S. Lidke. 2011. ErbB1 dimerization is promoted by domain co-confinement and stabilized by ligand binding. Nat. Struct. Mol. Biol. 18: 1244-1249

87. Luo, H. T., B. H. Jiang, S. M. King, and Y. C. Chen. 2008. Inhibition of Cell Growth and VEGF Expression in Ovarian Cancer Cells by Flavonoids. Nutrition and Cancer-An International Journal 60: 800-809

88. Maddy, A. H. 1967. The organization of protein in the plasma membrane. In Formation and Fate of Cell Organelles. K. B. Warren, editor. Academic Press, New York and London. 255-273.

89. Maniatas, T., E. F. Frisch, and M. D. Sambrook. 1989. *Molecular Cloning: A Laboratory Manual*. Cold Spring Harbor Laboratory.

90. Manni, S., K. Kisko, T. Schleier, J. Missimer, and K. Ballmer-Hofer. 2014. Functional and structural characterization of the kinase insert and the carboxy terminal domain in VEGF receptor 2 activation. FASEB J. 28: 4914-4923

91. Maruyama, I., and J. Y. Shen. 2012. Brain-derived neurotrophic factor receptor TrkB exists as a preformed dimer in living cells. FASEB J. 26

92. Matsumoto, T., and L. Claesson-Welsh. 2001. VEGF receptor signal transduction. Sci. STKE. 2001: re21

93. Meyers, G. A., D. Day, R. Goldberg, D. L. Daentl, K. A. Przylepa, L. J. Abrams, J. M. Graham, M. Feingold, E. Rawnsley, A. F. Scott, and E. W. Jabs. 1996. FCFR2 exon IIIa and IIIe mutations in Crouzon, Jackson-Weiss, and Pfeiffer syndromes: Evidence for missense changes, insertions, and a deletion due to alternative RNA splicing. American Journal of Human Genetics 58: 491-498

94. Meyers, G. A., S. J. Orlow, I. R. Munro, K. A. Przylepa, and E. W. Jabs. 1995. Fibroblast-Growth-Factor-Receptor-3 (Fgfr3) Transmembrane Mutation in Crouzon-Syndrome with Acanthosis Nigricans. Nat. Genet. 11: 462-464

95. Mohammadi, M., I. Dikic, A. Sorokin, W. H. Burgess, M. Jaye, and J. Schlessinger. 1996. Identification of six novel autophosphorylation sites on fibroblast growth factor receptor 1 and elucidation of their importance in receptor activation and signal transduction. Mol. Cell. Biol. 16: 977-989

96. Mohammadi, M., G. McMahon, L. Sun, C. Tang, P. Hirth, B. K. Yeh, S. R. Hubbard, and J. Schlessinger. 1997. Structures of the tyrosine kinase domain of fibroblast growth factor receptor in complex with inhibitors. Science 276: 955-960

97. Mohammadi, M., S. K. Olsen, and O. A. Ibrahimi. 2005. Structural basis for fibroblast growth factor receptor activation. Cytokine & Growth Factor Reviews 16: 107-137

98. Mohammadi, M., J. Schlessinger, and S. R. Hubbard. 1996. Structure of the FGF receptor tyrosine kinase domain reveals a novel autoinhibitory mechanism. Cell 86: 577-587

99. Neher, E. 1992. Ion channels for communication between and within cells. Neuron 8: 605-612

100. Nessa, A., S. A. Latif, N. I. Siddiqui, M. A. Hussain, M. R. Bhuiyan, M. A. Hossain, A. Akther, and M. Rahman. 2009. Angiogenesis-a novel therapeutic approach for ischemic heart disease. Mymensingh. Med. J. 18: 264-272

101. Oling, F., J. Sopkova-de Oliveira Santos, N. Govorukhina, C. Mazères-Dubut, W. Bergsma-Schutter, G. Oostergetel, W. Keegstra, O. Lambert, A. Lewit-Bentley, and A. Brisson. 2000. Structure of membrane-bound annexin A5 trimers: A hybrid cryo-EM–X-ray crystallography study. J. Mol. Biol. 304: 561-573

102. Olsen, S. K., O. A. Ibrahimi, A. Raucci, F. M. Zhang, A. V. Eliseenkova, A. Yayon, C. Basilico, R. J. Linhardt, J. Schlessinger, and M. Mohammadi. 2004. Insights into the molecular basis for fibroblast growth factor receptor autoinhibition and ligand-binding promiscuity. Proceedings of the National Academy of Sciences of the United States of America 101: 935-940

103. Olsson, A. K., A. Dimberg, J. Kreuger, and L. Claesson-Welsh. 2006. VEGF receptor signalling - in control of vascular function. Nat. Rev. Mol. Cell. Biol. 7: 359-371

104. Ornitz, D. M. 2000. FGFs, heparan sulfate and FGFRs: complex interactions essential for development. BioEssays 22: 108-112

105. Ornitz, D. M., and N. Itoh. 2001. Fibroblast growth factors. Genome Biology 2

106. Ornitz, D. M., J. S. Xu, J. S. Colvin, D. G. Mcewen, C. A. MacArthur, F. Coulier, G. X. Gao, and M. Goldfarb. 1996. Receptor specificity of the fibroblast growth factor family. J. Biol. Chem. 271: 15292-15297

107. Park, W. J., G. A. Bellus, and E. W. Jabs. 1995. Mutations in Fibroblast Growth-Factor Receptors - Phenotypic Consequences During Eukaryotic Development. American Journal of Human Genetics 57: 748-754

108. Park, W. J., G. A. Meyers, X. Li, C. Theda, D. Day, S. J. Orlow, M. C. Jones, and E. W. Jabs. 1995. Novel Fgfr2 Mutations in Crouzon and Jackson-Weiss Syndromes Show Allelic Heterogeneity and Phenotypic Variability. Human Molecular Genetics 4: 1229-1233

109. Passos-Bueno, M. R., A. L. Sertie, A. Richieri-Costa, L. G. Alonso, M. Zatz, N. Alonso, D. Brunoni, and S. F. M. Ribeiro. 1998. Description of a new mutation and characterization of FGFR1, FGFR2, and FGFR3 mutations among Brazilian patients with syndromic craniosynostoses. American Journal of Medical Genetics 78: 237-241

110. Passos-Bueno, M. R., W. R. Wilcox, E. W. Jabs, A. L. Sertié, L. G. Alonso, and H. Kitoh. 1999. Clinical spectrum of fibroblast growth factor receptor mutations. Human Mutation 14: 115-125

111. Patterson, G. H., S. M. Knobel, W. D. Sharif, S. R. Kain, and D. W. Piston. 1997. Use of the green fluorescent protein and its mutants in quantitative fluorescence microscopy. Biophys. J. 73: 2782-2790

112. Payrastre, B., M. Plantavid, C. Etievan, G. Ribbes, C. Carratero, H. Chap, and L. Dousteblazy. 1988. Characterization of Plasma-Membranes from A431 Cells, Isolated by Self-Generating Percoll Gradient - A Rapid Isolation Procedure to Obtain Plasma-Membranes with Functional Epidermal Growth-Factor Receptors. Biochim. Biophys. Acta 939: 355-365

113. Placone, J., L. He, N. Del Piccolo, and K. Hristova. 2014. Strong dimerization of wild-type ErbB2/Neu transmembrane domain and the oncogenic Val664Glu mutant in mammalian plasma membranes. Biochim. Biophys. Acta 1838: 2326-2330

114. Placone, J., and K. Hristova. 2012. Direct Assessment of the Effect of the Gly380Arg Achondroplasia Mutation on FGFR3 Dimerization Using Quantitative Imaging FRET. PLoS ONE 7: e46678

115. Plotnikov, A. N., J. Schlessinger, S. R. Hubbard, and M. Mohammadi. 1999. Structural basis for FGF receptor dimerization and activation. Cell 98: 641-650

116. Qutub, A. A., G. F. Mac, E. D. Karagiannis, P. Vempati, and A. S. Popel. 2009. Multiscale models of angiogenesis. IEEE. Eng. Med. Biol. Mag. 28: 14-31

117. Reardon, W., A. Smith, J. W. Honour, P. Hindmarsh, D. Das, G. Rumsby, I. Nelson, S. Malcolm, L. Ades, D. Sillence, D. Kumar, C. DeLozier-Blanchet, S. Mckee, T. Kelly, W. L. McKeehan, M. Baraitser, and R. M. Winter. 2000. Evidence for digenic inheritance in some cases of Antley-Bixler syndrome? Journal of Medical Genetics 37: 26-32

118. Reardon, W., R. M. Winter, P. Rutland, L. J. Pulleyn, B. M. Jones, and S. Malcolm. 1994. Mutations in the Fibroblast Growth-Factor Receptor-2 Gene Cause Crouzon-Syndrome. Nat. Genet. 8: 98-103

119. Robertson, S. C., J. A. Tynan, and D. J. Donoghue. 2000. RTK mutations and human syndromes - when good receptors turn bad. Trends Genet. 16: 265-271

120. Ruch, C., G. Skiniotis, M. O. Steinmetz, T. Walz, and K. Ballmer-Hofer. 2007. Structure of a VEGF-VEGF receptor complex determined by electron microscopy. Nat. Struct. Mol. Biol. 14: 249-250

121. Rutland, P., L. J. Pulleyn, W. Reardon, M. Baraitser, R. Hayward, B. Jones, S. Malcolm, R. M. Winter, M. Oldridge, S. F. Slaney, M. D. Poole, and A. O. M. Wilkie. 1995. Identical Mutations in the Fgfr2 Gene Cause Both Pfeiffer and Crouzon Syndrome Phenotypes. Nat. Genet. 9: 173-176

122. Sarabipour, S., and K. Hristova. 2013. FGFR3 Transmembrane Domain Interactions Persist in the Presence of Its Extracellular Domain. Biophys. J. 105: 165-171

123. Sarabipour, S., and K. Hristova. 2013. Glycophorin A transmembrane domain dimerization in plasma membrane vesicles derived from CHO, HEK 293T, and A431 cells. Biochim. Biophys. Acta 1828: 1829-1833

124. Sarabipour, S., and K. Hristova. 2015. FGFR3 Unliganded Dimer Stabilization by the Juxtamembrane Domain. J. Mol. Biol.

125. Sarabipour, S., C. King, and K. Hristova. 2014. Un-induced high-yield bacterial expression of fluorescent proteins. Anal. Biochem. 449: 155-157

126. Schlessinger, J. 2000. Cell signaling by receptor tyrosine kinases. Cell 103: 211-225

127. Schlessinger, J. 2004. Common and distinct elements in cellular signaling via EGF and FGF receptors. Science 306: 1506-1507

128. Schlessinger, J., A. N. Plotnikov, O. A. Ibrahimi, A. V. Eliseenkova, B. K. Yeh, A. Yayon, R. J. Linhardt, and M. Mohammadi. 2000. Crystal structure of a ternary FGF-FGFR-heparin complex reveals a dual role for heparin in FGFR binding and dimerization. Molecular Cell 6: 743-750

129. Scott, R. E. 1976. Plasma membrane vesiculation: A new technique for isolation of plasma membrane. Science 194: 743-745

130. Scott, R. E., and P. B. Maercklein. 1979. Plasma-Membrane Vesiculation in 3T3-Cells and Sv3T3 Cells .2. Factors Affecting the Process of Vesiculation. J. Cell Sci. 35: 245-252

131. Scott, R. E., R. G. Perkins, M. A. Zschunke, B. J. Hoerl, and P. B. Maercklein. 1979. Plasma-Membrane Vesiculation in 3T3-Cells and Sv3T3-Cells .1. Morphological and Biochemical Characterization. J. Cell Sci. 35: 229-243

132. Sengupta, P., A. Hammond, D. Holowka, and B. Baird. 2008. Structural determinants for partitioning of lipids and proteins between coexisting fluid phases in giant plasma membrane vesicles. Biochimica et Biophysica Acta-Biomembranes 1778: 20-32

133. Shaner, N. C., P. A. Steinbach, and R. Y. Tsien. 2005. A guide to choosing fluorescent proteins. Nature Methods 2: 905-909

134. Shen, J. Y., and I. N. Maruyama. 2011. Nerve growth factor receptor TrkA exists as a preformed, yet inactive, dimer in living cells. FEBS Lett. 585: 295-299

135. Shibuya, M., and L. Claesson-Welsh. 2006. Signal transduction by VEGF receptors in regulation of angiogenesis and lymphangiogenesis. Experim. Cell Res. 312: 549-560

136. Singer, S. J. 1971. The molecular organization of biological membranes. In Structure and Function of Biological Membranes. L. I. Rothfield, editor. Academic Press, New York. 145-222.

137. Singer, S. J., and G. L. Nicolson. 1972. The fluid mosaic model of the structure of cell membranes. Science 175: 720-731

138. Singh, D. R., M. M. Mohammad, S. Patowary, M. R. Stoneman, J. A. Oliver, L. Movileanu, and V. Raicu. 2013. Determination of the quaternary structure of a bacterial ATP-binding cassette (ABC) transporter in living cells. Integrative Biology 5: 312-323

139. Smith, N. R., D. Baker, N. H. James, K. Ratcliffe, M. Jenkins, S. E. Ashton, G. Sproat, R. Swann, N. Gray, A. Ryan, J. M. Jurgensmeier, and C. Womack. 2010. Vascular Endothelial Growth Factor Receptors VEGFR-2 and VEGFR-3 Are Localized Primarily to the Vasculature in Human Primary Solid Cancers. Clinical Cancer Research 16: 3548-3561

140. Snyder, B., and E. Freire. 1982. Fluorescence energy transfer in two dimensions. A numeric solution for random and nonrandom distributions. Biophys. J. 40: 137-148

141. Spivakkroizman, T., M. A. Lemmon, I. Dikic, J. E. Ladbury, D. Pinchasi, J. Huang, M. Jaye, G. Crumley, J. Schlessinger, and I. Lax. 1994. Heparin-Induced Oligomerization of Fgf Molecules Is Responsible for Fgf Receptor Dimerization, Activation, and Cell-Proliferation. Cell 79: 1015-1024

142. Spivakkroizman, T., M. A. Lemmon, I. Dikic, J. E. Ladbury, D. Pinchasi, J. Huang, M. Jaye, G. Crumley, J. Schlessinger, and I. Lax. 1995. How do Heparin and Heparan-Sulfate Activate Fgf-Mitogenic Activity. Trends in Glycoscience and Glycotechnology 7: 447-449

143. Stoeckenius, W., and D. M. Engelman. 1969. Current models for the structure of biological membranes. J. Cell Biol. 42: 613-646

144. Studier, F. W. 2005. Protein production by auto-induction in high-density shaking cultures. Protein Expr. Purif. 41: 207-234

145. Sun, X., E. N. Meyers, M. Lewandoski, and G. R. Martin. 1999. Targeted disruption of Fgf8 causes failure of cell migration in the gastrulating mouse embryo. Genes & Development 13: 1834-1846

146. Takahashi, H., and M. Shibuya. 2005. The vascular endothelial growth factor (VEGF)/VEGF receptor system and its role under physiological and pathological conditions. Clinical Science 109: 227-241

147. Tanner, K. G., and J. Kyte. 1999. Dimerization of the extracellular domain of the receptor for epidermal growth factor containing the membrane-spanning segment in response to treatment with epidermal growth factor. J. Biol. Chem. 274: 35985-35990

148. Thompson, T. E. 1964. The properties of bimolecular phospholipid membranes. In Cellular Membranes in Development. Academic Press, New York. 83-96.

149. Tsai, F. J., C. F. Yang, J. Y. Wu, C. H. Tsai, and C. C. Lee. 2001. Mutation analysis of Crouzon syndrome and identification of one novel mutation in Taiwanese patients. Pediatrics International 43: 263-266

150. Tsuzuki, Y., C. M. Carreira, M. Bockhorn, L. Xu, R. K. Jain, and D. Fukumura. 2001. Pancreas microenvironment promotes VEGF expression and tumor growth: Novel window models for pancreatic tumor angiogenesis and microcirculation. Laboratory Investigation 81: 1439-1451

151. Vajo, Z., C. A. Francomano, and D. J. Wilkin. 2000. The molecular and genetic basis of fibroblast growth factor receptor 3 disorders: The achondroplasia family of skeletal dysplasias, Muenke craniosynostosis, and Crouzon syndrome with acanthosis nigricans. Endocrine Reviews 21: 23-39

152. van Rhijn, B. W. G., R. Montironi, E. C. Zwarthoff, A. C. Jobsis, and T. H. van der Kwast. 2002. Frequent FGFR3 mutations in urothelial papilloma. Journal of Pathology 198: 245-251

153. van Rhijn, B. W. G., A. A. G. van Tilborg, I. Lurkin, J. Bonaventure, A. De Vries, J. P. Thiery, T. H. van der Kwast, E. C. Zwarthoff, and F. Radvanyi. 2002. Novel fibroblast growth factor receptor 3 (FGFR3) mutations in bladder cancer previously identified in non-lethal skeletal disorders. European Journal of Human Genetics 10: 819-824

154. Veatch, S. L., P. Cicuta, P. Sengupta, A. Honerkamp-Smith, D. Holowka, and B. Baird. 2008. Critical fluctuations in plasma membrane vesicles. Acs Chemical Biology 3: 287-293

155. Wang, F., M. Kan, K. McKeehan, J. H. Jang, S. J. Feng, and W. L. McKeehan. 1997. A homeo-interaction sequence in the ectodomain of the fibroblast growth factor receptor. J. Biol. Chem. 272: 23887-23895

156. Warnock, D. E., C. Roberts, M. S. Lutz, W. A. Blackburn, W. W. Young, and J. U. Baenziger. 1993. Determination of Plasma-Membrane Lipid Mass and Composition in Cultured Chinese-Hamster Ovary Cells Using High-Gradient Magnetic Affinity-Chromatography. J. Biol. Chem. 268: 10145-10153

157. Webster, M. K., and D. J. Donoghue. 1996. Constitutive activation of fibroblast growth factor receptor 3 by the transmembrane domain point mutation found in achondroplasia. EMBO J. 15: 520-527

158. Webster, M. K., and D. J. Donoghue. 1997. FGFR activation in skeletal disorders: Too much of a good thing. Trends Genet. 13: 178-182

159. Wells, A. 1999. EGF receptor. International Journal of Biochemistry & Cell Biology 31: 637-643

160. White, S. H., A. S. Ladokhin, S. Jayasinghe, and K. Hristova. 2001. How membranes shape protein structure. J. Biol. Chem. 276: 32395-32398

161. Wilkie, A. O. M. 2005. Bad bones, absent smell, selfish testes: The pleiotropic consequences of human FGF receptor mutations. Cytokine & Growth Factor Reviews 16: 187-203

162. Wilkie, A. O. M., G. M. Morriss-Kay, E. Y. Jones, and J. K. Heath. 1995. Functions of fibroblast growth factors and their receptors. Curr. Biol. 5: 500-507

163. Wolber, P. K., and B. S. Hudson. 1979. An analytic solution to the Förster energy transfer problem in two dimensions. Biophys. J. 28: 197-210

164. Yamagishi, N., S. Teshima-Kondo, K. Masuda, K. Nishida, Y. Kuwano, D. T. Dang, L. H. Dang, T. Nikawa, and K. Rokutan. 2013. Chronic inhibition of tumor

cell-derived VEGF enhances the malignant phenotype of colorectal cancer cells. Bmc Cancer 13

165. Yang, Y., P. Xie, Y. Opatowsky, and J. Schlessinger. 2010. Direct contacts between extracellular membrane-proximal domains are required for VEGF receptor activation and cell signaling. Proceedings of the National Academy of Sciences of the United States of America 107: 1906-1911

166. Zenaty, D., P. Bretones, C. Lambe, I. Guemas, M. David, J. Leger, and N. de Roux. 2006. Paediatric phenotype of Kallmann syndrome due to mutations of fibroblast growth factor receptor 1 (FGFR1). Mol. Cell Endocrinol. 254-255: 78-83

167. Zhang, X. Q., O. A. Ibrahimi, S. K. Olsen, H. Umemori, M. Mohammadi, and D. M. Ornitz. 2006. Receptor specificity of the fibroblast growth factor family - The complete mammalian FGF family. J. Biol. Chem. 281: 15694-15700

168. Zhang, X. W., J. Gureasko, K. Shen, P. A. Cole, and J. Kuriyan. 2006. An allosteric mechanism for activation of the kinase domain of epidermal growth factor receptor. Cell 125: 1137-1149

Curriculum Vitae

Contact Information

Name:	Sarvenaz Sarabipour
Address:	3400-North Charles Street-Maryland Hall-Room 206 Baltimore-Maryland 21218-USA
Email:	ssarabi2@jhu.edu
Date of Birth:	30 April 1984
Place of Birth:	Tehran, Iran

Education

[2009- 20 March 2015] Doctor of Philosophy in Materials Science and Engineering, Johns Hopkins University, USA

[2013] Masters in Materials Science and Engineering, Johns Hopkins University, USA

[2007-2008] Masters in Radiobiology, Université de Sherbrooke, Québec, Canada

[2004-2007] Bachelor of Science (Advanced), Double major in Physics & Mathematics, University of Sydney, Sydney, Australia

[2003] High school Certificate, Tabriz, Iran

Fellowships

[2007-2008] M.Sc Fellowship from department of Radiobiology Université de Sherbrooke, Canada

Awards and Honors

[2010] Student Research Achievement Award (SRAA) in Membrane Structure and Assembly, American Biophysical Society, USA.

[2006] Best undergraduate presentation prize of Student Research Symposium of the ACT/NSW Branch of the Australasian College of Physical Scientists and Engineering in Medicine (MedPhys06), Australia.

[2006] Summer Studentship in Department of PET & Nuclear Medicine, Royal Prince Alfred Hospital, Sydney, Australia.

[2006] Travel Award from Institute of Medical Physics, University of Sydney to present at the 14th World Congress in Medical Physics and Biomedical Engineering 2006 in Seoul, Korea.

[2005-2006] Membership in Talented Students Program (TSP) in School of Physics, University of Sydney, Australia.

[2005] first year mathematics prize from School of Mathematics and Statistics, University of Sydney, Australia.

[2004] Second Prize and successful entry in the innovation competition of School of Physics, University of Sydney to design and build an elastically powered Mars Rover, Australia.

[2002] 34th place in National English language Competition held by Education Ministry in Iran.

Teaching Experience

[2014 Spring semester] Taught and instructed “Fluorescence properties” for Biomaterials Lab II course.

[2012 Fall semester] presented a lecture for Prof.Kalina Hristova’s Class in membrane biophysics (EN.510.426) on Receptor Tyrosine Kinases, Department of Materials Science and Engineering, Johns Hopkins University.

[2008-2009] Teaching Assistant for a year for Physical Chemistry Labs II and III at Department of Chemistry, Johns Hopkins University.

[2005-2006] Employment as Casual Academic (Physics Tutor) for a year in second year undergraduate physics labs, University of Sydney.

[2005-2006] private tutoring for undergraduate Physics and Mathematics.

Research Experience

Biophysics and Biochemistry of cells (Molecular biology and quantitative fluorescence Imaging), protein engineering and purification, Immunochemistry, mammalian cell culture, confocal and two-photon quantitative imaging, western blotting gel electerophoresis, Flow cytometry. Plasma Physics, Medical Physics, Radiobiology (physical chemistry of low energy ion, electron and photon beams impacted on biofilms).

Language Skills

Persian (Farsi), Native Speaker

Azeri, Native Speaker

Turkish, Fluent

English, Fluent, Certificated from University of Sydney English Teaching center.

French, Beginner

Publications

1. **Sarabipour.S**, Bosi.S.G, Hill.B and Baldock.C. A preliminary study of the measurement of slice-width dose profiles (SWDP) on diagnostic x-ray CT scanners

using PAGAT polymer gel dosimeters with optical CT read-out. *Journal of Physics: Conference Series* 56 (2006) 280–282.

2. Bosi.S.G, Brown.S, **Sarabipour.S**, De Deene.Y, Baldock.C. Light scattering artefacts in a funnel phantom using optical CT. *Physics in Medicine and Biology*, Vol. 54, (2), (2009), pp. 275-283(9).

3. Chen F, **Sarabipour S**, Hristova K. Multiple Consequences of a Single Amino Acid Pathogenic RTK Mutation: The A391E Mutation in FGFR3. *PLoS ONE* 8(2): e56521 (2013).

4. **Sarabipour.S** and Hristova.K, Glycophorin A transmembrane domain dimerization in plasma membrane vesicles derived from CHO, HEK 293T, and A431 cells. *Biochimica et Biophysica Acta (BBA) – Biomembranes*, Vol. 1828, Issue 8, (2013), Pages 1829–1833.

5. **Sarabipour.S** and Hristova.K, FGFR3 transmembrane domain interactions persist in the presence of its extracellular domain, *Biophysical Journal,* Vol.105, Issue 1, 2July2013, Pages 165-171.

6. **Sarabipour.S**, Christopher King, Hristova.K, Uninduced high-yield bacterial expression of fluorescent proteins, *Analytical Biochemistry,* 449, 155-157 (2014).

7. **King.C, Sarabipour.S**, Byrne.P, Leahy.D and Hristova.K, The FRET signatures of non-interacting proteins in membranes: simulations and experiments, *Biophysical Journal,* 106 (6), 1309-1317 (2014).**I am a co-First author.**

8. **Sarabipour S** and Hristova K. FGFR3 unliganded dimer stabilization by the juxtamembrane domain. *Journal of Molecular Biology in Press 14Feb 2015.*

9. **S.Sarabipour,** R.B.Chan, B.Zhou, G. Di Paolo and K.Hristova, Analytical characterization of plasma membrane derived vesicles produced via osmotic and chemical vesiculation. Accepted manuscript. *Biochimica et Biophysica Acta* (*BBA)-Biomembranes* March 2015.

10. **S.Sarabipour** and K.Hristova, Mechanism of FGF receptor signal transduction across the plasma membrane. *Manuscript in preparation 2015.*

11. **S.Sarabipour,** Kurt Ballmer-Hofer, K.Hristova, Mechanism of VEGFR2 signal transduction across the plasma membrane. *Manuscript in preparation 2015.*

Conference proceedings

1. **Sarabipour S**, Fulton R, Baldock C. Optical motion tracking techniques to monitor chest deformation during respiration. *Proceedings of EPSM 2006, Engineering and Physical Sciences in Medicine incorporating Australian Biomedical Engineering Conference 2006 in Queensland, Australia.* Available on page 5.

2. **Sarabipour S**, Bosi SG, Hill B, Baldock C.A preliminary study of measurement of slice-width dose profiles (SWDP) on diagnostic CT scanners using PAGAT polymer gel dosimeters with optical CT read-out. *Proceedings of DOSGEL 2006, 4th International Conference on Radiotherapy Gel Dosimetry 2006 in Sherbrooke, Canada*.

3. **Sarabipour S**, Bosi SG, Hill B, Baldock C. Optical Evaluation of Normoxic PAGAT polymer gel dosimeters used to measure SWDP on diagnostic CT scanners. *Proceedings of WC2006, 14th World Congress on Medical Physics and Biomedical Engineering 2006 in Seoul, Korea.*

4. **Sarabipour.S**, Deng.Z, Huels.M Fragmentation of DNA components by hyperthermal heavy ion (Ar+ and Xe+) impact in the condensed phase p.2732, *37th COSPAR Scientific Assembly* 13-20 July 2008, in Montréal, Canada.

5. **Sarabipour.S,** Deng.Z, Huels.M . Hyperthermal heavy ion damage to DNA bases. *APS March meeting* New Orleans, LA, USA 2008.

6. **Sarabipour.S,** Hristova.K, Quantitative Measurements of Receptor Interactions in Mammalian Cells: Implications for Human Pathologies, *Biophysical Society meeting* Baltimore, MD, USA 2013.

7. **Sarabipour.S,** Li.E, Hristova.K, Effect of FGFR3 Juxtamembrane Domain on FGFR3 Dimerization, *Biophysical Society meeting* Baltimore, MD, USA 2010.

8. **Sarabipour.S**, Frishman.A, Hristova.K, Homodimerization of FGFR2 and FGFR3 in cell derived vesicles, *FASEB meeting (Molecular Biophysics of Membrane)* Snowmass, CO, USA 2012.

9. **Sarabipour.S**, Hristova.K, The strength of side chain Hydrogen bonds in Plasma membrane, APS March meeting Baltimore, MD, USA 2013.

10. **Sarabipour.S**, Hristova.K, GpA dimerization in plasma membrane vesicles derived from CHO, HEK 293T, and A431 cells, 245th ACS National meeting, New Orleans, LA, USA 2013.

11. **Sarabipour S**, Hristova K. Mechanism of VEGFR2 activation, FASEB meeting molecular biophysics of membranes, Big Sky, Montana, USA 2014.